17

# THE SYNTHESIS, STRUCTURE AND CHEMISTRY OF SOME NOVEL ORGANOMETALLIC DENDRIMERS

A thesis submitted to the
**UNIVERSITY OF CAPE TOWN**
In fulfillment of the requirements for the degree of

**DOCTOR OF PHILOSOPHY**

by

**MEREDITH ANN HEARSHAW**
**B.Sc(HONS)**



Department of Chemistry
University of Cape Town
Rondebosch, 7701
South Africa

December 1999

*" Consider, for instance, one of the white flakes that are obtained by salting a solution of soap. At a distance its contour may appear sharply defined, but as we draw nearer its sharpness disappears..... The use of a magnifying glass or microscope leaves us just as uncertain, for fresh irregularities appear every time we increase the magnification, and we never succeed in getting a sharp, smooth impression, as given, for example, by a steel ball."*

*Jean Perrin (1906)*
*quoted: Benoit B. Mandelbrot,*
*The Fractal Geometry of Nature (1982)*

Parts of this thesis have been published in:

(i) M. A. Hearshaw and J. R. Moss, *Chem. Commun.*, 1999, 1.

(ii) M. A. Hearshaw, A. T. Hutton, J. R. Moss and K. J. Naidoo in, *Advances in Dendritic Macromolecules,* ed. G. R. Newkome, JAI Press, Greenwich, CT, 1999, vol. 4, pp. 1-60.

## ABSTRACT

The synthesis and chemistry of several series of novel organometallic dendritic wedges and small dendrimers containing iron, ruthenium, cobalt and tungsten have been investigated. The compounds have been synthesised using the convergent methodology of Hawker and Fréchet. Haloalkyl complexes such as $Cp^*Fe(CO)_2(CH_2)_3Br$ and $CpRu(CO)_2(CH_2)_3Br$ were used for the synthesis of the dendrimers. In this approach, the metal and ligand system remain on the periphery of the dendrimer. The synthesis proceeds *via* successive coupling and activation steps. Many of the dendritic wedges decomposed during the activation procedure. All the dendritic wedges and first generation dendrimers were soluble in common organic solvents and were characterised by IR, $^1H$ and $^{13}C$ NMR spectroscopy, mass spectrometry and microanalysis where possible. The organoruthenium dendrimers are significantly more stable at room temperature and in solution than all the iron analogues. The steric hindrance imparted by the cobaloxime ligand allowed only the zero-generation dendrimer to be synthesised. Several heterobimetalllic dendritic wedges were synthesied as well as a hybrid block copolymer. The surface functionalisation of bromobenzyl-terminated dendrimers was attempted. The data are discussed and some properties and reactions of the compounds are described.

The x-ray crystal structures of a dendritic precursor, $[CpFe(CO)_2(CH_2)_3Br]$ (space group $P2_1/c$) and first generation ruthenium dendritic wedge (space group Cc) have been determined at low temperature. Calculated molecular structures were generated with the HYPERCHEM™ program; the dendritic wedges are fairly open structures while the first generation dendrimer adopts a more spherical shape. Cyclic voltammetry studies were carried out on several of the iron and ruthenium dendrimers. The cyclic voltammograms of all the complexes showed a single irreversible oxidation peak; this suggests that there is no interaction or communication between the metals. The thermal behaviour of some of the organoiron dendrimers was also investigated by thermogravimetric analysis and differential scanning calorimetry. The latter traces generally showed one endothermic peak which could be assigned to melting. The chemical reactivity of a first generation ruthenium dendrimer was investigated; this dendrimer was found to react more slowly than the mononuclear complexes. This first generation dendrimer, supported on silica, was tested as a catalyst in the Fischer-Tropsch synthesis. This mono-atomic ruthenium dendrimer was found not to have sufficient catalytic activity for this purpose. The chemical and physical properties of these dendrimers are discussed.

# SCOPE OF THIS THESIS

Dendrimers are a new class of polymers that attracted much attention since their "birth" in the early 1980's. This is because their novel molecular architecture is so different from traditional linear polymers and so many new properties and applications have been proposed for these compounds. In the early years, the dendrimers tended to be organic in nature. Several years later, other elements such as phosphorus and silicon as well as transition metals such as iron, ruthenium and nickel were included in dendrimer synthesis. Two main methods of synthesis have been developed and refined over the last few years. These are the divergent approach in which synthesis proceeds in an outward fashion and the convergent approach where the synthesis begins at what will eventually become the periphery of the molecule. Each method has its own advantages and disadvantages.

The work presented in this thesis explores the synthesis and chemistry of several series of organometallic dendrimers containing iron, ruthenium, tungsten and cobalt. The convergent approach was used to synthesise all the dendrimers in this thesis for the reason of having a greater degree of control over the placement of the functional groups in the dendrimer. The new dendrimers and dendritic wedges could be characterised by standard methods of analysis. Some physical properties including the electrochemical and thermal behaviour of these new compounds have been examined. Chemical reactivity studies were carried out on selected dendrimers to compare their behaviour with analogous mononuclear compounds. Structural studies were carried out to gain information on the conformation of the dendrimer, in particular the location of the metal-ligand system in the dendrimer. If the dendrimer is to be used as a catalyst, the metal and its ligand system must be on the surface of the dendrimer and available to reactants. Finally, a first generation organoruthenium dendrimer was tested as a supported catalyst in the Fischer-Tropsch synthesis.

Chapter 1 gives an overview on the synthetic methodology developed for use in dendrimer synthesis and discusses some general properties and applications of these new compounds. Chapter 2 examines the synthesis, characterisation and some reactions of iron-containing dendrimers. Some structural and physical properties of these dendrimers are investigated. Chapter 3 looks at the chemical reactivity and some physical properties of some ruthenium-containing dendrimers. The X-ray structure of a first generation dendritic wedge is presented. Chapter 4 looks at the synthesis and characterisation of some

cobaloxime dendrimers. Chapter 5 examines the preparation and characterisation of some heterobimetallic dendrimers and dendritic block copolymers. The attempted surface functionalisation of some organic dendrimers with metals is also discussed. Chapter 6 presents a summary and some conclusions of all these investigations.

## LIST OF ABBREVIATIONS

| | |
|---|---|
| ASF | Anderson-Shultz-Flory |
| $^{n}$Bu | n-butyl (-$CH_2CH_2CH_2CH_3$) |
| $^{t}$Bu | tert-butyl (-$C(CH_3)_3$) |
| $CBr_4/PPh_3$ | Carbon tetrabromide/triphenyl phosphine mixture |
| CORE | 1,1,1-tris(4'hydroxyphenyl) ethane |
| Cp | cyclopentadienyl ($\eta$-$C_5H_5$) |
| Cp* | pentamethylcyclopentadienyl ($\eta$-$C_5Me_5$) |
| [Co] | cobaloxime |
| CSD | Cambridge structural database |
| CV | cyclic voltammetry |
| dppm | bis(diphenylphosphino) methane |
| DSC | Differential Scanning calorimetry |
| EI | electron impact |
| Equiv | equivalent |
| Fp | $CpFe(CO)_2$- |
| Fp* | $Cp^*Fe(CO)_2$- |
| Fp acyl | $CpFe(CO)(PPh_3)\{C(O)\}$- |
| FAB-MS | fast atom bombardment mass spectrometry |
| FT-IR | fourier transform infra-red |
| $M^+$ | parent molecular ion |
| Me | methyl (-$CH_3$) |
| MS | mass spectrometry |
| NMR | nuclear magnetic resonance |
| PAMAM | poly(amidoamine) |
| PEG | poly(ethylene) glycol |
| Ph | phenyl (-$C_6H_5$) |
| Py | pyridine (-$C_5H_5N$) |
| R.T. | room temperature |
| SEC | size exclusion chromatography |
| TBAP | tetrabutylammonium perchlorate |
| THF | tetrahydrofuran |

| | | |
|---|---|---|
| TLC | thin layer chromatography | |
| TGA | Thermogravimetric analysis | |
| TOS | time on stream | |
| NMR | s | singlet |
| | d | doublet |
| | t | triplet |
| | m | unresolved multiplet |
| | br | broad |

An example of the terminology used in the experimental section for a dendritic benzyl alcohol:

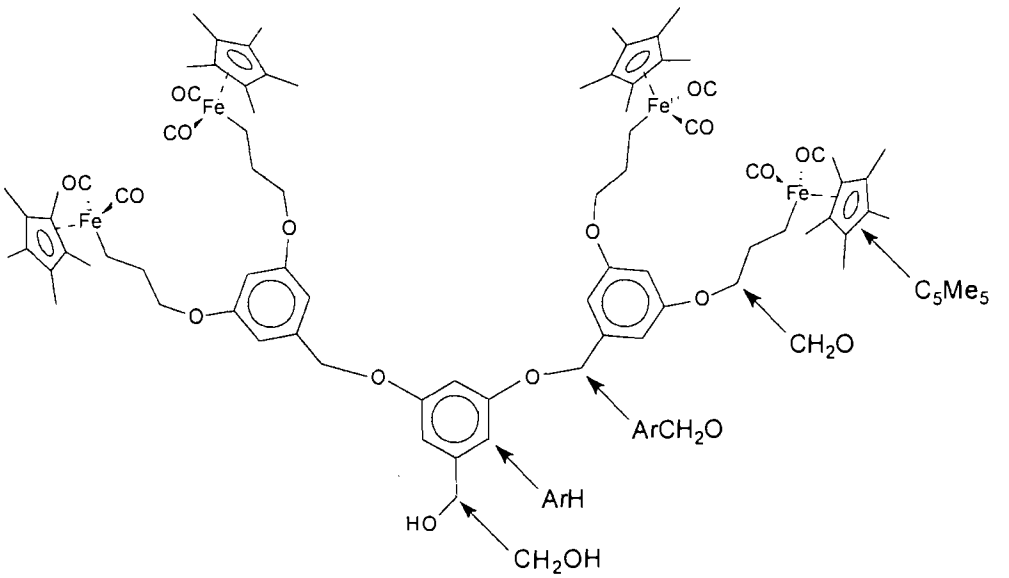

## TABLE OF CONTENTS

# Chapter 1

# A review on dendrimers

Biological macromolecules such as DNA and proteins have existed in nature for thousands of years, whereas the history of synthetic polymers is relatively short.[1] Nature has the ability to manipulate and control the structure of molecules in three dimensions. Collagens and enzymes are some of the best-known examples of three-dimensional polymers in which their synthesis is controlled to give a molecular architecture with a specific and highly efficient function. Staudinger's discovery of random coil polymers 60 years ago, represented the first of four major architectural classes of macromolecules (Figure 1.1).[1] In the last ten years there has been an explosion in activity in the area of three-dimensional molecules and supramolecular chemistry.[2-5]

The rising demand for materials with improved and novel properties has now switched the emphasis in polymer research from traditional linear polymers (Class I) to a new class of materials with highly controlled molecular architectures (Class IV).[1]

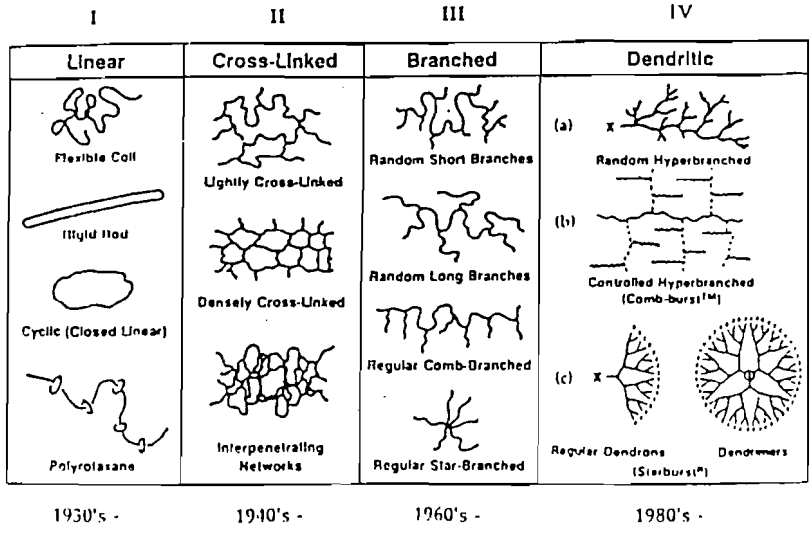


**Figure 1.1** Four major macromolecular architectures (Classes I-IV).[1]

This new family of highly branched three-dimensional molecules, termed dendrimers, arborols or starburst polymers has sparked significant interest because the molecular architectures involved are so different from traditional linear polymers. Numerous articles, on these polymers including many reviews, have been published in recent years.[6-13]

Dendrimers resemble trees in growth, structure and appearance, and, just as there are spaces between the branches of a tree, there are also spaces within the molecular structure. The word 'dendrimer' is derived from a combination of the Greek '*dendron*' (tree) and oligo*mer*.[1b] 'Arborol' is derived from the Latin for tree.[13] Dendritic macromolecules are characterised by repeating layers or 'generations' of building blocks (B) which radiate from a central core (C).[14] The surface groups (S) contain functional groups which are used to increase the branching until an almost globular shape with a dense surface is reached (Figure 1.2).

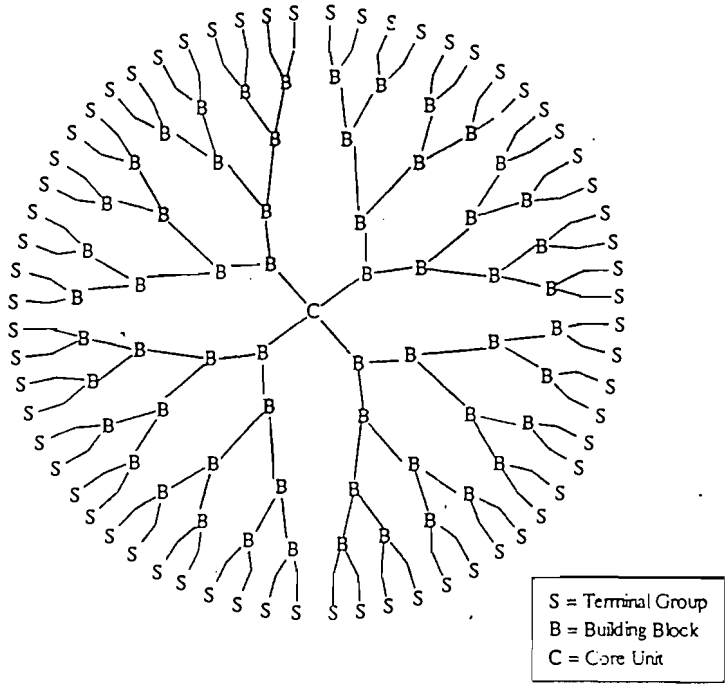


**Figure 1.2** Schematic representation of a dendritic macromolecule.[2]

A closely related class of materials, comprising hyperbranched macromolecules, are also highly branched, but differ from dendrimers in that they have a less regular structure and often contain a number of structural defects and missing branches.[13]

The development of dendrimers took place very slowly until the 1980's. In the 1940's, Flory[14] published a series of papers providing theoretical and experimental evidence for the formation of branched-chain, three-dimensional macromolecules. Vögtle and co-workers[15] reported the first cascade-like synthesis of branched polyamines in 1978, using a stepwise repetitive procedure of consecutive Michael-type addition-reduction steps (Scheme 1.1). Denkelwalter[16] subsequently synthesised polylysine macromolecules; however, the molecules contained some defects. By 1985 two synthetic groups, headed by Tomalia[17] and Newkome,[18] published their synthetic strategies towards cascade synthesis. Each group used different building blocks and strategies, but they both sought to find a systematic construction for the preparation of high molecular weight symmetrically branched molecules. Tomalia[17] worked on polyamidoamine (PAMAM) macromolecules, while Newkome[18] reported the synthesis of arborols possessing terminal hydroxyl moieties.

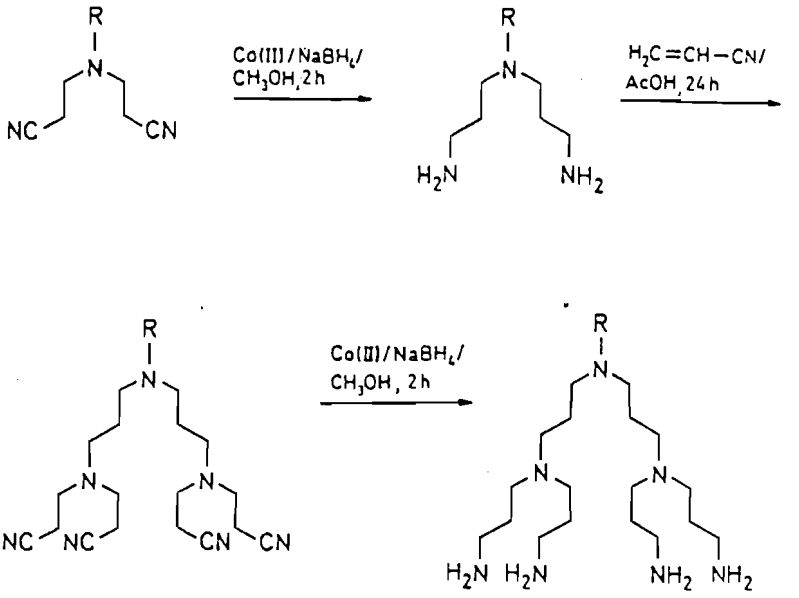


**Scheme 1.1**

Today, many structural classes of dendrimers are known, including dendritic polyethers,[19] polyamides,[20] polyols,[21] polyphenylenes[22] and poly(crownethers)[23] (for example Figure 1.3). Tomalia's PAMAM dendrimers[17] and Meijer's poly(propylenimine) dendrimers[24] are now even commercially available.

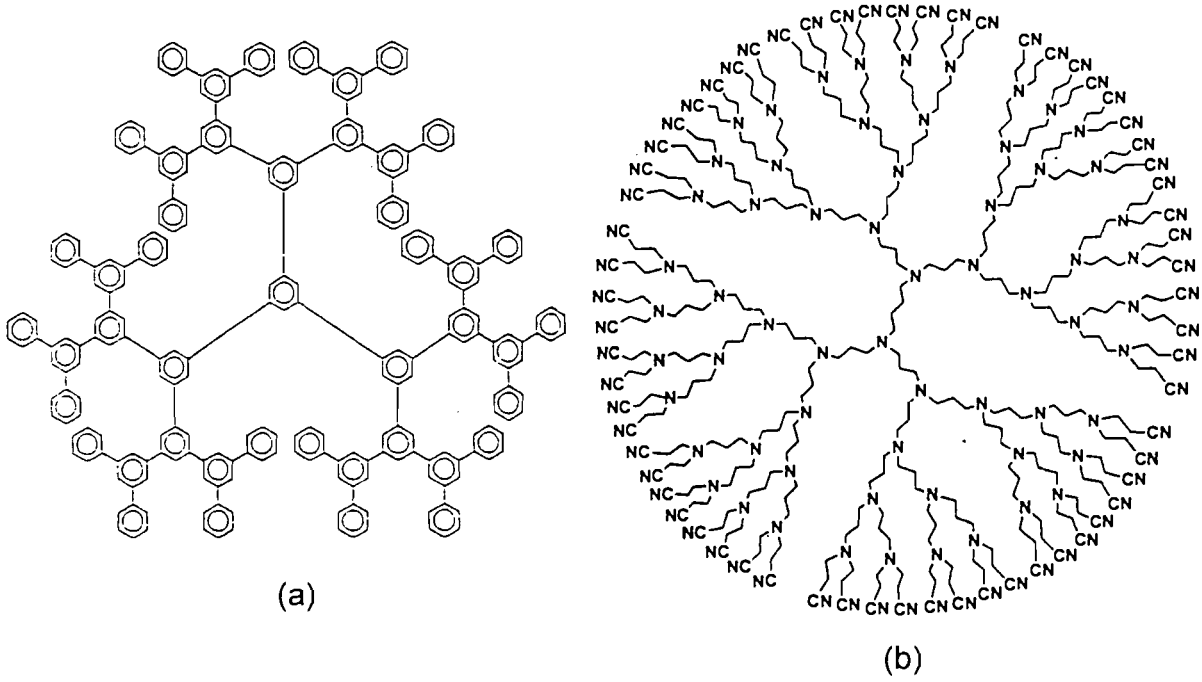


**Figure 1.3** (a) Polyphenylene[22] and (b) poly(propylenimine)[24] dendrimers.

## 1.1 Synthetic strategies

The distinguishing requirement of dendrimer synthesis is the ability to synthesise very high molecular weight polymers with narrow molecular weight distributions in a controlled manner. Two fundamentally different strategies have developed for the synthesis of dendritic macromolecules, with each method having its own advantages and disadvantages. In the divergent or starburst approach, independently pioneered by Tomalia[17] and Newkome,[18] growth of the dendrimer begins at the central core and proceeds radially outward via a two-step process (Scheme 1.2).

The first step is reaction of the core molecule with a monomer unit which contains at least two protected branching sites. The second step involves deprotection of the introduced branching sites which regenerates the reactive chain ends to give the next generation dendritic macromolecule. Repetition of this two-step process leads to larger and larger dendrimers.

The diverse chemistry of silicon offers many reactions that are suitable for the construction of dendrimers, and many carbosilane, carbosiloxane and silane dendrimers have been described. Roovers[25] and Van der Made[26] independently

reported a series of carbosilane dendrimers using different synthetic methodologies.

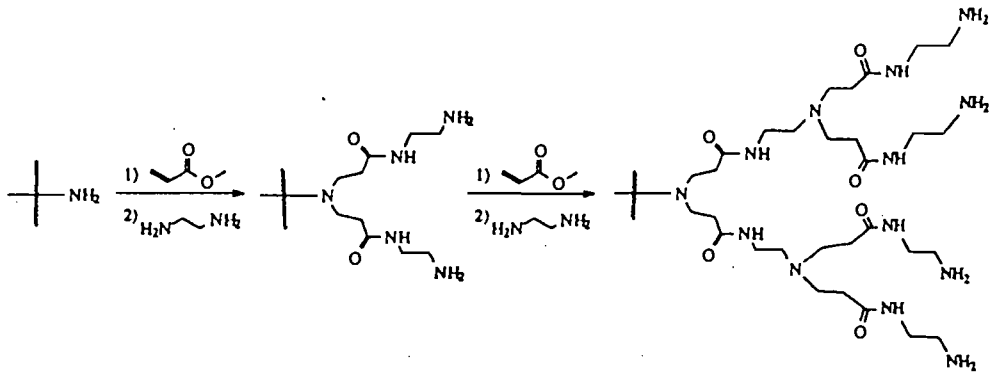

**Scheme 1.2**

Roovers[25] synthesised carbosilane dendrimers via repetitive Pt-catalysed additions of dichloromethylsilane to an alkene (Scheme 1.3).[25b] Van der Made,[26] however, prepared dendritic silanes up to the fifth generation, starting from tetraallylsilane and using repetitive alkenylation-hydrosilylation cycles. Many other groups have subsequently used silicon frameworks to anchor a variety of functional groups to the surface; an example in seen in Seyferth's[27] water-soluble carbosilane dendrimers.

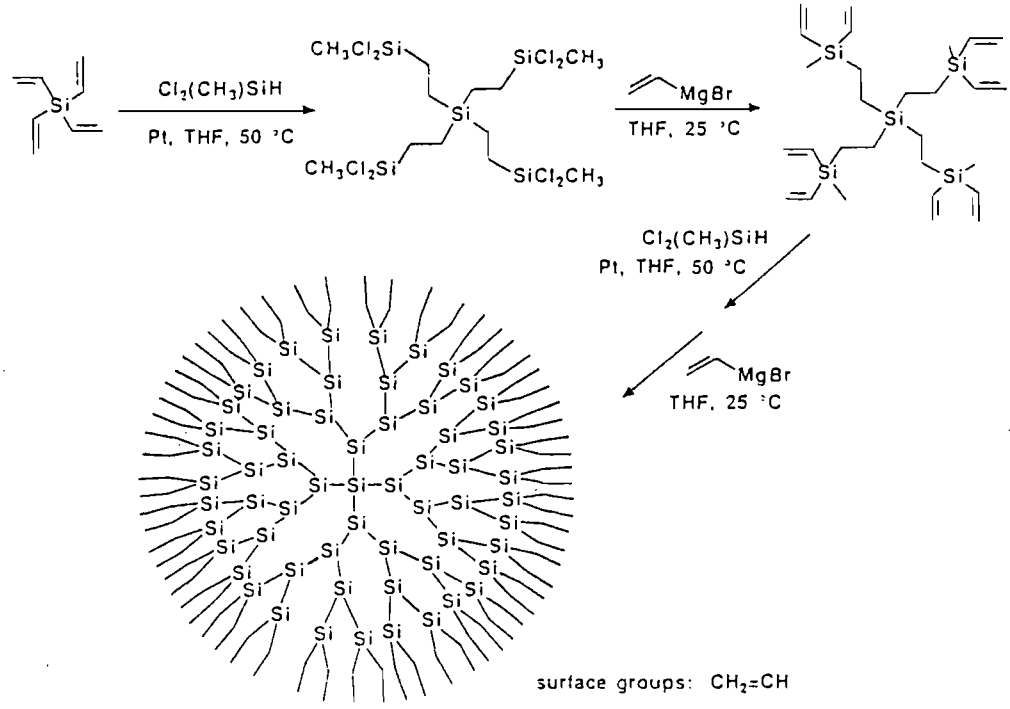


**Scheme 1.3**

A characteristic feature of this starburst approach is that the probability of defects in the structure increases as the dendrimer becomes larger. In the synthesis of higher generation dendrimers, large excesses of reagent are required to achieve ideally branched dendrimers, but this usually makes purification difficult. It also becomes difficult to detect defects spectroscopically once the dendrimers grow larger; therefore the reactions should proceed in high yield and side reactions must be minimised and controlled.

A few years later, in 1990, a second method was developed to try to overcome some of the difficulties associated with the starburst approach. This second method, termed the convergent approach, was independently reported by Fréchet[28] and Miller,[29] can provide extremely accurate control over molecular architecture (Scheme 1.4).[14] Fréchet and co-workers have since reported an accelerated synthesis of dendritic macromolecules through the use of 'hypermonomers', which are more highly branched monomers.[28c]

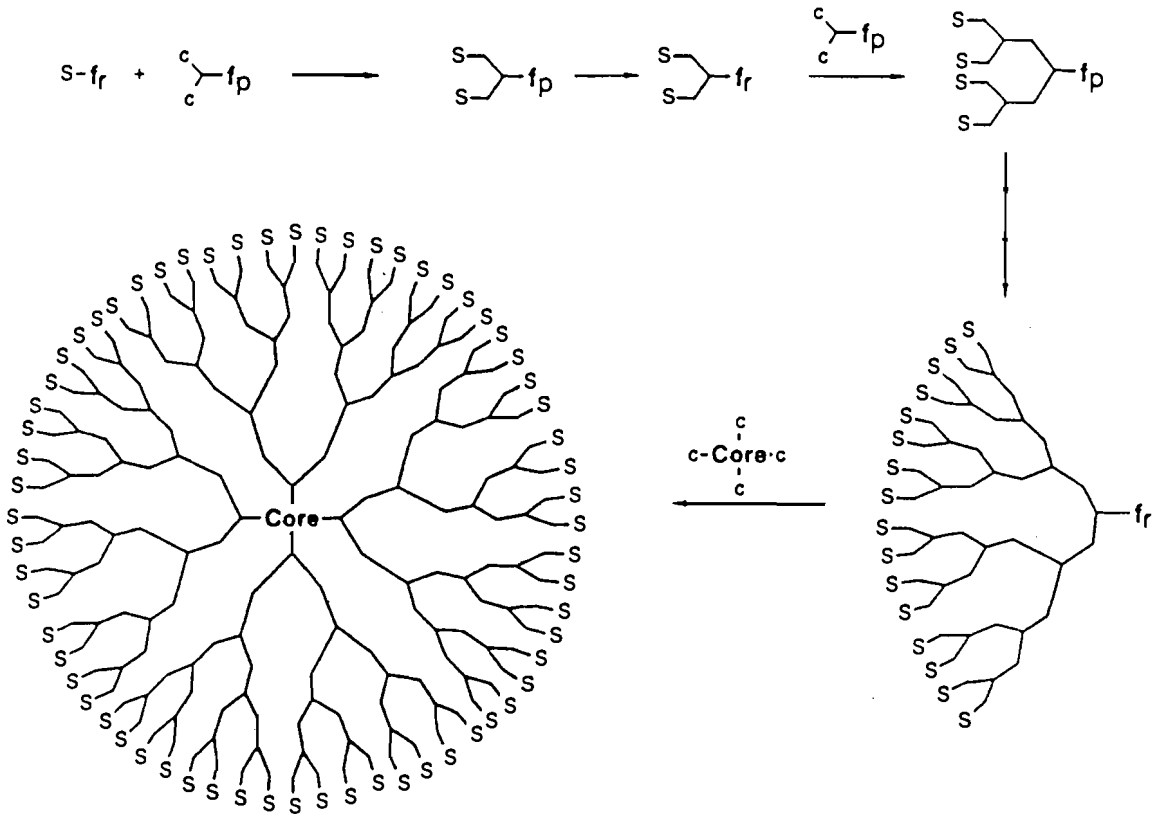


Scheme 1.4

This process works in the reverse way to the divergent approach in that synthesis is begun at the periphery of the molecule (S), and proceeds inwards. Activation of the focal point ($f_p$) regenerates the reactive functional group ($f_r$) that can again be coupled with the monomer unit. Repetition of this two step process results in an increase in the number of layers of monomer units, and hence generation number, and leads to larger and larger dendritic fragments. The final reaction step involves attachment of a dendritic wedge to a polyfunctional core. In this approach simultaneous additions at a progressively larger number of sites are avoided which allows greater control over the final macromolecular architecture. The early work of Hawker and Fréchet[28e] focussed on the convergent synthesis of a series of functionalised polyether macromolecules, such as this water-soluble polyarylether dendrimer with 32 carboxylate surface groups (Figure 1.4).[28]

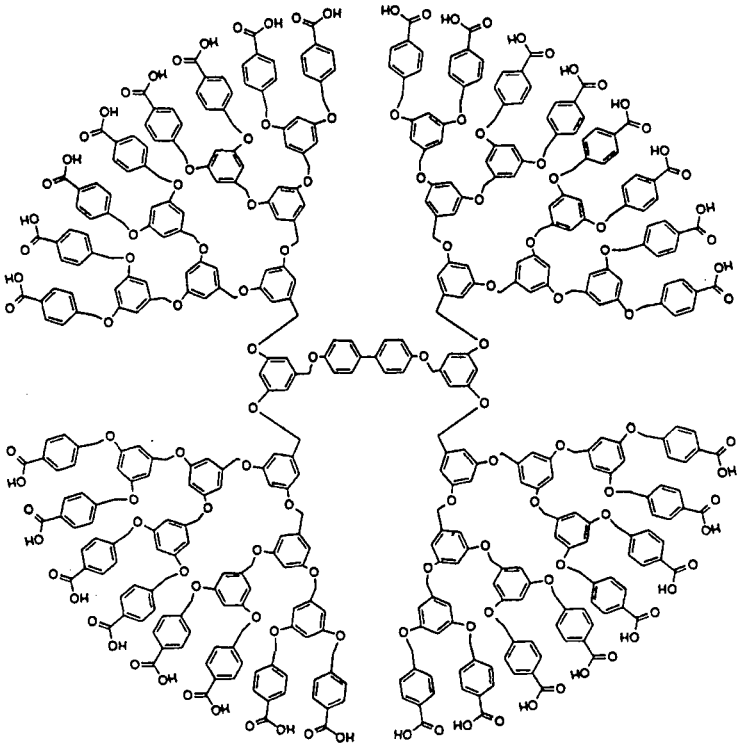

**Figure 1.4** Hawker and Fréchet's polyayrlether water-soluble macromolecule.[28e]

Miller and Neenan[29] reported a convergent synthesis of hydrocarbon-based dendrimers using 1,3,5-trisubstituted benzene and later, polyaryl molecular trees based on Pd-catalyzed aryl-aryl coupling. Moore[30] has succeeded in designing 'molecular antennae' which can funnel electrons to the focal point of the molecule (Figure 1.5).

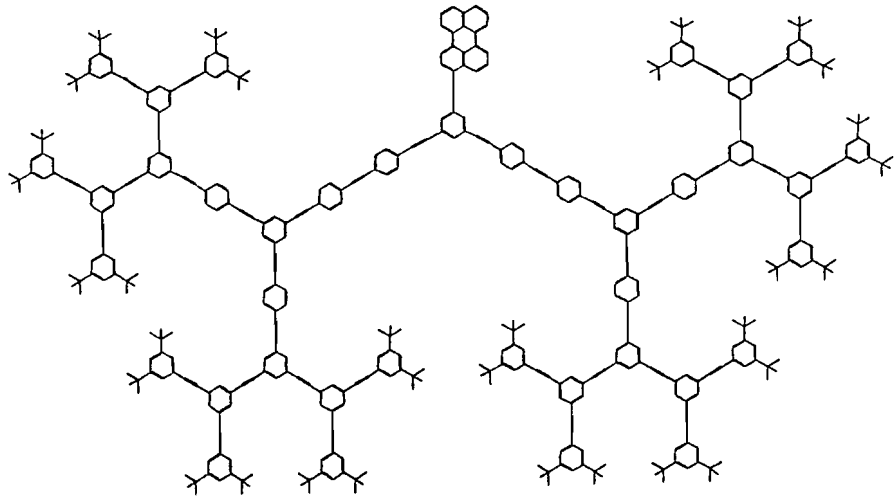

**Figure 1.5** Moore's dendritic molecular antennae.[30]

The convergent approach has several advantages for the synthesis of lower molecular weight dendrimers, while the starburst approach is superior for the synthesis of dendrimers with molecular weights above 100 000 amu. In the convergent approach, there are a limited number of side reactions possible because of the small number of reaction steps involved, and large excesses of reagent are avoided. This allows the products to be purified by recrystallisation or flash chromatography. Reactions can be monitored by spectroscopic methods at each stage, thus avoiding defects later on.

The convergent approach offers a high degree of control over the placement of functional groups in the dendritic wedges; for this reason block copolymers can be synthesised. For example, Fréchet and co-workers[31] reported the synthesis of a novel class of AB and ABA block copolymers using a linear hydrophilic B block such as polyethylene glycol (PEG) or polyethylene oxide (PEO) and a spherical, hydrophobic A block dendritic polyether bromide (Figure 1.6).[31]

## 1.2 Dendrimers containing special functional groups

The functionalisation of dendritic macromolecules is now an important aspect of dendrimer synthesis and has received much attention. Engel and Rengan[32] synthesised a series of cascade molecules in which the core and branch points were ammonium or phosphonium ion sites. Newkome *et al.*[33] prepared carborane superclusters, the idea being to render boron clusters soluble in an aqueous environment for use in cancer treatment.

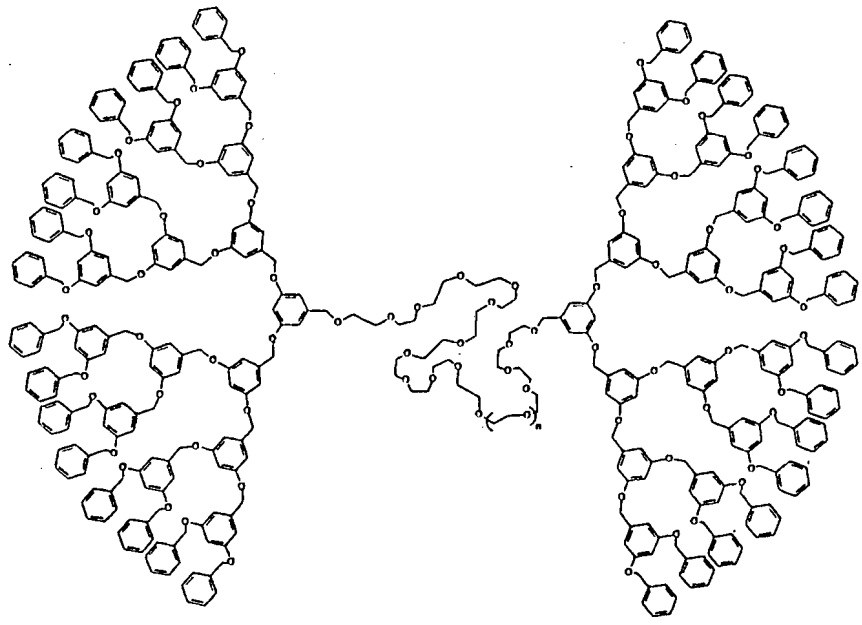

**Figure 1.6** An ABA block copolymer reported by Fréchet and co-workers.[31]

The structure and properties of dendritic micelles are important areas of research owing to the similarity of such micelles to natural systems. Studies have shown that dendritic micelles are capable not only of molecular inclusion but also of solubilising hydrophobic molecules in aqueous solutions.[34] Meijer and de Brabander-van den Berg's[35b] dendritic box elegantly demonstrates the potential of dendrimers as hosts for other molecules. The 64 end groups of a poly(propylene imine) dendrimer were reacted with protected amino groups, resulting in a chiral shell. Guest molecules such as Bengal Rose, a carboxylic acid dye, were encapsulated inside the box and could be selectively released (Figure 1.7).[35b] Dye-in-the-box systems might also be useful as fluorescent markers for pores in the nanometer range. Newkome and co-workers[35c] have succeeded in preparing 'unimolecular micelles' with a completely hydrophobic (alkane) interior.

Liquid crystal properties for dendrimers were first reported by Friberg in 1988.[36] Percec and coworkers[37] synthesised a novel class of thermotropic liquid-crystalline polymers possessing tertiary carbon-branching centres. The formation of a nematic phase suggested that in such cases even higher generation dendrimers should not exhibit a spherical or disc shape (Figure 1.8).[37]

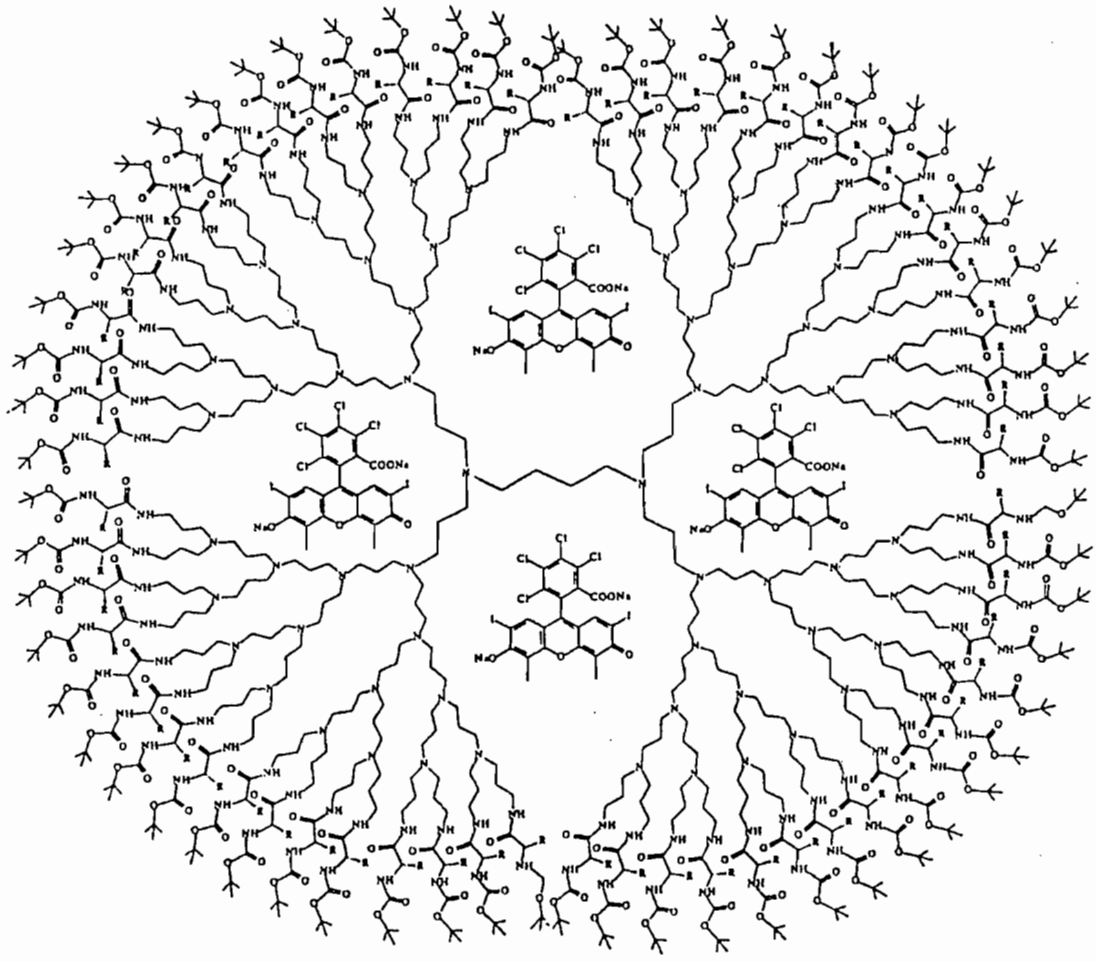

**Figure 1.7** Meijer and de Brabander's 'dendritic box' with encapsulated Bengal Rose molecules.[35a]

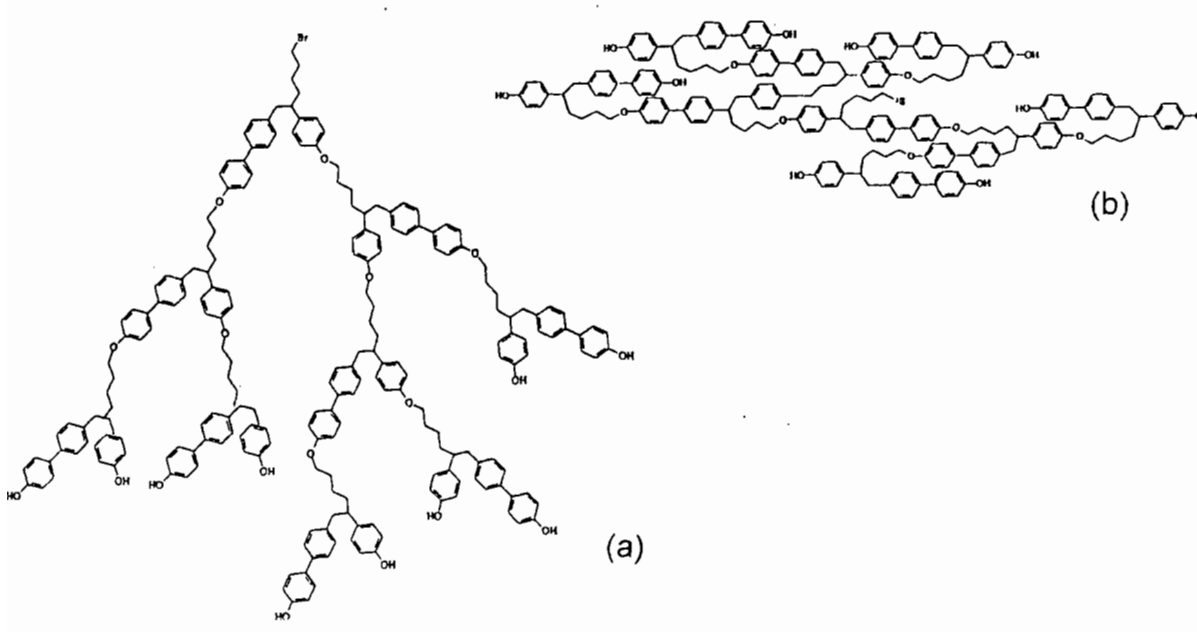


**Figure 1.8** A hyperbranched liquid-crystalline dendrimer:[37]
(a) isotropic state (b) nematic state.

Chirality can also be incorporated into dendrimers. Chow and Mak's [38] interest lies in the use of chiral dendrimers in chiral resolution and recognition. They have synthesised and characterised some optically active, homochiral, monodispersed dendrimers, in which the chiral unit was derived from optically active tartaric acid. Preliminary investigation of the optical rotation of these compounds revealed that the molar rotation was proportional to the number of tartrate units.

Togni and co-workers[39] have prepared a series of chiral organometallic dendrimers for use in asymmetric catalysis, an area of research still in its infancy. Chiral ferrocenyl ligands have shown proven efficiency in a number of asymmetric catalytic reactions, and incorporation of the Josiphos ligand into dendritic structures has resulted in a multisite ligand system that allows highly enantioselective rhodium-catalysed hydrogenation of dimethyl itaconate in methanol (Figure 1.9).

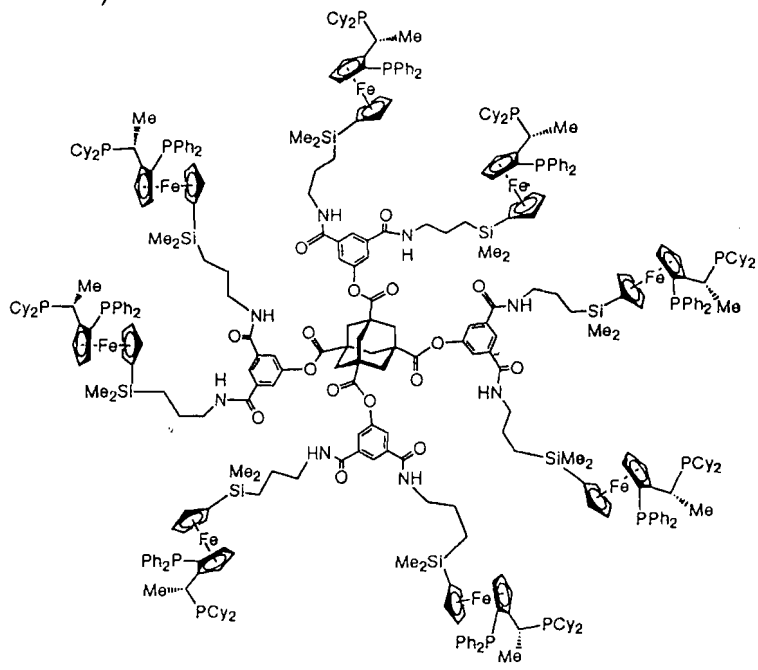

**Figure 1.9** a catalytically active chiral dendrimer.[39]

The use of dendrimers in self-assembly processes is another area of current interest. Zimmerman and co-workers[40] have used a hydrogen bond-mediated self-assembly process as a tool for generating large structures from smaller subunits. Hydrogen-bonded carboxylic acid dimers were linked to the core of a polyether dendrimer, which resulted in the dimers self-assembling to form cyclic hexamers.[40] Huck *et al.*,[41] on the other hand, used a building block containing

two coordinatively unsaturated palladium centres that were capable of self-assembly. Light scattering experiments were used to show how the nature of the building block affected the size of the self-assembled hyperbranched sphere.[41]

### 1.3 Inorganic and organometallic dendrimers

The preparation of dendritic macromolecules has not been limited to those purely organic in nature and many groups have now reported the synthesis of dendrimers containing inorganic and organometallic fragments. Some important and representative examples are highlighted here.

A vast amount of work on phosphorus-containing dendrimers has been produced by Majoral's group over the last few years.[42] To date, they have produced the largest phosphorus-containing dendrimers built (up to the 10th generation) and possessing either aldehyde groups or phosphorus–chlorine bonds on the surface.[42d] The reactive terminal phosphino groups allow the surface of the dendrimer to be complexed to transition metals such as Fe, Ru, Pd, Pt and Rh, with the hope of producing new and interesting catalysts (Figure 1.10).[42e,f]

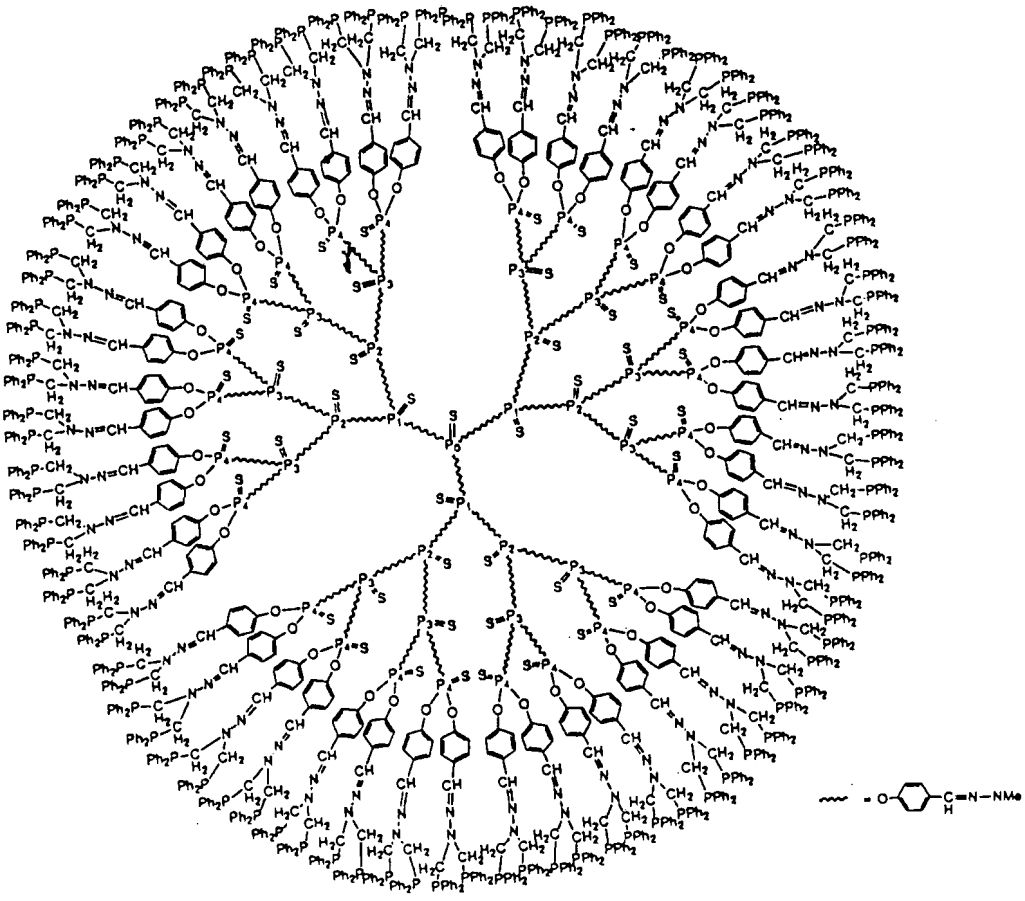

**Figure 1.10** Schematic drawing of a fourth generation phosphorus dendrimer.[42b]

There are many advantages to including a transition metal either at the core or at the periphery of a dendrimer. The first inorganic transition-metal molecular trees were designed by Balzani and co-workers,[43] who developed a versatile synthetic strategy leading to luminescent and redox-active dendrimers (Scheme 1.5). Ru(II) and Os(II) polypyridine complexes are well known for their luminescent properties. The synthesis was based on a divergent construction with the metal ion (ruthenium or osmium) acting as a key link and branching point. These compounds could be used as electrochemical molecular devices and antennae for harvesting light fo solar energy conversion because they strongly absorb visible light.[43]

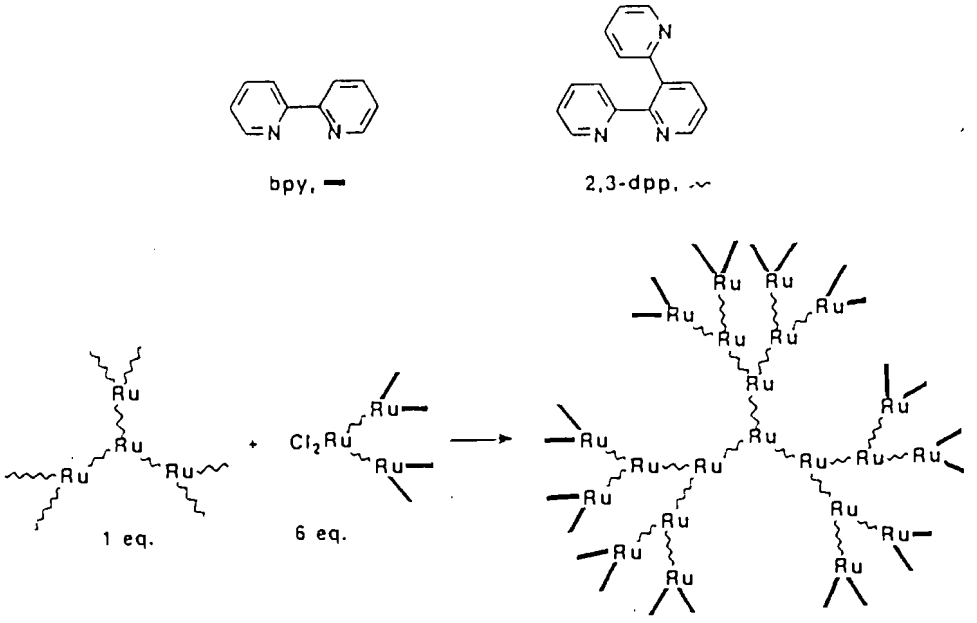


**Scheme 1.5**

The groups of Newkome[44] and Constable[45] have also prepared highly branched metallomacromolecules based on terpyridine ligands. Preconstructed cores were assembled and the dendritic fragments were linked by $Ru^{2+}$ ions. Their approach, using the coordination properties of appropriate ligands to multiply bind metals provides a useful alternative to carbon-carbon or carbon-heteroatom bond formation for the assembly of dendrimers (Figure 1.11).[44b]

Liao and Moss,[46] on the other hand, prepared large organometallic dendrimers containing metal-carbon σ-bonds up to the fourth generation with $CpRu(CO)_2$ moieties positioned exclusively on the periphery of the molecule.

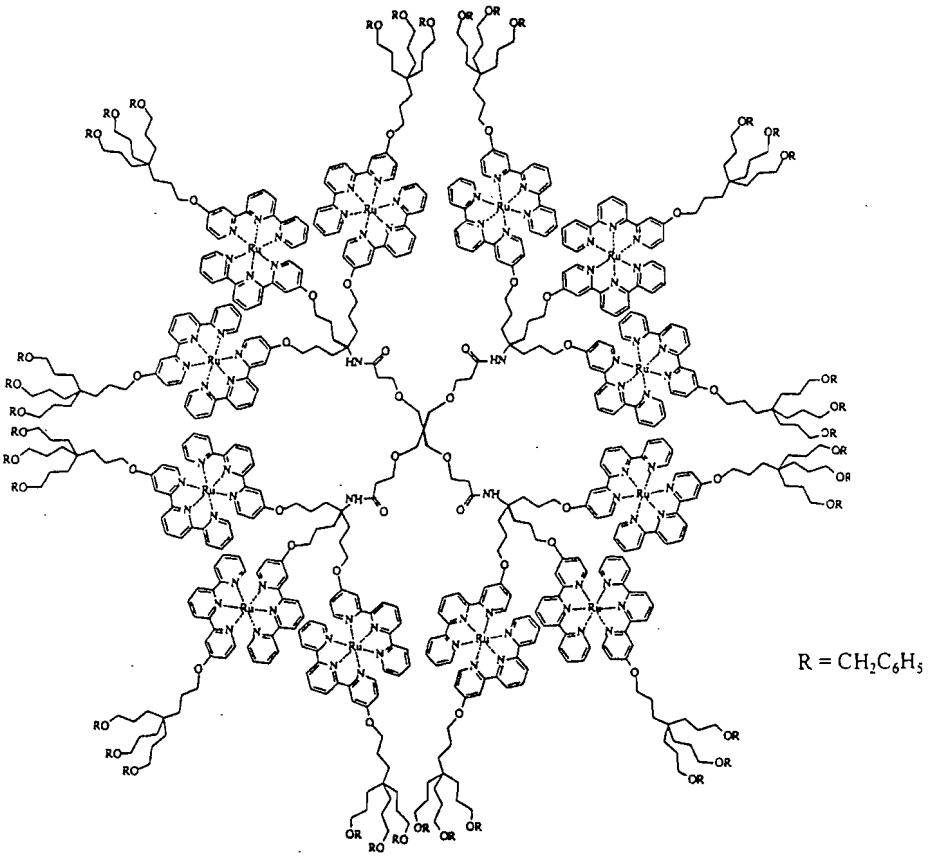


**Figure 1.11** Newkome's dodeca-ruthenium dendrimer.[44]

Many ferrocene-containing dendrimers have been prepared due to the stability of the ferrocene entity and the ease with which it can be functionalised. Cuadrado and co-workers have shown that silicon[47a,b] and amine-based[47c,d] dendrimers with surface functionalities can be built up in a logical and step-wise fashion by this method. The ferrocene moieties behave as electronically isolated units, and the dendritic molecules undergo a simultaneous multielectron transfer at the same potential. These are the first organometallic dendritic molecules displaying electronic interactions between transition-metal atoms in the dendritic structure (Figure 1.12a).[47a] Cuadrado's group has also used silicon-based dendrimers to position $CpFe(CO)_2$ groups and $\eta^6$-coordinated $Cr(CO)_3$ moieties at the periphery of the dendrimers.[47e] Astruc and co-workers[48], in a series of papers, have described how they have elegantly built up multimetallic compounds also containing ferrocene groups at the surface. They used $FeCp^+$ as a core for the synthesis of hexa- and hepta-iron sandwich complexes.[48a] These star-shaped molecules have independent redox-centres and are excellent

candidates for multielectron redox catalysis.[48a,b] Recently, they synthesised amido-ferrocene dendrimers which were found to be useful for the recognition of small anions (Figure 1.12b).[48d]

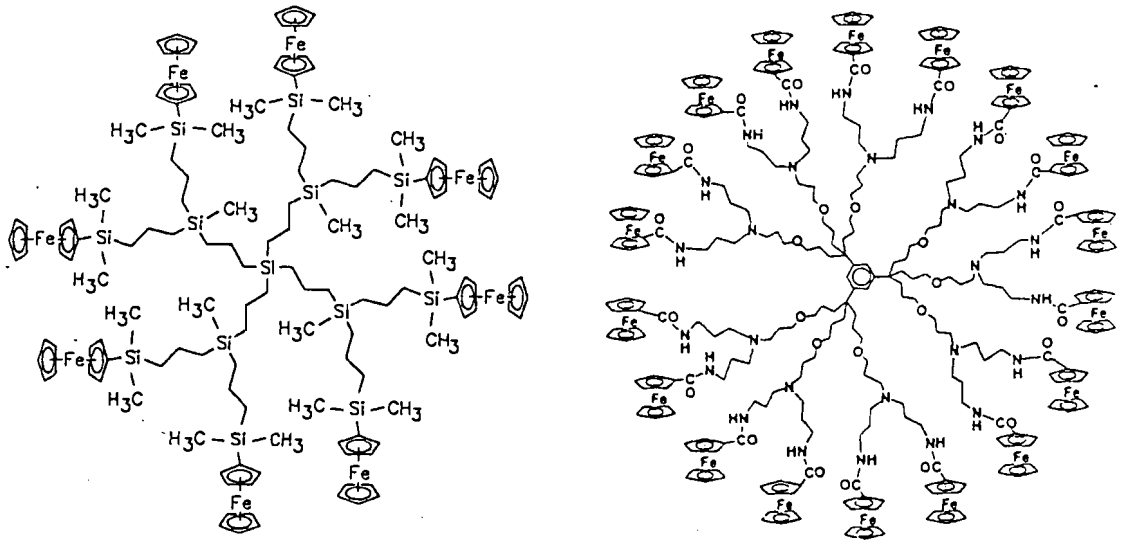

**Figure 1.12** (a) A ferrocene-terminated silicon dendrimer[47a] and (b) Astruc's polyamido ferrocene dendrimer.[48d]

Gorman[49] has prepared an encapsulated electroactive molecule in which the dendrimer acts as an insulating coating around an electroactive iron-sulfur core. These compounds can contribute to understanding biological electron transfer processes.

The incorporation of platinum and palladium into dendritic structures has been achieved by a number of workers.[50-52] Achar and Puddephatt[50] successfully used oxidative-addition reactions of Pt(II) to Pt(IV) to build up large alkyl-platinum dendrimers, containing up to 28 platinum atoms.[50c] The $Pt_{12}$ complex is shown in Figure 1.13. Huck *et al.*[51] used building blocks containing a labile coordinating cyano group and two kinetically inert bis(thioether) palladium complexes for the controlled assembly of palladium-based metallodendrimers. The introduction of transition metal ions such as Ni(II) and Pt(II) was made possible by use of a PCP rather than a SCS 'pincer' ligand[51a] (Figure 1.14). Heterobimetallic dendrimers containing Pt(IV) units arranged in a concentric fashion around a central organic moiety with ferrocenyl groups directed towards the periphery of the molecule have also been prepared.[52]

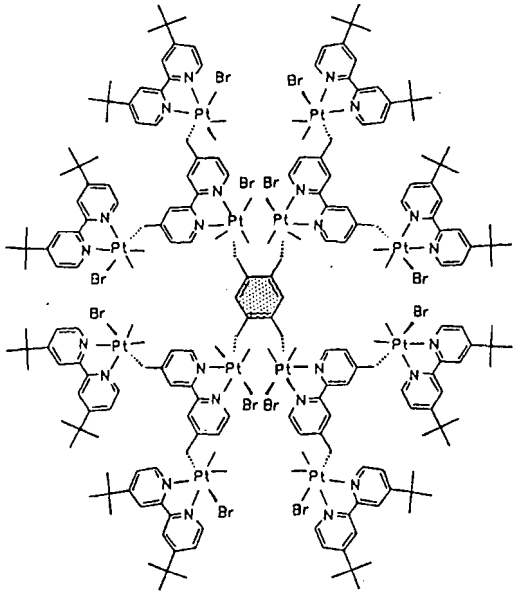

**Figure 1.13** Puddephatt's $Pt_{12}$ dendrimer.[50c]

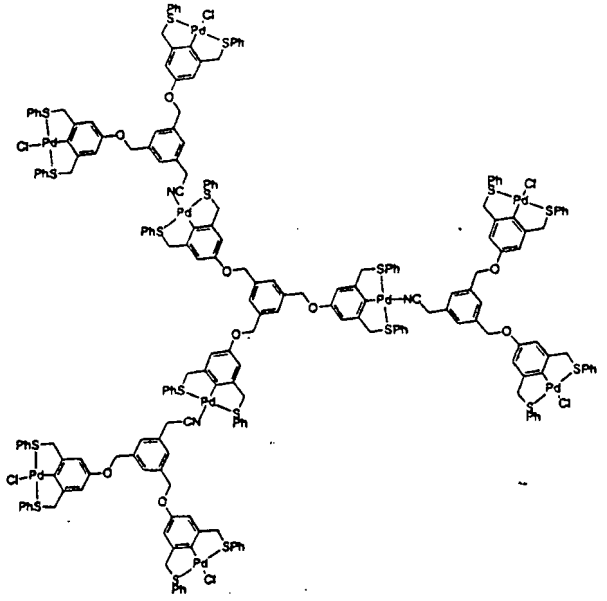

**Figure 1.14** Huck's palladium-based dendrimer.[51]

## 1.4 Structural features and physical properties of dendrimers

One of the driving forces in the study of these highly branched macromolecules has been the belief that these new materials will have fundamentally different properties when compared with traditional linear polymers.[17] Traditional linear polymers are characterised by a random coil structure with only two chain ends. At high molecular weights, the chain ends are negligible and the physical properties are dominated by chain entanglements and the presence or absence of functional groups attached to the polymer backbone. Dendrimers, on the other hand, have a dense globular structure, so should avoid some of these chain entanglements.

Several groups have done computations on model dendrimers using Monte Carlo methods or molecular dynamics simulations.[57] The first studies (on PAMAM dendrimers) by de Gennes and Hervet[58] showed the chain ends to be on the periphery, and density to be minimum at the core, maximum at the surface. Computational studies on the PAMAM dendrimers by Naylor *et al.*[59] indicated that, above the fourth generation, dendrimers adopt a globular structure with large hollow cavities inside, suggesting the possibility of binding or entrapment

of small molecules in the interior. These studies also suggested an elecron-density minimum at the centre of the dendrimer.[59] Lescanec and Muthukumar,[57a] however allowed for the inward folding of chain ends in their calculations, which resulted in the prediction of a density maximum between the core and the periphery. Investigations by Naidoo and co-workers[60] on Fréchet type poly(benzylphenyl ether) dendrimers functionalised with arene tricarbonylchromium(0) groups showed a transition from an extended to a globular structure as the generation number increased. Although chain ends were found in all regions of the dendrimer to some extent, most were still located on the periphery of the molecule or in a solvent-accessible area for those dendrimers studied.

Generally speaking, lower generation dendrimers tend to exist in relatively open forms, but as successive layers are added, the dendrimers adopt a spherical three-dimensional structure. There is, of course, a point at which steric congestion will prevent further growth of the dendrimer. This is called the starburst limit generation, beyond which polymer branching can no longer take place in an ideal fashion and defects start to develop.[57] For example, it has been shown that an ideally branched polyethylenimine dendrimer can only grow to the fourth generation, but ideally branched polyamidoamine dendrimers have been reported up to the ninth generation.[8]

For classical polymers, such as polystyrene, there is a linear relationship between the logarithms of molecular weight and intrinsic viscosity. The viscosity increases sharply with molecular weight according to the Mark-Houwink-Sakurada equation:[61]

$[\eta] = KM^a$ in which $[\eta]$ is the intrinsic viscosity of the polymer
M is its molecular weight (i)
K and *a* are constants for a given polymer

This relationship does not hold for dendrimers and other macromolecules once a threshold molecular weight is reached. This can be explained by the fact that the volume of a dendrimer increases cubically, whereas the mass increases exponentially during generation growth.[61] This behaviour is demonstrated graphically in Figure 1.15.

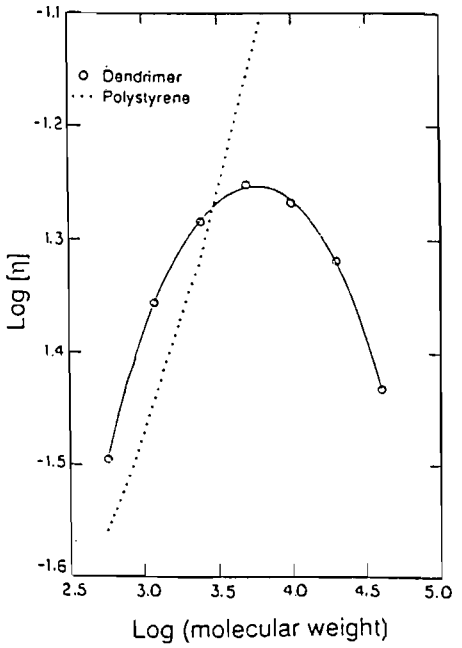


**Figure 1.15** Plot of log [η] vs log[mol. weight] for dendritic polyether macromolecules based on 3,5-dihydroxybenzyl alcohol.[61]

Dendrimers also differ from linear poymers in terms of their solubility. For example, for dendritic polyphenylenes, solubility enhancements of more than 100 000 times when compared with their mononuclear analogues have been reported.[61] This confirms that the shape as well as the functionality of the molecule, has a great effect on the molecular interactions and other parameters that control solubility and miscibility.

In contrast to the solution properties described above, the thermal properties (such as the glass transition temperature, $T_g$ and degradation) of dendrimers and functionally analogous linear polymers are similar. The glass transition temperature is an important characteristic of a polymeric material. Fréchet and co-workers.[62] have reported a comprehensive study on the glass transition temperatures of some dendritic polyethers and polyesters. The variation of glass transition temperature with molecular weight and chain-end composition follows a modified version of the chain-end free volume theory[62] after taking into account the large number of chain ends. The glass transition was found to be greatly affected by the polarity of the chain ends and internal monomer units, and $T_g$ was found to increase as the molecular weight increased, which is generally found for polymers.[62] Other properties, such as melt viscosity, chemical reactivity and intrinsic viscosity, were found to be dependent on the macromolecular architecture.[17]

## 1.5 Characterisation

The characterisation of these large, highly branched molecules has challenged classical methods of analysis. New spectroscopic techniques developed in the last few years, such as electrospray,[63] FAB and MALDI TOF mass spectrometries have given scientists a much better idea of the regularity of dendrimer structure and have started to convince those previously in doubt. A combination of spectroscopic and chromatographic techniques is generally used to characterise a dendrimer fully.

The high symmetry and monodispersity of dendrimers in theory allows their characterisation to be accurately determined. The detection of failed sequences is very important as these well affect the physical properties of the dendrimer. NMR spectroscopy,[64] especially $^{13}C$ NMR, has proved to be particularly useful since the highly ordered and symmetrical branching sequence allows small changes in the focal-point group, terminal groups and interior building blocks to be readily observed. The dendrimer generation can be confirmed by comparison of the focal-point group resonance integration with that of other resonances. Chromatographic techniques such as TLC and HPLC can also be used to monitor reactions in progress.

Size exclusion chromatography is particularly useful with dendrimers synthesised by the convergent approach since their molecular weight basically doubles at each generation step. A comparison of size exclusion chromatography traces for a narrow molecular weight polystyrene standard and a dendritic macromolecule of comparable elution time is shown in Figure 1.16.[28a] It is found that the traces for dendritic macromolecules have much narrower peak widths, which is consistent with their monodispersed nature. Dendrimers themselves are now replacing polystyrenes as calibration standards to eliminate the effects of the differences in character between the two types of molecules.[65]

In general, due to their high molecular weight, dendrimers have been difficult to crystallise and so only a few single-crystal structures have been determined. Kriesel *et al.* [66] recently reported the synthesis and X-ray structure of a first-generation, ruthenium polycationic dendrimer. Other chemical techniques such as infrared spectroscopy and elemental microanalysis offer little structural information since the various functionalities involved at different stages of

growth are quickly overwhelmed by the bulk of the dendritic macromolecule and the sensitivities of the techniques do not allow these small differences to be accurately observed.

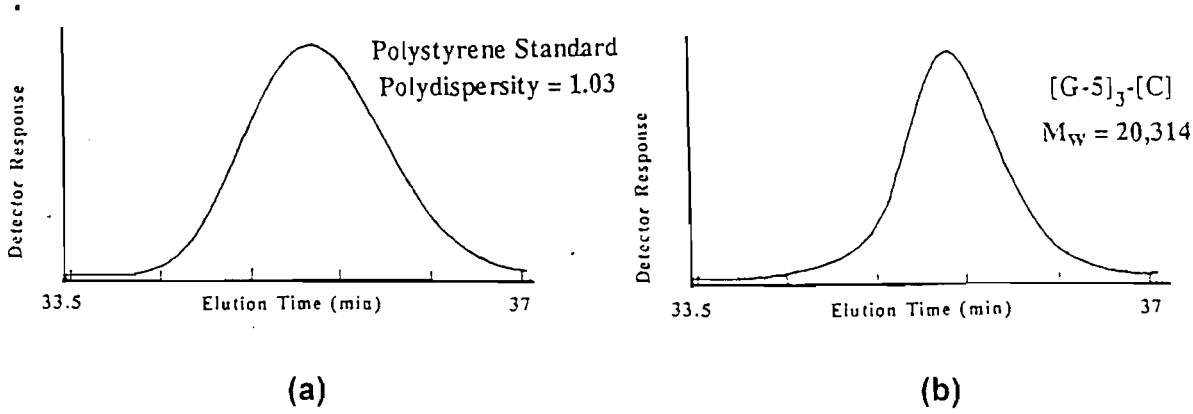


**Figure 1.16** Comparison of size exclusion chromatography traces for (a) a narrow molecular weight polystyrene standard and (b) a dendritic macromolecule of comparable elution time.[65]

## 1.6 Applications of dendrimers

Over the last decade, dendrimers have emerged as a new class of aesthetically appealing and synthetically challenging macromolecules. Indeed, much of the early work focussed on the synthetic aspect, using a diverse array of building blocks. Attention has now shifted towards the properties and applications of these molecules. The potential applications of these exciting molecules are abundant and include the use of dendrimers as micelles,[67] as hosts for biologically important guests,[8] as thin films precursors[68] and as electro- and photo-active materials[69] (Scheme 1.6).[9]

Molecular trees also have potential uses as hosts for the transport of biologically important materials. For example, a novel drug delivery system is given by a layer block dendrimer with surface functional groups that make the polymer water soluble, ester linkages that make it biodegradable and inner layers built of a drug and so designed that upon degradation, a uniform supply of the drug is delivered.[8]

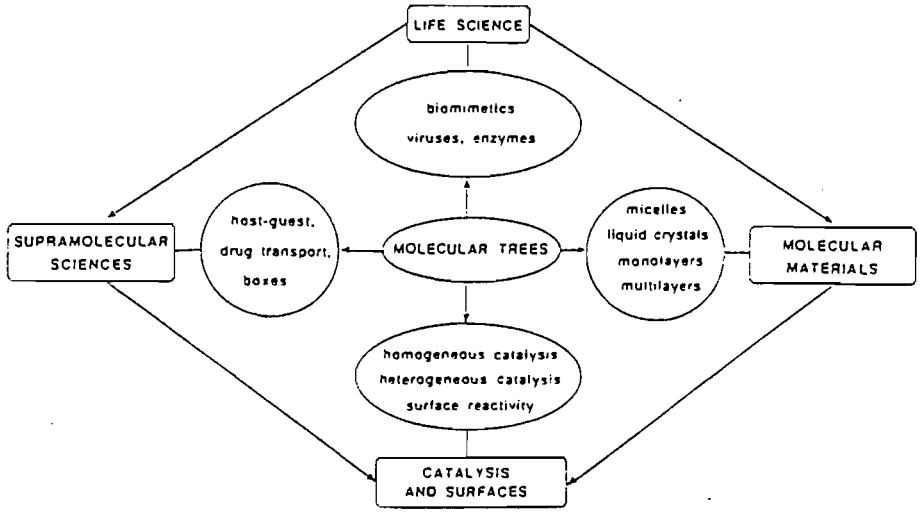


**Scheme 1.6**

The use of metal-containing dendrimers in catalysis is perhaps one of the most exciting applications of these molecules. An ideal polymeric catalyst should be a soluble, multifunctional macromolecule favouring configurations in which all active sites would always be exposed in the reaction mixture. There is great scope for combining the benefits of homogeneous catalysts, such as faster kinetics and accessibility of metal sites, with the ease of separation of heterogeneous catalysts. One approach is to anchor homogeneous catalysts to polymer supports. Dendrimeric catalysts are expected to retain the benefits of homogeneous catalysts owing to their spherical nature but should be easily recoverable from a product-containing solution because of their large size. Membrane filtration has been used for this purpose.[70]

One of the first examples of a dendritic catalyst was provided by van Koten and co-workers[71] Both the zero and first-generation polysilane dendrimers were functionalised with 4 and 12 catalytically active aryldiaminonickel(II) centres on the periphery respectively. The dendrimers (e.g. Figure 1.17) were successfully employed as homogeneous catalysts for the Karasch addition reaction of polyhalogenated alkanes to C=C double bonds.[71] Although the dendrimers exhibited slightly lower reactivity compared with the mono-nickel complexes, the regiospecificity was improved.

DuBois and co-workers[72] reported the synthesis of phosphorus-based dendrimers terminated with palladium complexes. Small dendrimers containing 12 or 15 phosphorus atoms metallated with $[Pd(MeCN)_4][BF_4]_2$ (Figure 1.18) have been shown to exhibit catalytic activity for the electrochemical reduction of $CO_2$. The phosphine-terminated dendrimers synthesised by Reetz *et al.*[73] which were complexed with transition metals such as iridium, palladium and rhodium, were successfully used to catalyse the Heck reaction of bromobenzene and styrene to form stilbene.

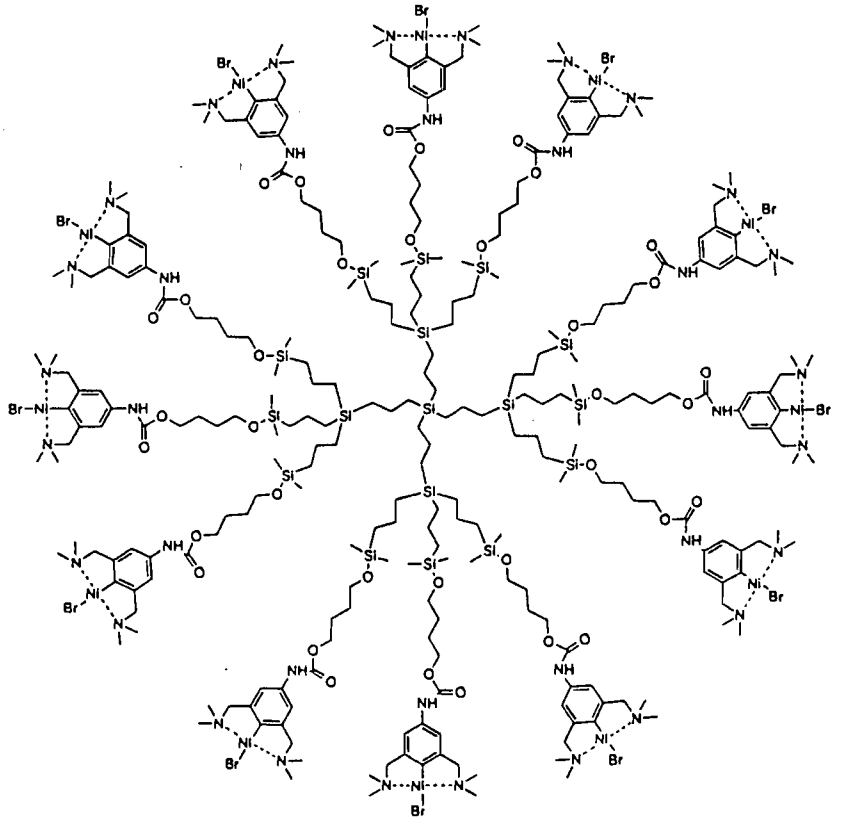

**Figure 1.17** The catalytically active carbosilane dendrimer.[71]

Brunner[74] has designed a class of expanded ligands for enantioselective transition-metal catalysis. The ligands consist of a chelating phosphine core surrounded by several layers of branching units built up with optically active groups. The catalytic reaction takes place at the core of the dendrimer and so the system resembles the prosthetic group of an enzyme, hence the term 'dendrizyme' (Figure 1.19).

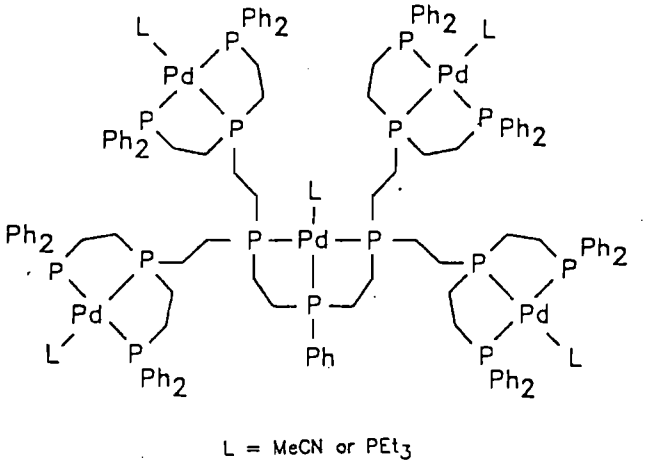


**Figure 1.18** A phosphorus-palladium dendrimer[73] (anions not shown).

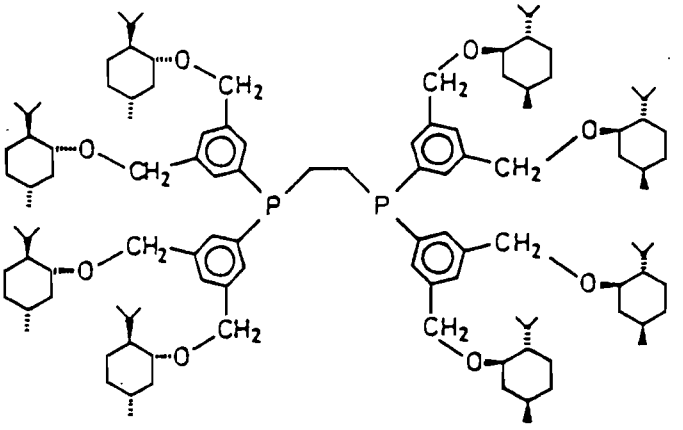

**Figure 1.19** Brunner's expanded ligand for enantioselective catalysis.[74]

Recently, Chow and Mak[75] reported the use of a bis(oxazoline)copper(II) dendrimer complex to catalyse a Diels-Alder reaction, while Moore, Suslick and co-workers[76] noted a similar increase in substrate selectivity in the epoxidation of olefins catalysed by manganese-porphyrindendrimers.

Another area of dendrimer applications is in the field of electronics. Miller's group[77] has added electronically active functionalities to the outer branches of PAMAM dendrimers in the hope of engineering a new class of three-dimensional conducting polymers that may have unique electrical properties.

The study of dendritic macromolecules has progressed rapidly in recent years. Their novel architecture promised many interesting properties and applications and many have been unveiled. However, a more in-depth study of these unique materials is needed to exploit their potential fully. In conclusion, this new class of dendritic compounds has opened new horizons in synthetic chemistry and hopefully this will lead to generations of new materials, both organic and inorganic.

# Chapter 2

# Synthesis, characterisation and reactivity studies on iron-containing organometallic dendrimers

## 2.1 Introduction

**The metal and ligand system**

Iron is the least expensive and most abundant of the transition metals; for this reason the chemistry of this element has been widely investigated.[78] Many organometallic iron complexes have been described in the literature and these are usually classified according to the hapticity of the ligand.[78] These include $\eta^1$ $\sigma$-alkyls, acyls, hydrides, $\eta^2$ cationic and neutral complexes, $\eta^1$ and $\eta^3$ allyl complexes, $\eta^4$ diene, $\eta^5$ complexes such as ferrocene and $\eta^6$ arene complexes.[79]

The chemistry of cyclopentadienyl (Cp) transition metal complexes has developed into an important area of organometallic chemistry since the discovery of ferrocene[80] in 1952.[81] Substitution of hydrogen by methyl groups in the Cp ligand has a great effect on the chemistry of the resulting transition metal complexes, as compared with that of the unsubstituted cyclopentadienyl analogues, due to both steric and electronic effects. Pentamethylcyclopentadienyl (Cp*) transition metal complexes are generally more soluble, tend to exhibit different crystallisation properties, show different kinetic and thermodynamic stabilities and have different reactivities towards reagents as compared with the corresponding Cp analogues.[82] The Cp ring is bonded to a transition metal in an $\eta^5$ manner, the $\eta^5$ bond being composed of:

(i) a $\sigma$- bond resulting from the donation of an electron pair from the filled orbital of the Cp ring to the empty d-orbital of the transition metal;

(ii) two orthogonal $\pi$ bonds resulting from the donation of an electron pair from each of the

bonding orbitals of the Cp ring into empty transition metal d-orbitals;

(iii) two δ- bonds resulting from the back donation of electron density from the transition metal d-orbitals into the two degenerate anti-bonding orbitals of the Cp ring.[81]

The substitution of all the hydrogen atoms on the Cp ring with methyl groups is expected to strengthen the bonds between the ring and a transition metal as a result of the increased electron density in the filled orbitals. The electron releasing effects of the methyl substituents on the Cp* ring increase the electron density on the transition metal and thus the bond between the transition metal and other ligands is strengthened. This was indeed true in the case of the $CpFe(CO)_2$- (Fp) and $Cp^*Fe(CO)_2$- (Fp*) dendrimers where the Fp* dendrimers were found to be significantly more stable than the Fp analogues.

Moss and co-workers[83] have prepared several series of haloalkyl complexes of the type $[L_mM(CH_2)_nX]$ where $L_mM$ = transition metal and its associated ligands (*e.g.* $CpFe(CO)_2$-); X = halogen (*e.g.* Cl, Br, I). The length of the alkyl chain in the complexes $[Fp(CH_2)_nX]$ , (X = Br, I) was varied from n = 3 to n = 8. The analogous $[Fp^*(CH_2)_nX]$ complexes are yellow crystalline solids and were found to be much more stable in air than the Cp analogues, both in solution and in the solid state. The bromides were more stable in air than the corresponding iodides. The halopropyl complex was found to be the most stable and for this reason was chosen as the starting point for the dendrimer synthesis. The presence of carbonyl groups in the haloalkyl complexes makes IR spectroscopy ideal for monitoring the progress of reactions.

The haloalkyl metal complexes used as the starting materials for preparation of the dendrimers were synthesised by reduction of the dimers $[CpFe(CO)_2]_2$ and $[Cp^*Fe(CO)_2]_2$ using standard literature procedures (Scheme 2.1).[84] In most cases, a Na amalgam was used. The reduction of the Fp dimer proceeds readily at room temperature, whereas the reduction of the Fp* dimer under the same conditions is more difficult and requires stirring overnight. $Na[Cp^*Fe(CO)_2]$ is very susceptible to oxidation and care was taken to do the reduction in an oxygen-free environment. An alternative approach that we used to prepare NaFp and NaFp* involved the use of sodium sand and a Na/K alloy. The yields of the resulting complexes were 80 – 90% after work-up indicating that the reduction was quantitative.

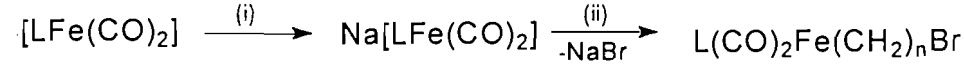


L = Cp, n = 3,6; L = Cp*, n = 3,5,7,11
(i) Na/K alloy, R.T. or Na/Hg, R.T.
(ii) $Br(CH_2)_nBr$ (n = 3,5,7,11)

| L | n | Cpd. no. |
|---|---|---|
| Cp | 3 | **1** |
| Cp | 6 | **2** |
| Cp* | 3 | **7** |
| Cp* | 7 | **8** |
| Cp* | 11 | **9** |

**Scheme 2.1**

The $[CpFe(CO)_2]_2$ and $[Cp^*Fe(CO)_2]_2$ dimers have been used as catalysts in reactions involving the replacement of ligands such as CO in transition metal complexes by Group 15 donor ligands. For example, the reaction of $[Mn_2(CO)_{10}]$ with triphenylphosphine goes to 80% completion in 90 and 180 minutes in the presence of $[CpFe(CO)_2]_2$ and $[Cp^*Fe(CO)_2]_2$ respectively. In the absence of these catalysts, the reaction would require either photochemical conditions or 7 hours for completion.[85] One of the aims of this project is to prepare dendrimers containing the $CpFe(CO)_2$- and $Cp^*Fe(CO)_2$- groups on the surface so that they could possibly be used as catalysts.

**Iron dendrimers in the literature**

The preparation of dendrimers containing metals, in particular transition metals, has received considerable attention in recent years. The incorporation of metals has resulted in compounds with potentially useful physical properties. Transition metals have been incorporated into dendrimers in all of the distinct parts of the dendrimer; in the repeating or branching unit, in the molecular core and on the periphery of the dendrimer.

To date, the majority of iron-containing dendrimers in the literature involve ferrocene. The main reasons for this are the high thermal stability of the ferrocene ligand and the ease with which the ligand can be functionalised. Two main groups have published most of the

literature in this field. Cuadrado[47] and co-workers have prepared several silicon and amine-based dendrimers with surface functionalities (Scheme 2.2). They showed that the ferrocenyl moieties behave as electronically isolated units and the dendritic molecules undergo a simultaneous multi-electron transfer at the same potential. A conspicious challenge is to construct well-defined dendrimers possessing redox-active organometallic units linked together in close proximity so that there could be electronic communication between the metal sites in the dendrimer.[47] Recently, Köllner and Togni[39] reported the preparation of dendritic ligands containing up to eight ferrocenyl diphosphines for use in asymmetric catalysis (see Chapter 1).

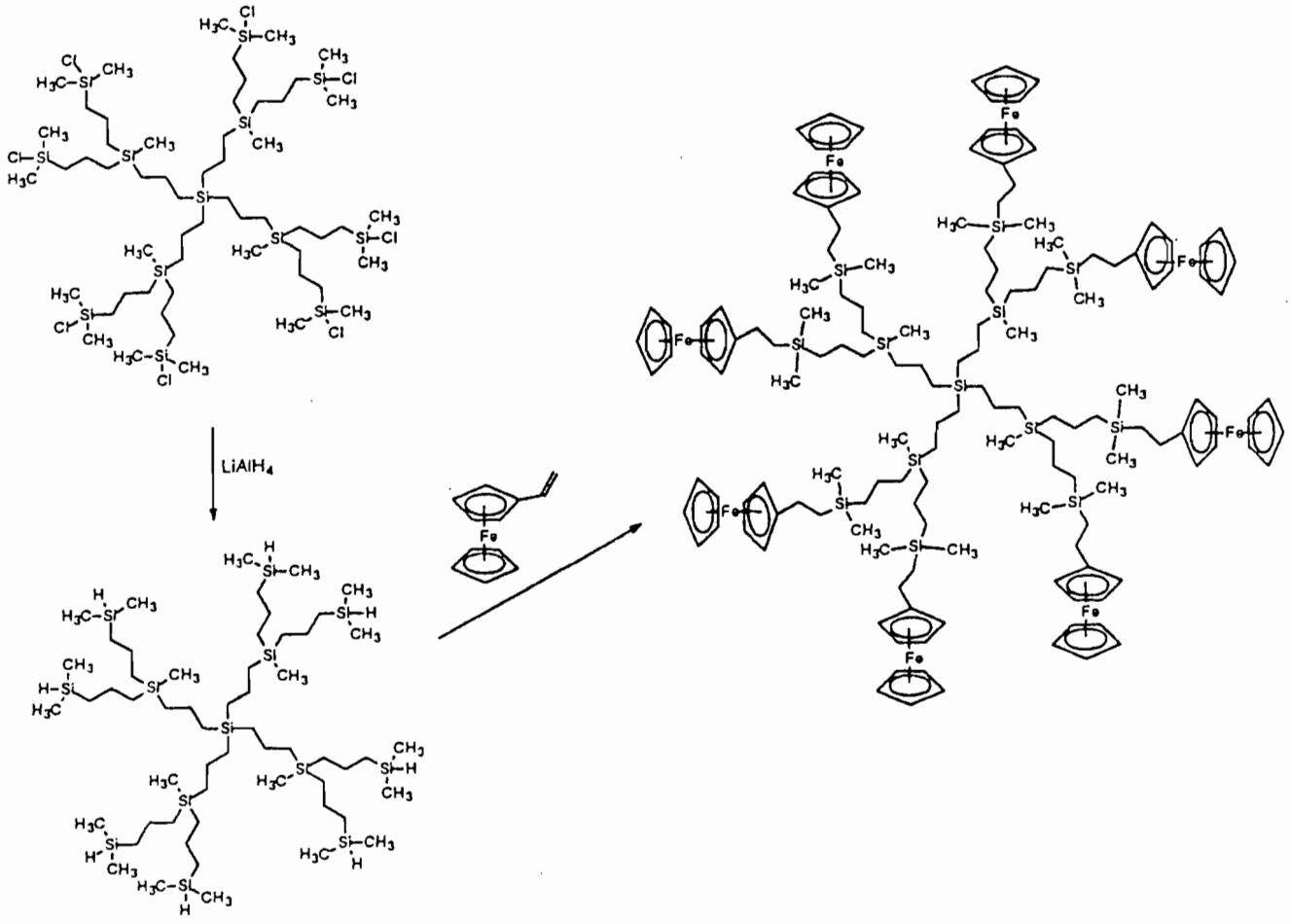


**Scheme 2.2**

**Dendrimer Notation**

A systematic nomenclature for dendrimers has been described.[86] The notation represented below will be used in the following four chapters of this thesis for all the dendrimers synthesised. The complexes are also numbered (in bold) throughout the text.

The general formula used is:

$Mn_1Gn_2X$ *e.g.* Fp3G1OH where

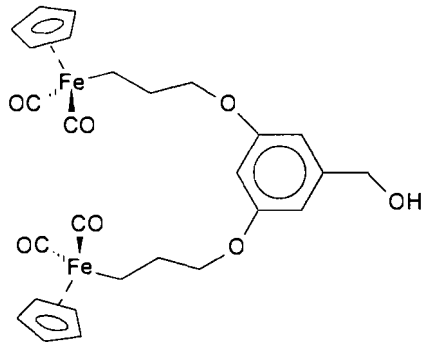


M: is the organometallic functional group on the periphery of the dendrimer
Fp = $CpFe(CO)_2$-, Fp* = $Cp^*Fe(CO)_2$- and Rp = $CpRu(CO)_2$- (Chapter III)

$n_1$: the length of the polymethylene chain, *i.e.* $n_1$ = 3 for $FpCH_2CH_2CH_2$-

G: this character represents the word 'generation'

$n_2$: the 'generation' number, *i.e.* the number of layers in the dendrimer

X: the functional group at the focal point of the dendrimer which could be:
OH or Br

The example above, Fp3G1OH would thus represent a first generation dendritic wedge with a benzyl alcohol functional group at the focal point. For a first generation wedge there would be two Fp groups on the periphery of the dendrimer. Fp6AG1OH would represent a first generation dendritic wedge containing two $Fp(CO)(PPh_3)\{C(O)\}(CH_2)_6$- groups.

The terminology $Mn_1Gn_2C$ is used to represent the attachment of the dendritic wedges to a chosen core molecule. 1,1,1-tris(4'-hydroxyphenyl)ethane was used as the core for most of the synthesis and is represented by CORE in the text.

**Proposed synthetic strategies**

Scheme 2.3 shows the convergent synthesis of poly(benzyl phenyl ether) dendrimers according to Hawker and Frechet.[28b] The synthesis begins at what will eventually be the periphery of the molecule and uses two repeating (coupling and activation) steps to build up the molecule to the desired size. The molecule goes through a "generation" of growth after each coupling occurs.[28b]

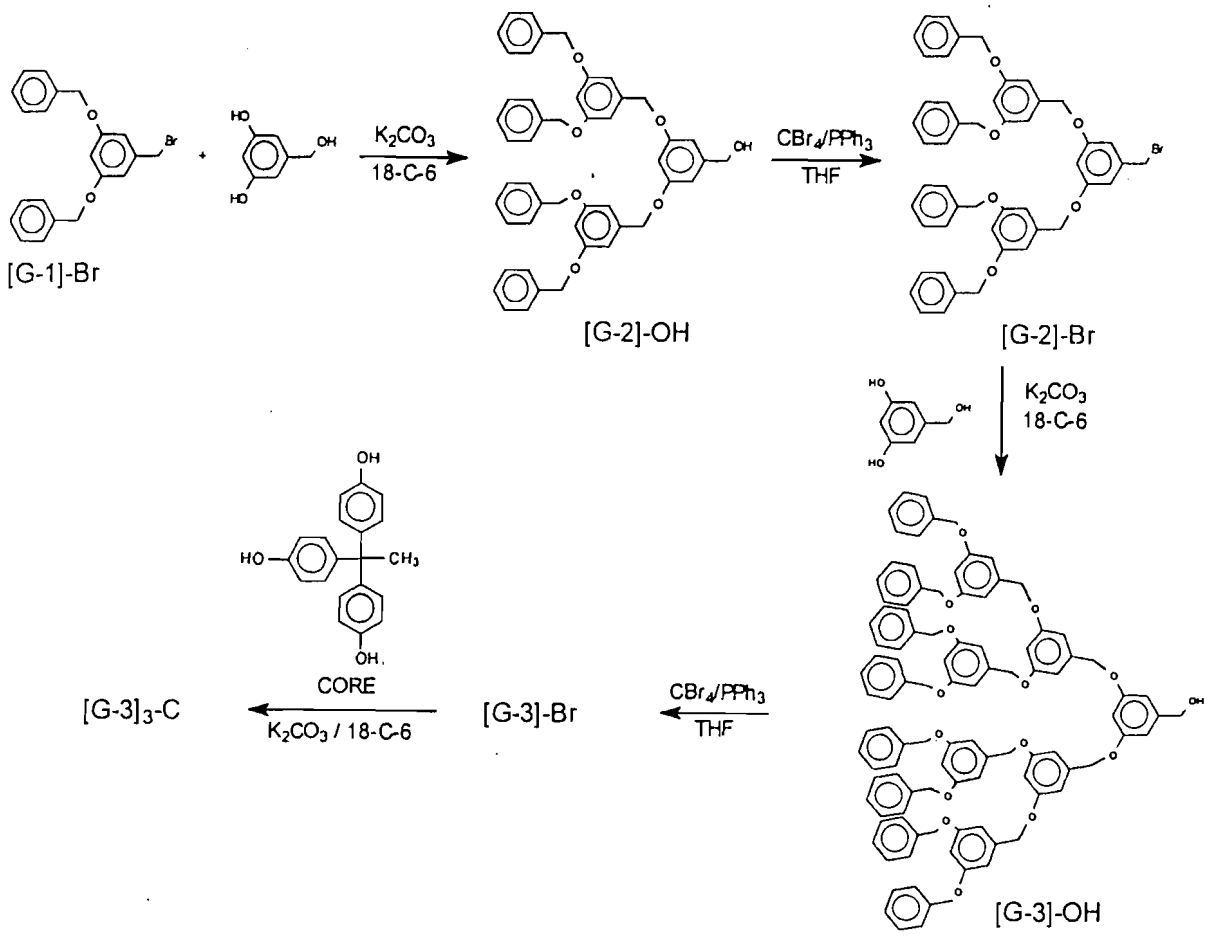


**Scheme 2.3**

In the first step, a benzyl halide is coupled to the branching monomer, in this case 3,5-dihydroxybenzyl alcohol to give a benzyl alcohol. The choice of branching monomer and methodology was based on the high yields that can be obtained for the formation of benzyl ethers from phenols and benzylic halides. The optimum reaction conditions for the coupling

were found to be potassium carbonate, with 18-crown-6 (18-C-6) in refluxing acetone. Potassium carbonate is a relatively weak base and only removes the more acidic phenolic hydrogens. This ensures that only the phenolic oxygens, and not the benzylic oxygen will react.

In the second step, the alcohol functionality is converted to a bromide. Several halogenating reagents were investigated and a carbon tetrabromide/triphenyl phosphine mixture was found to give the highest yields through all generations of growth. These coupling and activation steps can be repeated to build larger generation dendritic wedges. In the final step, the dendritic wedges are attached to a chosen core molecule. The convergent methodology is very adaptable and can be extended to include other branching monomers and coupling chemistries.

## 2.2 Synthesis and characterisation details of iron-containing dendrimers

In this chapter, we describe the synthesis of a series of new organoiron dendrimers. Liao and Moss[46] were the first to report the synthesis of organoruthenium dendrimers containing metal carbon σ-bonds. We aim to compare the physical and chemical properties of these iron- and ruthenium-containing dendrimers.

We have used the convergent methodology developed by Hawker and Fréchet[28] in our approach but have included a metal in the functionalised monomer. We have used bromo alkyl complexes of the type $[CpFe(CO)_2(CH_2)_nBr]$ (n = 3 or 6) , $[Cp^*Fe(CO)_2(CH_2)_nBr]$ ( n = 3 or 7 or 11) and $[CpFe(CO)(PPh_3)\{C(O)\}(CH_2)_6Br]$ as the functionalised monomers. It has been shown that these type of complexes are relatively inert and that reactions of haloalkyl complexes can be directed to the halo function.

The first step involves coupling of the haloalkyl complex with the branching monomer, in this case 3,5-dihydroxybenzyl alcohol, to give the first generation benzyl alcohol. In this way, the metal alkyl group becomes incorporated in the growing macromolecule.

**Activation methodologies and coupling reactions**

The solvent, reaction temperature and base were varied in order to try to optimise the reaction conditions. Acetone was found to be superior to THF and 1,4-dioxane as solvent. Potassium carbonate was preferred over cesium carbonate. The second reaction step

involves conversion of the alcohol functionality to a bromide functionality. Again, several brominating reagents can be used; these include a carbon tetrabromide/triphenyl phosphine mixture ($CBr_4/PPh_3$), phosphorus tribromide or n-bromosuccinimide. The carbon tetrabromide/triphenyl phosphine mixture was the halogenating agent of choice for the iron dendrimers as good yields were achieved with this reagent.

The core chosen for the majority of the reactions in this thesis was 1,1,1-tris(4'-hydroxyphenyl)ethane and the chemistry involved is similar to that used in the coupling steps. The convergent methodology was chosen as it allows accurate control over the number and placement of dendritic wedges on the core molecule. Reaction of some of the dendritic wedges with other core molecules is discussed in Sections 2.4.2 and 5.2.4.

### 2.2.1 The $CpFe(CO)_2(CH_2)_n$- system (n = 3 or 6)

The bromoalkyl iron complexes $CpFe(CO)_2(CH_2)_3Br$ **1** and $CpFe(CO)_2(CH_2)_6Br$ **2** were used as the functionalised monomers. Two molar equivalents of complex **1** or **2** were reacted with one molar equivalent of 3,5-dihydroxybenzyl alcohol in the presence of potassium carbonate and 18-crown-6 in refluxing acetone for two days (Scheme 2.4, shown for n = 3). The reaction was monitored by TLC eluting with a 70% $CH_2Cl_2$/hexane solution. The resulting benzyl alcohols **3** and **4** were purified by column chromatography. Yields of 40% and 32% respectively were obtained. Significant decomposition of the reaction mixture occurred after 2 days. Vigorous stirring throughout the reaction and light protection was necessary to optimise the product yields. Complexes **3** and **4** (*i.e.* Fp3G1OH and Fp6G1OH) are the first generation benzyl alcohols and were characterised by IR, $^1H$ and $^{13}C$ NMR and mass spectrometry. Both compounds were isolated as yellow oils and are moderately air and thermally stable. Attempts to improve the yields by increasing the temperature and changing the solvent were not successful and only resulted in more decomposition products.

Conversion of **3** and **4** to the corresponding benzyl bromides **5** and **6** was accomplished using $CBr_4/PPh_3$ in a minimum volume of THF (Scheme 2.4). The reaction, which is generally complete in 20 - 30 minutes, and was monitored by TLC eluting with 30% $CH_2Cl_2$/hexane solution. A large excess of $CBr_4/PPh_3$ is usually needed in order to achieve complete conversion, and the volume of THF used also affects the reaction outcome.

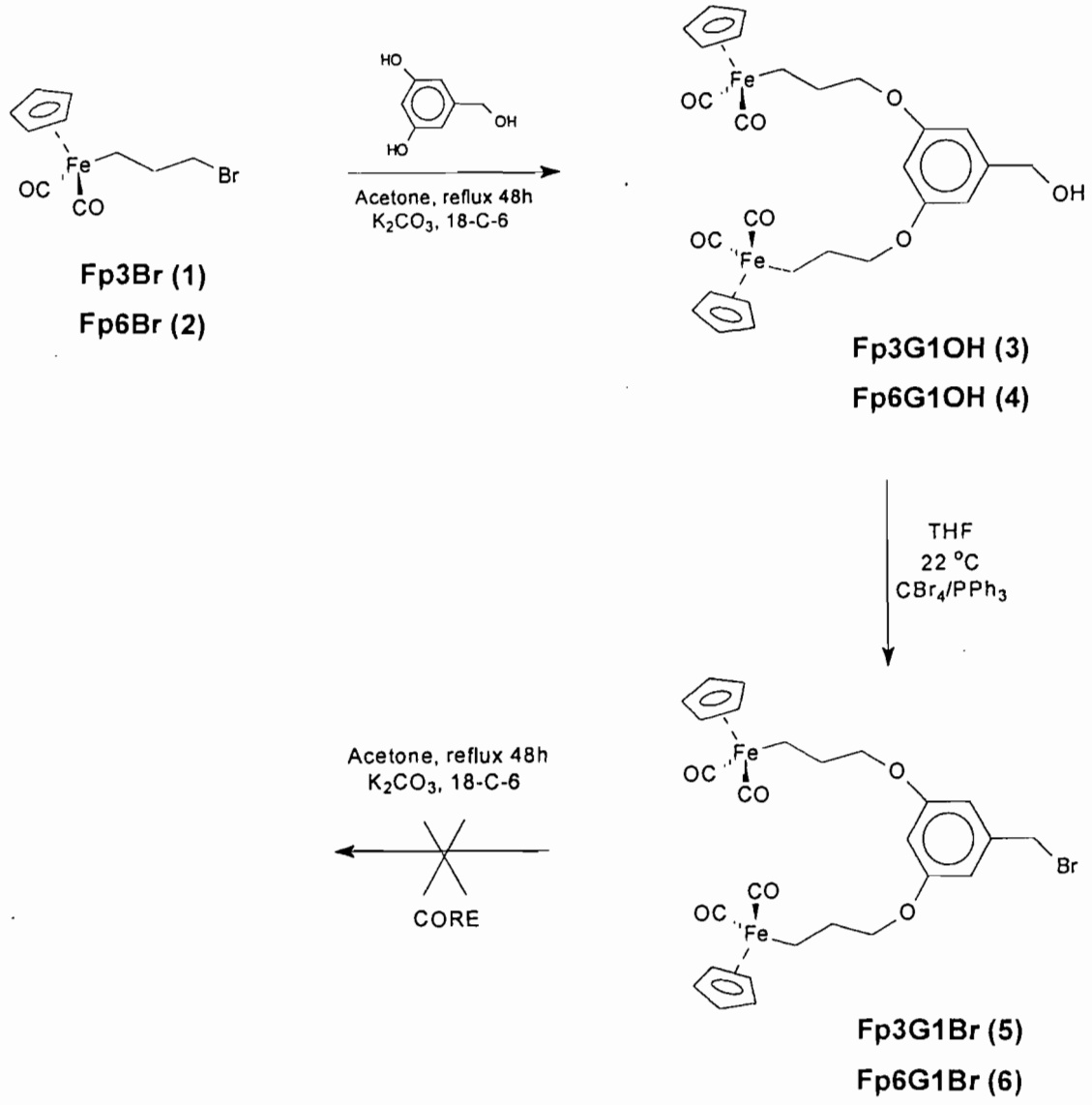


**Scheme 2.4**

The first generation benzyl bromides **5** and **6** were obtained in fairly good yields (70 – 80%) and characterised by standard methods but both iron compounds were unstable and showed decomposition after about 20 minutes under vacuum (p = 0.01 mm Hg).

Several attempts were made to react the benzyl bromides **5** and **6** with the core molecule, 1,1,1-tris(4-hydroxyphenyl)ethane in refluxing acetone failed (Scheme 2.4). None of the expected products were observed from TLC, except decomposition products. Full experimental details are given in the experimental (section 7.2).

### 2.2.2 The $Cp^*Fe(CO)_2(CH_2)_n$ system (n = 3 or 7 or 11)

In order to try to overcome instability problems with the Fp complexes, it was decided to change to the Fp* system. Cp* halogenoalkyl complexes have been shown to be more stable than their Cp analogues in many cases.[81,82]

A series of new organometallic dendritic wedges and first generation dendrimers have now been synthesised and characterised. Again two molar equivalents of the bromoalkyl complexes **7** - **9** were reacted with one molar equivalent of 3,5 dihydroxybenzyl alcohol in the presence of potassium carbonate and 18-crown-6 in refluxing acetone for 2 - 3 days (Scheme 2.5, shown for n = 3). The reactions were monitored by TLC eluting with a 50 - 70% $CH_2Cl_2$/hexane solution. The resulting "di-substituted" benzyl alcohols **11** - **13** were purified by column chromatography. A large amount of decomposition occurred after 2 days of refluxing, which resulted in low yields of the benzyl alcohols (*e.g.* 15% for **11**). Attempts to improve the product yields by changing solvents, reaction temperatures and bases were unsuccessful. Complexes **11** - **13** were isolated as yellow oils and appeared to be slightly more stable at room temperature than the Fp analogues prepared in section 2.2.1. Complex **11** was recrystallised from $CH_2Cl_2$/hexane; complexes **12** and **13** remained as a oils after attempted crystallisation. An intermediate product, the "mono-substituted" benzyl alcohol **10** was isolated as a minor product in the reaction of 3,5-dihydroxybenzyl alcohol with **7**. The equivalent "mono-substituted" benzyl alcohol was not observed in the case of the longer chain alkyl complexes **8** and **9**. This intermediate product was also not observed for the Fp complexes. This is presumably due to steric hindrance. Compound **10** was synthesised directly in a separate reaction by adjusting the molar ratios of the haloalkyl complex and the monomer unit to equal ratios. This compound was later used in the preparation of heterobimetallic dendrimers (see Section 5.2).

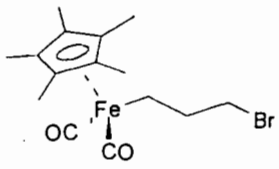


**Fp*3Br (7)**

**Fp*7Br (8)**

**Fp*11Br (9)**

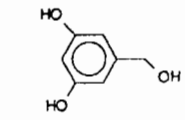


Acetone, reflux 48h
$K_2CO_3$, 18-C-6

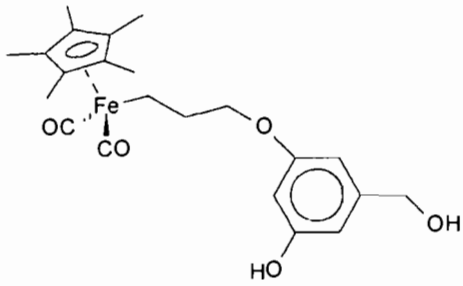


**mFp*3G1OH (10)**

\+

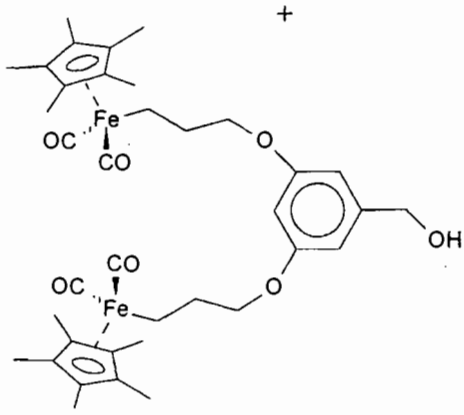


**Fp*3G1OH (11)**

**Fp*7G1OH (12)**

**Fp*11G1OH (13)**

THF
22 °C
$CBr_4/PPh_3$

**11**

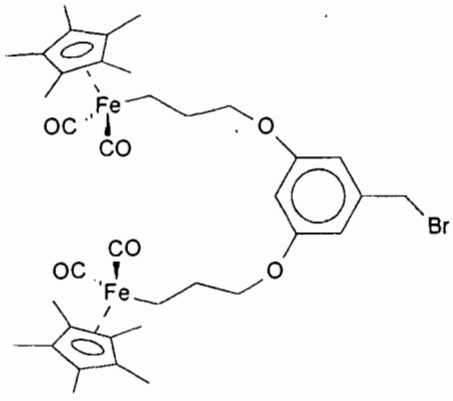


**Fp*3G1Br (14)**

**Scheme 2.5**

The activation of the benzyl alcohols **11** – **13** was attempted using $CBr_4/PPh_3$. The reactions are usually complete within 20 - 30 minutes and were followed by TLC. Again, an excess of the brominating agent was required to drive the reaction to go to completion. Benzyl alcohol **11** was converted to the corresponding benzyl bromide **14** as described previously. TLC showed that the longer chain benzyl alcohols **12** and **13** had been converted to the corresponding benzyl bromides but decomposed during the work-up procedure. All the benzyl bromide complexes prepared so far appear to be very unstable.

Finally, three equivalents of the first generation benzyl bromide **14** was reacted with the CORE molecule, 1,1,1-tris(4'hydroxyphenyl)ethane to give the first generation dendrimer **15** as a yellow oil (Scheme 2.6). The first generation dendrimer **15** contains six Fe atoms on the periphery of the dendrimer.

In an attempt to prepare the second generation dendritic wedge, the coupling and activation steps as described in Scheme 2.5 were repeated. Thus two molar equivalents of complex **14** were reacted with one molar equivalent of 3,5 dihydroxybenzyl alcohol in refluxing acetone. The first generation benzyl bromide **14** was then converted to the second generation benzyl alcohol **16** (Scheme 2.7). We have now built up a second generation dendritic wedge containing four Fe atoms. Attempts to prepare the second generation benzyl bromide failed and only decomposition products were observed.

Due to the low yields of these reactions and the instability of the products in solution at room temperature, it was very difficult to build up higher generation dendrimers with the Fp and Fp* system. Characterisation of all the organoiron dendritic wedges was also very difficult due to a number of factors: (i) very low yields, (ii) instability of the complexes at room temperature, particularly in solution and (iii) oily products which could not be recrystallised. Full experimental details are given in the experimental (section 7.2).

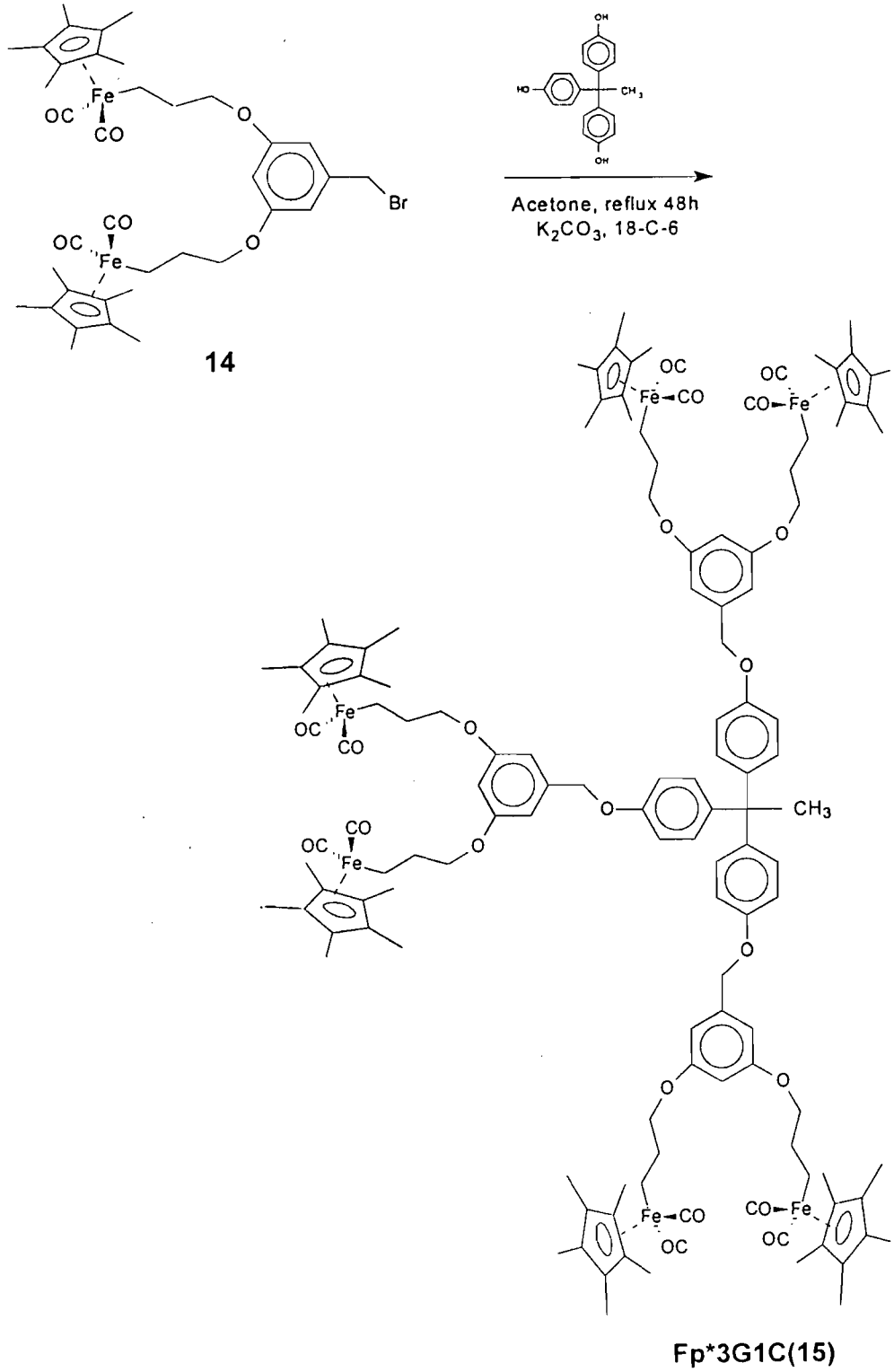


**Scheme 2.6**

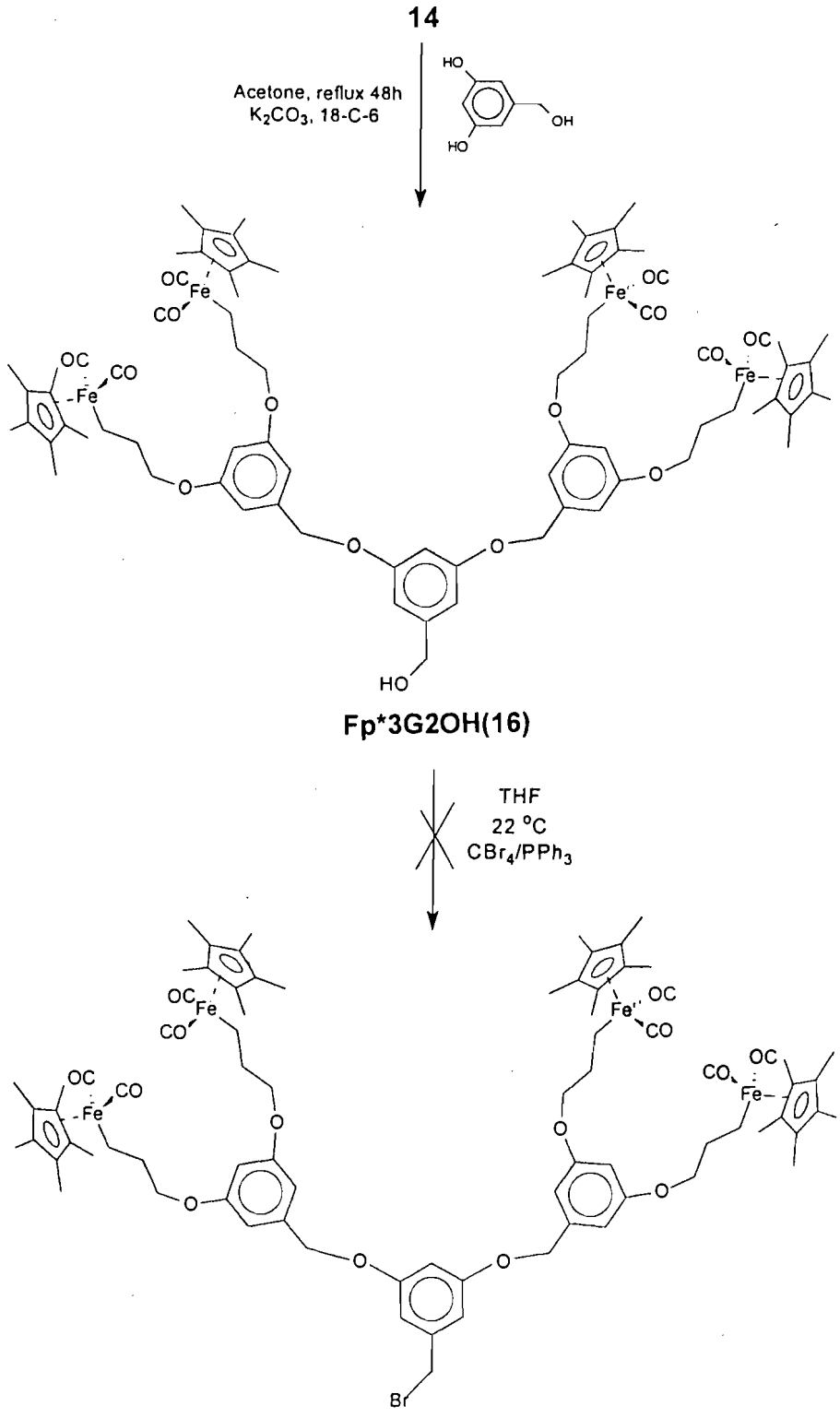
14
Acetone, reflux 48h
$K_2CO_3$, 18-C-6
HO
OH
HO
OC
Fe
CO
HO
Fp*3G2OH(16)
THF
22 °C
$CBr_4/PPh_3$
Br

**Scheme 2.7**

Up to this point, we have experienced few difficulties in the purification of these new dendrimers. This is because these dendrimers are highly soluble in common organic solvents such as dichloromethane, chloroform and acetone. However, it has been shown that the solubility of dendrimers usually decreases as the generation number increases.[46] The yields usually decrease slightly as well because of the increasing steric congestion around the focal point. These iron compounds usually separate out as oils during attempted crystallisation and are difficult to purify. The products are usually obtained as glassy solids even after drying the complexes under vacuum for several hours. Solvent could not be removed completely in some cases. This made microanalysis on these complexes extremely difficult as there was often a small amount of included solvent in the complex.

### 2.2.3 The $CpFe(CO)(PPh_3)\{C(O)(CH_2)_6\}$- system

The carbonyl insertion or alkyl migration reaction is one of the most widely studied reactions in organometallic chemistry. It is fundamentally important to catalytic processes, such as hydroformylation[78] and the Fischer-Tropsch process.[87] In a further attempt to improve the yields and find a more stable system, it was decided to investigate an iron acyl group as this could be easily prepared and was also expected to be more stable. The acyl starting materials were prepared by reaction of the haloalkyl complexes **1** and **2** with $PPh_3$ in refluxing benzene (Scheme 2.8). In the case of **1**, a carbene species **17** was formed; this has been reported previously.[84] In the reaction of **2** with $PPh_3$, the expected acyl compound **18** was synthesised in 88% yield. A chiral centre is present in **18**, when $PPh_3$ is coordinated to iron. No attempts were made to separate the optical isomers of **18**. Extensive studies on the chiral auxilliary, $Cp(CO)(PPh_3)Fe$ have shown that high stereospecificity of organic transformations can be achieved with this metal centre.[88]

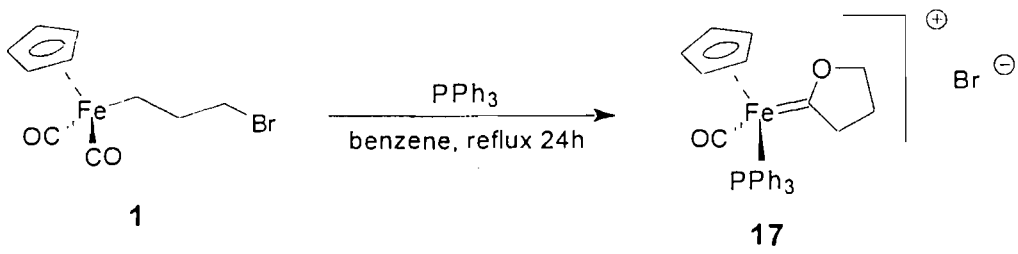


**1** **17**

**Scheme 2.8**

Scheme 2.9 shows the synthesis of the acyl organoiron dendritic wedges. The methodology used to prepare the dendritic wedges was the same as that described in sections 2.2.1 and 2.2.2.

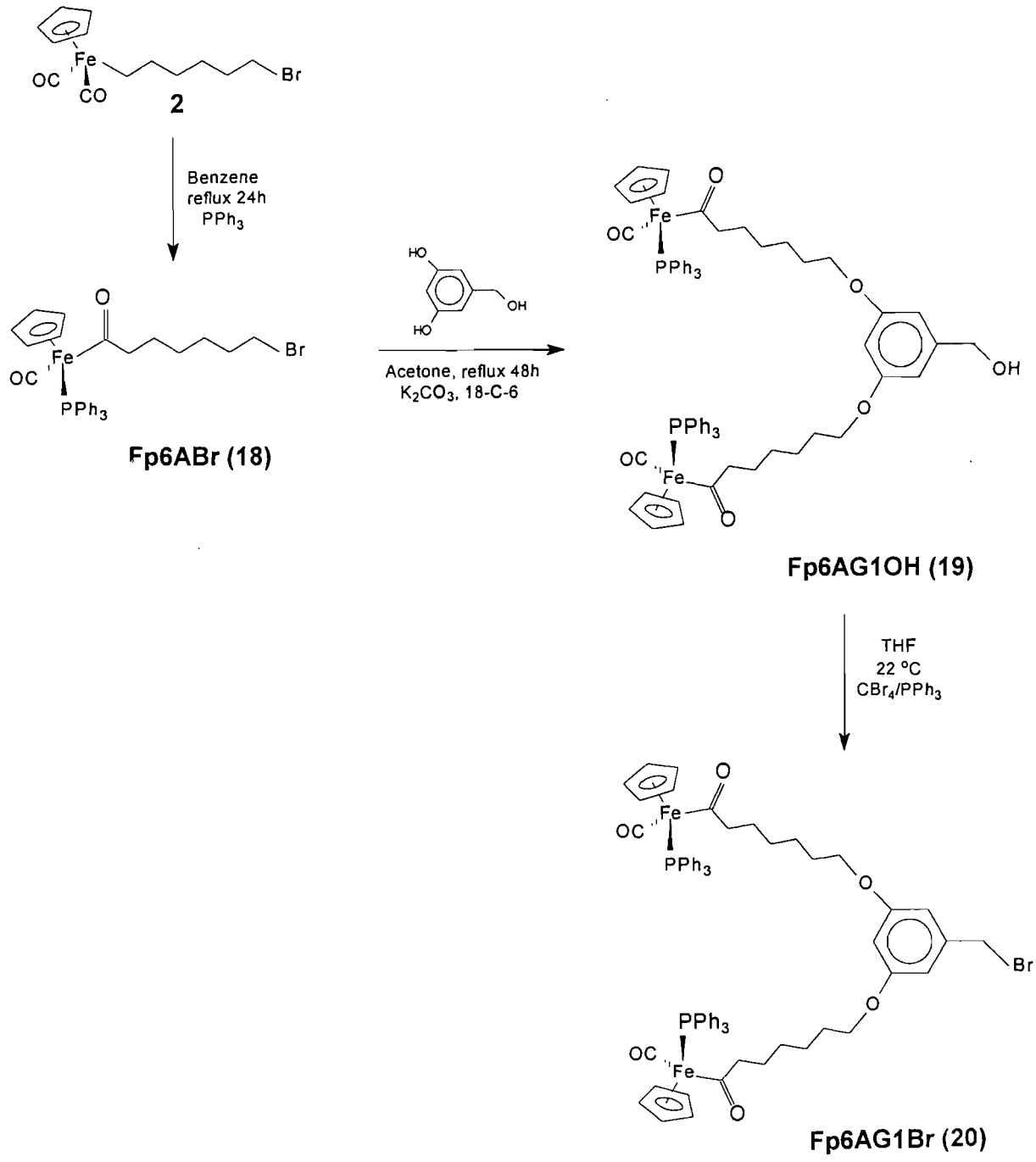


**Scheme 2.9**

The dendritic wedges **19** and **20** were isolated as orange oils which turned to orange foams upon drying under high vacuum. The yield of the acyl benzyl alcohol complex **19** is significantly higher than those of the alkyl Fp and Fp* complexes. The triphenyl phosphine group introduces a crowded environment around the iron atom which possibly stabilises the metal centre. Activation of **19** to the benzyl bromide **20** proceeds as before. The first generation iron acyl dendrimer **21** was prepared by reaction of **20** with the CORE molecule in refluxing acetone (Scheme 2.10).

The second generation wedge **22** was prepared by repeating the coupling reaction (Scheme 2.11). Complex **22** was also obtained as an orange foam after the work-up procedure. Attempted activation of **22** again resulted in mostly decomposition products being formed.

The activation procedure used for the organoiron dendrimers appears to be too harsh for complexes of this type. TLC showed evidence for the formation of the benzyl bromides in all cases, but, these complexes all decomposed (at least to some extent) during the work-up procedure. This was not expected as the analogous ruthenium dendrimers (described in Chapter 3) were relatively stable towards $CBr_4/PPh_3$. Other activation procedures such as the use of phosphorus tribromide, gave similar results.

All the iron acyl compounds were purified by column chromatography. A more polar solvent system was needed to elute the iron acyl dendrimers as compared with the Fp and Fp* alkyl dendrimers. In general, the iron acyl dendrimers were found to be much more stable at room temperature, in solution than the Fp and Fp* analogues. Full experimental details are listed in the experimental (section 7.2).

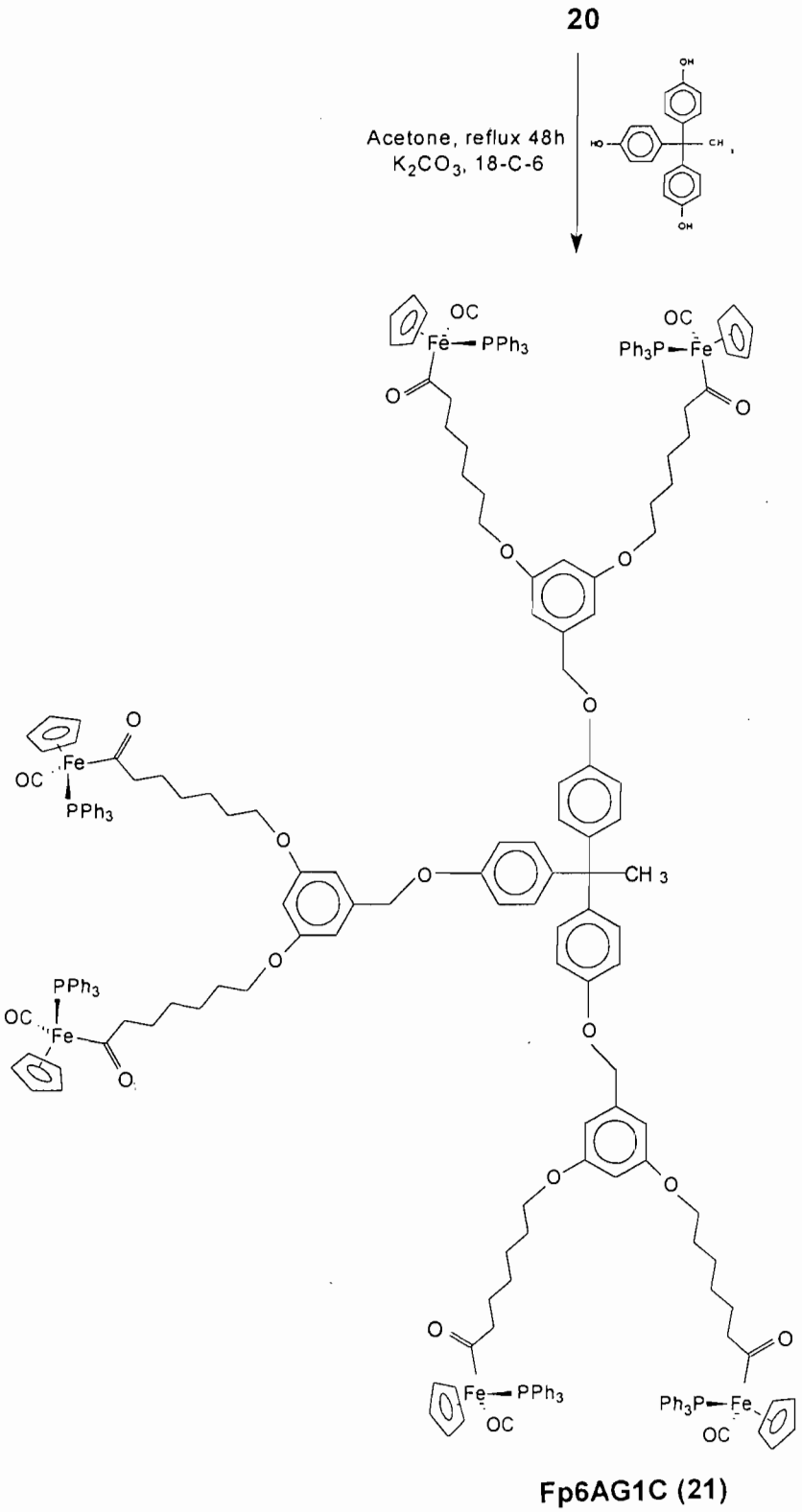


Scheme 2.10

**20**

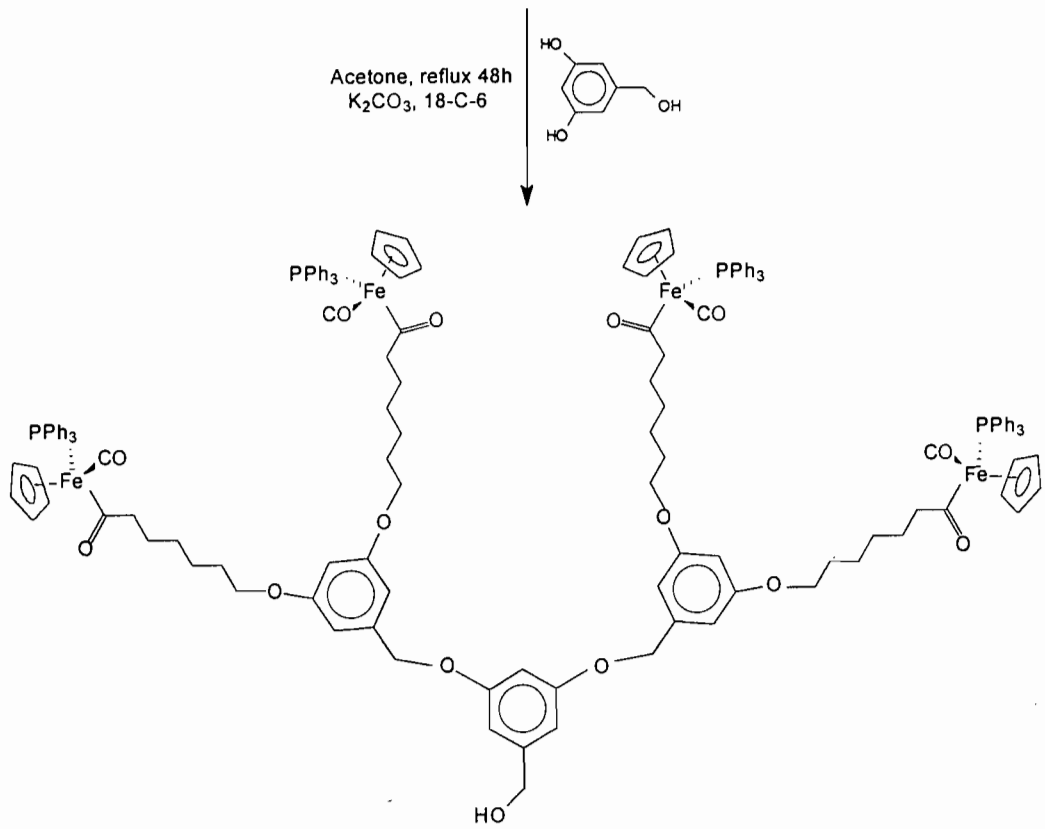


**Fp6AG2OH (22)**

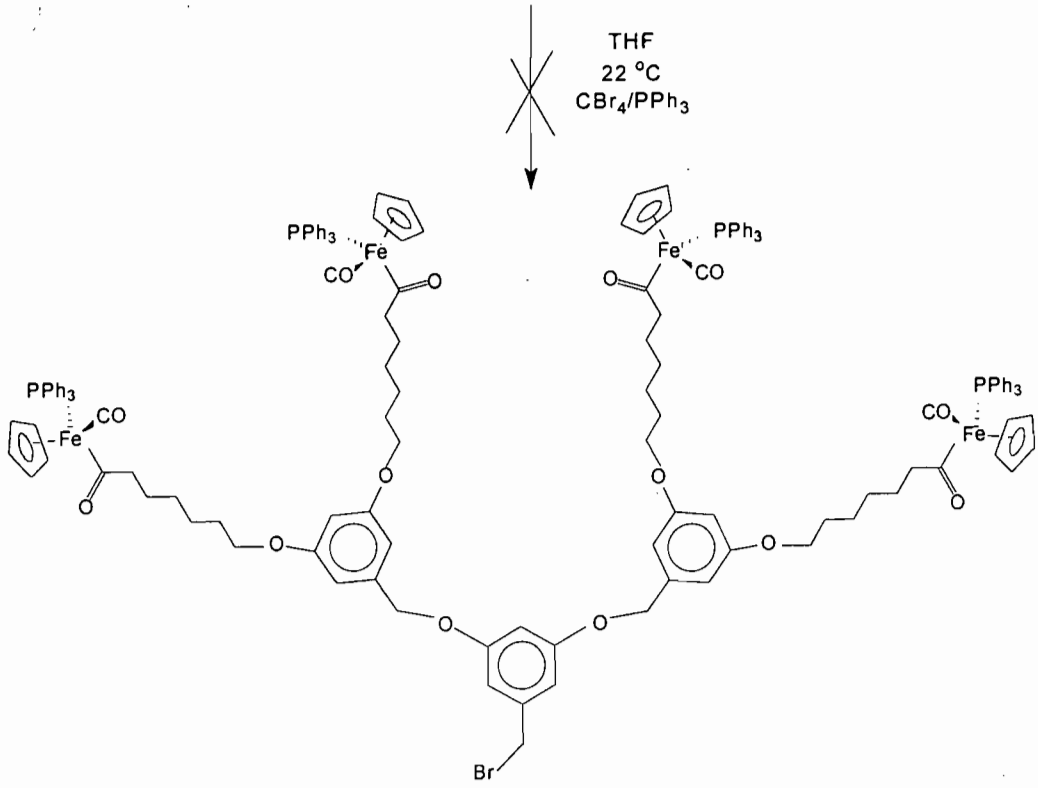


**Scheme 2.11**

### 2.2.4 Characterisation of the organoiron dendrimers

Many attempts were made to characterise all the new organotransition metals dendrimers and dendritic wedges by IR, $^{1}H$ and $^{13}C$ NMR spectroscopy, mass spectroscopy and elemental analysis. Many of the complexes prepared were unstable and decomposed while being purified or, while being analysed. For this reason, several of the complexes prepared could not be fully characterised. The data are given in the experimental section 7.1. The results are discussed in the following text.

#### IR Spectroscopy

The IR spectra of compounds **1** - **22** were recorded in $CH_2Cl_2$ from 2200 to 1500 $cm^{-1}$. Figure 2.1 shows the carbonyl region of the spectrum obtained for the three types of iron dendritic wedges **4**, **12** and **19**. The Fp and Fp* compounds showed two strong absorption bands at 1999, 1938 $cm^{-1}$ and 1980 and 1919 $cm^{-1}$ respectively. The shift of the carbonyl bands in the Fp* complexes to a lower frequency is due to the electron releasing effects of the Cp* ligand. The iron acyl dendrimers showed absorption bands at 1912 and 1603 $cm^{-1}$. The lower $\nu$(CO) stretch for the acyl complexes confirms the formation of a carbonyl inserted product. It was anticipated that the densely packed chain-ends may have effects on the $\nu$(CO) absorption bands. However, neither a band shift nor band distortion was observed in any of these dendrimers.

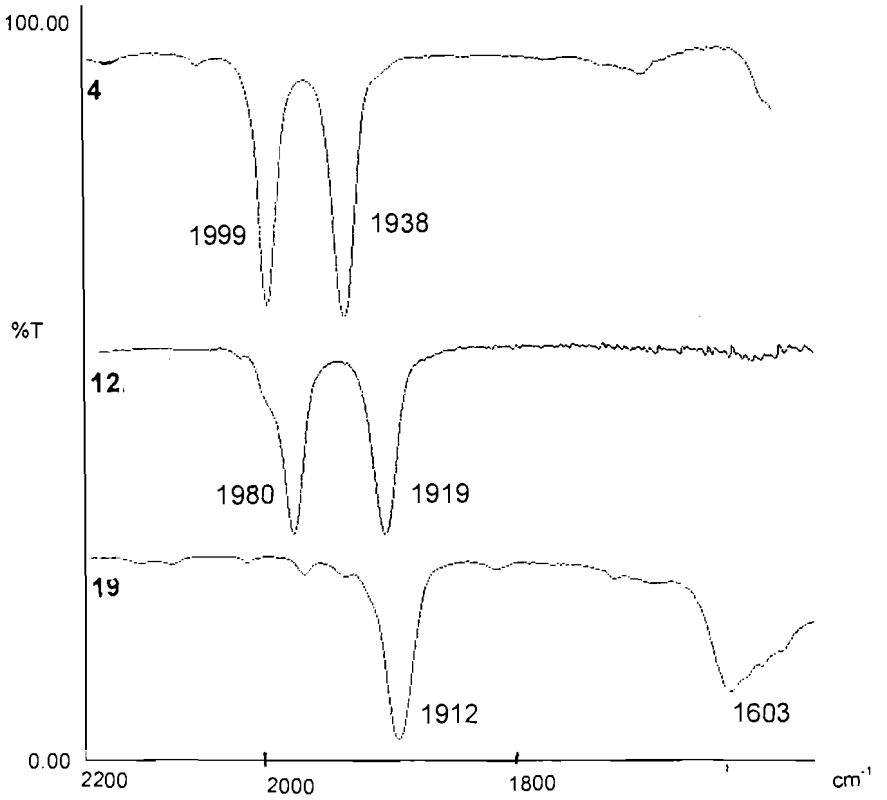


**Figure 2.1** The carbonyl region of the IR spectra obtained for **4**, **12** and **19**.

**$^{1}$H and $^{13}$C NMR Spectroscopy**

NMR spectroscopy has proved to be invaluable in the characterisation of the new dendrimers. All the dendrimers and dendritic wedges prepared were characterised by $^{1}$H and $^{13}$C NMR spectroscopy. A 400 MHz $^{1}$H NMR spectrum of Fp*3G1Br **14** is shown in Figure 2.2. In the Fp* compounds, the organometallic functional groups on the periphery of the molecule give four sets of resonances at positions δ 3.85 ($CH_2O$), 1.82 ($CH_2$), 1.74 ($Cp^*$) and 0.88 ($FeCH_2$). In the Fp compounds, the resonances occur at δ 4.69 (Cp), 3.80 ($CH_2O$), 1.82 ($CH_2$) and 1.38 ($FeCH_2$). The triplet observed at 3.85 ppm is important, since it confirms the formation of the first generation products. The other peaks indicated that the organometallic functional groups remain in the dendritic structure during the reactions. The doublet and triplet (sometimes unresolved) in the region δ 6 - 7 ppm was assigned to the aromatic protons.

The benzyl protons occur in the region δ 4.5 - 5 ppm. This region is important as it contains the resonances due to the functional groups at the focal point of the dendrimer. The benzyl alcohol protons occur at *ca.* 4.6 ppm, while the benzyl bromide shows an unresolved doublet at *ca.* 4.40 ppm. A further shift from 4.40 to 4.93 ppm of the same $CH_2$ resonance was observed when dendritic wedges were coupled to a core molecule. Figure 2.3 shows the dramatic shift of the focal benzyl $CH_2$ resonances in **11**, **14** and **15**.

The attachment of the dendritic wedges to a core molecule was also accompanied by a new resonance at 2.10 ppm, corresponding to the methyl protons of the core molecule, while the aromatic protons of the core molecule gave two additional doublets at 6.99 and 6.86 ppm. A complex AA'-BB' splitting pattern was observed for the core aromatic protons. In all cases, the integration of resonances was employed to further confirm whether the reaction of the benzyl bromide with the core molecule (or with 3,5-dihydroxybenzyl alcohol) had gone to completion.

$^{13}$C NMR spectroscopy was found to be less useful in characterisation of the products. This could be due to the limited sensitivity of the $^{13}$C nucleus, which cannot distinguish the subtle change of the chemical environment in the dendritic structure. However, all the spectra were assigned and the different functional groups could be distinguished. The 100 MHz $^{13}$C NMR spectrum of **13** is shown in Figure 2.4. The resonance due to the focal $CH_2$ group

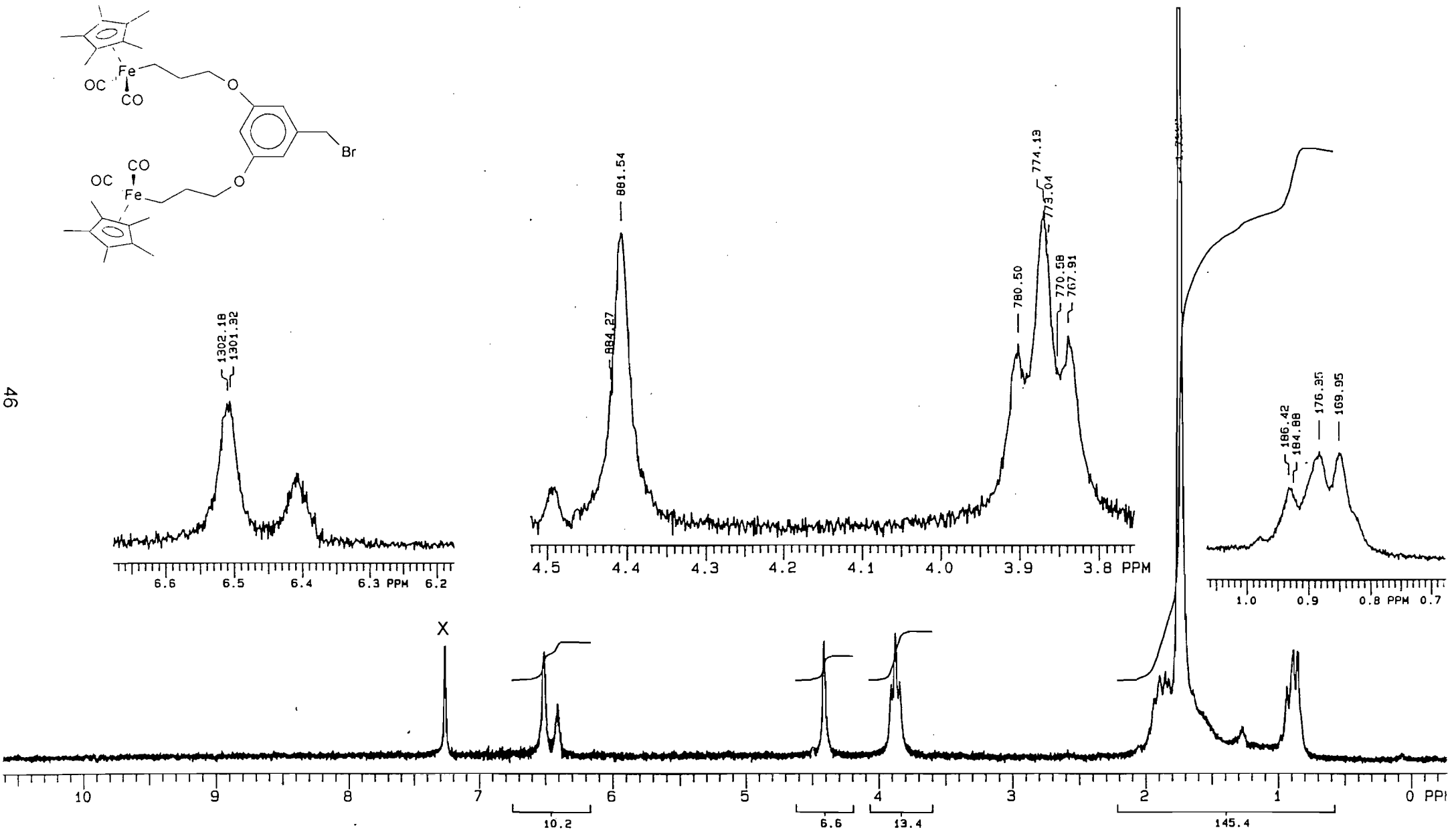


**Figure 2.2** A 400 MHz $^{1}$H NMR spectrum of **14**. X = solvent

(65.5 ppm) is clearly distinguishable from the various functional groups, such as $CH_2OAr$ (68.1) and CO (219.6 ppm).

The NMR spectra of the iron acyl complexes also show some characteristic features. The 200 MHz $^1H$ NMR spectrum of **20** is shown in Figure 2.5. Again, the triplet at 3.85 ppm confirms the formation of the benzyl alcohol wedge. Two magnetically non-equivalent protons in $\alpha$-$CH_2$ were observed at 2.83 and 2.55 ppm. This is because the $\alpha$-$CH_2$ group is prochiral. Similar effects have been observed before.[89] The large number of protons of the triphenyl phosphine group relative to the number of aromatic protons tend to "swamp" the aromatic protons. For this reason, the peaks at 6.36 and 6.51 ppm occur as unresolved doublets and triplets. Paramagnetic iron impurities also caused line broadening problems.

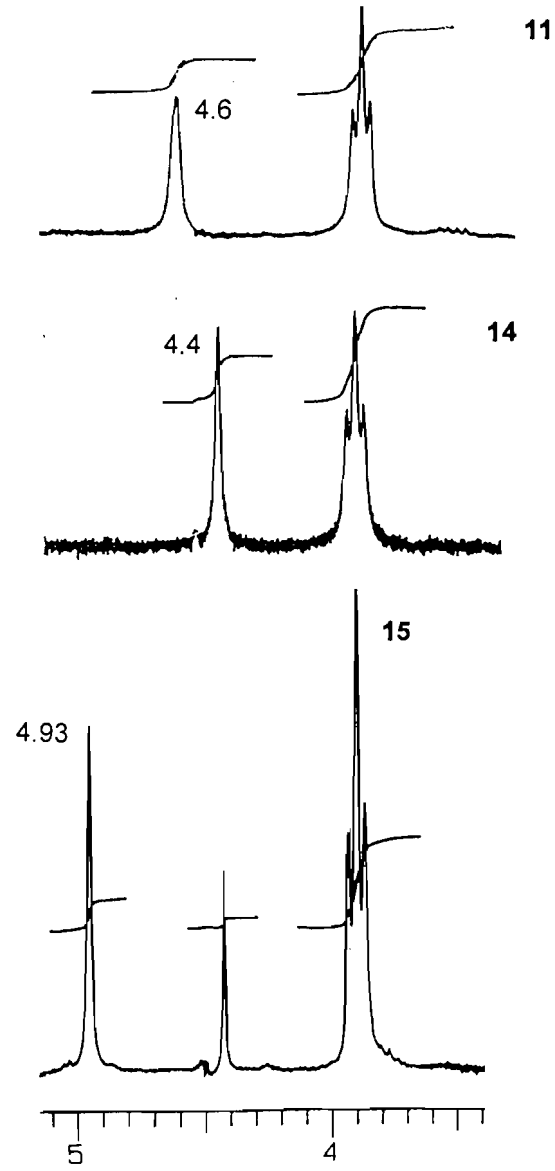


**Figure 2.3** Shift of the benzyl protons in **11**, **14** and **15**.

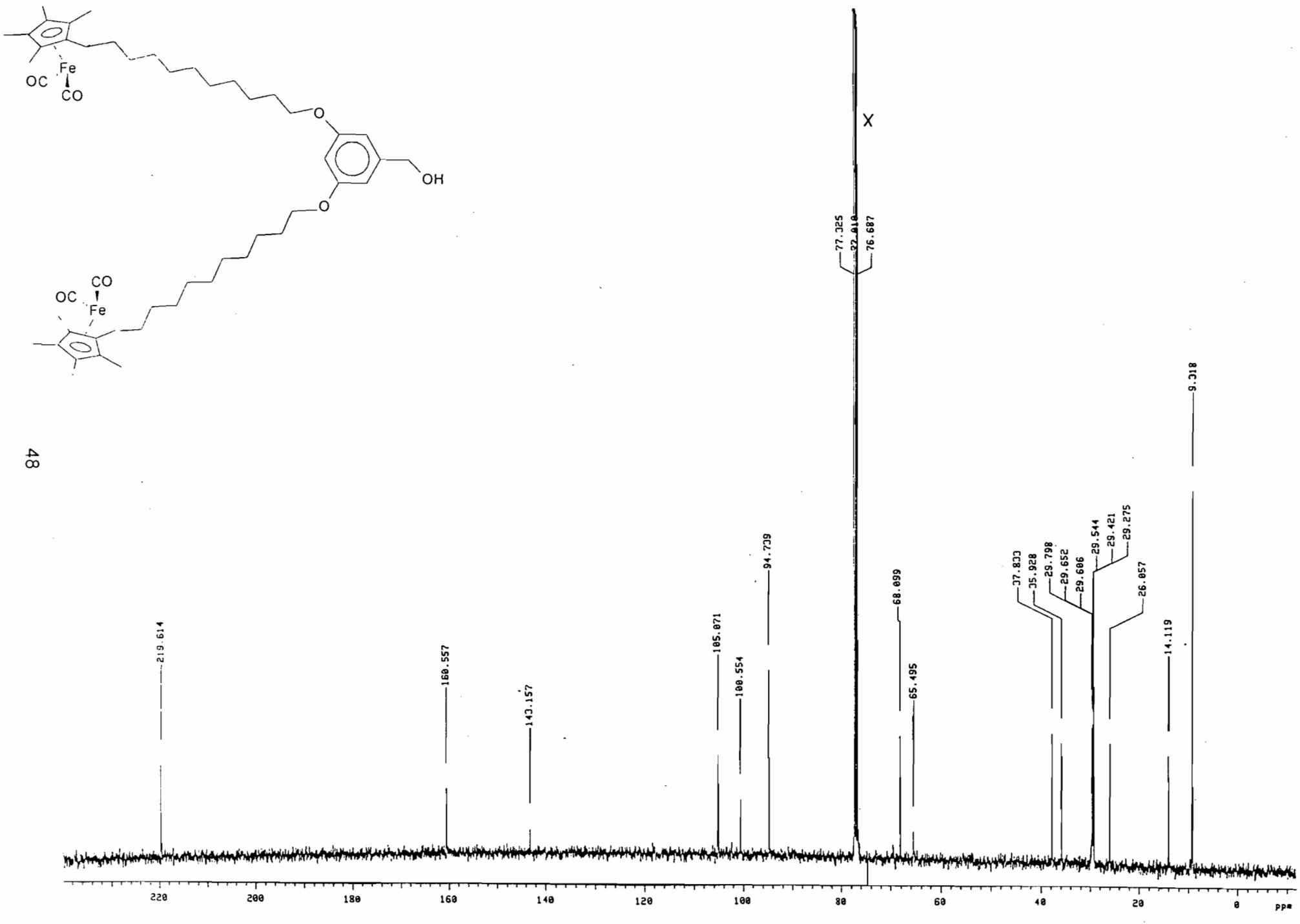


**Figure 2.4** A 100 MHz $^{13}C$ NMR spectrum of **13**. X = solvent

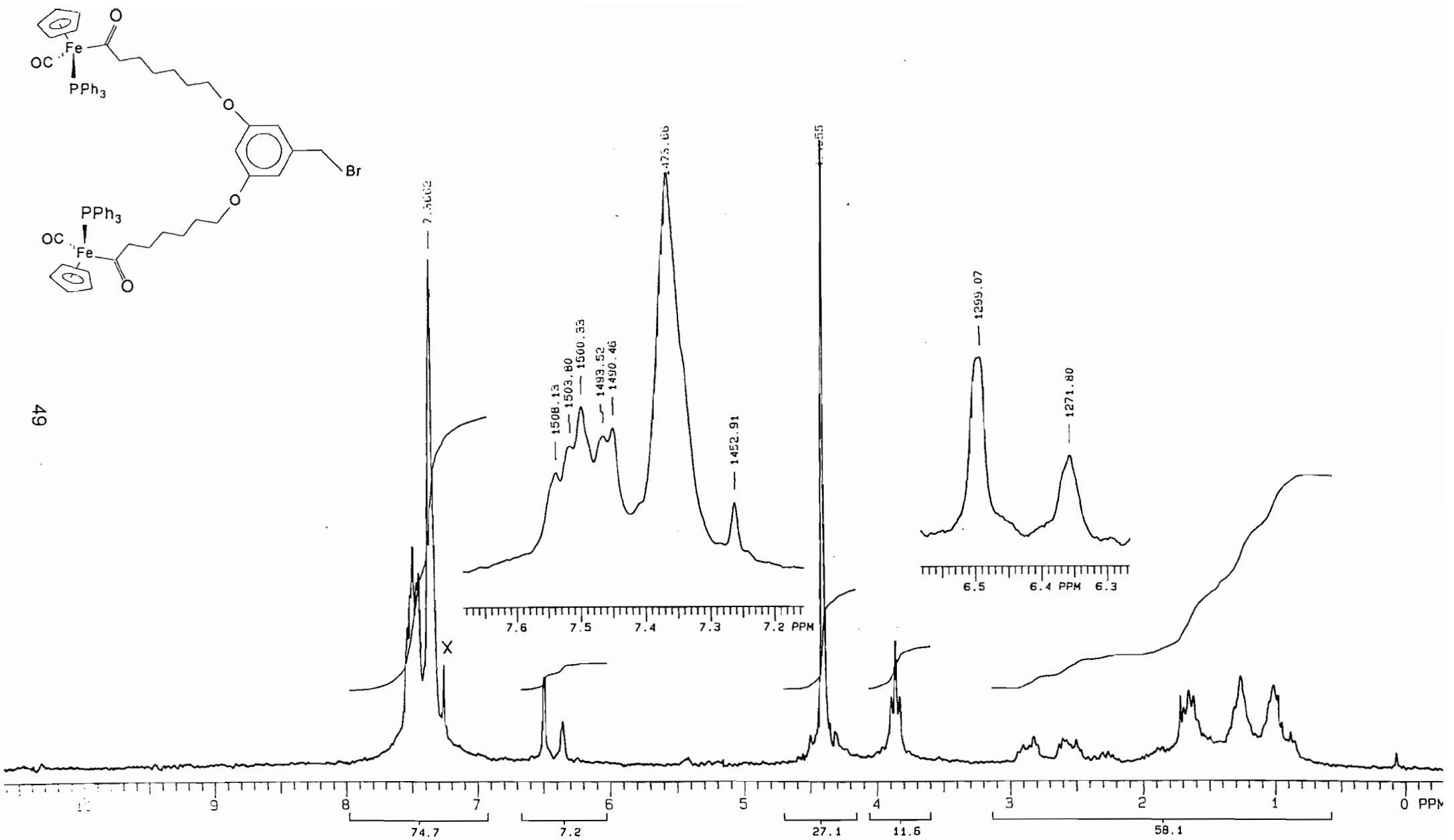


**Figure 2.5** A 200 MHz $^{1}$H NMR spectrum of **20**. X = solvent

**Mass Spectroscopy**

Mass spectroscopy, together with NMR and IR spectroscopy, is nowdays one of the standard methods of characterisation. The decomposition of organometallic ions can be divided into three groups:[90]

(i) the cleavage of metal-ligand bonds;

(ii) simple cleavage of bonds within the complex ligands;

(iii) fragmentation reactions with rearrangement.

In many cases, competition between all three degradation types is possible.[90] Thermal decomposition phenomena frequently complicate the mass-spectroscopic investigation of organometallic complexes, and not uncommonly lead to incorrect interpretations regarding the constitution or the purity of a compound.[91] For example, ferrocene appears as a thermolysis product in the mass spectra of cyclopentadienylcarbonyliron derivatives; this was indeed observed.[92]

The molecular weights of most of the dendrimers and dendritic wedges were confirmed by low electron impact (EI) or fast atom bombardment (FAB) mass spectroscopy, and the results are given in the experimental section. The FAB mass spectra generally showed molecular ion peaks at the expected positions for the lower molecular weight dendrimers. The elemental composition of molecular ion peaks was further confirmed by comparing its isotope pattern with the pattern generated from computer calculation. However, in the case of the higher molecular weight dendrimers, only daughter peaks at $(M - CO)^+$ and $(M - 2CO)^+$ were observed. The FAB mass spectra were complicated by the low intensity of peaks, complex isotope patterns of iron and the possible overlapping of fragments such as $M^+$-2CO-1, $M^+$-2CO-2 *etc.* For some complexes such as **15**, several techniques were attempted, such as FAB and EI, but the compound appeared to fragment very easily under the required conditions, and so the parent ion was not be observed.

Most of the mass spectra reported here are reasonable, since it has been shown that complexes of the type $[CpM(CO)_2[(CH_2)_nX]$ (where M = Fe, Ru; X = H, Br, I ) give very weak molecular ion peaks in their mass spectra. The ratio of peak intensities of $(P^+\text{-}2CO)/(P^+)$ is found to increase as the molecular weight of the complex increases. Figure 2.6 shows the FAB mass spectrum of **19**.

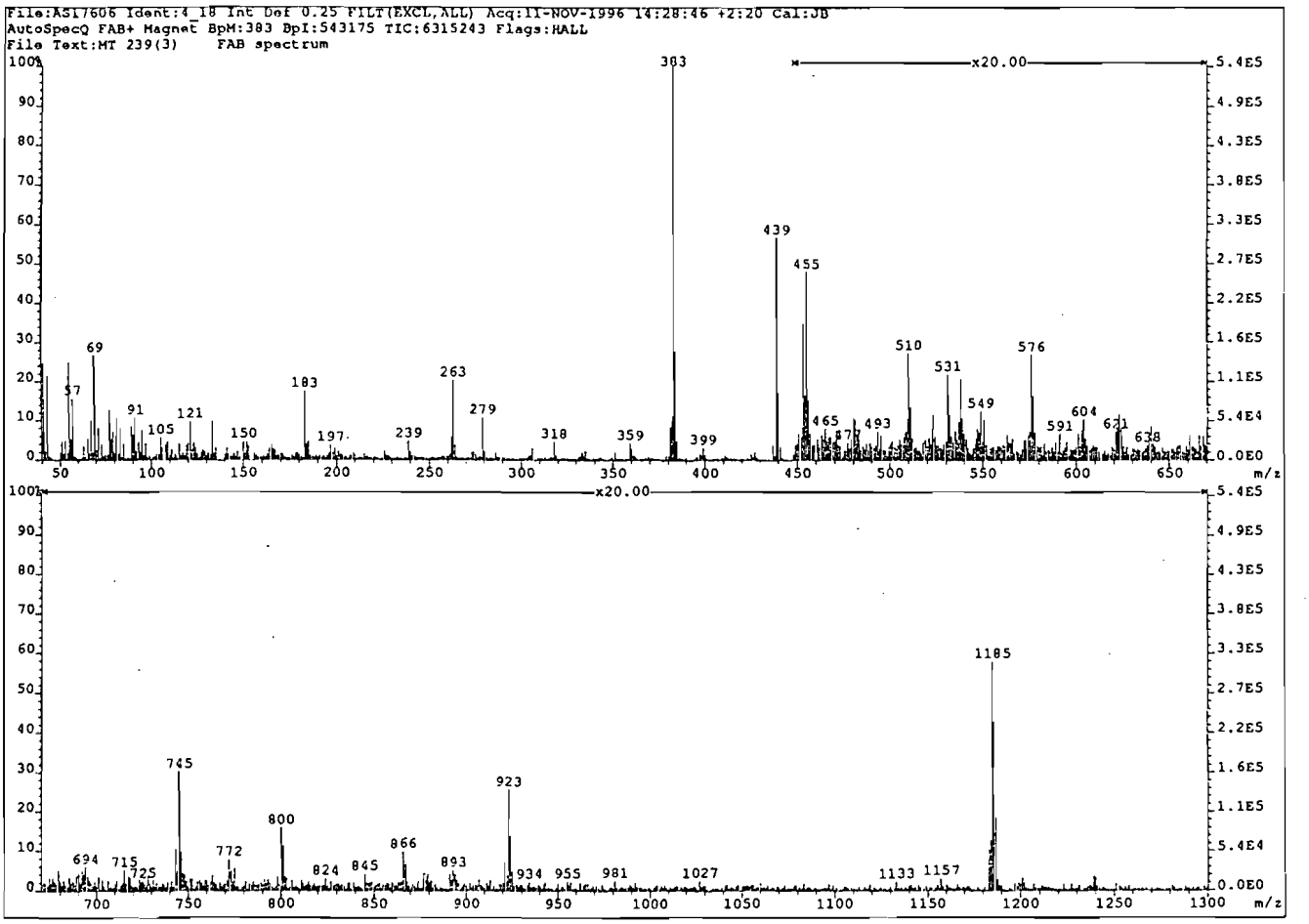


**Figure 2.6** FAB mass spectrum of **19**.

### Microanalysis

Microanalysis was attempted for all of the new dendrimers and dendritic wedges synthesised. In many cases, the results obtained deviated from the calculated values. Many of the complexes were unstable at room temperature and decomposed during the analysis. In some cases, solvent inclusion was believed to occur even though the complexes had been dried under vacuum for several hours. The included solvent agreed with residual solvent peaks in the $^{1}H$ NMR spectra (see experimental section 7.2 for details).

## 2.3 Structural studies and physical behaviour of selected dendrimer precursors and related compounds

Dendrimers are expected to exhibit interesting structural and physical properties when compared with traditional linear polymers due to their novel highly branched three-dimensional architecture. There has been much controversy over the exact shape of dendrimers in solution and many conflicting results have been obtained. de Gennes and Hervet[58] were the first to perform calculations on dendritic structures. They showed the chain ends to be on the periphery and found a density minimum at the core and a density maximum at the surface. Other studies have showed a density maximum between the dense core and the periphery.[57a] Monte Carlo calculations by Mansfield and Klushin[57b] found the chain ends to be distributed throughout the structure, and in close proximity to the core. They revealed a density maximum between the centre of mass and the periphery.[57] Calculations carried out on some Frechet type poly(benzylphenyl ether) dendrimers, functionalised with arene tricarbonylchromium(0) groups showed a transition from an extended to a globular structure as the generation number increased.[60] The chain ends were found to be in all regions of the dendrimer to some extent, although most were still located on the periphery or in a solvent-accessible area for those dendrimers studied. The simulations on the molecules were performed in vacuum. Vacuum simulations are comparable to simulations in a poor solvent.

Due to their novel architecture and high molecular weight, dendrimers are generally difficult to crystallise as they tend to form glasses rather than single crystals. Although many dendrimers containing a large variety of ligands and functional groups have been prepared, there are still very few crystal structures of dendrimers or dendritic wedges in the literature. Dendrimers which have been characterised by single x-ray crystallography include a second generation organosilicon dendrimer with hydrides at the termini[27a], a first generation platinum-acetylide dendrimer[52a] and a heterobimetallic Fe/Pt dendritic wedge (Figure 2.7).[52b]

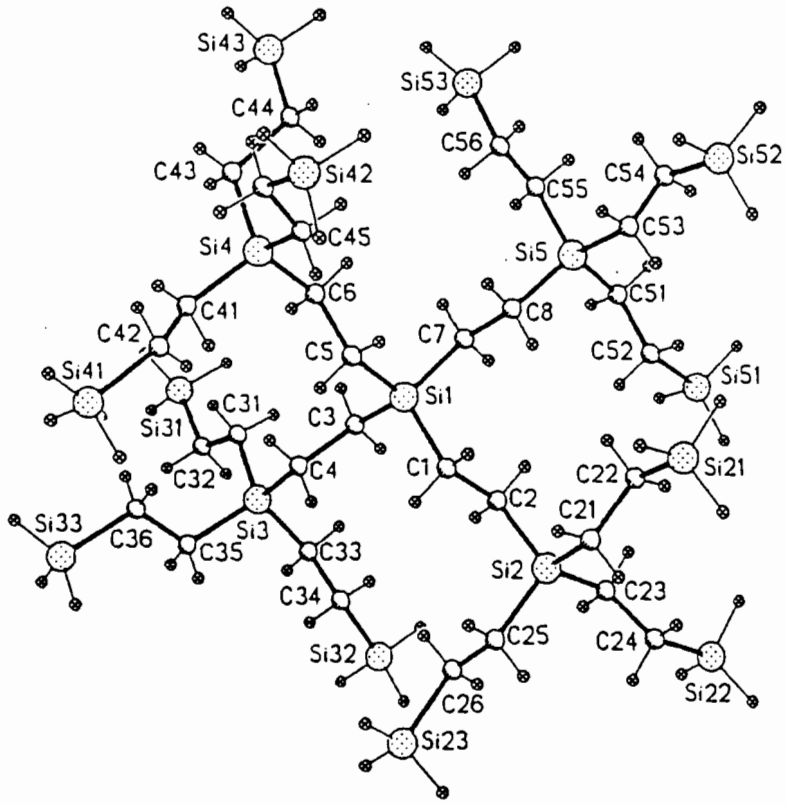


(a)

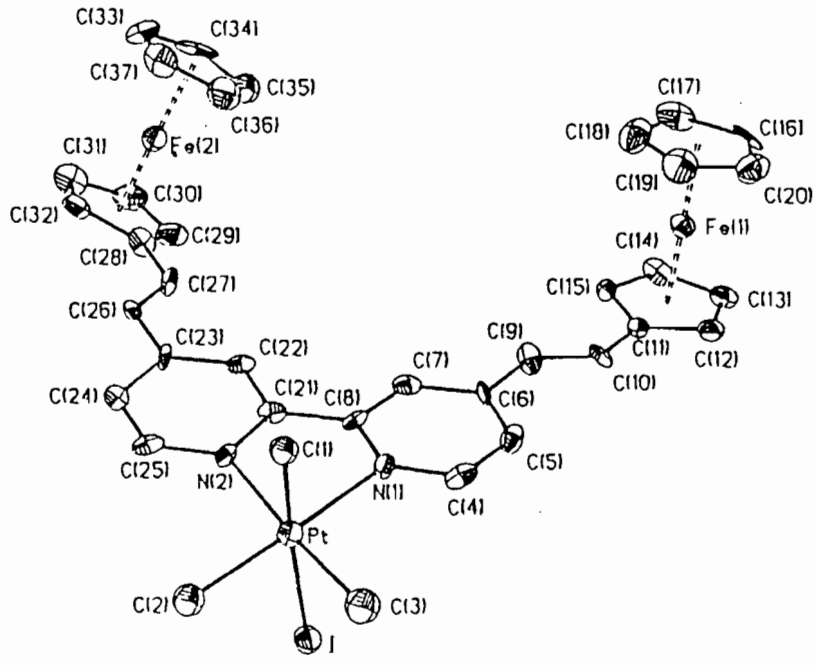


(b)

**Figure 2.7** Molecular structures of (a) a second generation organosilicon dendrimer[27a] and (b) a Pt-Fe dendritic wedge.[52]

### 2.3.1 Structure determination of Fp*3Br (7)

Suitable yellow single crystals were grown from a hexane solution at –15°C. Oscillation and Weissenberg photography revealed 2/m Laue symmetry, indicating the monoclinic crystal system. The lack of any systematic absences among general reflections on upper level Weissenberg photographs indicated the presence of a primitive lattice. There were no conditions on hkl, but conditions on h0l (l = 2n) and 0k0 (k = 2n) were observed. The space group $P2_1/c$ was unambiguously assigned from the data. The iron and bromine atoms were located using Patterson methods and the remaining non-hydrogen atoms found after successive difference Fourier syntheses. Successful structure refinement followed (see Table 2.1) and is described experimentally in Section 7.1. The initial data collected at 21°C suffered from severe decay (R = 0.173 in final refinement) and so data were recollected at -25°C providing a much improved refinement with a final R factor of 0.039. The molecular structure with the atomic numbering scheme is shown in Figure 2.8. Fractional atomic coordinates, anisotropic displacement parameters, bond lengths, bond angles and torsion angles appear in Appendix 1a (Tables A1 to A6) and structure factor data are included in Appendix 1b (on diskette).

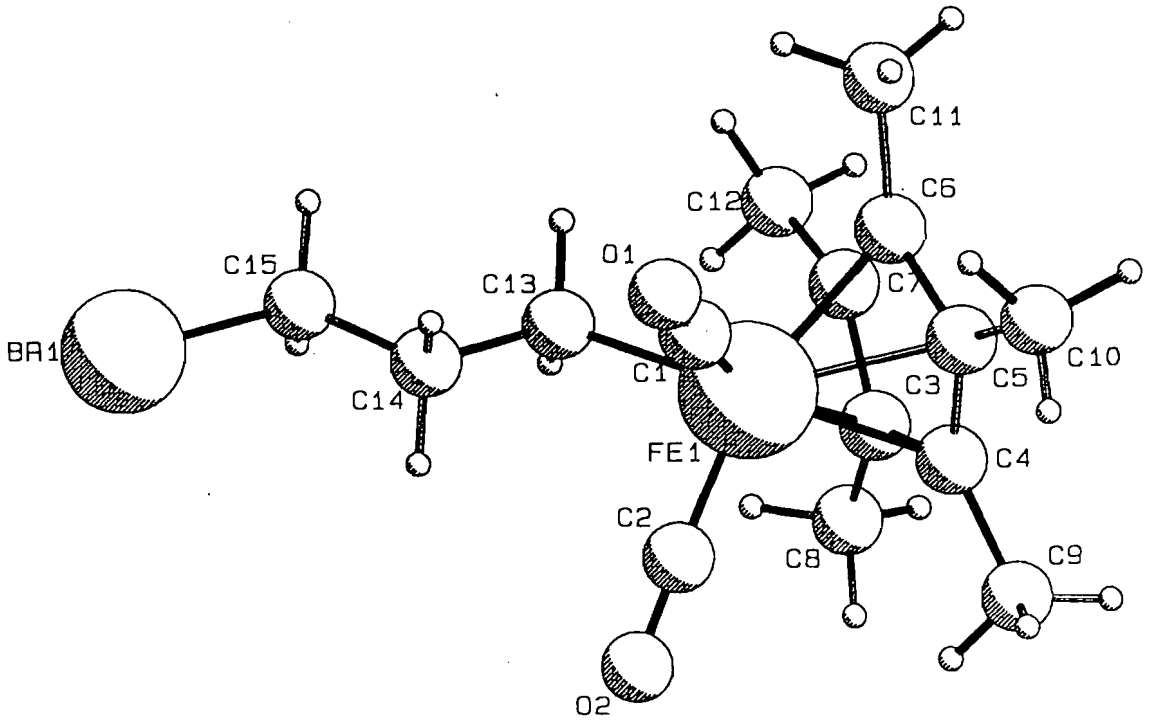


**Figure 2.8** Molecular structure of **7** showing atom labelling.

The pentamethylcyclopentadienyl ligand is bound to the metal atom in a $\eta^5$ manner, and there are two terminal carbonyl ligands. The Fe-C(Cp*) bond lengths are consistent within experimental error ranging from 2.099(4) – 2.114(5) Å. The Fe-C(Cp') average distance is slightly longer than the average Fe-C(Cp) distance reported for ferrocene, 2.056(2) Å.[93] This reflects the ability of the carbonyl ligands to bond more strongly to transition metals than Cp or Cp' ligands. The orientation of the pentamethylcyclopentadienyl ring atoms (C3 – C7), is planar with a mean deviation from the plane of 0.010(5) Å. The iron atom is displaced from this plane by 1.727(2) Å. The propyl chain is staggered as expected with C-C bond lengths averaging 1.507Å and the C-C-C angle averaging 110°(Figure 2.9). Other bond lengths and angles are within expected ranges for related published structures.[94],[95] An interesting aspect of this structure is its molecular packing, shown in Figure 2.10. The packing is determined mostly by van der Waals forces with no intermolecular hydrogen bonds detected. The molecules are all orientated with their long axes nearly normal to the (100) crystal planes. The screw axes parallel to b generate layers within which the molecules are in a very regular 'head-to-tail' antiparallel orientation. Operation of the c-glide on these layers generates molecular stacks parallel to c, two such stacks being shown in Figure 2.10.



**Figure 2.9** A stereoview of **7** showing the staggered chain conformation.

**Table 2.1** Details of intensity data-collection and structure refinement for **Fp*3Br (7)**.

| | |
|---|---|
| Colour/shape | yellow/ tabular |
| Empirical formula | $C_{15}H_{21}O_2FeBr$ |
| Formula weight /gmol$^{-1}$ | 369.082 |
| Temperature /K | 248 |
| Crystal system | Monoclinic |
| Space group | $P2_1/c$ |
| Unit cell dimensions: a/Å | 11.455(5) |
| b/Å | 12.438(4) |
| c/Å | 11.778(4) |
| β/° | 107.22(3) |
| Volume /Å$^3$ | 1603(1) |
| Z | 4 |
| Density (calculated) /gcm$^{-3}$ | 1.53 |
| Absorption coefficient /cm$^{-1}$ | 34.1 |
| F(000) | 752 |
| Crystal size /mm | 0.25 x 0.2 x 0.4 |
| θ range for data collection/° | 1 – 25 |
| Index ranges | 0,13; -14,0; -14,14 |
| Total no. reflections | 3107 |
| No. unique reflections | 2504 |
| $R_{int}$ | 0.0676 |
| Transmission/max; min; av. (%) | 85.05; 99.85; 95.31 |
| No. obs data [I>2σI] | 2034 |
| No. param. Refined | 189 |
| Final R indices | 0.039 |
| Rw | 0.043 |
| Weighting function | $[\sigma^2(F_o) + 0.001628F_o^2]^{-1}$ |
| Goodness-of-fit on $F^2$ | 1.19 |
| Scan width /° | 0.85 + 0.35tanθ |
| Aperture width/mm | 1.12 + 1.05tanθ |
| Largest diff.peak and hole/eÅ$^{-3}$ | 0.26; -0.21 |

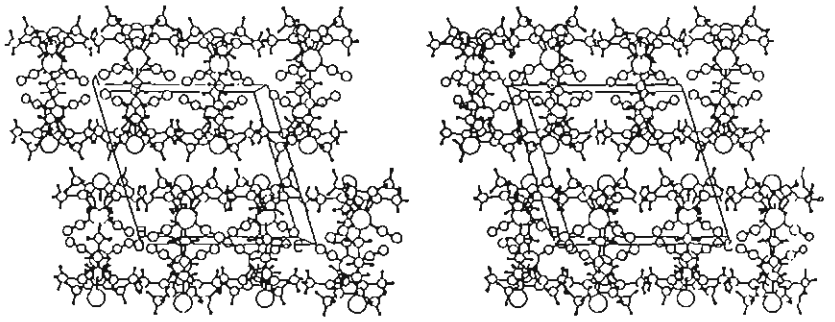

**Figure 2.10** Packing diagram for **7** viewed down the b-axis .



### Structure determination of the Fp dimer (23)

In an attempt to grow single crystals of the acyl benzyl alcohol **19**, crystals of a second and different species, were formed together with the crystals of **19**. Both crystals were orange in colour and visibly indistinguishable. The species was later shown to be a dimer, **23** (Figure 2.11). The x-ray structure confirmed that the compound is the diacyl species.

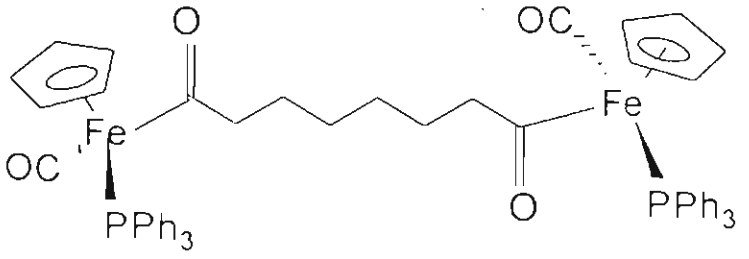


**Figure 2.11** Structure of the Fp dimer (**23**).

Rectangular orange crystals were grown from a $CH_2Cl_2$/hexane solution at –15°C. Oscillation and Weissenberg photography revealed 2/m Laue symmetry, indicating the monoclinic crystal system. The lack of any systematic absences among general reflections on upper level Weissenberg and precession photographs indicated the presence of a primitive lattice. There were no conditions on hkl but conditions on h0l (h+ l = 2n) and 0k0 (k = 2n) were observed. The space group $P2_1/n$ (alternative setting of $P2_1/c$) was assigned from these data. Both of the iron atoms were located using Patterson methods and the remaining non-hydrogen atoms found after successive difference Fourier syntheses. Five cycles of least-squares refinement were required for the positional and thermal factors to reach convergence. Successful structure refinement followed giving a final R factor of 0.075. Details of the intensity data-collection and structure refinement are listed in Table 2.2. Experimental details are given in section 7.1. The molecular structure with the atomic numbering scheme is shown in Figure 2.12. Fractional atomic coordinates, anisotropic displacement parameters, bond lengths, bond angles and torsion angles appear in Appendix 2a (Tables A1 to A6) and structure factor data are included in Appendix 2b (on diskette).

**Table 2.2** Details of intensity data-collection and structure refinement for the **Fp dimer (23)**.

| | |
|---|---|
| Colour/shape | Orange/ rectangular |
| Empirical formula | $C_{56}H_{52}O_4P_2Fe_2$ |
| Formula weight /gmol$^{-1}$ | 962.72 |
| Temperature /K | 233 |
| Crystal system | Monoclinic |
| Space group | $P2_1/n$ |
| Unit cell dimensions: a/Å | 9.343(3) |
| b/Å | 15.007(3) |
| c/Å | 33.177(5) |
| β/° | 93.18(2) |
| Volume /Å$^3$ | 4644(2) |
| Z | 4 |
| Density (calculated) /gcm$^{-3}$ | 1.38 |
| Absorption coefficient /cm$^{-1}$ | 7.37 |
| F(000) | 2008 |
| Crystal size /mm | 0.4 x 0.25 x 0.2 |
| θ range for data collection/° | 1 – 25 |
| Index ranges | -11, 11; 0,17; 0,39 |
| Total no. reflections | 8646 |
| No. unique reflections | 5769 |
| $R_{int}$ | 0.0326 |
| Transmission/max; min; av. (%) | 93.65; 99.68; 95.55 |
| No. obs data [I>2σI] | 3362 |
| No. param. refined | 328 |
| Final R indices | 0.075 |
| Rw | 0.065 |
| Weighting function | $[\sigma^2(F_o)]^{-1}$ |
| Goodness-of-fit on $F^2$ | 2.70 |
| Scan width /° | 0.75 + 0.35tanθ |
| Aperture width/mm | 1.12 + 1.05tanθ |
| Largest diff.peak and hole/eÅ$^{-3}$ | 0.71; -0.50 |

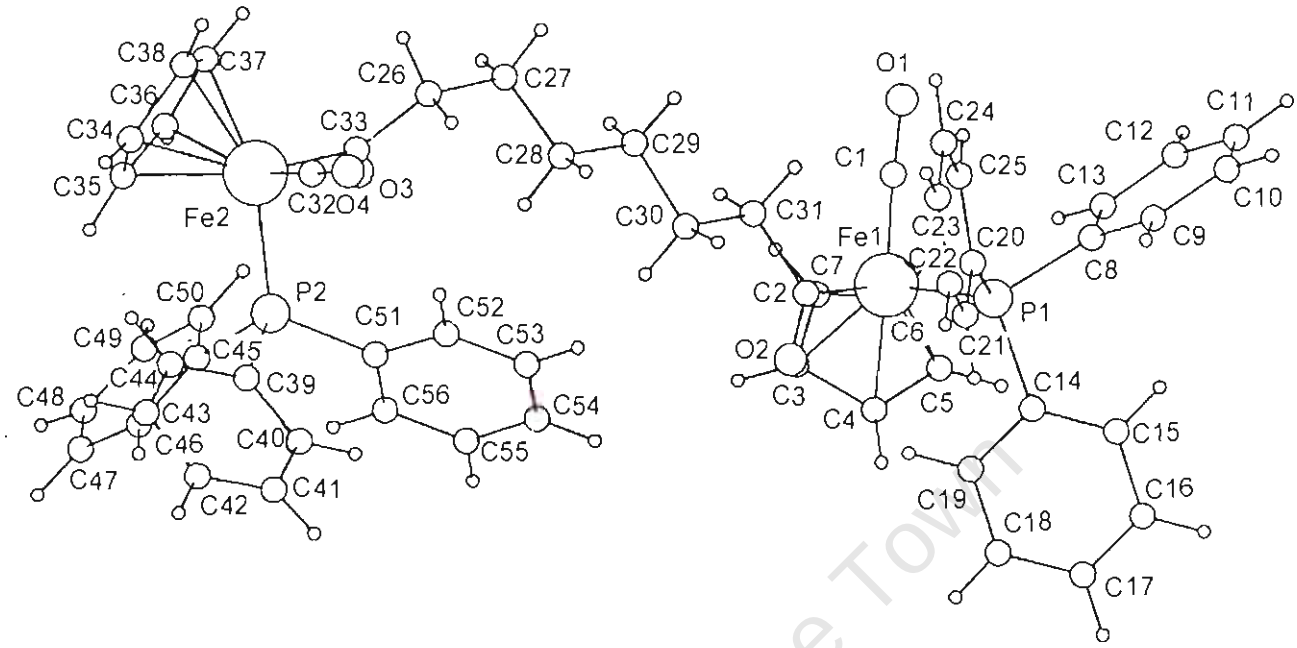


**Figure 2.12** Molecular structure of **23** showing atom labelling.

The structures of iron acyl complexes are usually described in terms of pseudo-octahedral arrangement of ligands around the iron atom.[96] The X-ray data obtained show that this structure corresponds closely to the generalised picture. The angles C(acyl)-Fe-C(carbonyl) and C(acyl)-Fe-P are between 90 and 95°, due to repulsion between the carbonyl groups. The dihedral angle, O(2)-C(2)-Fe(1)-C(1) of –167.3(9)° and corresponding angle O(3)-C(33)-Fe(2)-C(32) of 154.6(9)° indicates the approximate anti-arrangement of the free carbon monoxide ligand and the acyl carbonyl ligand. An average Fe-P distance of 2.2 Å indicates the spatial requirement for the iron atoms surrounded by such bulky ligands. Each phenyl ring is rotated about 90° with respect to the adjacent phenyl ring to give a propeller-like structure. Fe-C(Cp) bond lengths range from 2.08(1) – 2.16(1) Å. The cyclopentadienyl rings are planar with a mean deviation from the plane of 0.01 – 0.02 Å.

Each iron atom in the dimer is a chiral centre. The two chiral centres in the moleclue are different: one chiral centre is "R", the other "S". This is in accordance with other iron chiral compounds described in the literature.[88]

The alkyl chain adopts an extended staggered conformation, similar to Fp*3Br **7**. The alkyl chain however is slightly twisted in **23**, possibly due to the "trans" arrangement of the Cp groups. In this molecule, the Cp groups appear to be on opposite sides of the molecule, which differs from the conformation in other related acyl compounds without $PPh_3$ groups. The length of the alkyl chain and the presence of the $PPh_3$ group thus appear to influence the conformational properties of these iron acyl complexes.

C-C bond lengths average 1.507 Å and C-C-C angles average 110°. The stereoview shown in Figure 2.13 clearly illustrates these points. Other bond lengths and angles are within expected ranges for related published structures.[97,98]

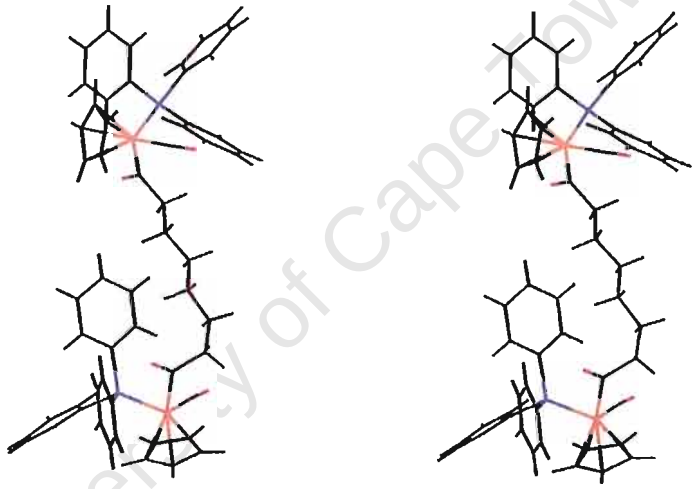



**Figure 2.13** A stereoview of **23**.

Selected bond lengths and angles are listed below:

| | | | |
|---|---|---|---|
| P1 – C8 | 1.84(9) Å | | |
| P1 – C14 | 1.84(9) Å | | |
| P1 – C20 | 1.83(9) Å | | |
| P2 – C51 | 1.82(1) Å | Fe1 – P1 | 2.184(3) Å |
| P2 – C39 | 1.82(1) Å | Fe2 – P2 | 2.217(3) Å |
| P2 – C45 | 1.86(1) Å | | |

There are four molecules in the unit cell as shown in Figure 2.14. The $2_1$ screw axis and n-glide result in the zig-zag type of arrangement that is observed. The Cp ring and one of the phenyl rings of the $PPh_3$ group of a symmetry related molecule appear to be nearly coplanar. It is the introduction of the $PPh_3$ group that introduces chirality into the molecule.

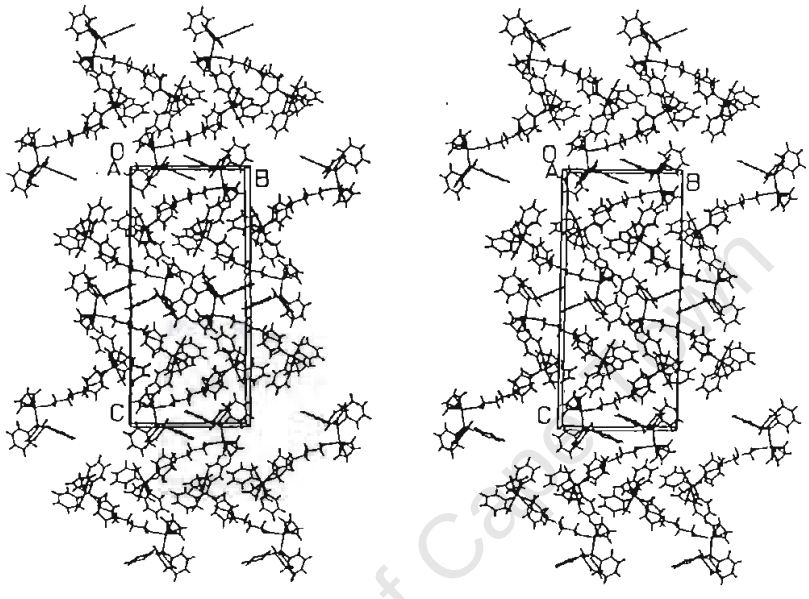


**Figure 2.14** Packing diagram for **23** viewed down the a-axis.

There are also some weak inter- and intramolecular interactions between carbonyl acceptors and phenyl donors.

| | | | |
|---|---|---|---|
| H19...O2 | 2.37(1) Å | C19-H19...O2 | 155.3(9) ° |
| H50...O3 | 2.48(1) Å | C50-H50...O3 | 150(1)° |
| H22...O2 | 2.25(1) Å | C22-H22...O2* | 166(1)° |

* denotes the symmetry related position –x, -y+1, -z+2

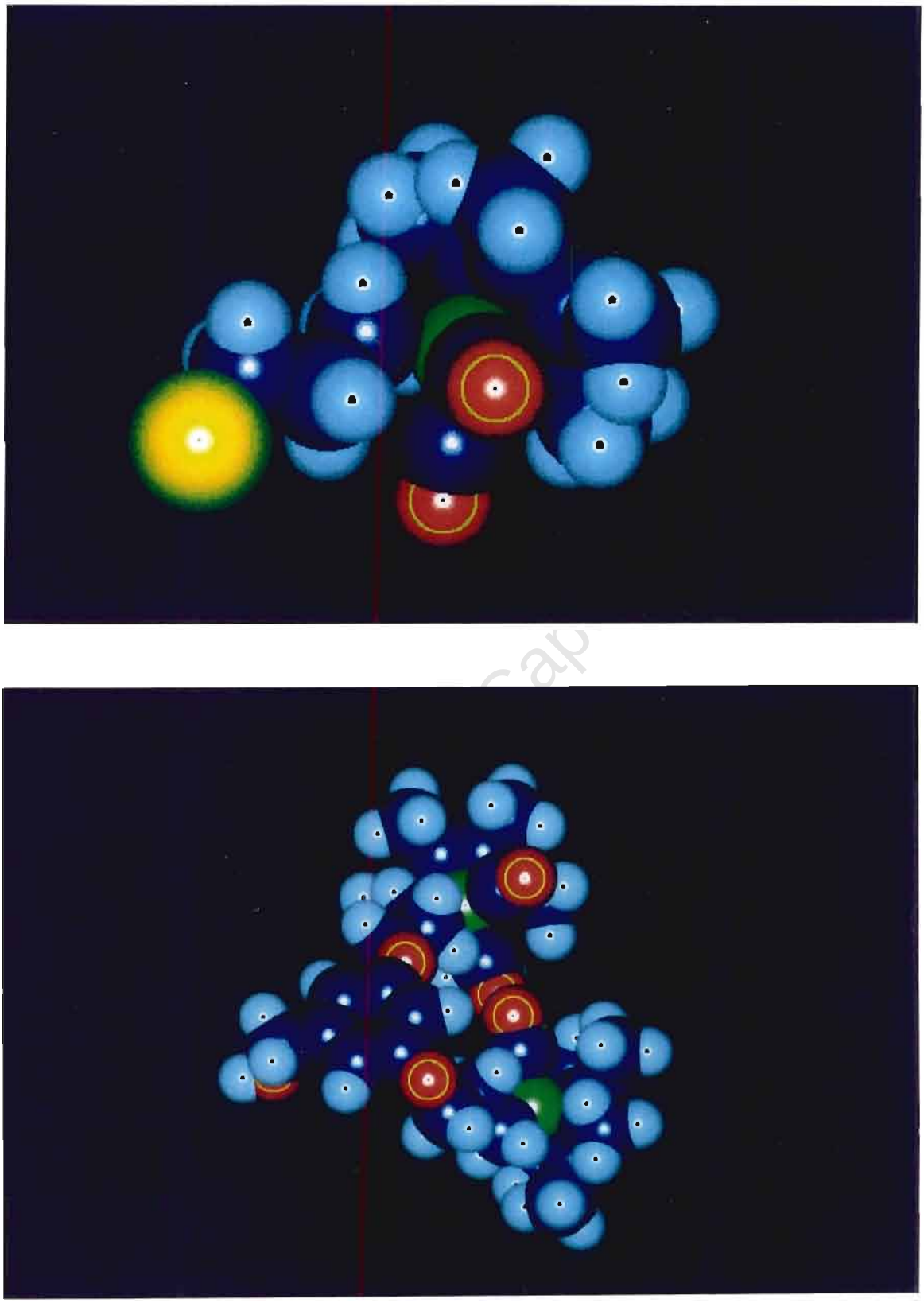

**Figure 2.15** Calculated space-filling models of (a) **7** and (b) **11**.

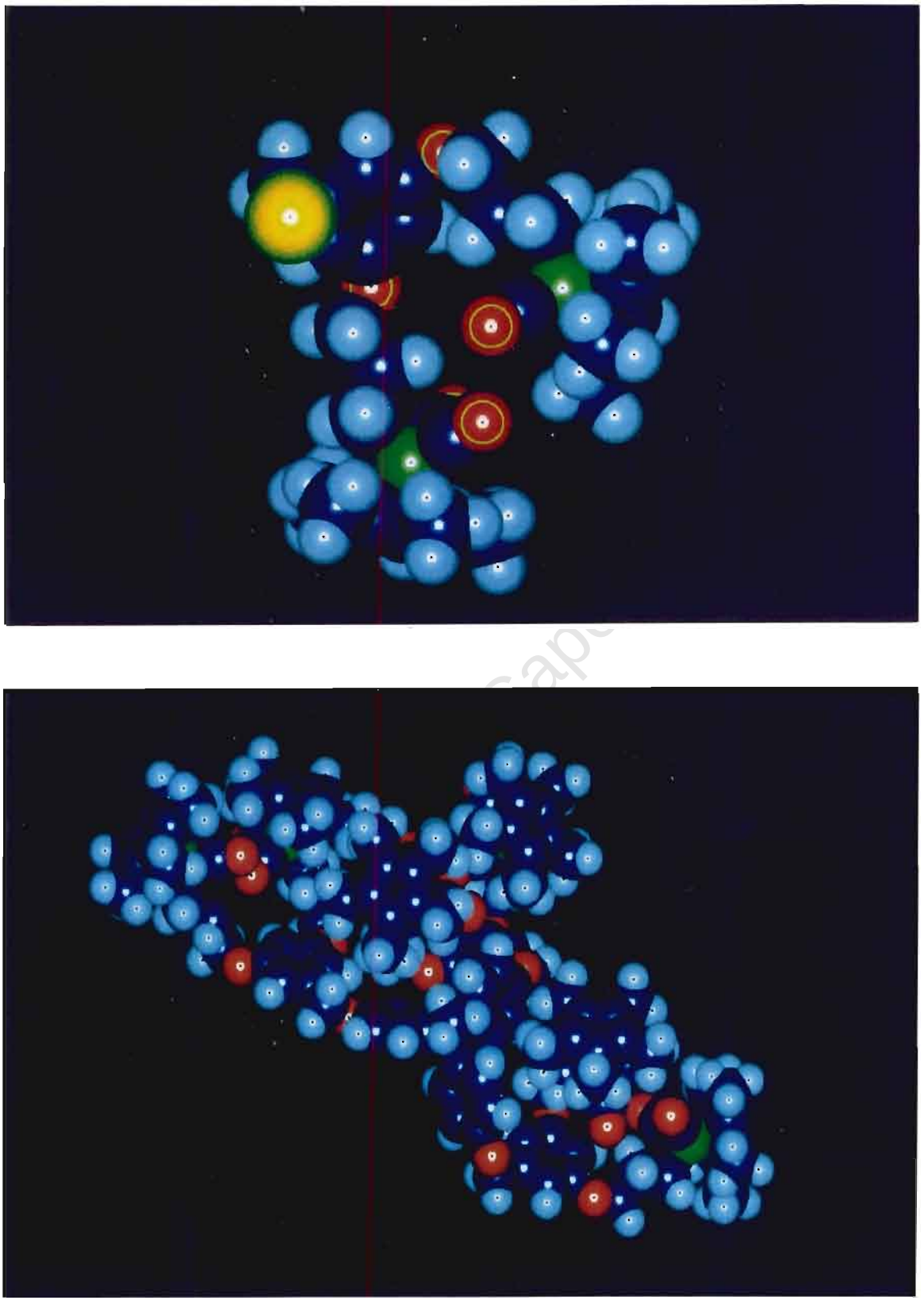

**Figure 2.15** Calculated space-filling models of (c) **14** and (d) **15**.

### 2.3.3 Electrochemical behaviour of organoiron dendritic wedges

Electron transfer reactions are of great importance in homogeneous catalytic reactions.[100] Cyclic voltammetry (CV) is a versatile electroanalytical technique for studying electron transfer processes and transient redox species over a wide potential range.[101] CV provides an excellent opportunity to study redox processes, particularly for organo-transition metal complexes.

The main focus of these cyclic voltammetry experiments was to determine whether there was any communication or interaction between the metal atoms on the surface of the dendrimer.

We specifically wished to see if oxidation of one of the metal atoms would affect the oxidation behaviour of the remaining metal atoms in the dendrimer. It might become progressively more difficult to oxidise the other iron atoms after one iron has been oxidised.

Several electrochemical studies have been carried out on ferrocene-containing dendrimers.[48d, 103] Cyclic voltammetric studies on poly(aryl ether) dendrimers containing 3, 6 or 24 surface ferrocene functionalities indicated that the ferrocenyl moieties are non-interacting redox centres. The metal centres were also shown to be electrochemically equivalent and oxidisable at the same redox potential.[103]

The apparatus used for the cyclic voltammetry experiments comprised of a three-electrode cell consisting of a $Ag/Ag^+$ reference electrode, a platinum wire auxiliary electrode and a platinum disc working electrode. The experiments were performed under an argon atmosphere. Full details of the experimental procedure can be found in the experimental (section 7.1).

The monomeric complex **7** (one Fe atom), dendritic wedge **14** (two Fe atoms) and first generation dendrimer **15** (six Fe atoms) were studied by CV at room temperature in acetonitrile solution. The cyclic voltammograms of complexes **7**, **14** and **15** are shown in Figure 2.16. All the scans were initially run in an oxidising direction (towards more positive potential) over various potential ranges and at a speed of 100 mV/sec.

For all three complexes, **7**, **14** and **15**, a single irreversible oxidation peak is observed. The peaks are all broad, possibly due to the low concentration of the solutions used. Table 2.3 lists the oxidation peaks of several dendritic wedges and the first generation six-metal dendrimer. The oxidation peaks occur at higher potentials in the dendritic wedges and dendrimer, *e.g.* at around 700 mV for complex **14** compared with mononuclear metal complex **7** which occurs at 567 mV. This indicates that the dendritic wedges are slightly more difficult to oxidise than the mononuclear compound, possibly because of the bulkiness of the increased number of Cp* ligands.

**Table 2.3** Cyclic voltammetry data for selected iron dendrimers and dendritic wedges

| **Compound** | **Oxidation peak, $E_{pa}$ /mV** |
|---|---|
| ferrocene (reference) | +147 |
| Fp*3Br (**7**) | +567 |
| 3,5-dihydroxybenzyl alcohol | +1181 |
| Fp*3G1Br (**14**) | +700 |
| Fp*3G1C (**15**) | +785 |

The voltammograms suggest that the oxidation of one of the metal atoms on the dendrimer surface does not affect the oxidation of the remaining metals. Multiple oxidation peaks would be expected if the oxidation of one metal influenced the oxidation behaviour of further metals in a complex.

The oxidation peaks also tend to be quite broad, more so for the dendrimer than the other complexes. This could be due to the simultaneous oxidation of all six of the metal atoms in the dendrimer from $Fe^{II}$ to $Fe^{III}$. These experiments are unable to show how many electrons are transferred but there are other techniques such as chronocoulometry that could be used to aquire such data.

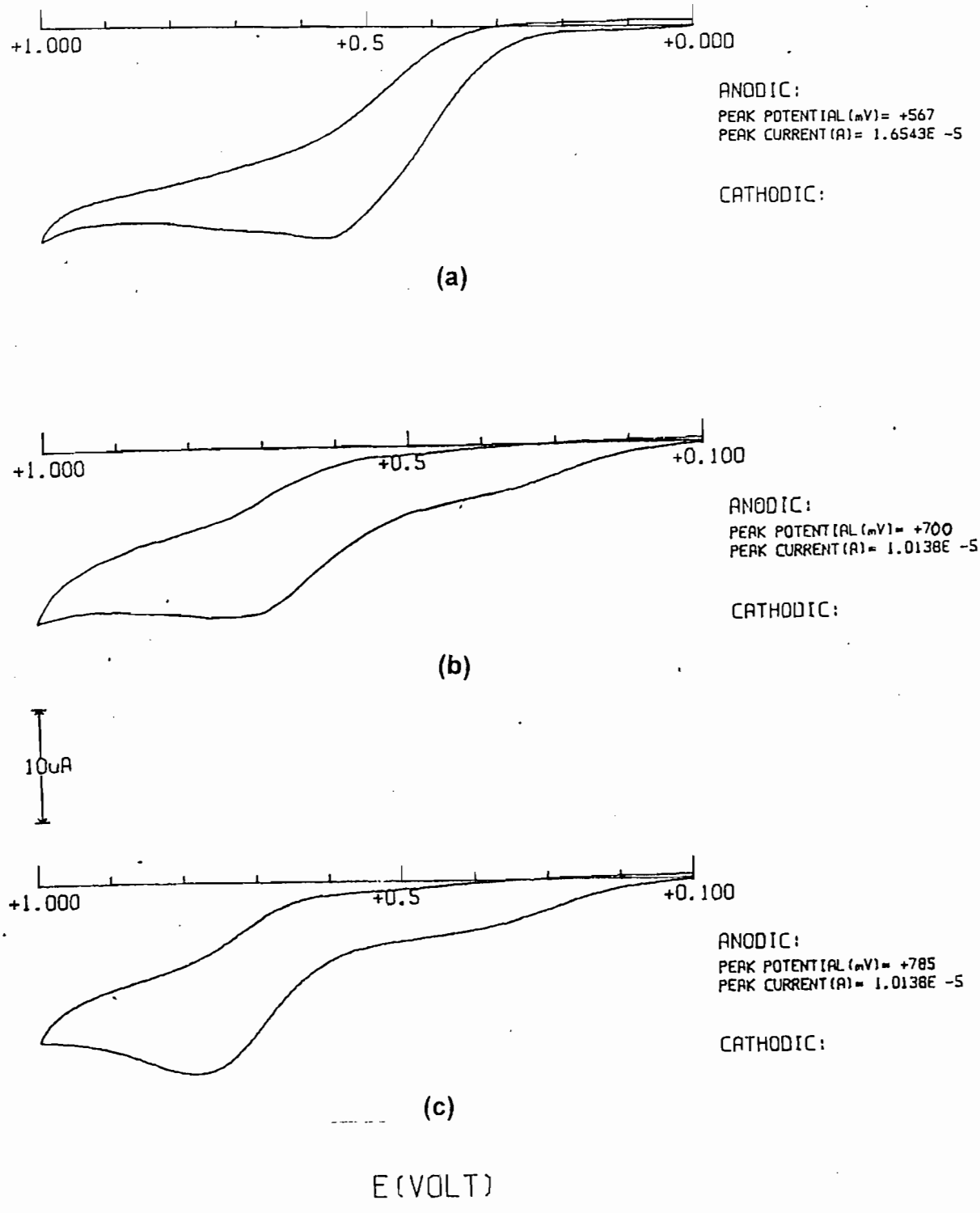


**Figure 2.18** Cyclic voltammograms of (a) **7** (b) **14** and (c) **15** in $CH_3CN$.

Other workers from our laboratories have found that the related complex, $[CpFe(CO)_2(CH_2)_6Br]$ **2** showed an irreversible oxidation peak at *ca.* 0.62 V, and a quasi-reversible redox couple at -0.15 V, which could only be seen after oxidation at *ca.* 0.6 V.[102] This indicated that a new species, possibly an acyl species, was formed at the electrode surface after the oxidation reaction. Although such a quasi-reversible redox couple was not evident in the CVs of the compounds examined here, we can assume that some new species was formed after oxidation that prevented the cycle from being reversible.

Cp iron alkyl carbonyl complexes undergo oxidatively induced carbonyl insertion reactions into the metal-alkyl bond. The consequent migration insertion occurs rapidly and gives a huge increase in the equilibrium constant for insertion in comparison to the neutral 18-electron complexes.[103] The induced alkyl migration or CO insertion reaction is a possible explanation for the irreversibility of the oxidation as shown by our complexes.

Giering *et al.* carried out CV studies on $[CpFe(CO)_2(CH_3)]$ in various solvents and at various temperatures.[104] They assigned the quasi-reversible couple to a solvent assisted carbonyl insertion product $[CpFe(S)(CO)(COR)]^+$ (where S = solvent), which was formed just after the oxidation reaction. A similar oxidatively induced CO insertion reaction has been shown to take place for complexes such as $CpFe(CO)(PPh_3)CH_3$.[105] The suggested mechanism for the alkyl-to-acyl migration of the 17-electron complex $CpFe(CO)(PPh_3)CH_3^+$ is a two-step process, the first step being a second-order process. Scheme 2.12 suggests a mechanism for a possible alkyl migration reaction occurring upon oxidation of the complexes in Table 2.3 The acetonitrile solvent acts as a nucleophile.

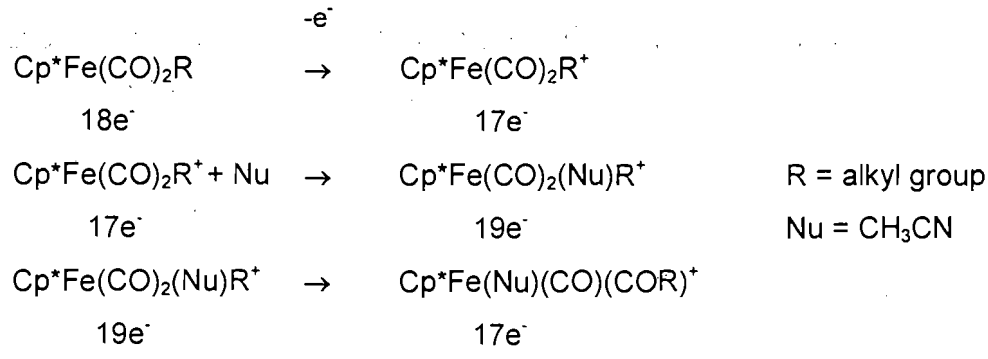


**Scheme 2.12**

**Table 2.4** TGA data for selected iron dendritic wedges and dendrimers.

| Compound | wt. Loss (%) | $T^d$/°C |
|---|---|---|
| Fp*3Br (**7**) | - | 118 |
| Fp*3G1OH (**11**) | - | 150 |
| M Fp*3G1OH(**10**) | 6.2[a] | 46.4 |
| Fp*3G1Br(**14**) | 7.7; 8.0 | 72.6; 129.1 |
| Fp6ABr (**18**) | 2[b] | 56 |
| Fp6AG1OH(**19**) | - | 128 |
| Fp6AG1Br(**20**) | <1[c] | 62 |

[a] small amount of included $CH_2Cl_2$

[b] small amount of included acetone

[c] small amount of included $CHCl_3$

[d] temperature corresponding to the onset of a peak

The DSC traces for all the complexes of interest were recorded over the temperature range 30 - 200 °C under nitrogen and the traces for **7**, **11**, **14** and **18** are shown in Figure 2.19. Additional DSC data is summarized in Table 2.5. Full experimental details can be found in the experimental (section 7.1).

The DSC traces generally showed one endothermic peak which could be assigned to melting (Figure 2.17). The peak temperatures corresponded with the melting points of the samples as determined using the hot-stage microscope. For Fp*3G1Br **14**, there is a sharp exothermic peak directly after the enothermic peak. This suggests that decomposition takes place immediately after melting. This result parallels the results found during synthesis.

In the case of **20**, the iron acyl benzyl bromide, there is an exothermic peak followed by an endothermic peak. The exothermic peak at 71 °C could be assigned to decarbonylation and the endothermic peak at 115 °C, to the melting of **20**. Iron acyl compounds are known to undergo decarbonylation fairly easily. The temperatures compared well with the melting point determined by the hot-stage microscope. Complexes of the type $[CpFe(CO)(PPh_3)R]$ are known to undergo β-hydride elimination to give alkenes and a hydride complex $[CpFe(CO)(PPh_3)H]$.[109] A broad endothermic peak for ferrocene has been observed for these type of complexes.[102] The Br and $PPh_3$ groups may play an important role in the thermal decomposition process but further studies would be needed to confirm this.

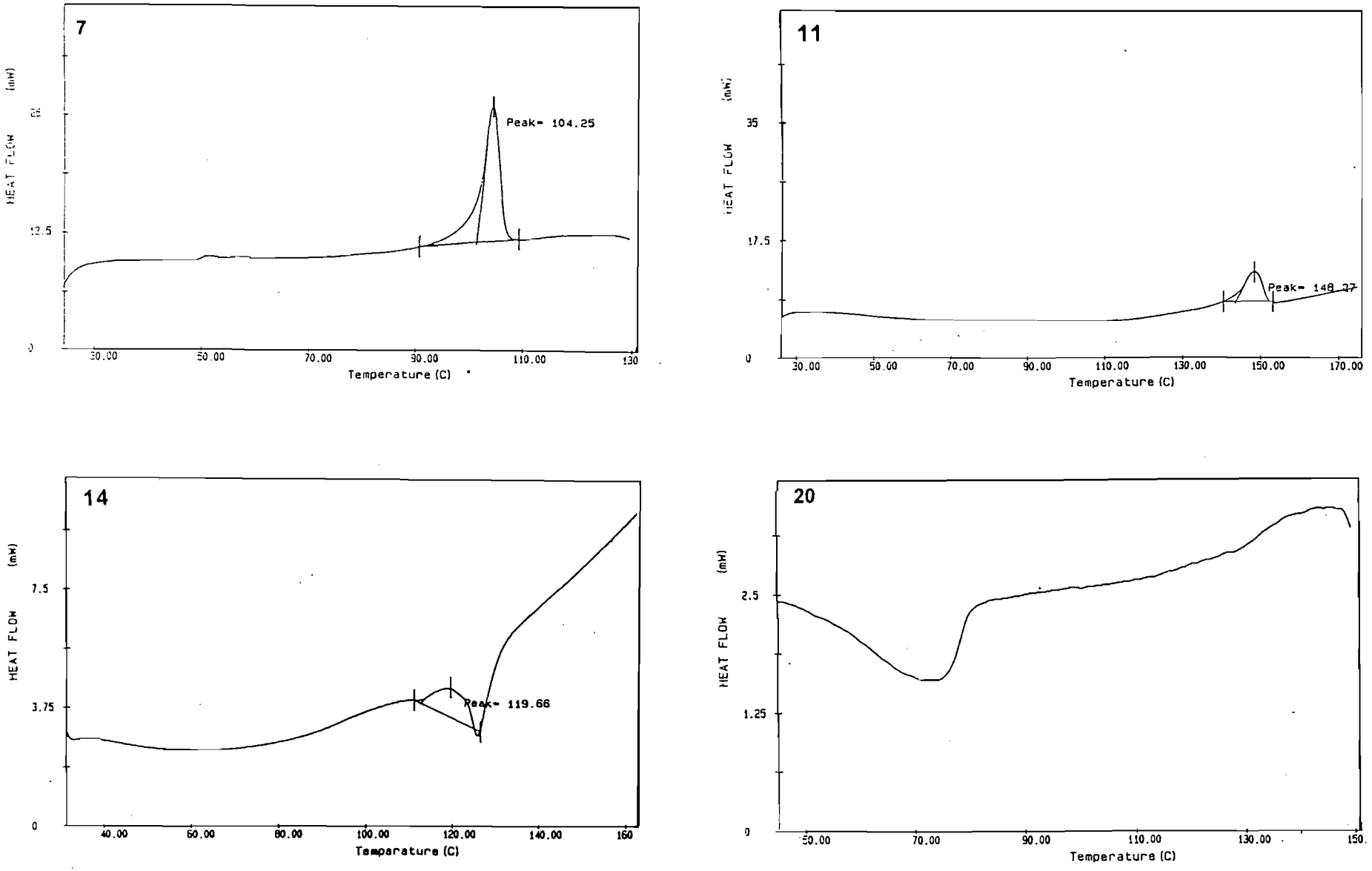


**Figure 2.19** DSC traces of complexes **7**, **11**, **14** and **20**.

**Table 2.5** DSC data for selected dendrimers and dendritic wedges.

| Compound | mp[a]/°C | $T_{max}$[b] / °C | $\Delta H_{endo}$[c] /kJmol$^{-1}$ | Explanation |
|---|---|---|---|---|
| Fp*3Br (**7**) | 98 – 102 | 104.3 (endo) | 59.92 | Melting |
| Fp*3G1OH (**11**) | 150 – 153 | 148.3 (endo) | 29.38 | Melting |
| m Fp*3G1OH(**10**) | 50 | 36.1 (endo)<br>48 | 3.63 | Solvent loss<br>Melting |
| Fp*3G1Br(**14**) | 125 | 119.7 (endo)<br>125.0 (exo) | 33.01 | Melting<br>Decomposition |
| Fp6ABr (**18**) | 102 | 103.5 (endo) | 37.18 | Melting |
| Fp6AG1OH(**19**) | 73 - 79 | >140 (endo) | 29.18 | Melting |
| Fp6AG1Br(**20**) | 63 - 74 | 71.2 (exo)<br>142.8 (endo) | 16.52<br>8.20 | Decarbonylation<br>Melting |
| Fp6AG1C(**21**) | oily | 36.2 (endo) | 8.58 | Melting |

[a] determined on a Kofler hotstage microscope

[b] temperature corresponding to the peak maximum

[c] calculated by Perkin Elmer PC Series DSC7 machine (in J/g)

The length of the hydrocarbon chain seems to have some effect on the thermal properties of the dendritic wedges. An increase in alkyl chain length caused a decrease in the melting temperature. A decrease in the melting temperature was also observed in going from the benzyl alcohol (*e.g.* **11**) to the benzyl bromide (e.g. **14**). This again confirms the increased stability of the benzyl alcohols relative to the benzyl bromides.

## 2.4 Chemical reactivity studies on organoiron dendritic wedges

There is little work in the literature on the reactivity of dendrimers; this is in contrast to the vast amount of literature available on mononuclear complexes.[84,110,111] We initially investigated a dendritic wedge and reacted it with several tertiary phosphine and nitrogen donor ligands that can form chelate complexes. Again we wished to determine whether the metal centres would act independently or not, if they were electronically linked via a spacer ligand.

### 2.4.1 Attempts at linking the metal centres of a dendritic wedge

Several experiments with a variety of reagents were carried out to try to link the metal centres of a dendritic wedge (Scheme 2.13 and 2.14). The aim of these experiments was to try to establish if we could generate electronic communication between the two metal centres. Electrochemistry would be a simple and useful method of determining whether the two metals (either two different metals such as Fe-Ru or the same two metals e.g. Fe-Fe) behaved independently or not. The focal point of the dendrimer would remain intact and still be available for reaction. These bridged-metal compounds would represent a new class of dendritic systems and their physical behaviour might be different from that of the Fp, Fp* and Fp acyl dendrimers already prepared.

The iron benzyl alcohol wedge, **4**, was reacted with several phosphorus and nitrogen ligands in refluxing benzene for 24 hours. Table 2.7 summarises the results given by the results shown in Schemes 2.13 and 2.14.

**Table 2.7** Reaction of **4** with phosphine and nitrogen ligands.

| Ligand | Product no. | IR $\nu$(CO)[a] /cm$^{-1}$ |
|---|---|---|
| Triphenylphosphine | **19** | 1911, 1598 |
| dppm* (1:1 mol) | **25**<br>**24** | 2000, 1940, 1916, 1596 (major)<br>2000, 1940, 1596 (minor) |
| dppm (excess) | **24** | 2000, 1940, 1593 |
| 4,4'-bipyridyl (excess) | **26b** | 1918, 1595 |
| 4,4'-bipyridyl + oxidant | **27** | 2000, 1940, 1592 |
| 1,4 phenylene diamine | **28** | 1992, 1947, 1597 |

* dppm = bis (diphenylphosphino) methane

[a] IR spectra recorded in $CH_2Cl_2$

Benzene, reflux 22h
PPh3
Benzene, reflux 24h
Ph2PCH2PPh2
(1:1 mol)
ex
Ph2PCH2PPh2
19
25 (major)
+
24 (minor)
25

Scheme 2.13

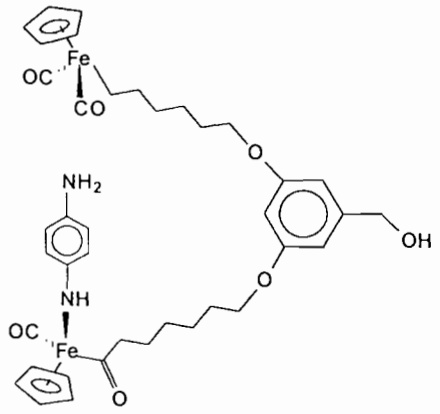

28

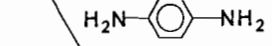

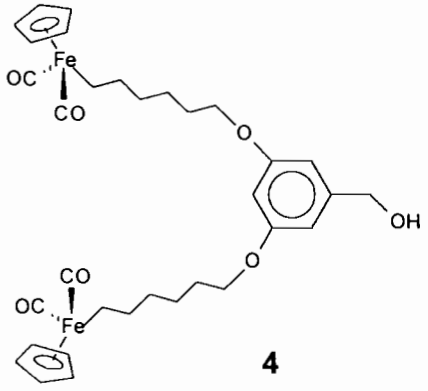

4

Benzene, reflux 22h

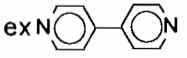

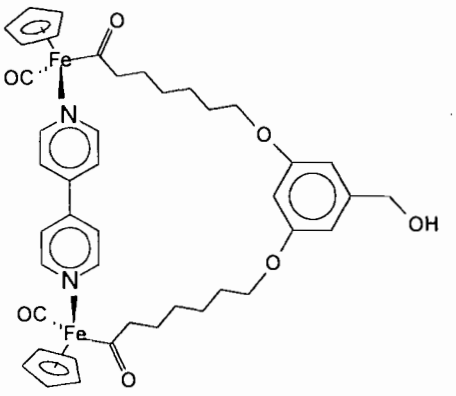

26a

OR

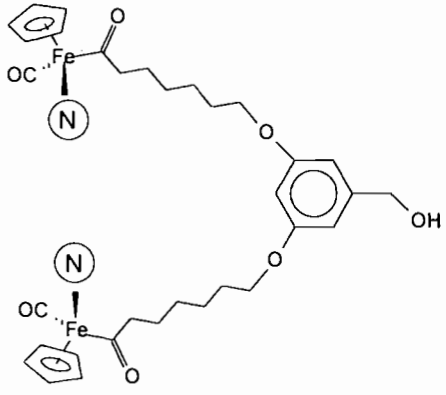

26b

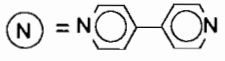

Benzene, reflux 24h

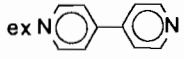

+ oxidant

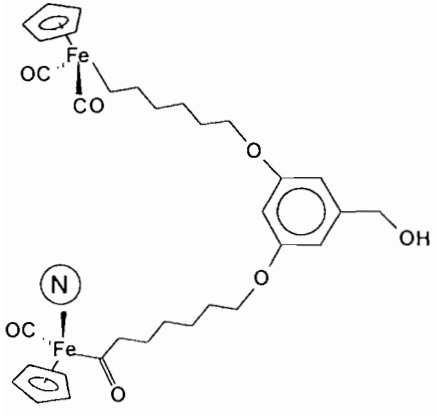

27

Scheme 2.14

IR spectroscopy proved effective for monitoring the progress of the reactions. The number and position of the carbonyl bands in the IR spectra were used to predict the substitution patterns. A new carbonyl band at around 1600 $cm^{-1}$ and a shift in the terminal carbonyl band to around 1916 $cm^{-1}$ suggested the formation of an acyl species. Reaction of $PPh_3$ with **4** in refluxing benzene (Scheme 2.13) gave the "disubstituted" benzyl alcohol **19** which we have prepared previously via another route (see section 2.2.3). In the reaction of **4** with bis(diphenylphosphino)- methane (dppm) (1:1 mol ratio) two products were isolated. The IR spectrum of the major product, **25** showed four carbonyl bands of equal intensity suggesting that only one of the iron centres had been substituted with the phosphine ligand. $^{31}P$ NMR spectroscopy of **25** confirmed this: a doublet at 73.2 ppm confirms the coordinated phosphorus and a second doublet at 23.8 ppm confirms the free phosphorus (Figure 2.18).

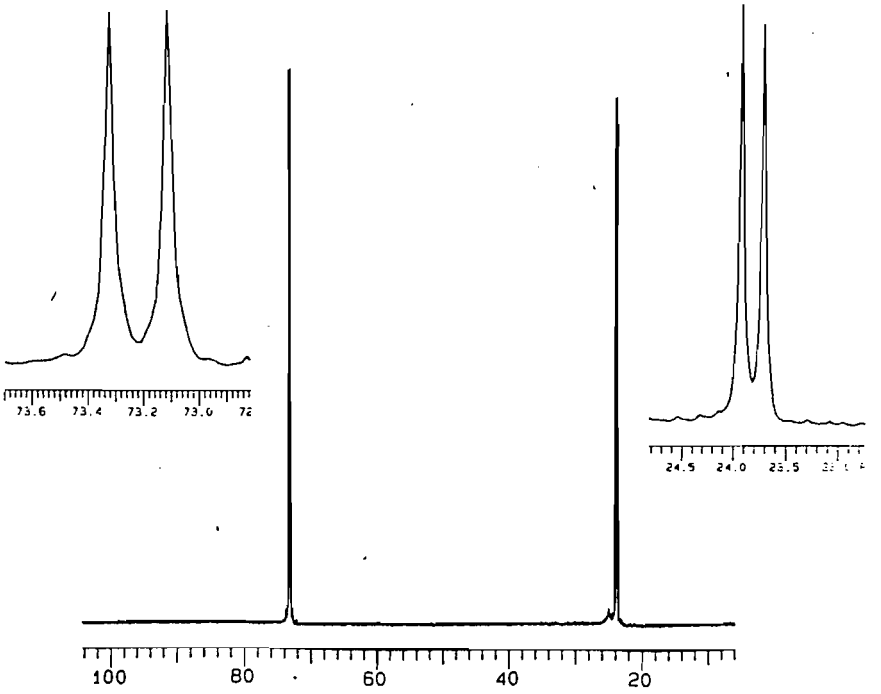


**Figure 2.18** The 80 MHz $^{31}P$ NMR spectrum of **25**.

The IR spectrum of the minor product **24** showed three bands, suggesting that only one of the iron centres had been substituted. A product where the two phosphorus atoms bridge one iron centre was proposed (Scheme 2.13). The reaction was repeated using excess dppm, and again gave the phosphorus bridged species **24**. The bis dppm is very bulky due to the diphenylphosphine groups and this is perhaps the reason for the ligand not linking the iron centres. The bite angle of the dppm ligand is also a factor that should be considered. A less sterically hindered phosphine ligand or a ligand with a slightly longer tether such as bis(diphenylphosphino)ethane might link the two metal centres.

The dendritic wedge, **4** was also reacted with a series of nitrogen donor ligands (Scheme 2.14). The IR spectrum of the reaction product from **4** with 4,4'-bipyridyl showed two carbonyl peaks; *viz* one terminal and one acyl peak. This suggested that either the bridged product, **26a** or di-substituted product **26b** had formed. $^1$H NMR spectroscopy of the reaction product confirmed the latter **26b** by integration of the aromatic protons.

It has been shown that addition of an oxidant can induce a redox-catalysed carbonylation reaction.[112] The reaction with 4,4'bipyridyl was repeated in the presence of the ferrocenium cation which was generated by addition of $AgBF_4$ to ferrocene in THF. The reaction was monitored by IR spectroscopy. However this oxidant did not seem to make much difference and compound **27** was suggested as the product that was formed. $^1$H NMR spectroscopy confirmed this.

The above ligands were not successful in linking the metal atoms of the dendritic wedge. The 4,4-bipyridyl is very rigid and can only span a certain distance. The length of the alkyl chain in the dendritic wedge possibly undergoes free rotation around the ether oxygen and thus the iron atoms are further apart than expected. A more flexible ligand might have been better for these reactions.

Isonitrile ligands are known to function as both bridging and terminal ligands.[113] A preliminary reaction of the haloalkyl complex, Fp6ABr with $^t$butyl isocyanide was carried out. The IR spectrum showed two new carbonyl bands at 1941 and 1610 $cm^{-1}$ and an additional band at 2127 $cm^{-1}$ due to the CNR stretch. This suggests that a ligand of this type might be suitable for linking the metal centres.

### 2.4.2 Reactions of dendritic wedges with a variety of core molecules

The selection of the reactive core is of great importance since it determines the size, multiplicity and specific functions of the dendrimer.[114] The three-dimensional shape of the dendrimer can also be varied depending on whether a bi-functional, tri-functional or tetra-functional core is used. A variety of cores have been used, these include: benzene-1,3,5-tricarbonyl trichloride,[115] pentaerythritol[116] and $C_{60}$.[117] Very recently, the synthesis of a series of diphosphine ligands having phosphorus donor atoms in the core of a carbosilane dendrimer, and their use in palladium catalysed allylic alkylation was reported.[118]

The iron dendritic wedges were reacted with a variety of dendritic wedges in order to see what effect the cores had on the properties of the dendrimers. Several bi-functional and tri-functional cores were used:

(i) 1,1,1-trishydroxy ethane (see section 2.2);

(ii) benzene-1,3,5-tricarbonyl trichloride;

(iii) polyethylene glycol 2000 (see section 5.2.4).

Three equivalents of Fp6AG1OH **19** was reacted with benzene-1,3,5-tricarbonyl trichloride in THF at room temperature (Scheme 2.15). After the work-up procedure, a yellow oil **29** was isolated in 38% yield. This trichloride core has been successfully used in previous experiments to build up dendrimers containing 1,3-diaminopropan-2-ol units.[117] Full experimental details can be found in (section 7.2).

**19**

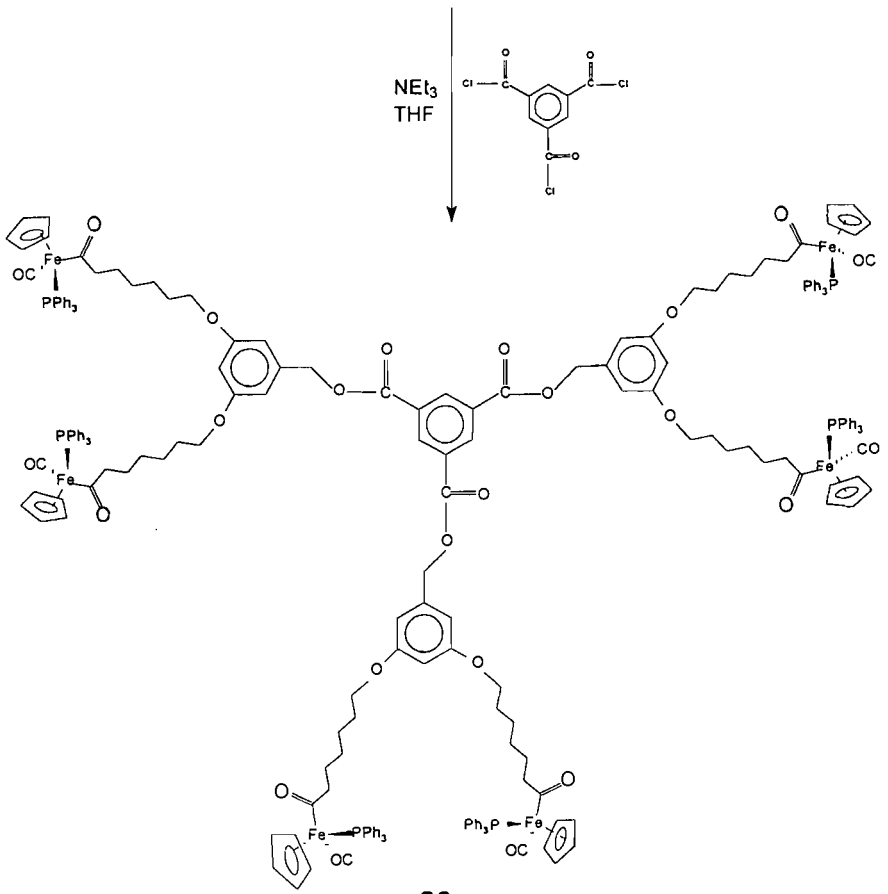


**29**

**Scheme 2.15**

## 2.5 Conclusions

In this chapter, several new organometallic dendritic wedges and first generation dendrimers have been synthesised and characterised. The convergent approach was found to be suitable, since any defects in the dendrimers could easily be detected. We have also investigated the physical and chemical behaviour of some of these complexes. The Fp compounds were found to be unstable and the benzyl bromide complexes **5** and **6** decomposed very rapidly, particularly in solution. The Fp* ligand was then introduced and several novel dendritic wedges **10** – **14** and a first generation dendrimer **15** were synthesised. The Fp* complexes were found to be more stable than the corresponding Fp complexes, but the yields of the coupling step were poor for most reactions. Several unsuccessful attempts were made to improve these yields; it was proposed that the steric bulk of the Cp* ligand causes too much congestion around the 3,5-dihydroxybenzyl alcohol molecule. The second generation dendritic wedges were also synthesised, but again the benzyl bromide complex decomposed in solution. In a final attempt to improve the yields of these reactions and the stability of the complexes, we introduced the iron acyl ligand into the dendrimer synthesis. The complexes prepared with this ligand were significantly more stable than the Fp and Fp* complexes and the yields of the coupling step also improved.

Generally, dendrimer synthesis requires high-yielding steps. The synthesis of large dendrimers is therefore extremely difficult when the synthetic steps are low yielding and the complexes unstable.

All the organoiron dendrimers and dendritic wedges synthesised were soluble in common organic solvents and could be purified by column chromatography. However, most of the complexes were obtained as oils and did not crystallise under the conditions attempted. The compounds were successfully characterised by IR spectroscopy and $^{1}H$ and $^{13}C$ NMR spectroscopy. Parent ions or ions given by the loss of carbonyl groups were generally observed in the mass spectra. Elemental analysis was difficult as most of the complexes decomposed during the analysis. Solvent inclusion in many of the complexes was observed.

We have also looked at the structural features of some dendrimer precursors and a first generation dendrimer. The x-ray crystal structure of the dendrimer precursor **7** shows the alkyl chain to adopt a staggered conformation. The molecules also pack regularly, in a "head-to-tail" fashion. Molecular modelling studies showed the dendritic wedges, **13** and **14** to be fairly open structures, while the first generation dendrimer **15** adopts a more spherical structure.

Cyclic voltammetry studies on several of the organoiron dendritic wedges all showed a single irreversible oxidation peak. This suggests that the oxidation behaviour of one of the metals on the dendrimer surface did not influence the oxidation behaviour of the other metals in the complex.

The thermal behaviour of several of the complexes was also investigated by TGA and DSC. The DSC traces generally showed one endothermic peak which could be assigned to melting. The functional group and the alkyl chain length of the dendritic wedges influence the endotherm temperature. The acyl complexes underwent decarbonylation prior to melting.

Finally, some chemical reactivity studies on the dendritic wedges were performed. Several attempts were made to try to link the metal centres of the dendritic wedges using tertiary phosphine and nitrogen donor ligands. Both the phosphine and nitrogen donor ligands showed coordination to one iron centre only, possibly due to the tether length. Future experiments to link the metal centres will include the use of isonitrile or thiophene ligands. The core was also varied to produce a variety of dendrimers.

# Chapter 3

# Chemical reactivity and structural studies on organoruthenium dendrimers

## 3.1 Introduction

The chemistry of ruthenium alkyl complexes has been well documented in the literature.[119] Much of the early work on organotransition metal compounds has focussed on mononuclear compounds $L_nMR$[120a], or binuclear $L_nRMMXL_n$[120b] (X = R, H etc.) or $L_nMR^1ML_n$[120c,120d] ($R^1$ = bridging hydrocarbyl group) e.g. $[(\eta^5\text{-}C_5H_5)(CO)_2RuCH_2CH_2Ru(CO)_2[(\eta^5\text{-}C_5H_5)]$[120e].

The chemistry of the ruthenium alkyl complexes, $[CpRu(CO)_2\{(CH_2)_nR\}]$ (R = $CH_3$ or $C_4H_9$) has been studied along with that of the analogous iron and osmium alkyl compounds.[121] The ruthenium complexes are significantly more stable to air and light than their iron analogues (but less stable then the osmium complexes) and thus are useful precursors for other functionalised ruthenium compounds. Scheme 3.1 lists the synthesis and some reaction pathways of $[(\eta^5\text{-}C_5H_5)Ru(CO)_2R]$ compounds.

Iron and ruthenium alkyl compounds are particularly significant as models for metal alkyl intermediates in a variety of important homogeneous and heterogeneous catalytic reactions such as the Fischer-Tropsch[87] synthesis as well as in the hydrogenation, hydroformylation[78] and polymerisation of alkenes (see section 3.5).[89,90]

Liao and Moss[46] used these ruthenium haloalkyl complexes as starting materials to prepare a series of organometallic dendrimers containing Ru-C σ-bonds on the periphery of the dendrimer. They prepared organoruthenium dendrimers up to the fourth generation containing 48 metal atoms and with a molecular mass of over 18,000 amu. Figure 3.1 shows a fourth generation organoruthenium dendritic wedge.

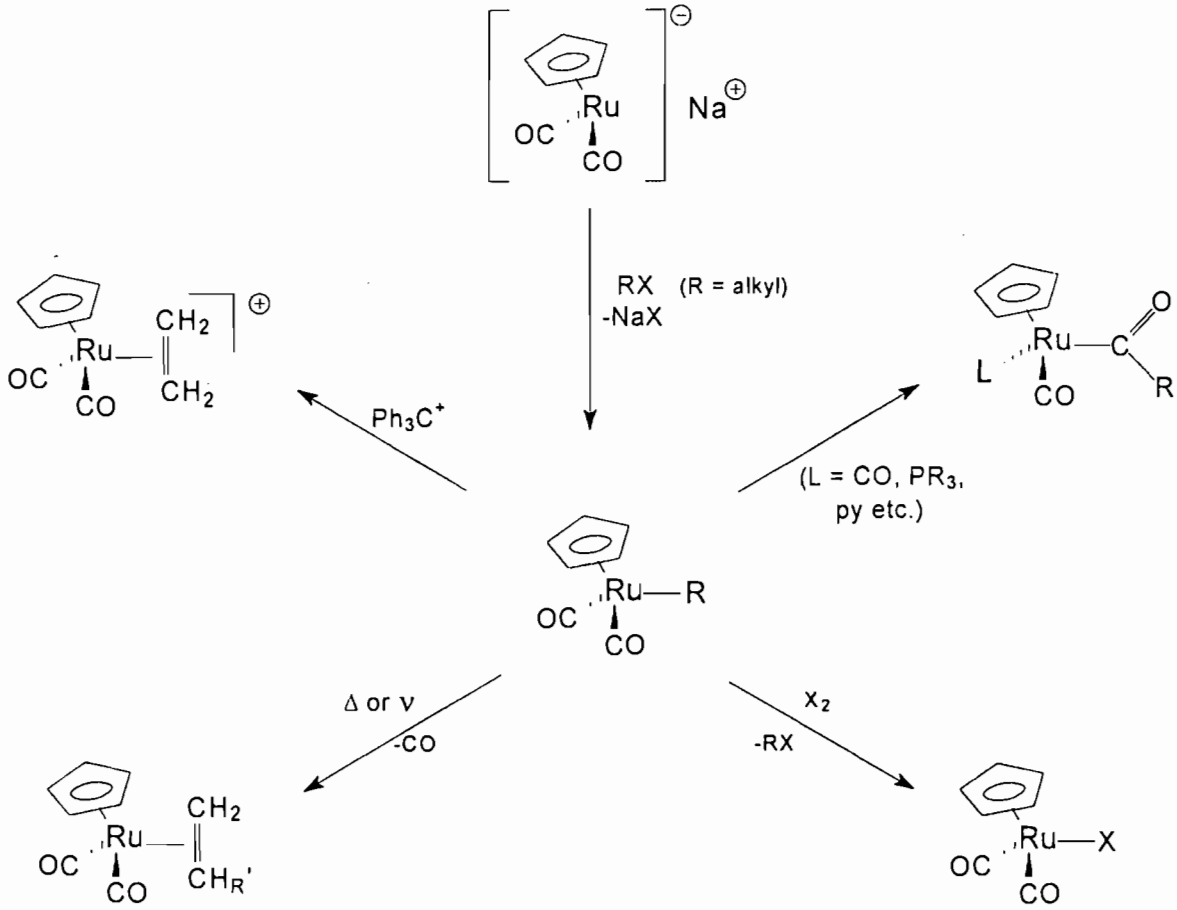


**Scheme 3.1**

Ruthenium has been incorporated into dendrimers at the core,[122] at the periphery[42d] (Figure 3.2) and throughout the dendrimer structure.[45] The mode of bonding has also varied from the use of ruthenium metal centres as linkers and branching points[43] through to dendrimers assembled via metal connectivity at multiple sites.[44b]

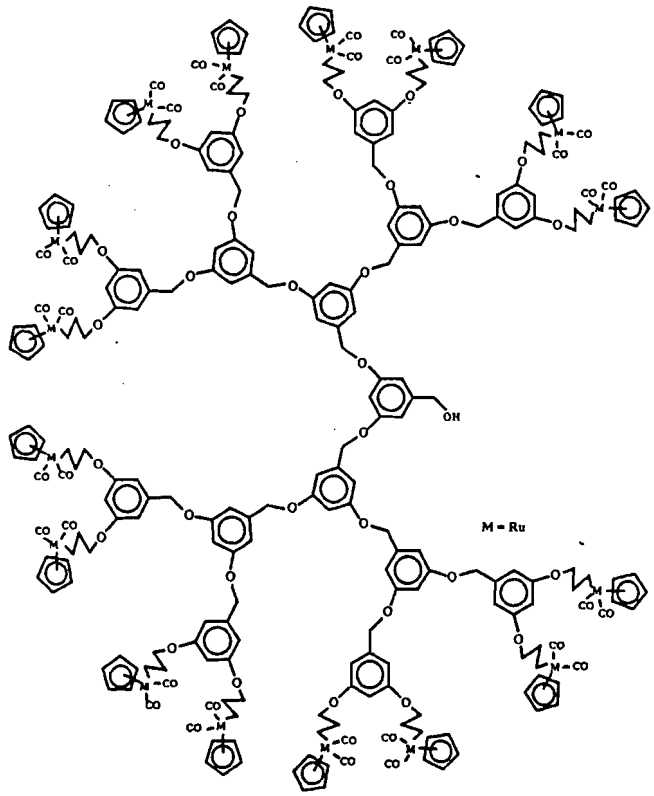


**Figure 3.1** A fourth generation organoruthenium dendrimer.[46]

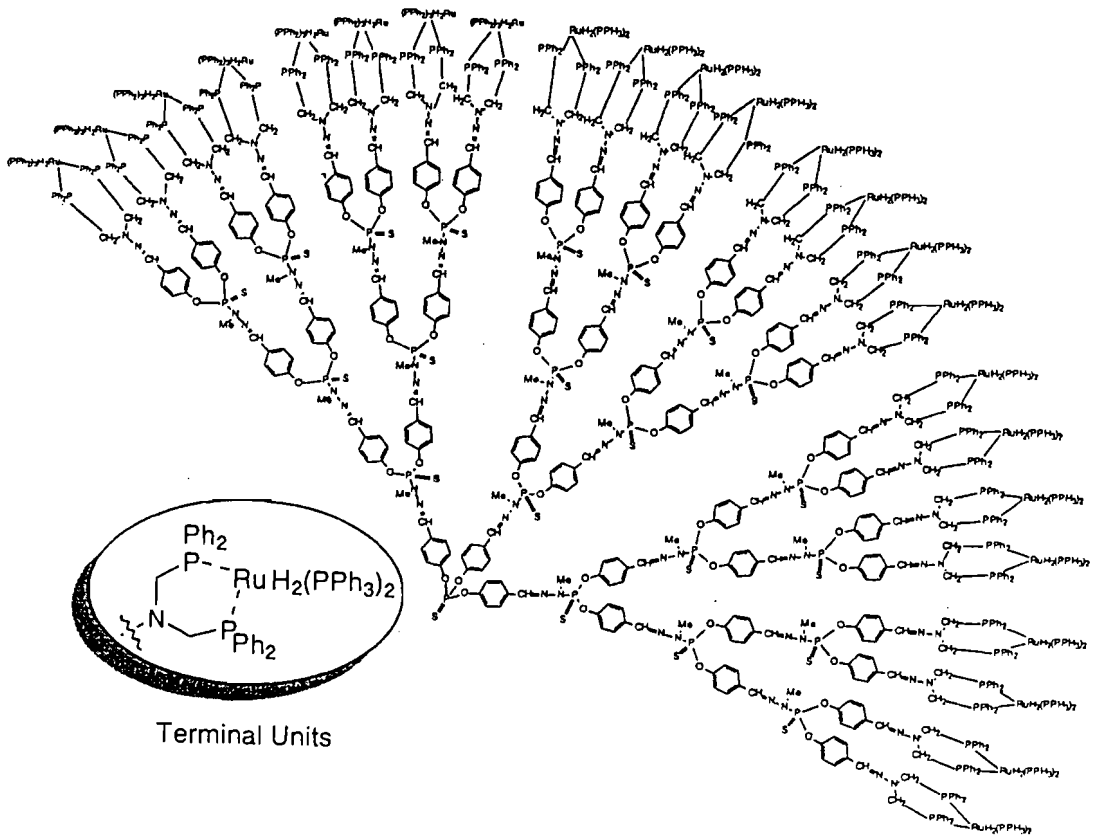


**Figure 3.2** Surface modification with Ru complexes.[42d]

Several groups have synthesised ruthenium-containing dendrimers using 2,2':6',2"-terpyridine as a connecting ligand for complexation with metal systems (Figure 3.3). As shown in Scheme 3.2, Constable *et al.*[9] reacted nucleophile (a) with bis(bromomethyl)benzene to give bromide (b) possessing an electrophillic site away from metal, which was subsequently reacted with 4,4'-dihydroxy-2,2'-bipyridine. The resulting complex (c) is a dinuclear complex possessing two terpyridyl Ru(II) moieties linked by an uncomplexed bipyridine ligand. Coordination to transition metals such as Fe(II) and Co(II) afforded the desired heptanuclear metallomacromolecule (d).

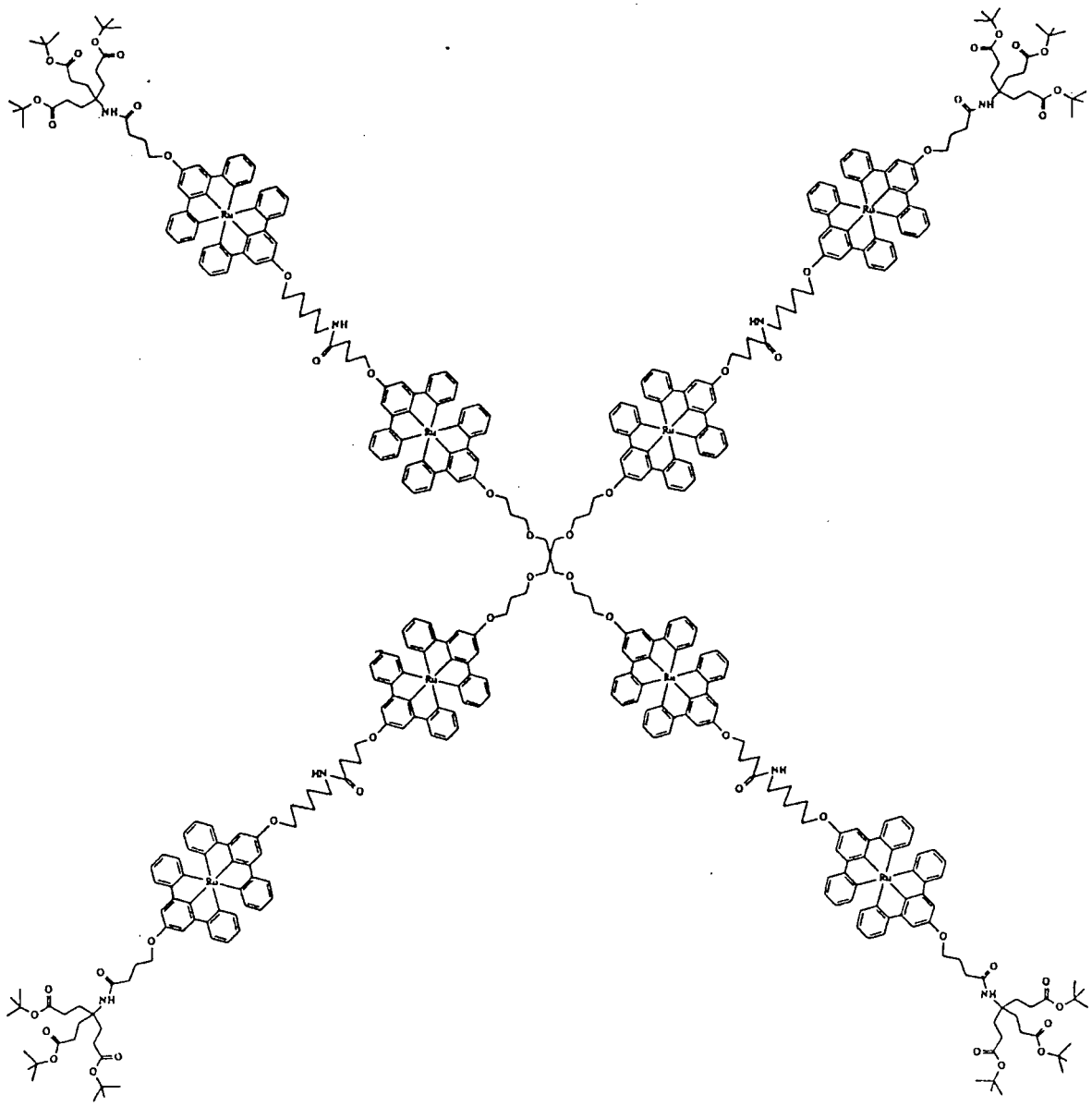

**Figure 3.3** Newkome's dendritic complex with -(Ru)-(x)-(Ru)- connectivity.[44b]

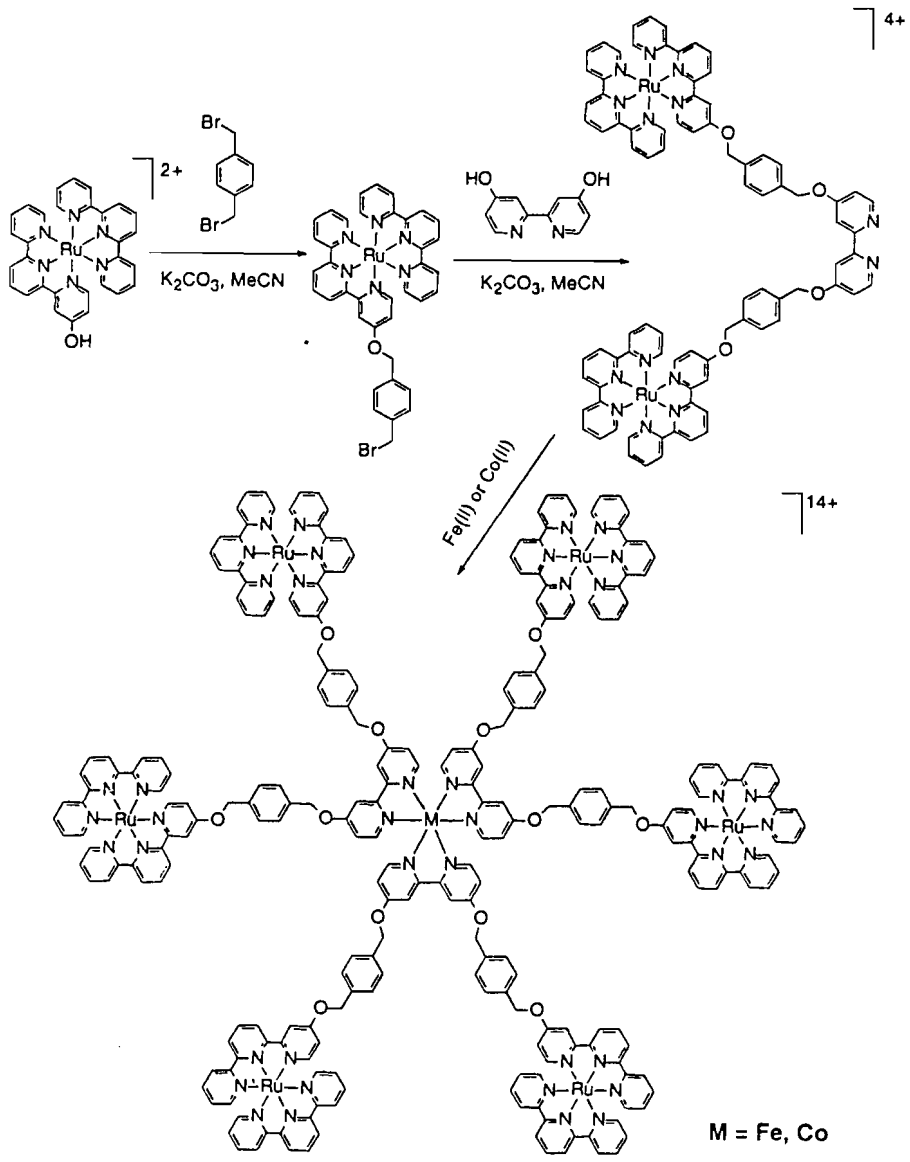


**Scheme 3.2**

## 3.2 Synthesis and characterisation of organoruthenium dendrimers

### 3.2.1 The $CpRu(CO)_2(CH_2)_3$- system

The synthesis of the organoruthenium dendrimers and dendritic wedges **31** - **33** reported in this section was carried out according to literature procedures.[46] Although the synthesis of these dendrimers has been reported previously[46], no reactivity studies have been reported, nor have any physical properties investigated. As for the iron dendrimers, the convergent methodology of Hawker and Fréchet[28] was used to build up the

organoruthenium dendrimers because it allows precise control over the number and placement of functional groups in the dendrimer. Scheme 3.3 shows the synthetic procedure followed.

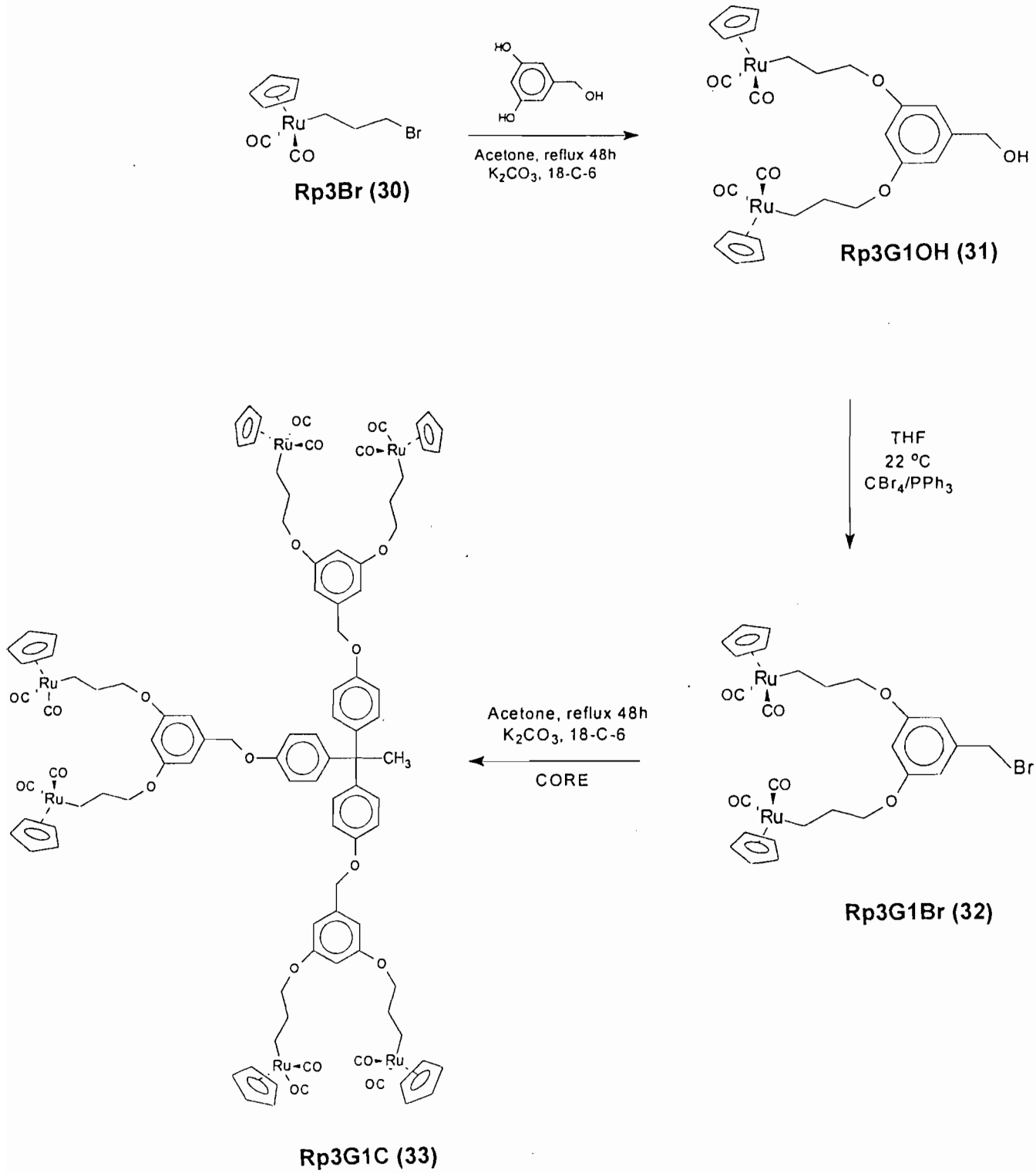


Scheme 3.3

The reactions were carried out in a stepwise fashion and the dendritic wedges were isolated, purified, and characterised by standard analytical and spectroscopic methods after each step. The bromoalkyl complex, **30** was used as the functionalised monomer and reacted with 3,5-dihydroxybenzyl alcohol to give the first generation benzyl alcohol, **31**. The optimised reaction conditions included the use of acetone as the solvent, 18-crown-6 and potassium carbonate as the base. Conversion of the alcohol functionality **31** to the bromide functionality **32** was achieved with a $CBr_4/PPh_3$ mixture in THF. These coupling and activation steps can be repeated to build larger generation dendritic wedges and finally the dendritic wedge is attached to the core molecule, 1,1,1-tris(4'-hydroxyphenyl)ethane. In a typical reaction, 3 molar equivalents of the benzyl bromide wedge **32** were reacted with 1 molar equivalent of the core molecule in the presence of potassium carbonate and 18-crown-6 in refluxing acetone for 48 hours to give **33** (Scheme 3.3).

### 3.2.2 Characterisation of organoruthenium dendrimers

The dendrimer precursors and first generation dendrimer were all obtained as colourless oils after column chromatography on alumina. Recrystallization from $CH_2Cl_2$/hexane or ether/hexane mixtures afforded the products as white crystalline solids. A white glassy solid was obtained upon drying **33** under vacuum for several hours. The characterisation data for the compounds prepared is summarised in Tables 3.1 -3.3.

**Table 3.1** Characterisation data for selected organoruthenium dendrimers.

| Compound | Appearance | Yield (%) | m.p. (°C) | $\nu_{max}$(CO) ($cm^{-1}$)[a] |
|---|---|---|---|---|
| Rp3Br(**30**) | pale yellow oil | 82 | - | 2017, 1945 |
| Rp3G1OH (**31**) | white crystalline solid | 85 | 90 – 92 | 2013, 1948 |
| Rp3G1Br (**32**) | white crystalline solid | 62 | 105-108 | 2013, 1949 |
| Rp3G1C (**33**) | white glassy solid | 50 | - | 2014, 1948 |

[a] IR spectra recorded in $CH_2Cl_2$

All the compounds show two strong ν(CO) bands in their IR spectra in $CH_2Cl_2$ solution. These bands appear at *ca.* 2013 and 1948 $cm^{-1}$ for the ruthenium compounds and at 1999 and 1938 $cm^{-1}$ for the analogous iron compounds, suggesting that the C-O bond in the iron compounds is weaker than the C-O bond in the ruthenium compounds.

Table 3.2 $^{1}H$ NMR data for selected organoruthenium dendrimers[a]

| Compound | $Ar^{CORE}$ | ArH | $C_5H_5$ | $ArCH_2O$ | $CH_2Br$ | $CH_2O$ | $CH_3$ | $\beta CH_2$ | $RuCH_2$ |
|---|---|---|---|---|---|---|---|---|---|
| Rp3Br (**30**) | - | - | 5.24 | - | 3.30(t, 7Hz) | - | - | 2.06(qu) | 1.62(m) |
| Rp3G1OH (**31**) | - | 6.49(d, 2Hz)[b]<br>6.38(t, 2Hz) | 5.25 | 4.61(br d)[c] | - | 3.86(t, 7Hz) | - | 2.01(m) | 1.68(m) |
| Rp3G1Br (**32**) | - | 6.45(d, 2Hz)<br>6.32(t, 2Hz) | 5.19 | - | 4.35 | 3.79(t, 7Hz) | - | 1.95(m) | 1.63(m) |
| Rp3G1C (**33**) | 6.98(d, 9Hz)<br>6.86(d, 9Hz) | 6.56(d, 2Hz)<br>6.40(t, 2Hz) | 5.25 | 4.96(br d)[c] | - | 3.86 | 2.10 | 2.01(m) | 1.72(m) |

[a] Measured in $CDCl_3$ relative to TMS (δ 0.00 ppm)
[b] J given in Hz (in brackets)
[c] broad unresolved doublet

Table 3.3 $^{13}C$ NMR data for selected organoruthenium dendrimers[d]

| Compound | CO | $Ar^{CORE}$ | ArH | $C_5H_5$ | $CH_2OAr$ | $ArCH_20$ | $\underline{C}CH_3$ | $CH_2$ | $CH_2Br$ | $\underline{C}CH_3$ | $RuCH_2$ |
|---|---|---|---|---|---|---|---|---|---|---|---|
| Rp3Br (**30**) | | - | - | | - | - | - | | - | - | -9.32 |
| Rp3G1OH (**31**) | 202.10 | - | 160.60; 143.16<br>105.08; 100.50 | 88.55 | 71.05 | 65.51 | - | 38.50 | - | - | -9.36 |
| Rp3G1Br (**32**) | 202.08 | - | 160.45; 139.46<br>107.41; 101.40 | 88.56 | 71.09 | - | - | 38.46 | 33.93 | - | -9.28 |
| Rp3G1C (**33**) | 202.00 | 156,81; 141.95<br>129.57; 113.28 | 160.48; 139.28<br>105.63; 100.66 | 88.49 | 70.99 | 70.05 | 50.5 | 38.42 | - | 31.0 | |

[d] Measured in $CDCl_3$ relative to TMS (δ 0.0 ppm)

$^{1}H$ and $^{13}C$ NMR spectroscopy is extremely useful for detecting defects in branching in the dendritic wedges prior to complexation with a core molecule. All the dendrimers were characterised by $^{1}H$ and $^{13}C$ NMR spectroscopy and the data obtained (Tables 3.2 and 3.3) agreed well with that reported in the literature. The $^{1}H$ NMR spectrum of **31** and $^{13}C$ NMR spectrum of **33** are shown in Figures 3.4 and 3.5 respectively. The triplet at 3.86 ppm in the $^{1}H$ NMR spectrum is important as it confirms the formation of the first generation products. The doublet and triplet at 6.38 and 6.49 ppm respectively confirm the correct ratio of aromatic protons. The peaks in the region 4.5 - 5 ppm were assigned to the benzyl protons. A shift of the benzyl $CH_2$ resonance from *ca.* 4.6 to 4.4 ppm was observed when the benzyl alcohol, **Rp3G1OH** was converted to the benzyl bromide, **Rp3G1Br**. This region is therefore very useful for confirming whether the activation step has proceeded to completion or not. A further shift of these $CH_2$ protons from *ca.* 4.4 to 4.9 ppm was observed when the dendritic wedges were coupled to the core molecule to form **Rp3G1C**. $^{13}C$ NMR spectroscopy was also used to confirm the products. The data listed in Tables 3.1 – 3.3 agrees well with the literature.[46]

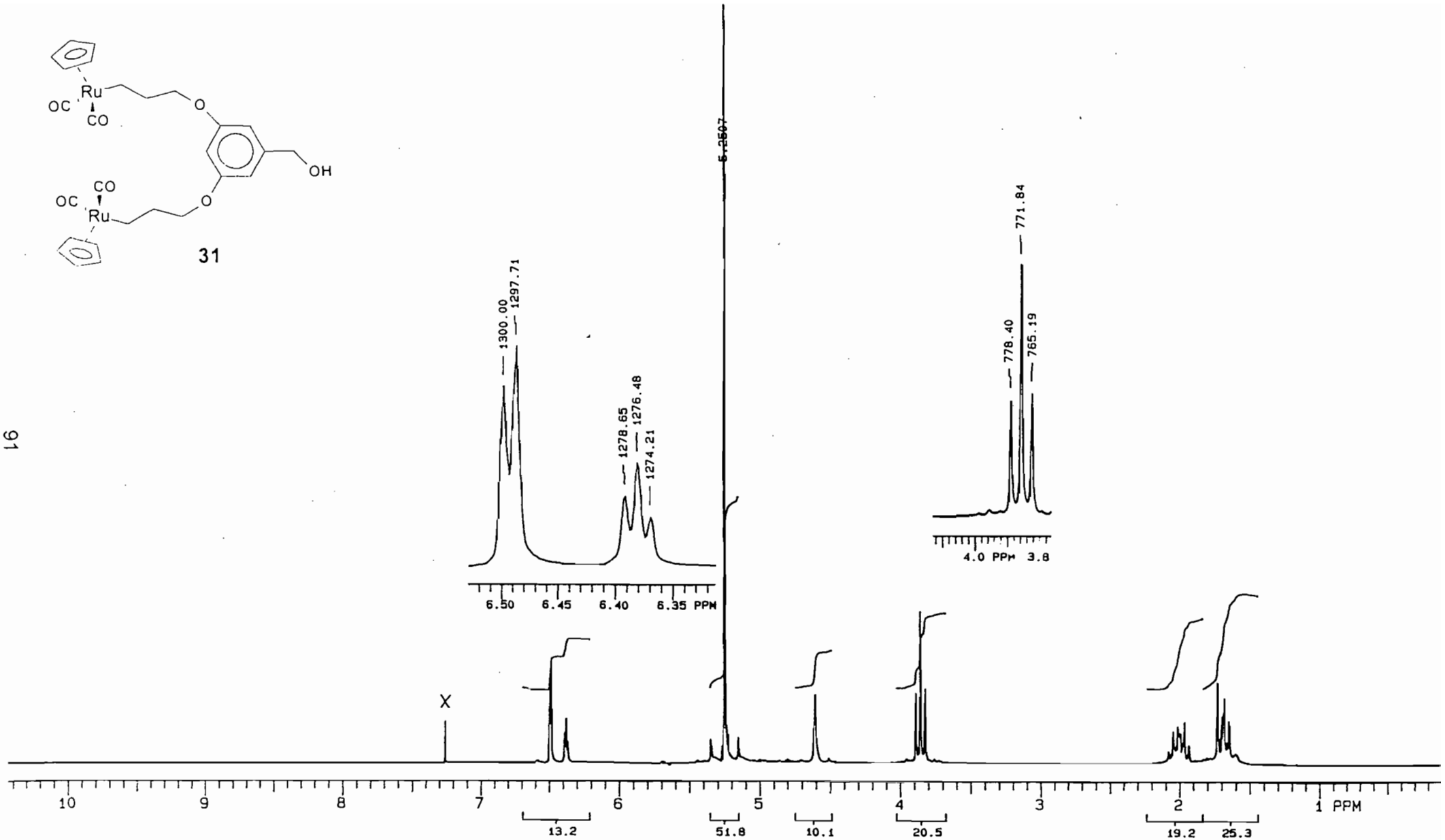


**Figure 3.4** A 200 MHz $^{1}$H NMR spectrum of **32**. X = solvent

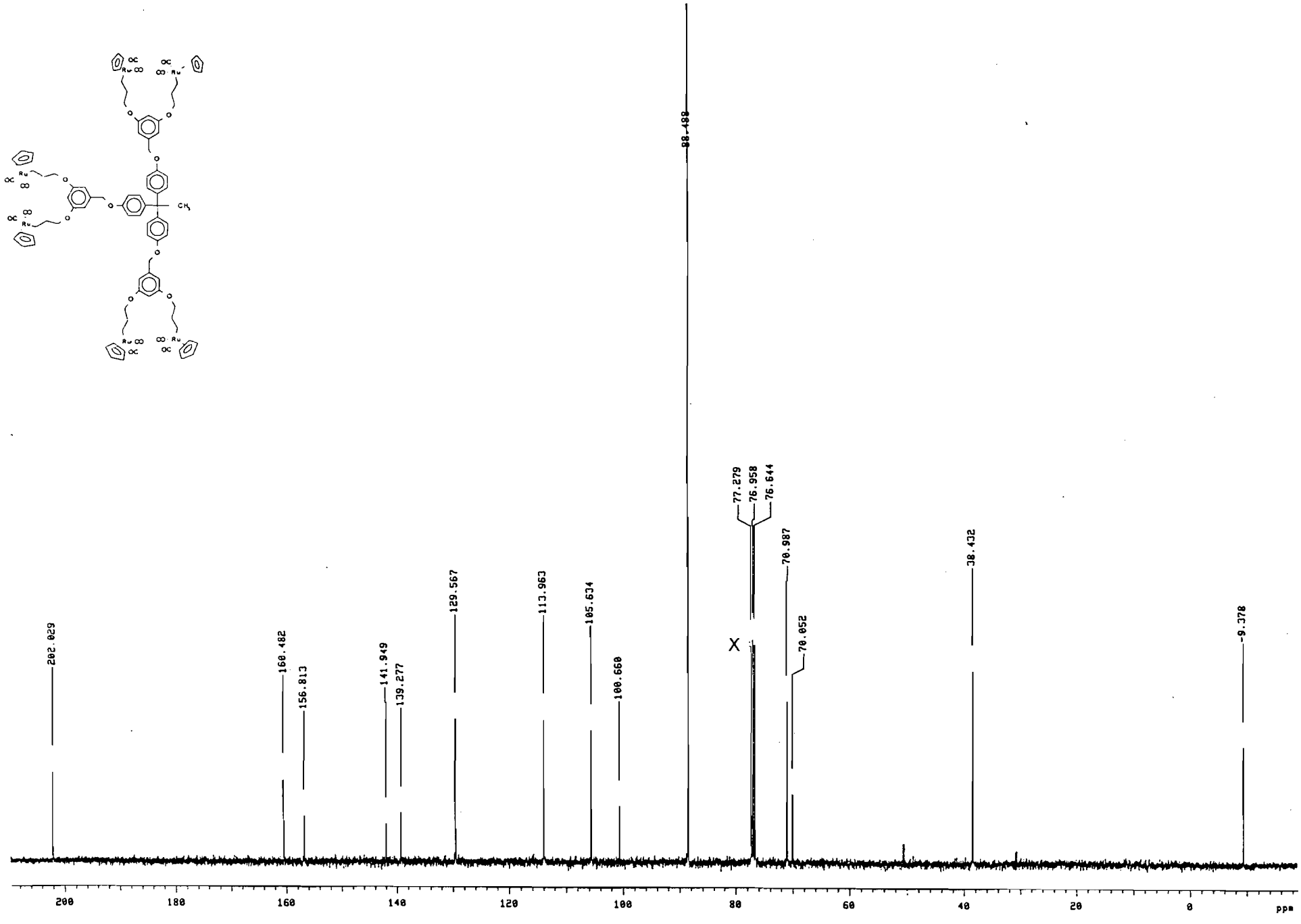


**Figure 3.5** A 100 MHz $^{13}C$ NMR NMR spectrum of **33**. X = solvent

## 3.3 Structural studies and physical behaviour of selected dendrimers

### 3.3.1 X-ray crystallography

We wished to determine the crystal structure of a first generation dendrimer, such as **33** but compound **33** crystallised as a glassy solid, so that was not possible. The highest unit that could be obtained in crystalline form was the first generation dendritic wedge, **32**. Nevertheless, the data obtained still yield valuable information regarding the metal-ligand environment in the dendrimer fragment and also confirm the synthesis of compound **32**.

Due to the difficulty of growing suitable crystals of dendrimers for X-ray diffraction, very few crystal structures of dendrimers have appeared in the literature. Recently the single-crystal structure of a first generation carbosilane dendrimer terminated with $Cp^*Ru^+$ groups was reported (Figure 3.6a).[123] A ball-and-stick model of the molecular structure is shown in Figure 3.6b.

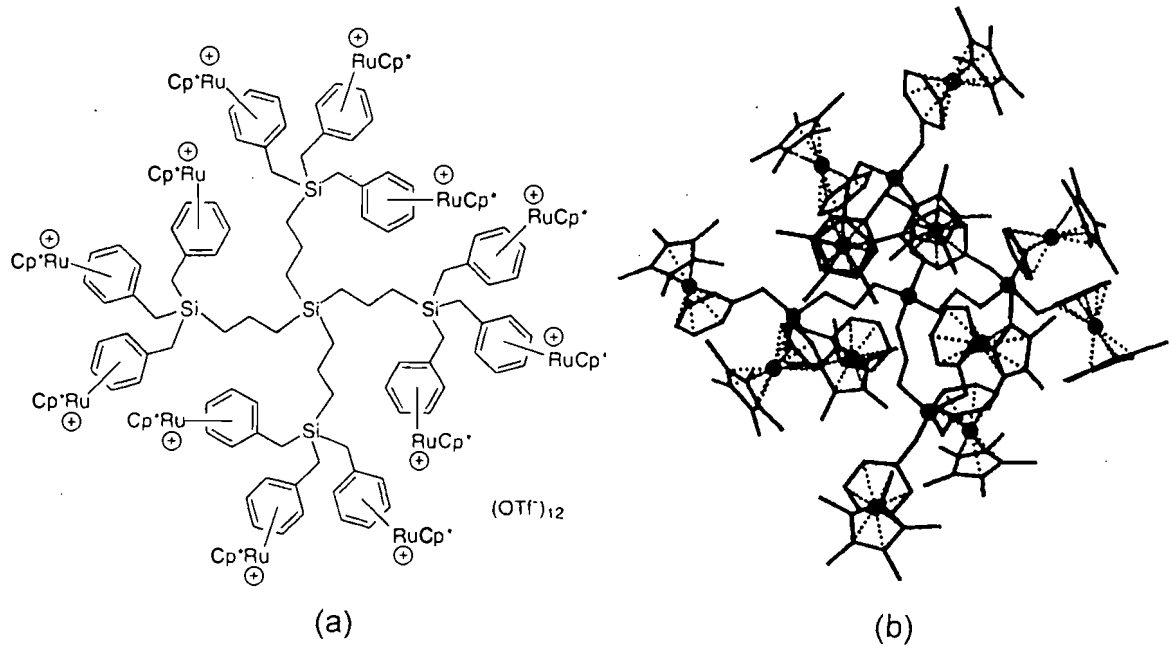


**Figure 3.6** (a) The $Cp^*Ru^+$ terminated dendrimer (b) a ball-and-stick model.

The dendrimer crystallised in an orthorhombic unit cell of space group *Fdd2*. There are 16 dendrimers per unit cell with an overall cell volume of 105 761 $Å^3$. The 12 triflate anions are closely associated with the dendrimer dodecacations, with 9 of them residing within the periphery of the dendrimer. There is some disorder in two triflates, and an associated solvent molecule, but an *R* value of 7.89% was still obtained. The diameter of

the cation was estimated from a space-filling model as being 23-28 Å. The somewhat irregular shape is not unexpected for early generation dendrimers. From the ball-and-stick model (Figure 3.6b), it can be seen that the dendrimer has an approximate $C_2$ axis passing through the central silicon atom. The structure can be described as a fairly "open" body-centred cubic lattice. This is the largest dendrimer in terms of molecular weight and volume to be characterised by single-crystal X-ray diffraction.

### 3.3.1 Structure determination of Rp3G1Br (32)

Colourless needles were grown with difficulty from a layered $CH_2Cl_2$/hexane solution at −15°C. Oscillation, Weissenberg and precession photography revealed 2/m Laue symmetry, indicating the monoclinic crystal system. Conditions limiting possible reflections were as follows: hkl: (h + k = 2n); h0l: (l = 2n; {h = 2n}); 0k0: (k = 2n), which indicated space group Cc (non-centric) or C2/c (centric). Intensity data statistics confirmed Cc as the correct space group. Manual Patterson methods were attempted, but the structure had to be solved by direct methods. Five cycles of least-squares refinement were required for the positional and thermal factors to reach convergence. The structure was successfully refined, giving a final R factor of 0.046. Details of the data-collection and refinement are shown in Table 3.4. Experimental details can be found in section 7.1. The molecular structure with the atomic numbering scheme is shown in Figure 3.7. Fractional atomic coordinates, anisotropic displacement parameters, bond lengths, bond angles and torsion angles appear in Appendix 3a (Tables A1 to A6) and structure factor data are included in Appendix 3b (on diskette).

**Table 3.4** Details of intensity data-collection and structure refinement for **Rp3G1Br (32)**.

| | |
|---|---|
| Colour/shape | Colourless/needles |
| Empirical formula | $C_{27}H_{27}O_6Ru_2Br$ |
| Formula weight /gmol$^{-1}$ | 729.64 |
| Temperature /K | 233 |
| Crystal system | Monoclinic |
| Space group | Cc |
| Unit cell dimensions: a/Å | 8.635(6) |
| b/Å | 35.49(3) |
| c/Å | 8.954(3) |
| β/° | 95.39(4) |
| Volume /Å$^3$ | 2732(2) |
| Z | 4 |
| Density (calculated) /gcm$^{-3}$ | 1.77 |
| Absorption coefficient /cm$^{-1}$ | 25.71 |
| F(000) | 1440 |
| Crystal size /mm | 0.15 x 0.25 x 0.06 |
| θ range for data collection/° | 1 – 25 |
| Index ranges | 0,10; 0,42; -10,10 |
| Total no. reflections | 2622 |
| No. unique reflections | 2356 |
| $R_{int}$ | 0.0 |
| Transmission/max; min; av. (%) | 93.26; 99.93; 95.73 |
| No. obs data [I>2σI] | 1965 |
| No. param. Refined | 189 |
| Final R indices | 0.046 |
| Rw | 0.048 |
| Weighting function | $[\sigma^2(F_o) + 0.000506F_o^2)^{-1}$ |
| Goodness-of-fit on $F^2$ | 1.53 |
| Scan width /° | 0.75 + 0.35tanθ |
| Aperture width/mm | 1.12 + 1.05tanθ |
| Largest diff.peak and hole/eÅ$^{-3}$ | 0.47; -0.25 |

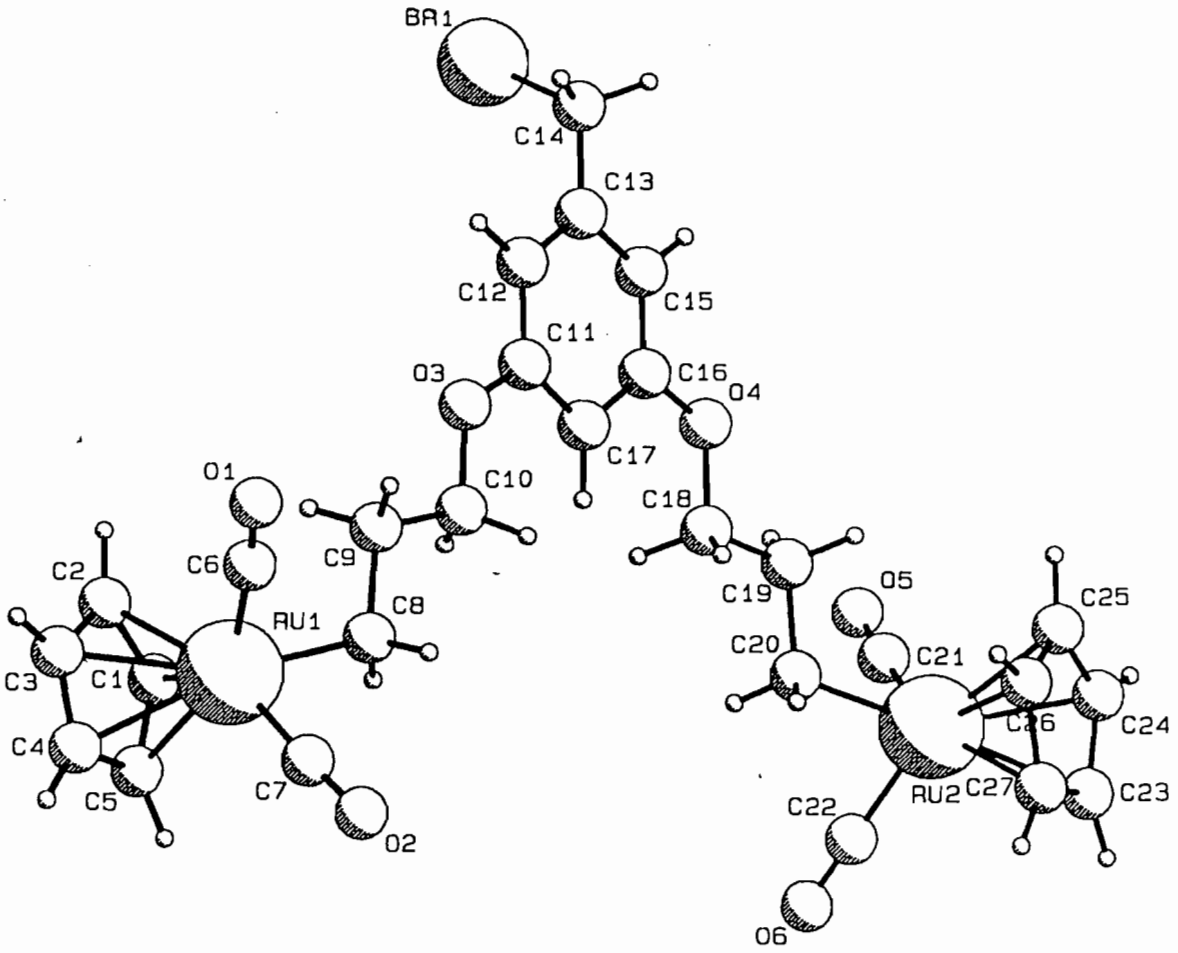


**Figure 3.7** Molecular structure of **32** showing atom labelling.

The molecule is pseudosymmetrical ($C_2$) if the Br atom is ignored. The propyloxy chains are staggered as predicted, with average C-C bond distances of 1.52Å. The Cp rings are planar with a mean deviation from the plane of 0.01Å. Ru-C(Cp) bond distances range from 2.23(2) to 2.27(2) Å and C-C(Cp) 1.40(3) – 1.43(3) Å. The Cp groups appear to be 'trans' to each other with respect to the plane of the benzyl ring. The crystal structure of a related complex, $[CpRu(CO)_2]_2(CH_2)_5$, shows the two Cp groups to lie on the same side of the Ru1-Ru2 axis, i.e. in a 'cis' orientation.[124] This could be due to the length of the alkyl chain. The bond angles C(CO)-Ru-$CH_2$ and C(CO)-Ru-C(CO) are close to 90° indicating an octahedral arrangement around the ruthenium with the Cp ligand occupying three co-ordination sites. This was also found for the iron dimer described previously (pp. 56). Figure 3.8 shows a stereoview of the crystal packing viewed down the c-axis.

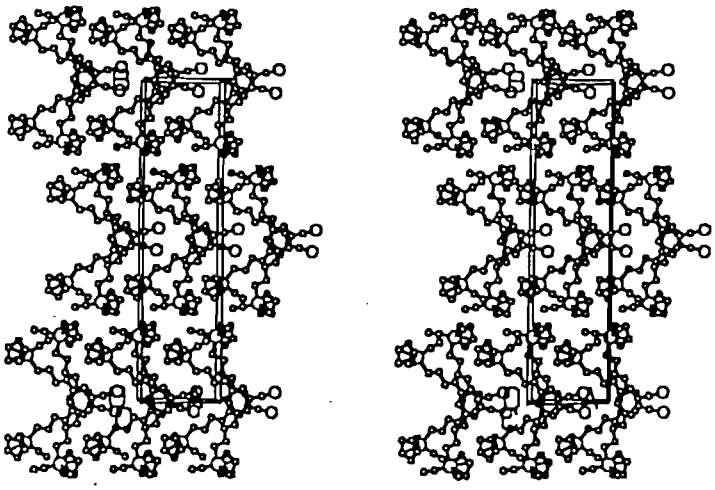

**Figure 3.8** Stereoview of **32**.

Some favourable intermolecular Cp...Cp interactions are listed below and shown in Figure 3.9.

| | |
|---|---|
| C23...C1 | 3.30(2) Å |
| C24...C2 | 3.37(3) Å |
| C27...C1 | 3.39(2) Å |

The Br atoms and Cp rings are positioned in alternating domains along b. The non-centrosymmetric space group gives a 'polarity' to the crystal structure- all molecules facing the same way *ie.* C-Br vectors are roughly parallel to the a-axis.

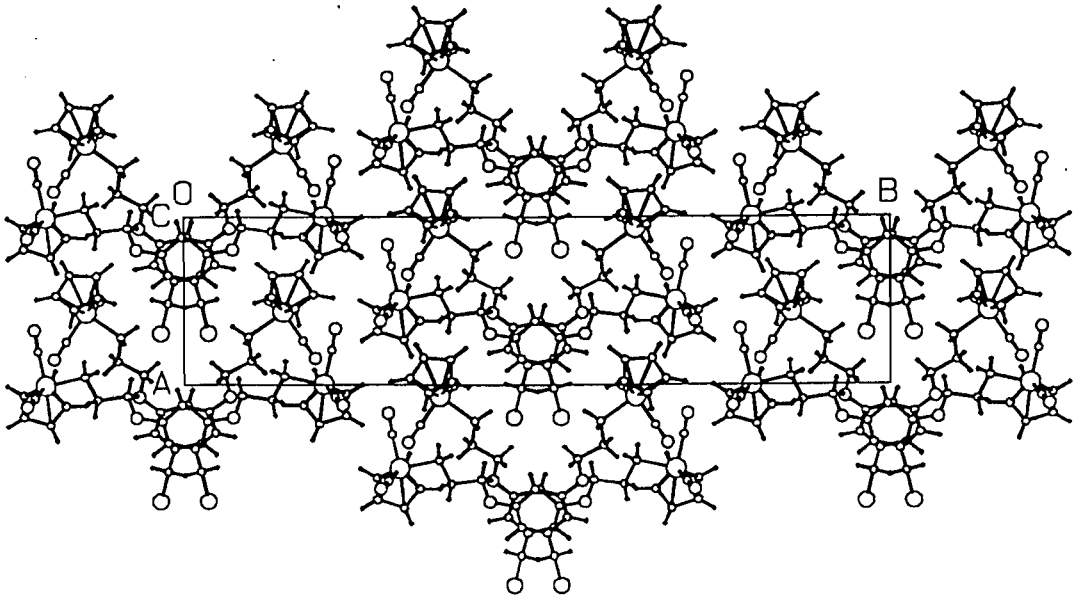


**Figure 3.9** Packing diagram for **32** viewed down the c-axis.

### 3.3.2 Molecular modelling studies using HYPERCHEM™

Computer assisted molecular models have been used in many areas of chemistry to predict the shapes of molecules. It has generally been found that as the size of the dendrimer increases, the shape changes from being star-like to being more spherical (see section 2.3 for a more detailed discussion). We used the HYPERCHEM[99] modelling program to determine how the predicted structure of the first generation ruthenium benzyl bromide, **32** (Figure 3.10) would differ from the x-ray crystal structure (Figure 3.7). The model differs slightly from the crystal structure. In the crystal structure, both propyl chains are extended and the cyclopentadienyl rings face away from each other whereas the model shows only one of the chains to be extended, and the other chain to be slightly folded.

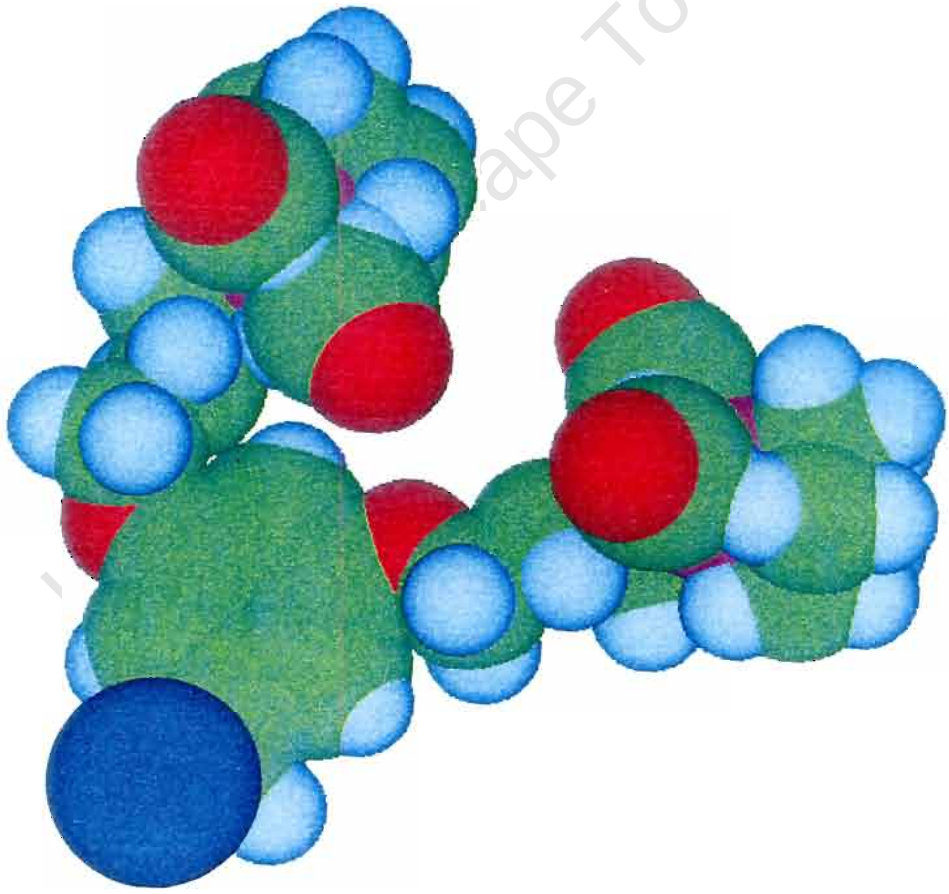

**Figure 3.10** Calculated structure of **32**.

### 3.3.3 Electrochemical behaviour of selected organoruthenium dendrimers

As described in Chapter 2, the primary motivation for performing these cyclic voltammetry experiments was to determine whether there was any communication or interaction between the ruthenium metal atoms on the surface of the first generation dendrimer. The oxidation behaviour of the dendritic wedge **31** and first generation ruthenium dendrimer **33** and was studied by cyclic voltammetry (Figure 3.11).

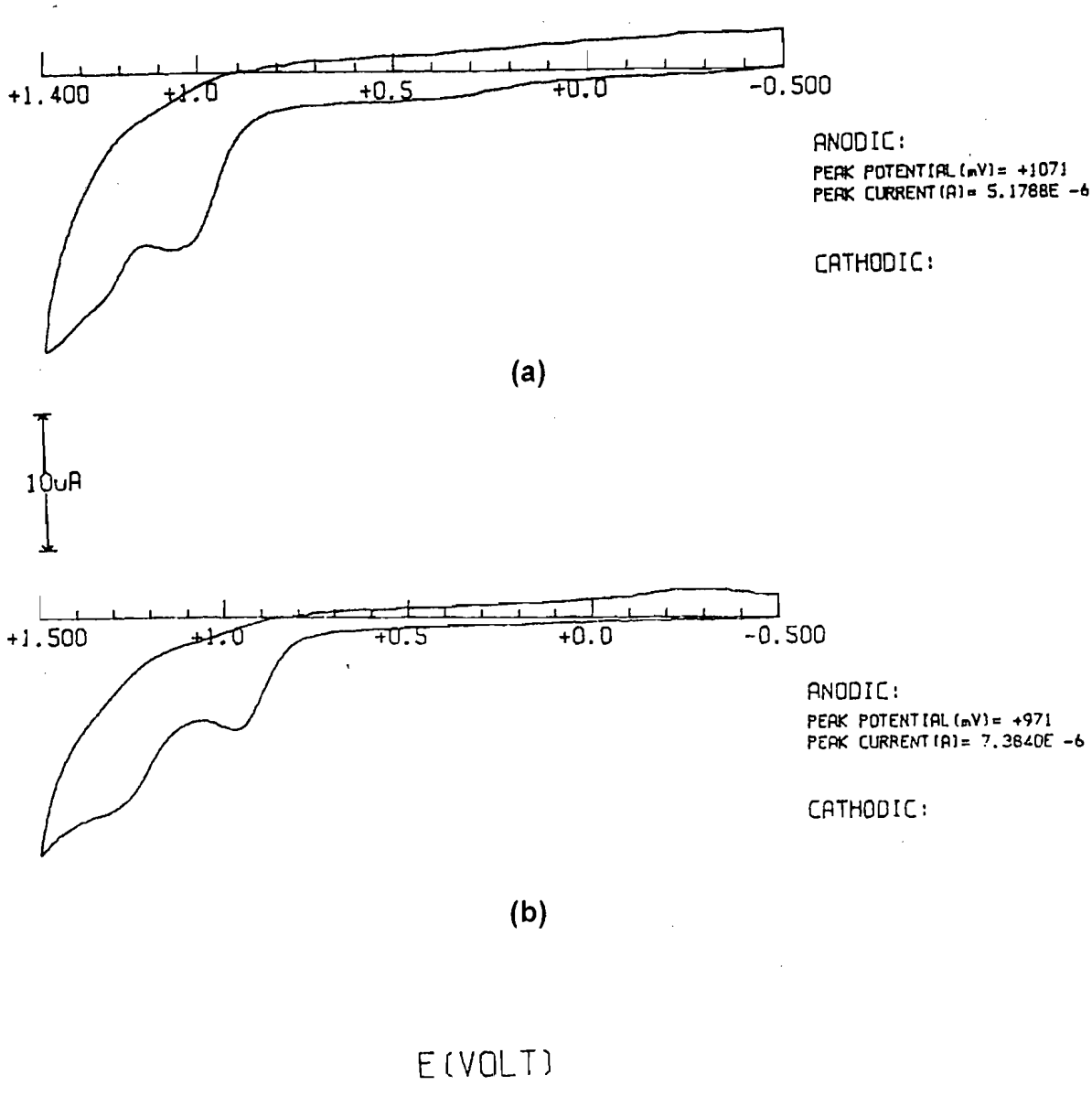


**Figure 3.11** Cyclic voltammograms of (a) **31** and (b) **33** in $CH_3CN$.

The cell consisted of a three-electrode system with a $Ag/Ag^+$ reference electrode, a platinum wire auxilary electrode and a platinum disc working electrode. The experiments were carried out under argon as described in Section 2.3.3.

In both cases, a single irreversible oxidation peak is observed. In contrast to the iron dendrimers, the oxidation peak for **31** appears at a slightly higher potential, *viz* 1071 mV compared with that for the first generation dendrimer **33** at 971 mV, *i.e.* **31** is slightly more difficult to oxidise than **33**. The reason for this difference could possibly be some influence by the Cp* ligand in the case of the iron complexes. Nevertheless, the single oxidation peak for both complex **31** (2 Ru atoms) and **33** (6 Ru atoms) suggests that there is no communication between the metals, as one would have expected multiple oxidation peaks for **33** if there had been any interaction between the metals. As explained in section 2.3.3, a possible reason for the irreversible oxidation behaviour could be an induced alkyl migration reaction. The new species formed after oxidation has taken place cannot be reduced under the conditions applied.

## 3.4 Chemical reactivity studies on a 1st generation dendrimer

Previous studies have examined the chemical behaviour of mononuclear and binuclear complexes.[112] We wished to determine whether the organometallic dendrimer behaves as a 'mononuclear' type complex or if the metal sites on the dendrimer can react independently. Several reactions were carried out on the dendrimer precursor, **31** and the first generation dendrimer **33**. Similar reactions have been carried out previously with mononuclear compounds of the type $CpRu(CO)_2R$.

### 3.4.1 Reaction with $PPh_3$

Some reactions of the organoruthenium dendrimers with tertiary phosphines were carried out to compare the reactivity of the mononuclear complex, **30** with the dendrimer precursor, **31** and the first generation dendrimer, **33**. **31** and **33** were refluxed with triphenylphosphine in benzene for 2 days. The reactions were monitored by IR spectroscopy. **31** showed no reaction in benzene, and only reacted after 5 days of refluxing in xylene to form the acyl species, **34** (Scheme 3.4). In contrast, the corresponding iron benzyl alcohol, **4** underwent alkyl migration in benzene to give the acyl species, **19** in 24 hours (Scheme 2.13). This reactivity parallels that of the mononuclear FpR and RpR complexes.[125] The first generation dendrimer, **33** also showed no reactivity after refluxing with triphenylphosphine in benzene for 3 days. The

solvent was replaced with xylene, and after a further 24 h refluxing, a weak acyl peak appeared at 1592 $cm^{-1}$ confirming the formation of **35** (Scheme 3.5). However, most of the starting material remained unreacted. This could be due to steric hindrance because of the bulkiness of the $PPh_3$ ligand. In the dendrimer precursor, **31** the alkyl chains are fairly flexible and can accomodate the bulky $PPh_3$ ligand. The dendrimer, **33** is already a more sterically congested complex, so that addition of a bulky ligand such as $PPh_3$ is very difficult.

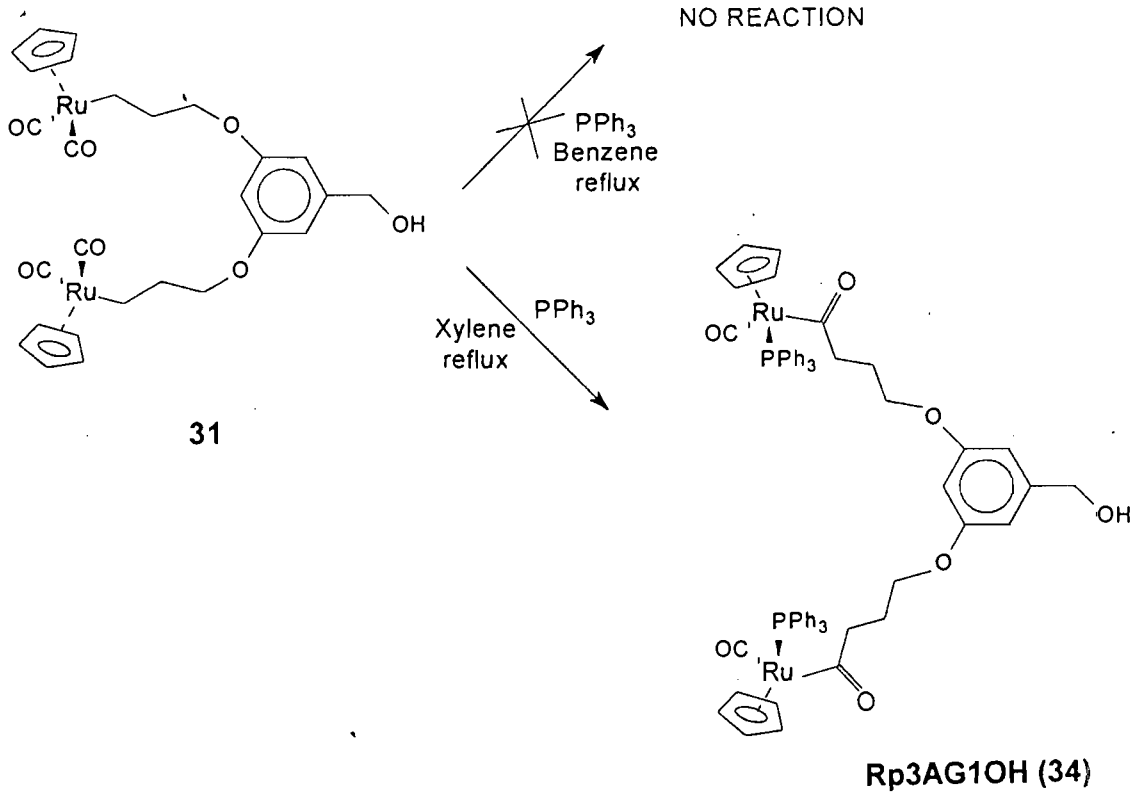


**Scheme 3.4**

A previous study on the rates of alkyl migration in the series of compounds, $[CpM(CO)_2R]$ (M = Fe, Ru, Os and R = $CH_3$ to $n$-$C_{18}H_{37}$) has shown a definite trend in reactivity.[125] The metal alkyl complex, $CpM(CO)_2R$ was reacted with a ten-fold excess of $PPh_3$ in xylene. Changing the metal from Fe to Ru while keeping the other ligands the same, was found to cause a decrease of about $10^3$ in the rate of alkyl migration. The analogous Os compounds showed no detectable reaction after 6 days.[125] Thus the rate of alkyl migration for the osmium alkyls must be at least $10^4$ times slower than that for the analogous ruthenium compounds. From these results it can be seen that the reactivity of compounds of this type with $PPh_3$ decreases in the order Fe > Ru >> Os. The reactivity of the iron and ruthenium dendrimers also seems to follow this trend.

### 3.4.2 Reaction with $I_2$

The electrophilic cleavage reaction of metal-carbon bonds in mononuclear alkyl compounds is well-known.[126] We were interested to see how the six-metal dendrimer, **33** would react in contrast to the related mononuclear compound, $CpRu(CO)_2(CH_2)_3R$ and the diruthenium compound $[Cp(CO)_2Ru(CH_2)_5Ru(CO)_2Cp]$ which reacts with $I_2$ according to equation (1)[127]:

$$[Cp(CO)_2Ru(CH_2)_5Ru(CO)_2Cp] + 2I_2 \rightarrow 2CpRu(CO)_2I + I(CH_2)_nI \qquad (1)$$

**33** was reacted with $I_2$ in $CH_2Cl_2$ at room temperature. The reaction was followed by IR spectroscopy till all the starting material had gone. An orange fraction was collected and later identified as a mixture of $CpRu(CO)_2I$ and the new iodine terminated dendrimer, **36** (Scheme 3.6). Thus, cleavage of Ru-$CH_2$ bonds on reaction with iodine occurs with the dendrimer too.

### 3.4.3 Reaction with $Ph_3CPF_6$

The reactions of mononuclear $[CpFe(CO)_2R]$ with trityl salts (such as $Ph_3CPF_6$) are known to give cationic alkene species $[CpFe(CO)_2(alkene)]^+$.[128] Binuclear compounds, $[Cp(CO)_2Fe(CH_2)_nFe(CO)_2Cp]$ give cationic species such as $[Cp(CO)_2Fe\text{-}(C_nH_{2n-1})Fe(CO)_2Cp]^+$ by hydride abstraction.[129] A single hydride abstraction was also observed in the related reaction of $[Cp(CO)_2Ru(CH_2)_5Ru(CO)_2Cp]$ with $Ph_3CPF_6$.[130]

The first generation ruthenium dendrimer **33** was reacted with six molar equivalents of $Ph_3CPF_6$ in $CH_2Cl_2$ at room temperature and the reaction was monitored by IR spectroscopy. After 24 hours reaction at room temperature, there was evidence in the IR spectrum for the high frequency band (2082, 2035 $cm^{-1}$) corresponding to the cationic metal alkene end of the molecule as well as for some unreacted sites in the dendrimer (Scheme 3.7). A grey white solid was obtained after the work-up procedure. The presence of four carbonyl bands in the IR spectrum suggested an alkene alkyl structure **37**. It appears that the formation of one cation affects the formation of further cations being formed.

In all these reactions, the first generation ruthenium dendrimer **33** reacted slower than the corresponding mononuclear complex. This was anticipated. Experimental details are listed in the experimental (section 7.3).

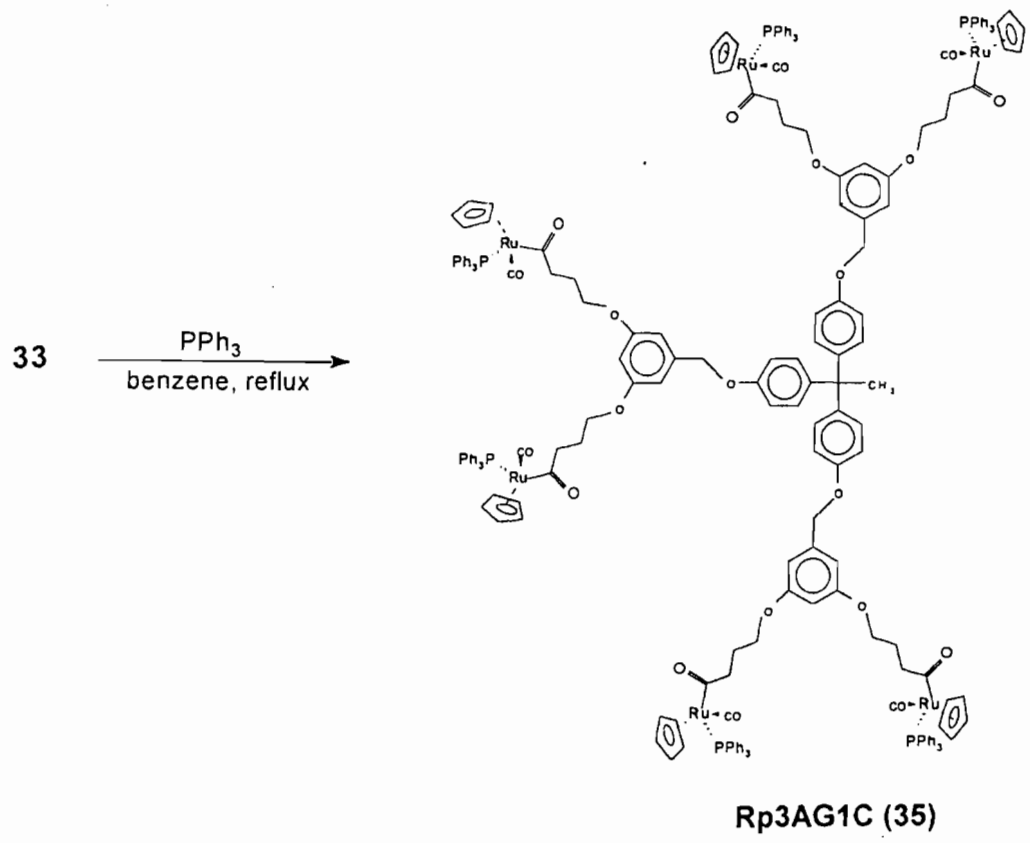


**Scheme 3.5**

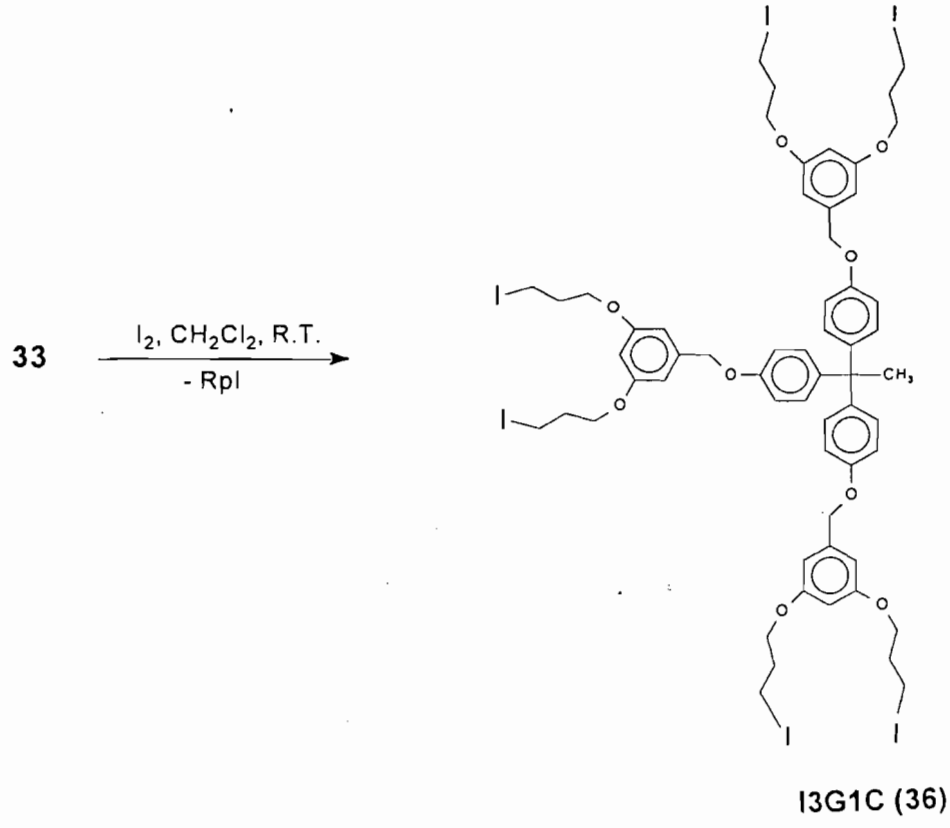


**Scheme 3.6**

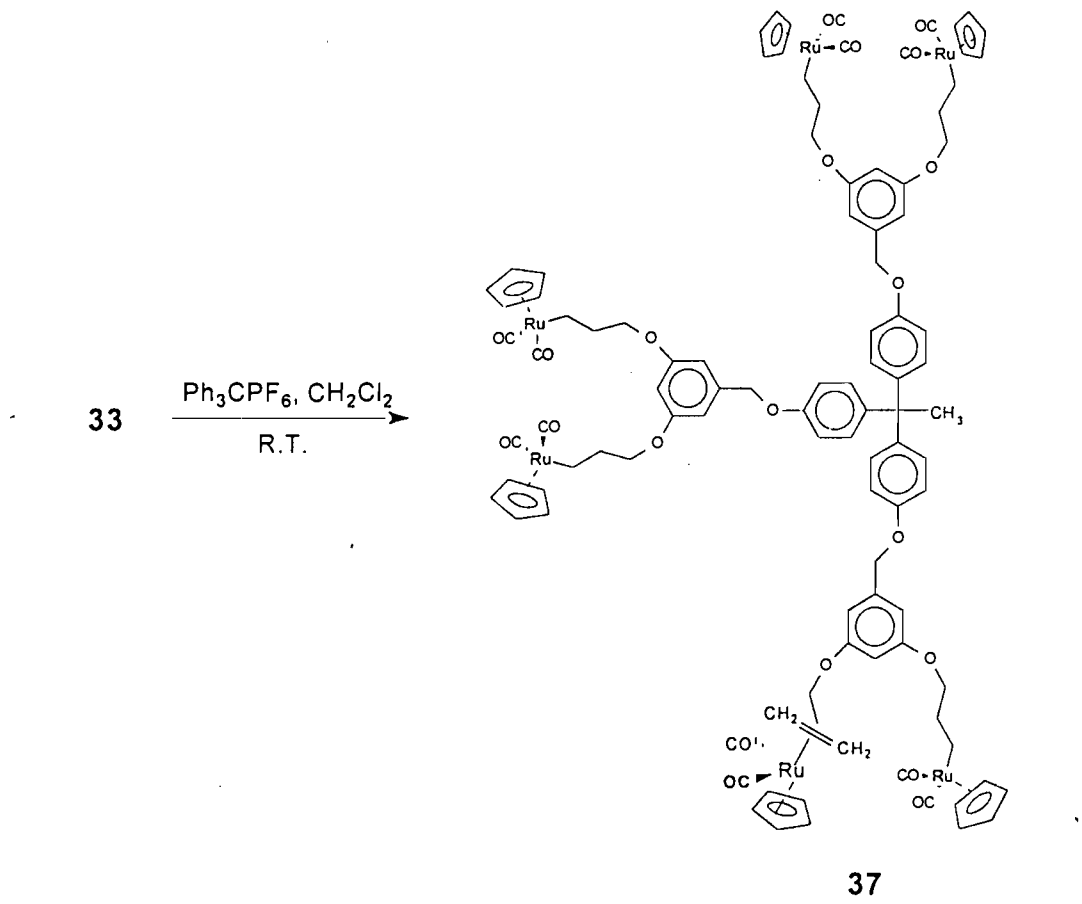


**Scheme 3.7**

## 3.5 Catalytic studies with a 1st generation dendrimer

### 3.5.1 Organometallic compounds in homogeneous and heterogeneous catalysis

Organometallic compounds have played a key role in catalysis, particularly homogeneous catalysis, since the early days of hydroformylation (1938), olefin polymerisation (1953) and acetaldehyde synthesis (1959). New knowledge regarding the structure and reactivity of organometallic compounds has created new catalytic processes in industry and improved conditions for catalytic processes already established, such as the replacement of cobalt by rhodium in the hydroformylation reaction.[131] Nevertheless, about 85 % of known catalytic processes in industry are dominated by heterogeneous catalysis.[132] Table 3.5 summarises the strengths and weaknesses of both types of catalysts.[120]

**Table 3.5** Advantages and disadvantages of homogeneous and heterogeneous catalysts.

| | **Homogeneous Catalysis** | **Heterogeneous Catalysis** |
|---|---|---|
| Activity | High | variable |
| Selectivity | high | variable |
| Reaction conditions | mild | harsh |
| Catalyst life | variable | long |
| Sensitivity toward catalyst poisons | low | high |
| Diffusion problems | none | may be important |
| Catalyst recycling | expensive | not necessary |
| Variability of steric and Electronic properties of catalyst | possible | not possible |
| Understanding of mechanism | fairly good | very poor (except for model systems) |
| Product separation | difficult | easy |

Organometallic catalysts have the advantage of generally being well-defined in terms of molecular structure and offer structural variability with the potential of tailor-made catalysts. The main disadvantages of homogeneous catalysis are difficulties in catalyst-product separation and their low thermal stability (< 200 °C) compared to classical, heterogeneous, supported catalysts. However, the mechanistic understanding of the catalytic cycles in homogeneous catalysis is superior, along with the possibility of influencing steric and electronic properties of these well-defined systems. The ideal catalyst would therefore combine the advantages of homogeneous catalysis such as activity and selectivity and minimise the disadvantages associated with catalyst recovery.

The catalytically active species can be immobilized on an inert support in several ways. Inorganic backbones (such as polysiloxanes) are generally prefered over organic polymers (such as polystyrene) as catalyst carriers because of their much higher thermal and mechanical stability. "Heterogeneous modifications" of homogeneous catalysts thus comprise both the supramolecular concepts of host-guest interactions[133] and the "ship-in-the-bottle" principle in zeolite catalysis.[134]

Dendrimers offer a possibility for developing materials that combine the most desirable features of homogeneous and heterogeneous catalysis, while minimizing the

disadvantages of both. The organometallic catalytic sites are expected to be dispersed in a controlled manner on the periphery of a dendrimer. This approaches the ideal situation of precisely defined catalytically active sites on a nanoscale particle.[12b] This is in contrast to the poorly-defined sites provided by homogeneous catalysts anchored on polymer supports. Each catalytic site in the dendrimer is expected to behave independently, and electrochemical studies on multiple ferrocenyl-containing dendritic molecules confirm the presence of multiple but noninteracting redox sites on the periphery.[52] As a result of the spherical shape of dendrimers, all the active sites should be exposed and readily accessible to reactants in the reaction mixture. The metallodendrimer's relatively high molecular weight should allow easy recovery from a reaction solution by methods such as ultrafiltration.

The aryldiaminonickel(II)-functionalised first-generation polysilane dendrimer reported in 1994 by Van Koten and coworkers[71] provided one of the first examples of catalysis by a dendrimer (see Figure 1.16, Chapter 1). They found the catalytic activity of the zero- and first-generation dendrimers (as shown by kinetic data) to be 20 and 30% less, respectively, than that of the analogous monomeric organometalllic complex $[Ni\{C_6H_3(CH_2NMe_2)_2\text{-}2,6\}Br]$. This suggests that the microenvironment of the active site needs improvement. However, the regioselectivity of the dendrimer equalled that of the monomeric complex.

Several other dendrimers containing phosphorus ligands that showed catalytic activity include phosphorus-based dendrimers terminated with palladium complexes,[72] and a phosphine core surrounded by several layers of optically active groups (see Figures 1.18 and 1.19, Chapter 1).[74] The phosphinterminated dendrimers synthesised by Reetz *et al.*[73] showed significantly higher catalytic activity of the dendrimers compared with that of the analogous monomeric complexes. This was attributed to the higher thermal stability of the dendritic complexes. In contrast, the monomeric parent compounds underwent partial decomposition to form Pd metal precipitates during the course of the reaction.

### 3.5.2 Catalytic studies on a 1st-generation dendrimer [135]

In these studies we have investigated the dendrimer as a heterogeneous catalyst precursor for the Fischer-Tropsch (FT) synthesis. Several CO hydrogenation reactions have been attempted with our first generation ruthenium dendrimer, **33** loaded on silica in order to answer two questions, namely: (i) does mono-atomic Ru catalyse the Fisher-Tropsch synthesis ? (ii) how many ruthenium atoms in close proximity are required for the synthesis of higher hydrocarbons ?

Catalysts for the F-T synthesis must possess multiple functionality, since the synthesis of higher hydrocarbons from syngas (CO + $H_2$) requires the adsorption of hydrogen and carbon monoxide, the cleavage of H-H and the C-O bond, the hydrogenation of carbonaceous surface species, the removal of surface oxygen species and the formation of C-C bonds.[136] Iron, cobalt, ruthenium and nickel are known to catalyse the formation of higher hydrocarbons from synthesis gas (syngas).[137] As the F-T reaction is catalysed by an ensemble of surface metal atoms, the minimal size of the ensemble is of interest.

Mono-atomic ruthenium exists in homogeneous complexes such as $Ru(CO)_5$ but ruthenium carbonyl can not be used under typical F-T conditions because of its high volatility. The approach we have taken is to anchor to a silica support a dendrimer, **33**. The ruthenium dendrimer contains mono-atomic ruthenium atoms on the periphery of the macromolecule. The "time-on-stream" behaviour during the CO hydrogenation was studied since the stability of the dendrimer under the Fischer-Tropsch reaction conditions was unknown. Some decomposition and/or leaching due to its slight solubility in apolar organic solvents was expected.

**Preparation and characterisation of the catalysts**

The ruthenium dendrimer was impregnated on silica gel (3% Ru loading) using the incipient wetness technique (see experimental section 7.3). The solvent was removed by applying a $N_2$ stream at room temperature. There was no further pretreatment of the sample. For comparison, a known $Ru/SiO_2$ catalyst was prepared by impregnation of silica gel with aqueous $RuCl_3 \cdot xH_2O$, also using the incipient wetness technique. In contrast to the dendrimer, the dried catalyst was pretreated in the FT-synthesis reactor. The known catalyst is assumed to have a ruthenium content of 0.8 wt% after reduction.

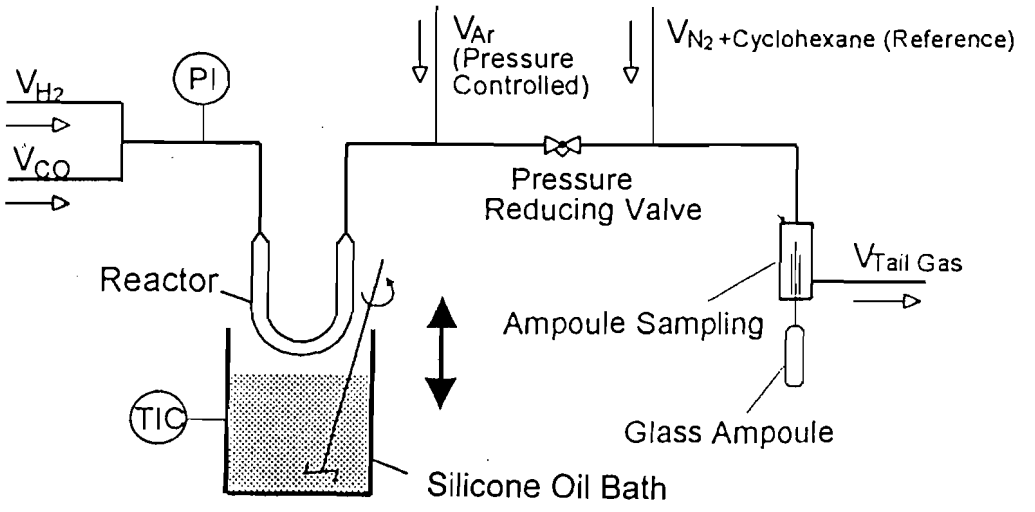


**Figure 3.12** Schematic of the apparatus used for the CO hydrogenation reaction.

The stability of the ruthenium dendrimer catalyst, Ru-dendrimer/$SiO_2$ in different environments was characterised by TGA under flow conditions using different gases: $N_2$, $H_2$, CO and a $H_2$/CO mixture. Figure 3.12 shows schematically the experimental set-up for the reactions. The apparatus was designed to detect the initial behaviour of each catalyst and to distinguish FT-activity from the expected decomposition of the ruthenium dendrimer which was expected. The small reactor was dipped into a pre-heated silicon oil bath to ensure a rapid heat-up of the catalyst bed. Rapid sampling was ensured using the ampoule sampling technique[138] which allows for the evaluation of mass balances and product spectra with high temporal resolution.

The TGA trace of Ru-dendrimer/$SiO_2$ in different environments is shown in Figure 3.13. Two steps of weight loss were observed. The first weight loss at <100 °C is probably due to evaporation of $CH_2Cl_2$ from the preparation step of the dendrimer. The second weight loss at >180 °C can be attributed to decomposition of the dendrimer, the dendrimer decomposing more rapidly in the hydrogen-rich ($H_2$ or $H_2$ + CO) atmospheres. This suggests that hydrogen is involved in the destruction of the dendrimer, *e.g.* by hydrogenolytic reactions. From these results, a reaction temperature of 170 °C was chosen for the CO hydrogenation reactions. This temperature is below the decomposition temperature of the dendrimer and at the same time it is sufficiently high for FT-synthesis. Pre-runs of FT-synthesis with the known Ru/$SiO_2$ catalyst showed that

a lower reaction temperature was not sufficient to guarantee reliable product data under the conditions used (because of GC detection limits).

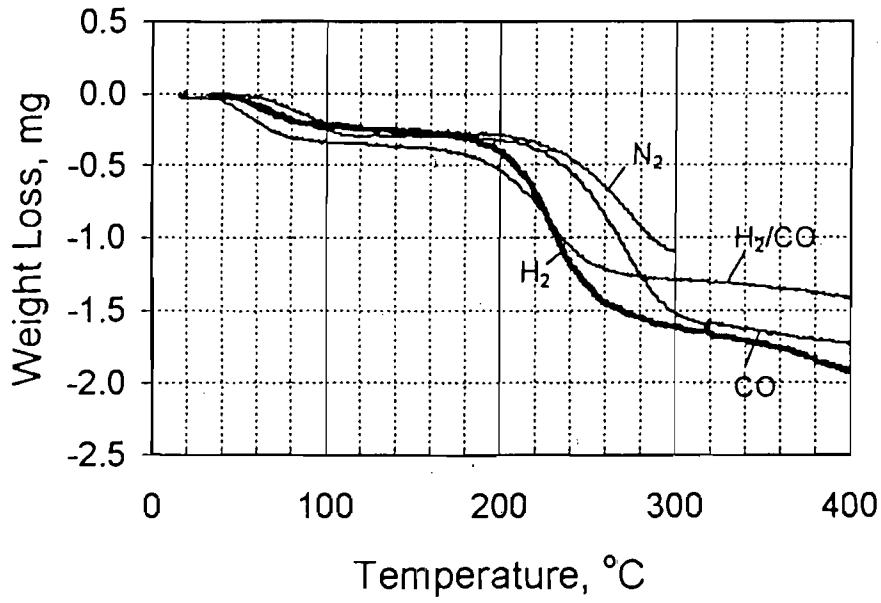


sample mass = 25 mg, heating rate = 5°C/min, flow rate = 30 ml(NTP)/min

**Figure 3.13** TGA trace of Ru-dendrimer/$SiO_2$ under different gas environments.

**The CO hydrogenation with the known Ru/$SiO_2$ catalyst**

Figure 3.14 shows the activity (expressed as total formation rates or yields of volatile organic compounds (voc) on a carbon basis) of the known Ru/$SiO_2$ catalyst as a function of time on stream (TOS). Approximately 4 minutes after the synthesis is initiated, the catalyst starts to deactivate rapidly. Steady state conversion levels are reached after about one day on stream ($Y_{voc}$ , 0.02 C-%). These low yields of organic compounds still allowed a detailed quantitative evaluation of F-T selectivities (see Figure 3.16).

Figure 3.15 shows an Anderson-Schultz-Flory (ASF) chart (logarithmic plots of molar product fractions versus carbon number), which can be taken as confirmation for the existence of polymerisation kinetics.[139] Very straight lines were obtained from from $C_3$ to $C_7$ or $C_9$, their slopes allowing for the calculation of chain growth probabilities of ca. 0.60$\pm$ 0.04 (decreasing with decreasing catalyst activity). Methane selectivities in the volatile organic compounds ranged between *ca.* 20 and 31 %-C (increasing with time on stream). The olefin contents in the respective hydrocarbon fractions of the same carbon number amounted to about 70 mol-% and were independent of carbon number. This

indicates the absence of secondary olefin hydrogenation, a reaction often occurring during FT-synthesis.[140]

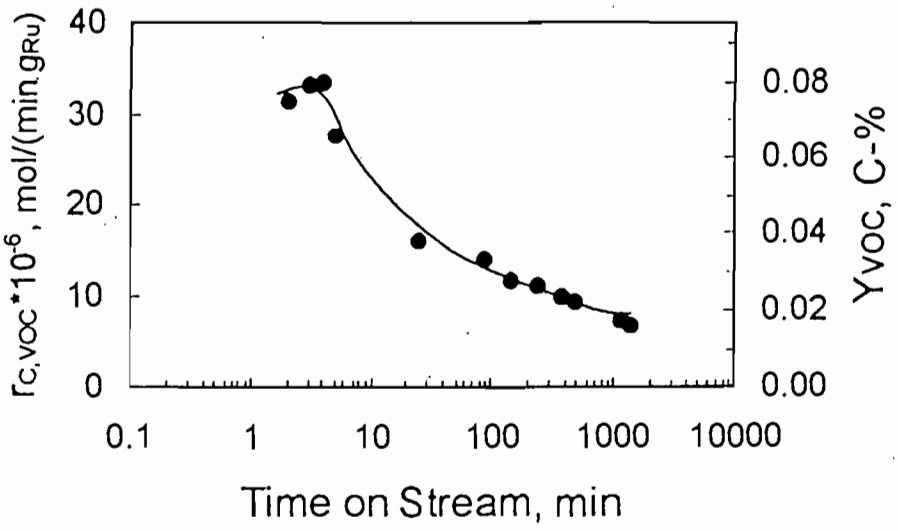


**Figure 3.14** Total formation rates and yields volatile organic compounds during FT-synthesis with $Ru/SiO_2$ catalyst.

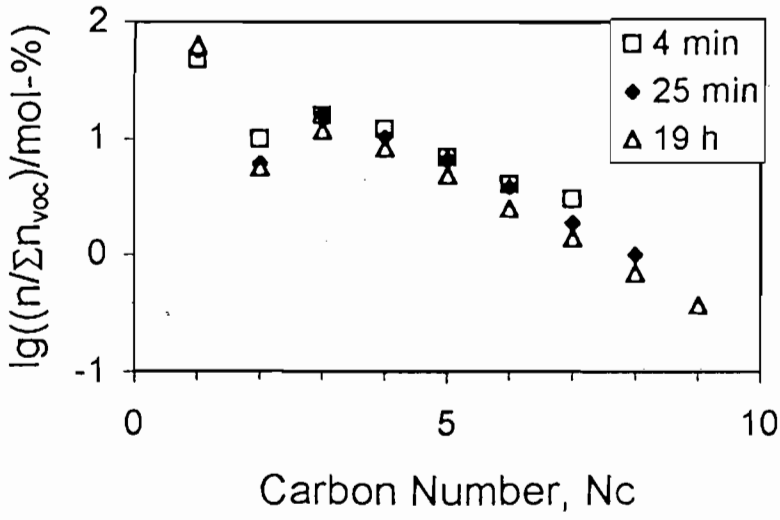


**Figure 3.15** ASF-distributions at 3 different reaction times. FT-synthesis with the known $Ru/SiO_2$ catalyst.

**CO Hydrogenation with Ru-dendrimer/$SiO_2$**

Figure 3.16 shows sections of a typical chromatogram obtained from samples taken during the CO hydrogenation. Comparison of the two chromatograms reveals little resemblance. Apart from a few identified peaks (such as those corresponding to propene and cyclopropane, methane, n-butene and methanol), the use of Ru-dendrimer/$SiO_2$ does not result in typical F-T product patterns ($C_3$ - $C_9$ fractions). The products formed are therefore believed to originate mainly from the decomposition of the dendrimer. Two additional peaks, marked X1 and X2 in the chromatogram, could not be identified.

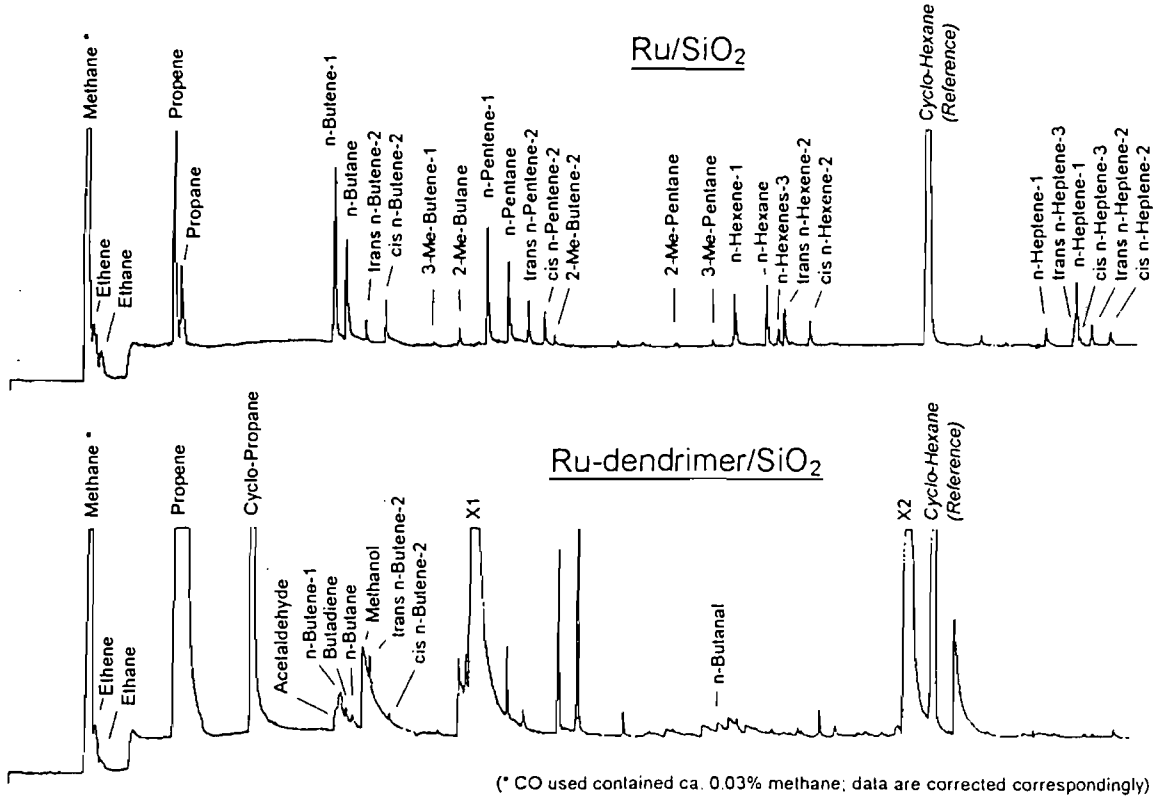


**Figure 3.16** Gas-chromatograms of product samples after a reaction time of 4 min: (a) CO hydrogenation with Ru/$SiO_2$ and (b) with the Ru-dendrimer/$SiO_2$.

Time resolved formation rates of the main products and the sum of all products during the CO hydrogenation with the ruthenium dendrimer are shown in Figure 3.17. The total

product formation rate passes through a maximum after *ca.* 4 minutes time on stream. At this time, more than 80 %C of the product consists of propene and cyclopropane. The maximum formation rates of the unknown compounds, X1 and X2 apppear earlier, indicating their formation to be comparatively faster. The product composition and the sharp decrease in the formation rates of organic compounds as a function of reaction time are clear indications that the dendrimer decomposes under the reaction conditions. X1, X2, propene and cyclopropane were also shown to be formed during thermal decomposition of the dendrimer in air. Integration (on a carbon basis) of all the product molecules formed during the 24 hour CO hydrogenation reaction suggests that only *ca.* 7% of the dendrimer decomposed.

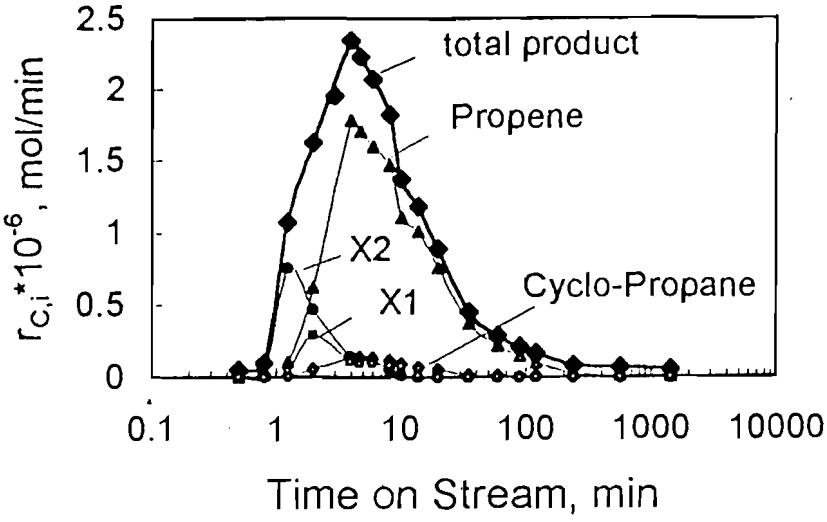


**Figure 3.17** Product formation rates (C-basis) as function of time on stream. CO hydrogenation with the Ru-dendrimer/$SiO_2$.

The amount of decomposition of the peripheral structure of the dendrimer can be estimated to be *ca.* 20% if one assumes that all product molecules bearing three carbon atoms (propene, propane, cyclopropane) to originate exclusively from $C_3$-units in the dendrimer (see Scheme 3.1). The effects of leaching of the ruthenium dendrimer by liquid reaction products can be excluded since no formation of liquids could be detected. Although the dendrimer decomposes and part of the ruthenium could have escaped the reactor as *e.g.* volatile ruthenium-carbonyls, the major fraction of the ruthenium should still be available for catalytic reactions. Inductively coupled plasma (ICP) experiments performed on Ru-dendrimer/$SiO_2$ before and after the CO hydrogenation reaction showed that the ruthenium remained on the silica after the dendrimer decomposed.

**Comparison of FT-activity of Ru-dendrimer/$SiO_2$ and the Ru/$SiO_2$ catalyst**

A direct comparison of FT-selectivities such as chain growth probability with the Ru/$SiO_2$ catalyst was not possible since CO hydrogenation with the ruthenium dendrimer showed no obvious FT-product patterns. The gas chromatograms obtained from samples of the dendrimer experiment showed the presence of compounds like ethene, ethane and linear $C_4$-hydrocarbons, which could theoretically be the result chain growth steps typical of FT. To confirm this, the molar formation rates of linear $C_4$- hydrocarbons (excluding butadiene) per gram ruthenium were plotted as a function of time on stream for the Ru/$SiO_2$ catalyst and for the Ru-dendrimer/$SiO_2$ (Figure 3.18).

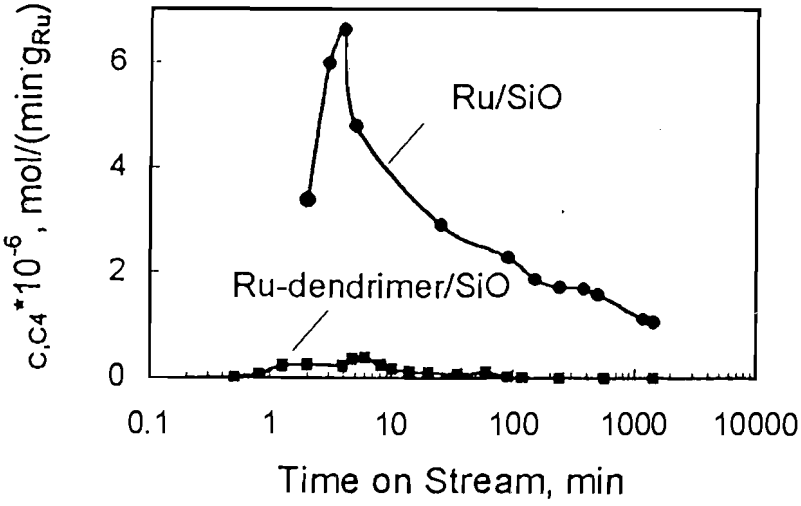


**Figure 3.18** Formation rates of C4-hydrocarbons (C-basis) during CO hydrogenation with Ru/$SiO_2$ and Ru-dendrimer/$SiO_2$.

A blank FT-activity of the reactor without catalyst was not detectable. Both formation rates passed through a maximum after 4-5 minutes, but, the rates with the Ru/$SiO_2$ catalyst were much higher (15-20 times) than those with the Ru-dendrimer/$SiO_2$ at all stages of the experiment. If one assumes an initial Ru-dispersion of 100% in the dendrimer, and a dispersion of *ca.* 10% for the Ru/$SiO_2$ catalyst, then the activity of the dendrimer should be at least two orders of magnitude higher with the standard catalyst. This disparity indicates that the monoatomic ruthenium in the dendrimer does not display any FT-activity. The $C_4$ products formed are probably due to hydroformylation of propene, which ruthenium is known to catalyse,[141] and further hydrogenation of the $C_4$-oxygenates (n-butanal was detected).

Thus, results from the time resolved CO hydrogenation with a standard $Ru/SiO_2$ catalyst and a Ru-dendrimer on a silica support suggest that mono-atomic ruthenium in the dendrimer is not able to catalyse FT-specific C-C bond formation. It can therefore be concluded that the minimal metal ensemble size is greater than one metal atom. Future work will be aimed at investigations with small metal clusters *e.g.* binuclear ruthenium organic compounds.

## 3.6 Conclusions

A series of ruthenium dendrimers have been prepared (according to established methods) and characterised by m.p., IR spectroscopy and $^{1}H$ and $^{13}C$ NMR spectroscopy. The yields for the ruthenium dendrimers are higher than those for the analogous iron dendrimers described in Chapter 2. The ruthenium dendrimers and precursors were found to be more stable in air at room temperature than the iron dendrimers.

The structural and physical behavioural properties of several dendrimer precursors and the first generation organoruthenium dendrimer, **33** have been investigated by x-ray crystallography, molecular modelling and cyclic voltammetry. It was not possible to grow suitable single crystals of the dendrimer **33,** but the x-ray crystal structure of the dendrimer precursor, **32** was successfully determined.

Electrochemical studies carried out on the dendrimer precursor, **31** and the dendrimer, **33** showed oxidation to be independent of the number of metal atoms present. This suggested that there was no communication or interaction between any of the metal atoms.

The chemical reactivity of the first generation dendrimer, **33** was also investigated. The dendrimer was indeed found to react differently from the mononuclear compound, $CpRu(CO)_2R$. The dendrimer tended to react more slowly than the mononuclear compound, most probably due to the congested steric environment of the dendrimer. In the reaction of **33** with $I_2$, all six metal sites on the dendrimer reacted with the $I_2$; however the reaction of **33** with $Ph_3CPF_6$ produced a mono-cationic species. The ruthenium dendrimer precursors also tended to be less reactive than the analogus iron dendrimers, which agreed with trends observed previously. These results suggest that this dendrimer does indeed behave differently to a monomeric species.

Finally, the first generation dendrimer, **33** was immobilised on silica and tested as a catalyst in Fischer-Tropsch synthesis. The dendrimer did not show Fischer-Tropsch activity, which may indicate that mono-atomic ruthenium is not sufficient to catalyse FT-specific C-C bond formation. The oxidation state of the ruthenium in the dendrimer could also be too high and might be corrected with a pretreatment procedure, as in the case of the standard ruthenium catalyst.

# Chapter 4

# Synthesis and characterisation of cobaloxime dendrimers

## 4.1 Introduction

Vitamin $B_{12}$ which contains cobalt, is one of the essential human nutrients.[142] The discovery of a direct cobalt-carbon bond in coenzyme $B_{12}$ (5'-deoxy-5'-adenosylcobalamin) indicated for the first time that organometallic reactions occur in biological systems. The macrocyclic ligand appeared to modify the properties of cobalt significantly, enabling it to form stable cobalt-carbon bonds, since only a few rather unstable compounds containing cobalt-carbon σ-bonds were known up to that point.[143a]

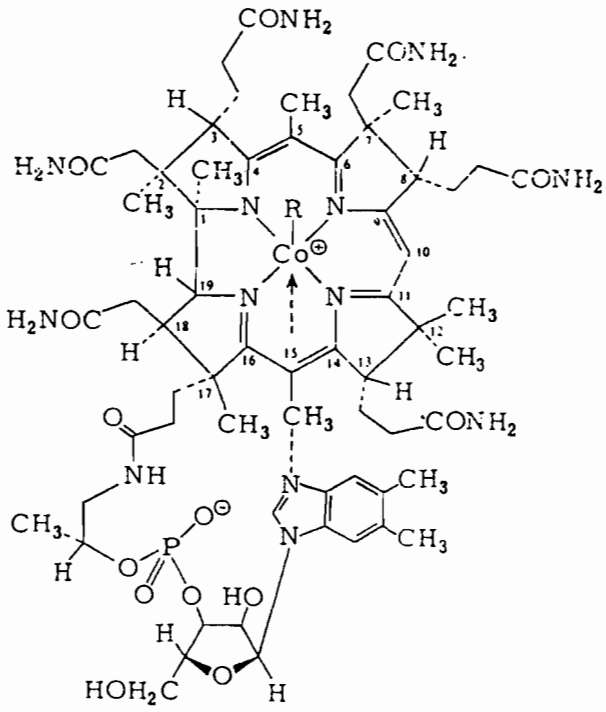

**Figure 4.1** Structure of an organocobalamin. In vitamin $B_{12}$, R = CN.

In 1964, Schrauzer and Kohnle[143b] reported that the reactions of the cobalt atom in vitamin $B_{12}$ (Figure 4.1) can be simulated with much simpler complexes. The cobalt(III) complexes of diacetyl-dioxime resemble vitamin $B_{12}$ so closely in their chemical properties that they were introduced as co-ordination chemical models of vitamin $B_{12}$. The term "cobaloximes" was derived to stress their similarity to the cobalamins. There is much documentation in the literature confirming the validity of cobaloximes as Vitamin $B_{12}$ model compounds.[143c] Other cobalt compounds such as cobalt chelates[3,144] have been proposed as alternative models, but the simple cobaloximes, abbreviated [Co], simulate the reactions of Vitamin $B_{12}$ most closely (Figure 4.2). These model compounds also have the advantage of being easily prepared in the laboratory.

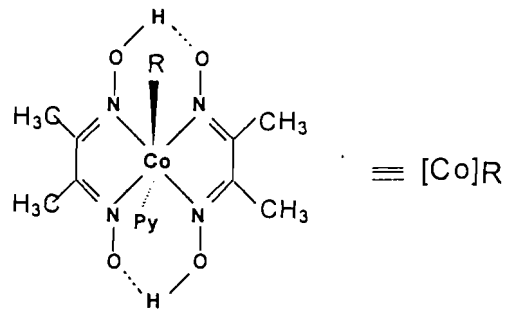


**Figure 4.2** A cobaloxime used as a model compound.

Model compounds and model systems with similar chemical properties and biochemical activity have been used for many years for studying biological systems. In view of the complicated structure of vitamin $B_{12}$, model compounds such as the cobaloximes provide a basis for understanding the mode of action of corrinoid coenzymes in enzymatic reactions. Studies on model compounds also increase the knowledge of the properties and reactions of organocobalt compounds.

The biological activities of vitamin $B_{12}$ coenzymes are associated with the presence of cobalt, whose oxidation-reduction potentials are modified by incorporation into the corrin system. The striking analogies between the chemical properties of the cobalt atom in vitamin $B_{12}$ and in the cobaloximes are primarily a consequence of the co-ordinating power of the four $sp^2$-hybridized nitrogen atoms. The partial positive charge on cobalt is slightly higher in the cobaloximes than in vitamin $B_{12}$, causing a firmer attachment of the axial bases in the model compounds as compared to the corrins. Although organocobalt

complexes of Vitamin $B_{12}$ and of model compounds are usually described as cobalt(III) compounds, this can cause confusion as the high covalency of the cobalt-carbon bond is ignored. It is more realistic to describe the nature of the axial cobalt-carbon bond in terms of equation (i) with structure (a) being the most important.

$$\underset{\mathbf{a}}{R\text{-}[Co]} \leftrightarrow \underset{\mathbf{b}}{R^{+}\ [Co^{-}]} \leftrightarrow \underset{\mathbf{c}}{R^{\cdot}\ [Co^{+}]} \qquad \text{(i)}$$

Cobalt(I) derivatives are some of the most powerful nucleophiles known and have been called "supernucleophiles". Cobalt(I) supernucleophiles react with conventional alkylating reagents, **RX** to yield organocobalt complexes, **R-[Co]**, the reactions being nucleophilic substitutions that occur with inversion of the α-carbon (Scheme 4.1).[145] Usually stable organocobalt compounds are only formed if the cobalt-bound carbon is primary or secondary.[146a]

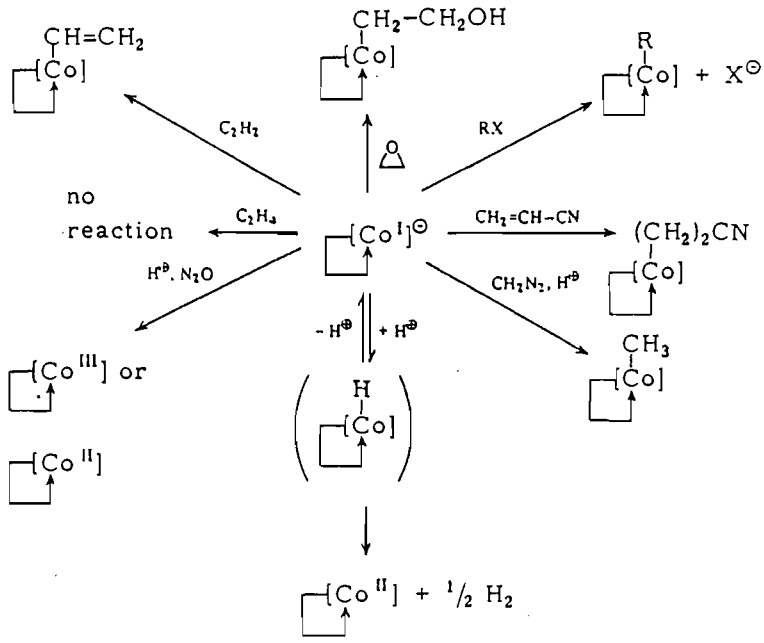


**Scheme 4.1**

Cobaloximes are known to undergo a variety of reactions. The covalent cobalt-carbon bond in the organocobalt complexes may be cleaved by nucleophillic- and electrophillic attack as well as reductive cleavage. Methylcobaloxime derivatives react with nucleophiles such as $Cl^{-}$, $CN^{-}$, $P(C_6H_5)_3$ and with cobalt(I) supernucleophiles

themselves.[146b,147] Reductive cleavage of cobalt-carbon bonds occurs preferentially with organocobalt complexes carrying electronegatively substituted alkyl residues.

Cobaloximes have potential uses as catalysts in organic reactions, in particular as metal-intermediates in intramolecular radical processes which could lead to the synthesis of complex carbocyclic frameworks.[148] As mentioned in Chapter 3, anchoring a cobaloxime catalyst to the surface of a dendrimer would make the catalyst easier to separate from the product by methods such as filtration or phase-layer separations. Reactions like radical cyclisation and stereoelectronically specific reactions would therefore be more accessible in industry. The aim of these experiments was to prepare a series of cobaloxime dendrimers which might have potential uses as catalysts in reactions of the types described above.

**Cobalt dendrimers in the literature**

Several cobalt-containing dendrimers have appeared in the literature. Cobalt has been included into dendrimers as Co(II)acetate[149], $Co(CO)_3$,[55] $Co_2(CO)_8$,[150] and as cobaltocenium units.[151] Seyferth *et al.*[11] reported cobalt-capped metallodendrimers up to the second generation. The terminal bis-cobalt complexes were formed via treatment of alkyne moieties on the carbosilane dendrimer with $Co_2(CO)_8$ (Scheme 4.2). Other cobalt-carbonyl dendrimers have been prepared by reaction of the carbosilane dendrimers with sodium cyclopentadienide followed by reaction with $Co_2(CO)_8$.[151b]

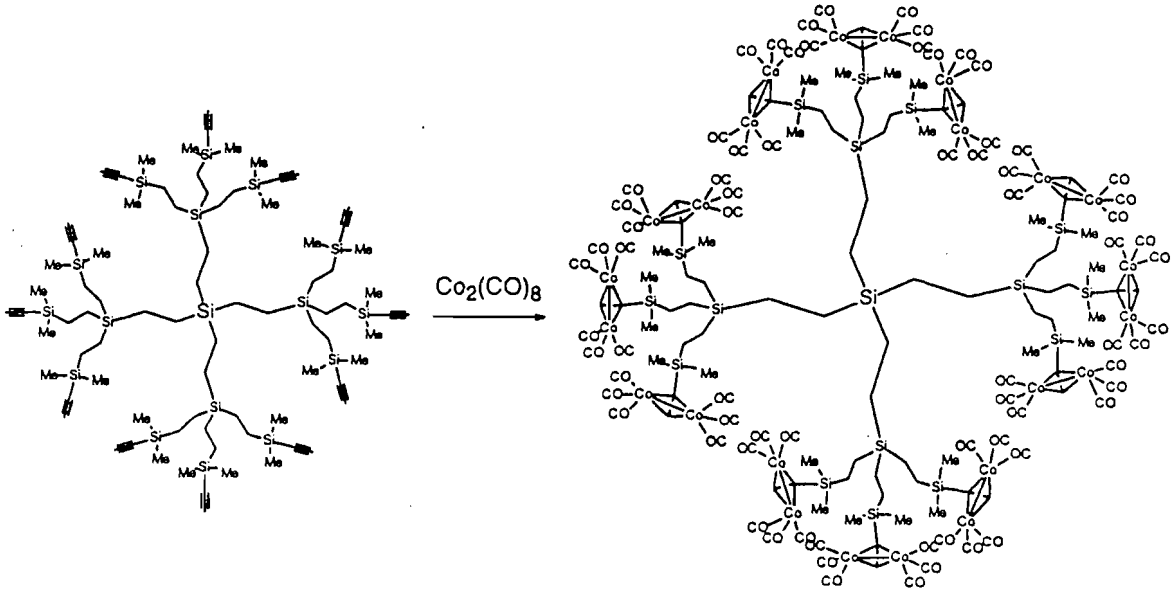


**Scheme 4.2**

Metallodendrimers up to the third and fourth generation have been used to form large supramolecular polycobaltocene complexes. β-Cyclodextrin derivatives were shown to facilitate aqueous solubilization of the reduced [$Cp_2Co(0)$] form via termini encapsulation.[151a] Figure 4.3 shows a polycobaltocene dendrimer containing 32 peripheral cobaltocenium subunits.

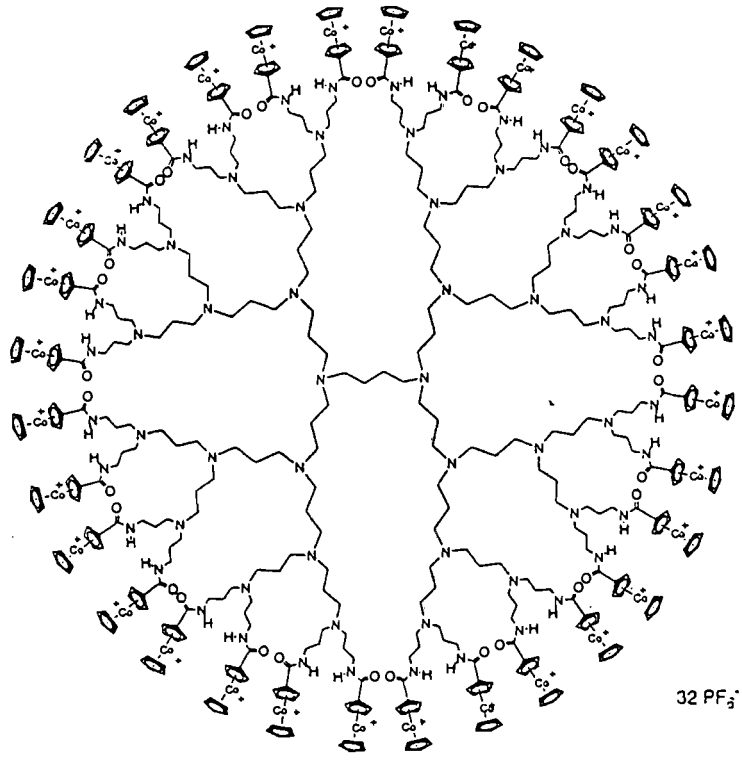


**Figure 4.3** A fourth generation polycobaltocene dendrimer that has been shown to co-ordinate β-cyclodextrin.[151b]

Recently Constable, Housecroft and co-workers[152] reported the synthesis of a dendritic tetrahedral polyphenylacetylene. Reaction of the acetylene moieties with $Co_2(CO)_8$ gave the dendritic cobalt-carbonyl complex (Figure 4.4). These complexes are potential precursors to the formation of metal oxide nanospheres.[152]

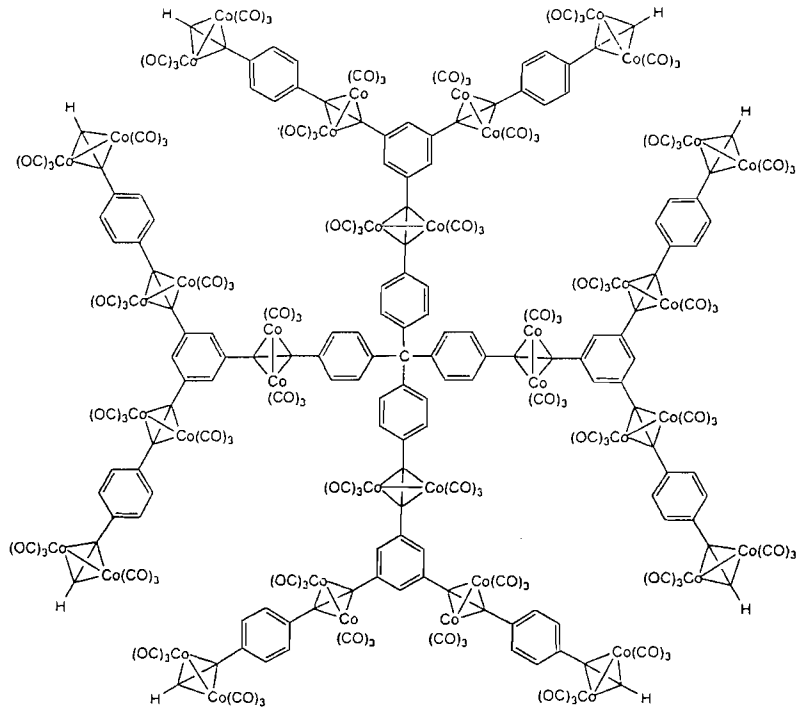

**Figure 4.4** A cobalt dendrimer containing 40 cobalt atoms.[152]

## 4.2 Synthesis and characterisation of cobaloxime dendrimers

### 4.2.1 The [Co] system

There have been no previous reports in the literature regarding the synthesis of cobaloxime dendrimers. Cobaloximes (which contain trivalent cobalt) will be represented by [Co] in this thesis. A similar strategy to that described in Chapters 1 and 2 was used to synthesise the cobaloxime dendrimers. The convergent approach was used to build up the cobaloxime dendritic wedges. Schemes 4.3 and 4.4 show the synthesis of the haloalkyl complexes and formation of the dendritic wedges respectively. Chloropyridinecobaloxime was synthesised according to literature procedure in good yields and used as our starting material for the bromoalkylpyridinecobaloxime complex.[146c] The bromopropyl-, bromobutyl- and bromohexyl-pyridinecobaloxime complexes, **38, 39** and **40** were prepared according to Finch and Moss[153] and isolated as yellow/orange solids (Scheme 4.3, shown for n = 6). Some characterisation data for these compounds is listed in Table 4.1.

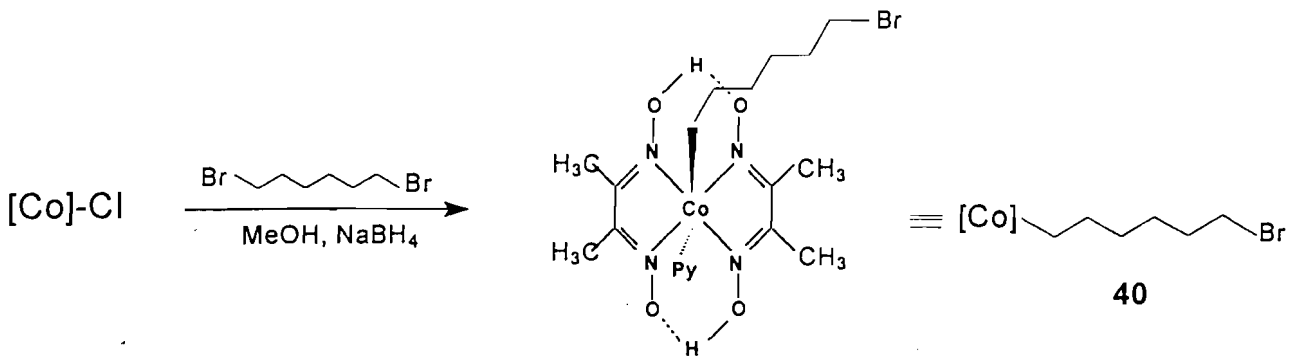


**[Co]3Br (38)**
**[Co]4Br (39)**
**[Co]6Br (40)**

**Scheme 4.3**

**Table 4.1** Characterisation data for cobaloxime dendrimer precursors.

| Compound | Appearance | Yield (%) | m.p. /°C | IR ν(Co-C)[a] /cm$^{-1}$ |
|---|---|---|---|---|
| [Co]3Br (**38**) | yellow/orange solid | 49 | 174-180 | 321 |
| [Co]4Br (**39**) | orange solid | 50 | 163-166 | 321 |
| [Co]6Br (**40**) | orange solid | 70 | 170(dec) | 319 |

[a] IR spectra recorded as a Nujol mull

We attempted to synthesise a series of cobalt dendrimers using the Hawker and Fréchet[28] methodology described in Chapters 2 and 3. The initial reactions were performed on the propyl cobaloxime complex, **38**. The complex was refluxed with 3,5-dihydroxybenzyl alcohol in acetone for 96 hours in the presence of 18-crown-6 and potassium carbonate (Scheme 4.4, shown for *n* = 6). TLC was used to monitor the reactions. $^1$H NMR spectroscopy however showed none of the expected benzyl alcohol product, only unreacted starting material. It was assumed that the length of the alkyl chain in the molecule was not sufficient to complex with the 3,5-dihydroxybenzyl alcohol monomer unit. The above reaction was then repeated with the butyl complex, **39**[154] and the hexyl complex, **40**. In both these cases, two products were obtained after refluxing

for long periods of time. The major product was identified as the "di-substituted" benzyl alcohol, **43** and **44** respectively by $^1$H NMR spectroscopy. The minor products were also identified by $^1$H NMR spectroscopy as the "mono-substituted" benzyl alcohols, **41** and **42**. These "mono-substituted" products form first as intermediates on route to the "di-substituted" products.

Column chromatography was used to purify the compounds. Silica gel was found to be superior to alumina for separating these cobaloxime complexes and the products were eluted with ethyl acetate/acetone mixtures. The products tended to tail on silica (and more so on alumina) which made separation of the product from any unreacted starting material difficult. The oily solids obtained after column chromatography were crystallised from $CH_2Cl_2$/pentane mixtures. The dark orange solids were subsequently dried under vacuum to remove solvent.

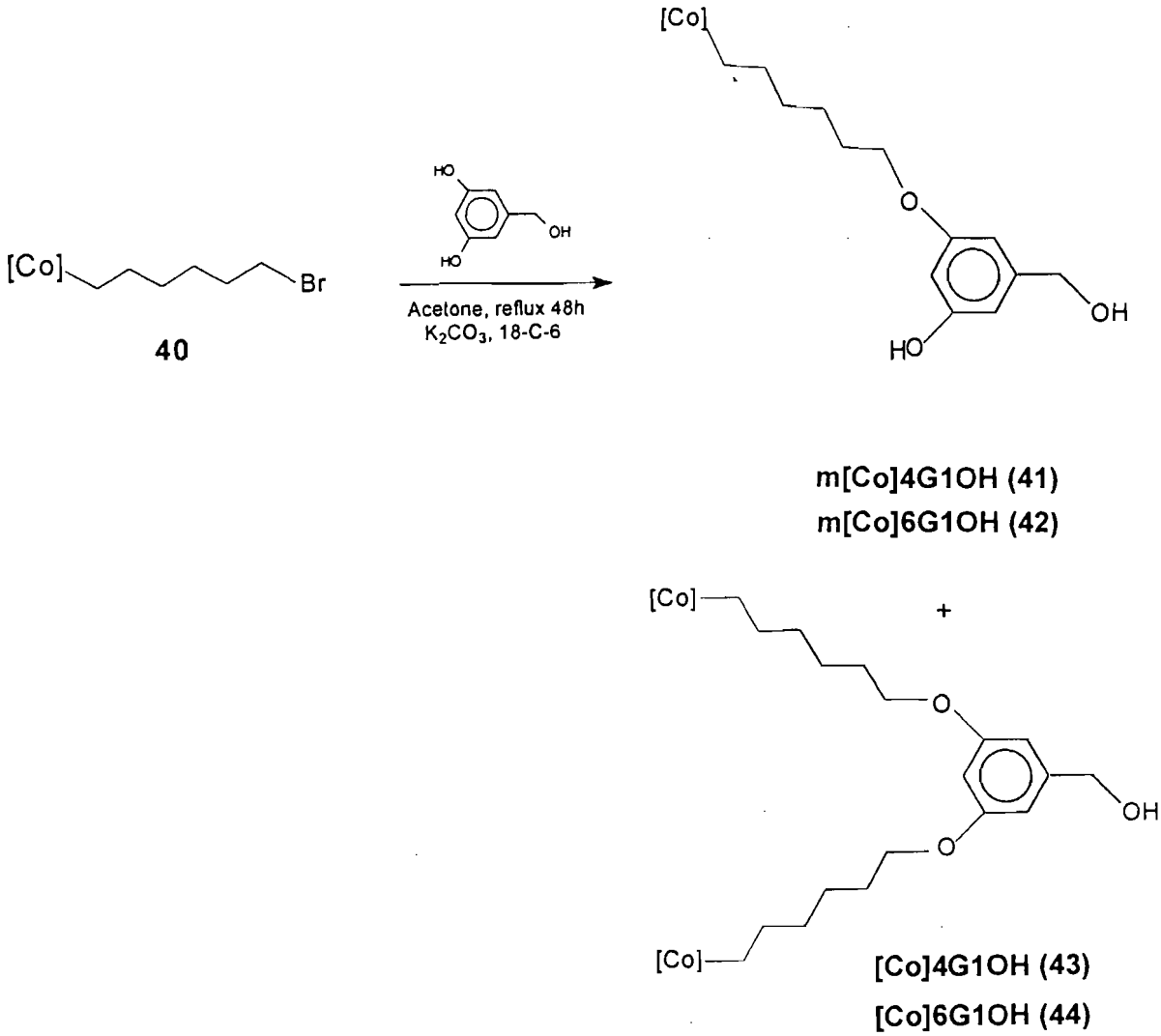


**Scheme 4.4**

The conversion of the bromohexylcobaloxime benzyl alcohol, **44** to the benzyl bromide **45** was attempted using two reagents: (i) $CBr_4/PPh_3$ and (ii) $PBr_3$[155] (Scheme 4.5). The first method gave a dark orange oil which was difficult to crystallise. Under vacuum, the complex decomposed to a brown oil. Activation with $PBr_3$ gave the required benzyl bromide, **45** in good yield (75%). Activation of the **43** with the $CBr_4/PPh_3$ mixture was also unsuccessful. This meant that reactions with the butyl complex could not proceed any further and so the first generation butylcobaloxime dendrimer could not be synthesised.

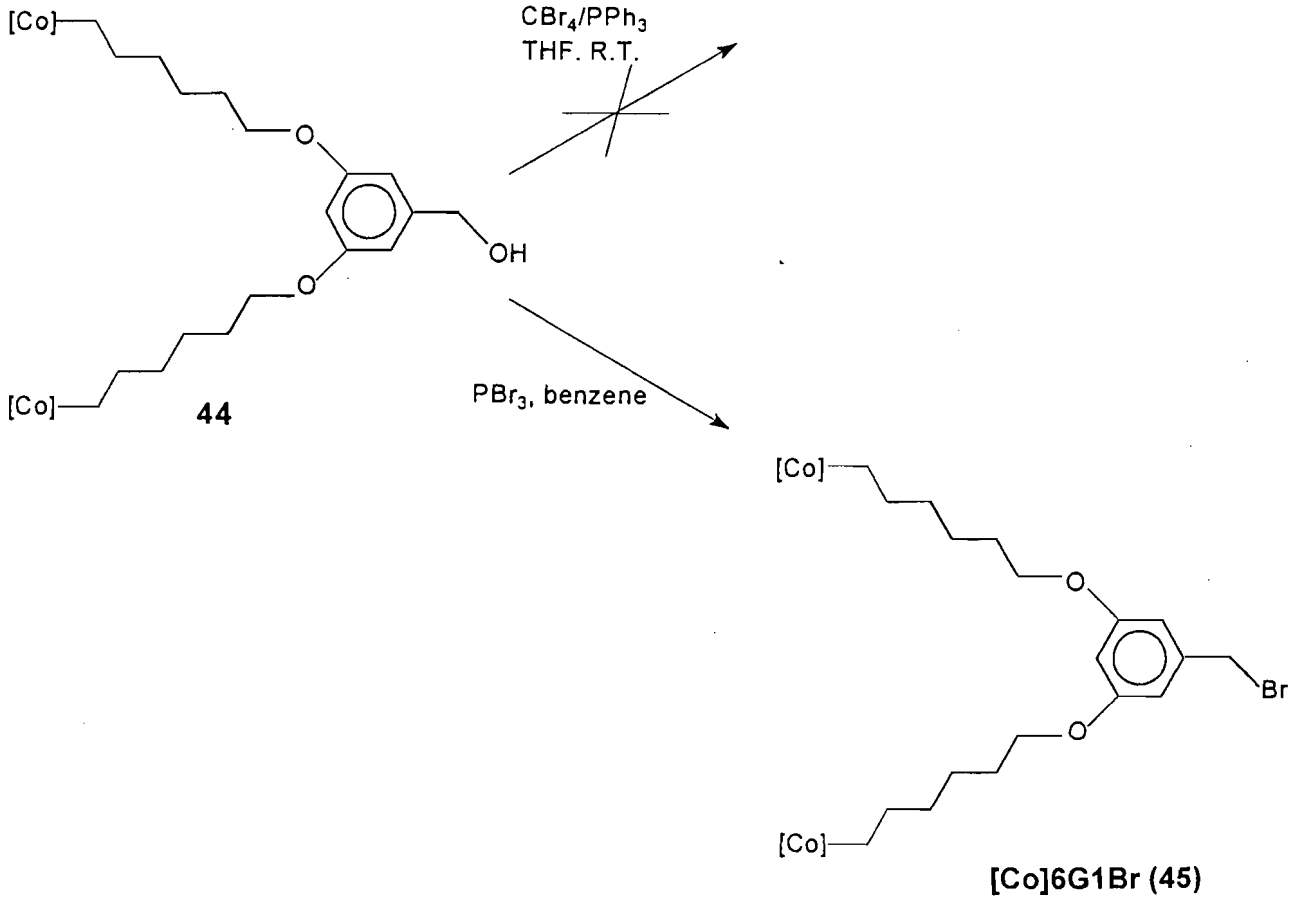


**Scheme 4.5**

Attempts to attach **45** to a core molecule were carried out in the same way as described previously for the iron- and ruthenium-containing dendrimers (see Chapters 2 and 3). Thus, the bromohexyl complex, **45** was refluxed in acetone with the CORE molecule,

$^1$H NMR spectroscopy of the isolated product however showed a mixture of the unreacted CORE molecule and **45**. The characteristic peak for the benzyl protons of the expected first generation dendrimer at *ca.* 4.9 ppm was not observed. Again, the most likely explanation for these results could be a steric one, that it is not possible to fit six cobaloxime moieties around a rigid core molecule such as the one used above.

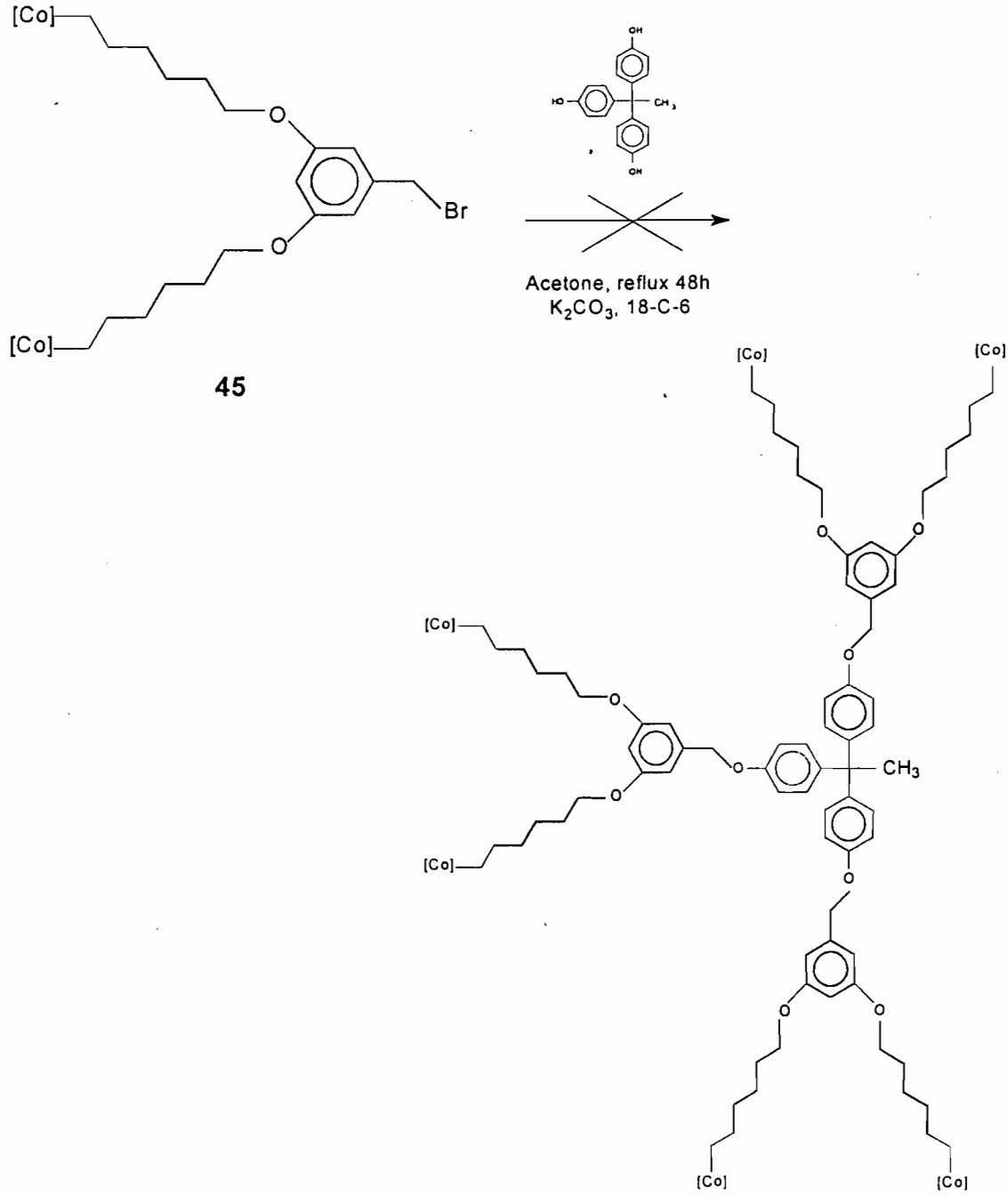


**Scheme 4.6**

However, the zero-generation dendrimer **46** was synthesised by reacting the bromo-butyl cobaloxime complex, **39** with the CORE molecule in refluxing acetone for 48 hours (Scheme 4.7). The product was isolated as an orange oil in low yield (20%). Full experimental details are given in the experimental (section 7.4).

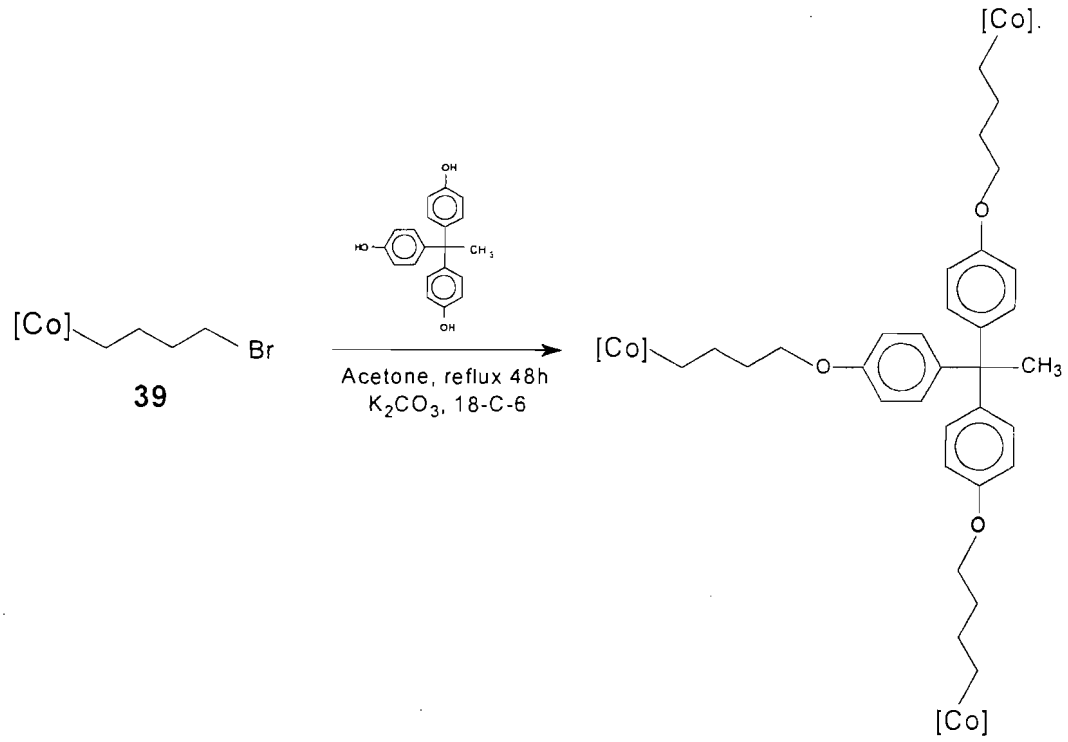


**Scheme 4.7**

### 4.2.2 Characterisation of cobaloxime dendrimers

Again $^1H$ and $^{13}C$ NMR spectroscopy was found to be very useful for identification of all the dendritic wedges, **41** - **45**. The number of peaks, as well as the integration, in the aromatic region of the $^1H$ NMR spectra confirmed either the "mono-substituted" (3 peaks) or "di-substituted" benzyl alcohol (2 peaks). The $^1H$ NMR spectrum of **43** is shown in Figure 4.5. The triplet at 3.82 ppm confirms the formation of the first generation benzyl alcohol. The triplet and doublet at 7.69 and 7.28 ppm respectively confirm the correct ratio of aromatic protons. The benzyl protons in the region 4.5 - 5 ppm are very sensitive to the functional group at the focal point of the dendritic wedge. In the cobaloxime benzyl alcohol, these benzyl protons appear at 4.57 ppm. An upfield shift of

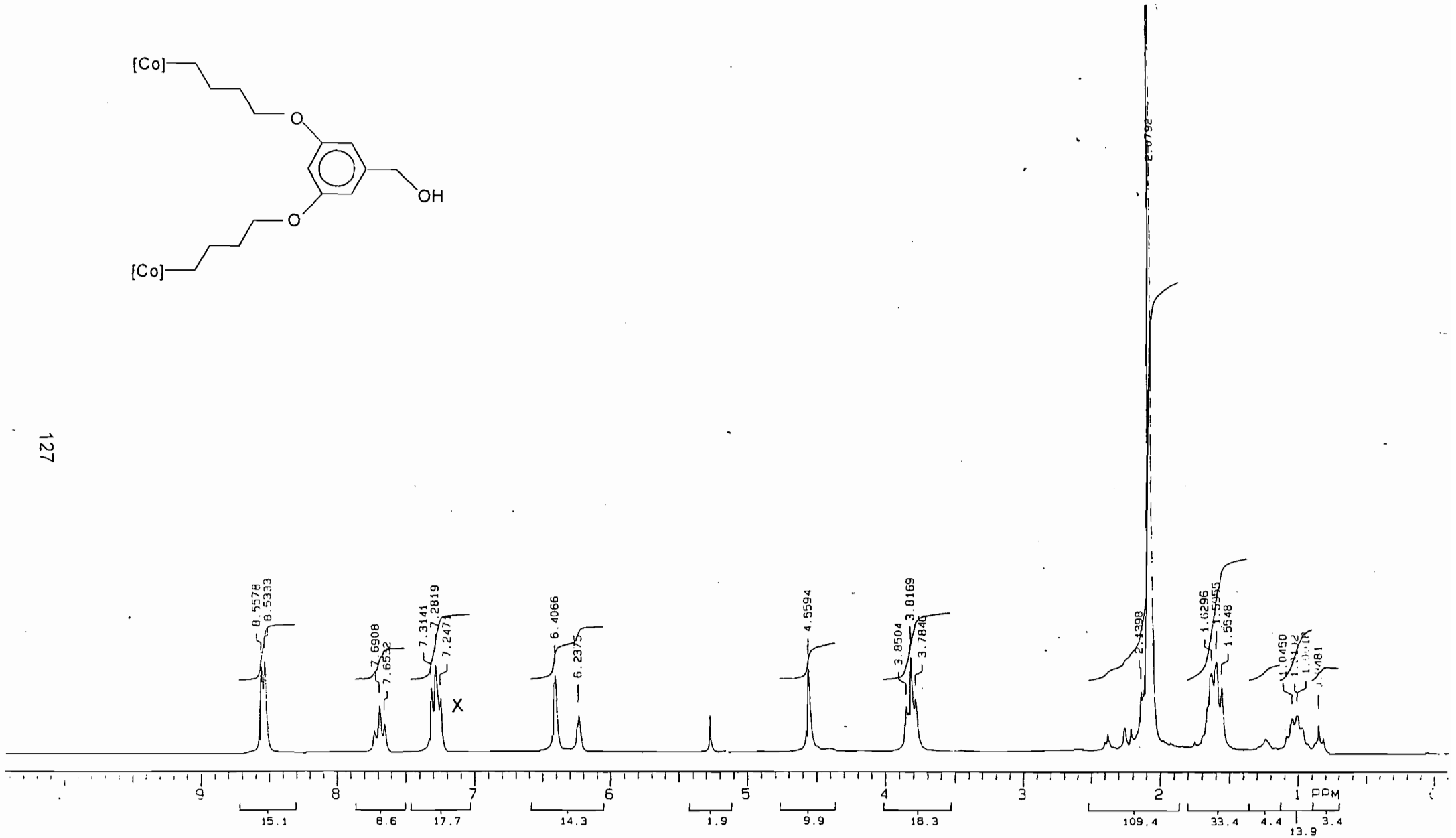


**Figure 4.5** A 400 MHz $^{1}$H NMR spectrum of **43**. X = solvent

*ca.* 0.4 ppm is usually observed upon activation to the benzyl bromide. Figure 4.6 shows part of the $^{1}H$ NMR spectrum of the zero generation dendrimer, **46**. The core aromatic protons occur as two doublets at 6.70 and 6.94 ppm. The benzyl protons occur as a triplet at 3.84 ppm confirming the formation of the dendrimer.

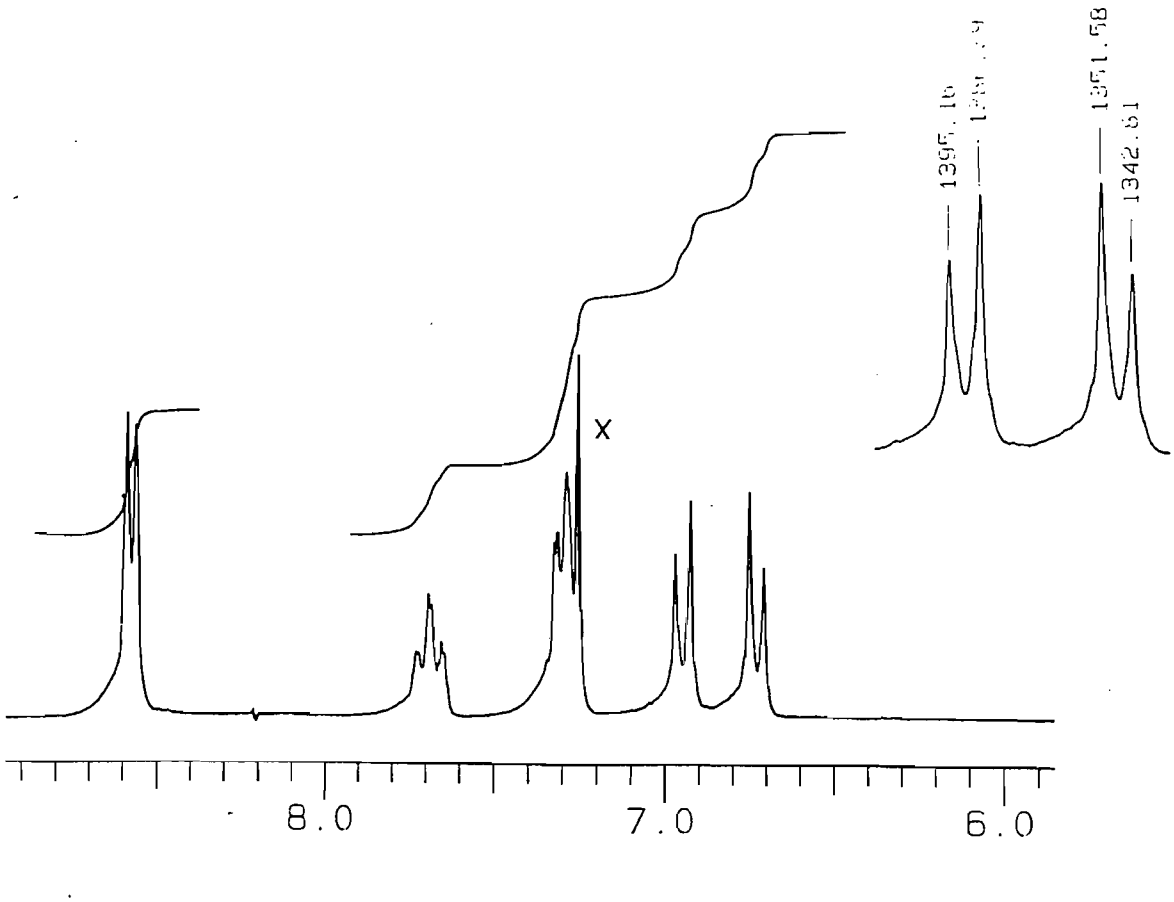


**Figure 4.6** A region of the $^{1}H$ NMR spectrum of **46**. X = solvent

$^{13}C$ NMR spectroscopy was also used to characterise the new dendrimers. A typical $^{13}C$ NMR spectrum of **43** is shown in Figure 4.7. The different environments of the aromatic carbons can clearly be seen by the four aromatic carbon peaks (160.41, 143.20, 105.13 and 100.11 ppm). Again the peak at 67.68 ppm for the benzyl carbon confirms the formation of the cobaloxime benzyl alcohol.

IR spectroscopy was also used to characterise these new compounds. The chloropyridinecobaloxime shows a strong band at 380 $cm^{-1}$ assigned to the νCo-Cl which disappears upon reaction with the bromoalkane. The new peaks at ca. 320 $cm^{-1}$ were assigned to ν(Co-C). Bands at 516, 452 and 427 $cm^{-1}$ were characteristic of cobaloxime compounds.

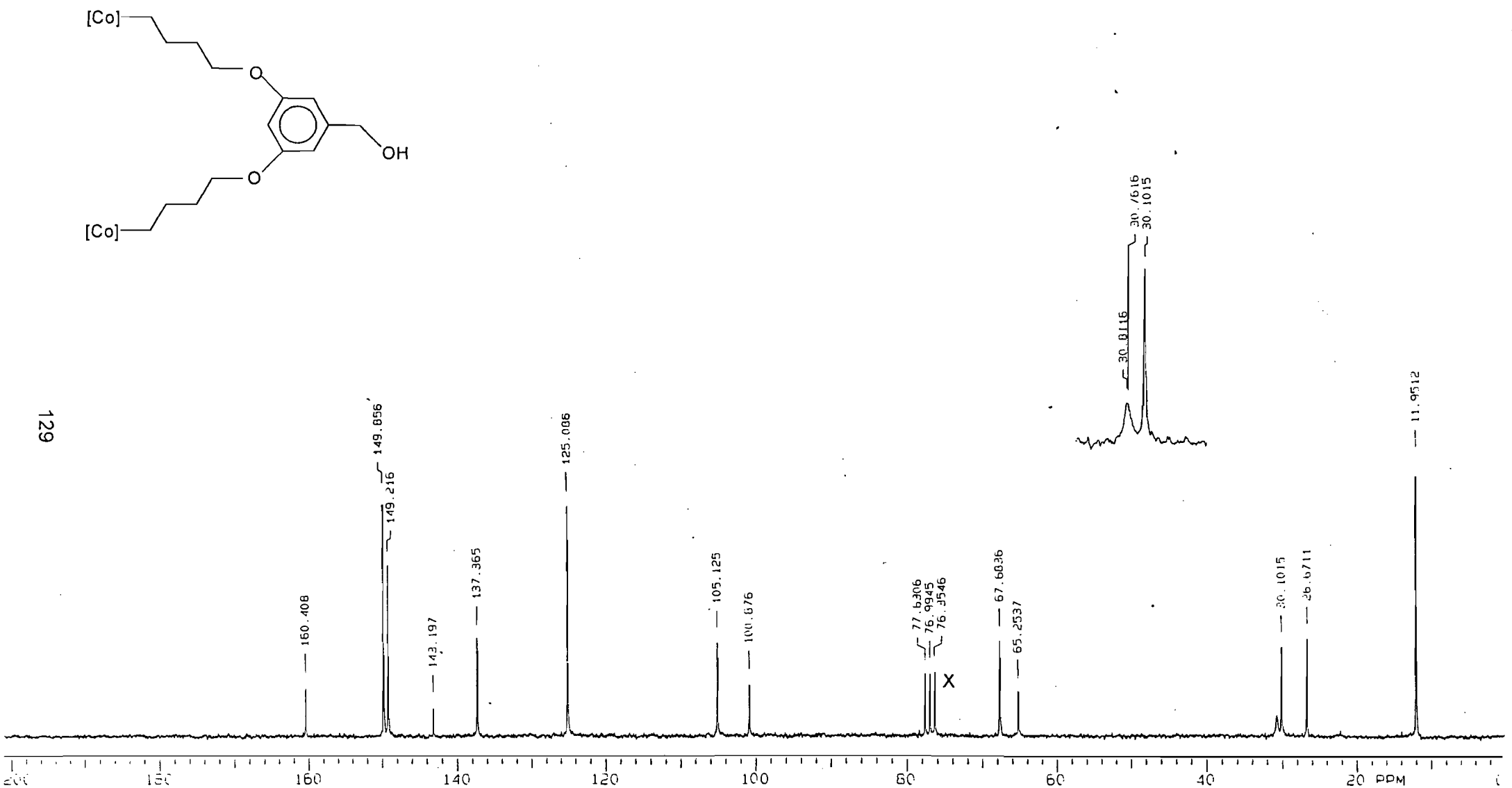


**Figure 4.7** A 100 MHz $^{13}C$ NMR spectrum of **43**. X = solvent

Elemental analysis on the new cobaloxime dendrimer precursors was attempted but the experimental data obtained did not agree well with the calculated data. The $^1$H NMR spectra of these complexes showed peaks for included solvent, even though the complexes were dried under high vacuum for three to five hours. This would account for some of the discrepancies observed with the elemental analysis.

FAB mass spectrometry was performed on several of the new complexes. In most cases, molecular ions for the parent ions were observed. For example, molecular ions for (P + 3) and (P + 1) in the case of **41** and **44** respectively were observed.

## 4.3 Conclusions

Several new cobaloxime dendrimer precursors have been synthesised and characterised. The alkyl chain length in the bromoalkylpyridinecobaloxime complex was found to influence the formation of the benzyl alcohol complex. The bromopropylcobaloxime benzyl alcohol complex, **[Co]3G1OH** was not formed, this was attributed to the steric bulk of the cobaloxime ligand. The bromobutyl- and bromohexyl-cobaloxime benzyl alcohols, **43** and **44** decomposed upon activation with a $CBr_4/PPh_3$ mixture. Activation of **44** with $PBr_3$ was successful. Attempts to prepare the first generation dendrimer failed. However, the zero generation dendrimer, **46** was successfully prepared.

Due to the difficulty of preparing cobaloxime dendrimers, no attempts were made to test the cobaloxime dendrimers or dendrimer precursors as catalysts as proposed in the introduction.

# Chapter 5

# Heterobimetallic dendrimers and block copolymers

## 5.1 Introduction to dendritic block copolymers

The synthetic methodology of the convergent growth approach allows precise control over the monomer units in the interior of the dendritic macromolecule. These methodologies permit the synthesis of novel dendritic block copolymers, which extend further the increasingly important fields of both dendritic macromolecules and block copolymers. Due to the three-dimensional globular nature of dendritic macromolecules, several unique architectures are conceivable; these include hybrid linear block copolymers and block copolymers based entirely on dendritic macromolecules.[2]

Traditional block copolymers (normally composed of one-dimensional linear blocks) are limited by the number of possible arrangements. On the other hand, three-dimensional systems such as dendritic macromolecules allow for a greater number of interesting and novel possibilities in terms of block copolymers. Figure 5.1 shows a schematic of the three types of block copolymers that can be obtained.[31] Dendritic segment-block colymers (a) are characterised by a radial geometry in which dendritic segments of differing chemistry radiate from a polyfunctional core. On the other hand, dendritic layer-block copolymers (b) result from the placement of concentric layers of segments of differing chemistry around a central core. Surface-block copolymers are characterised by the uniformity of their interior building blocks with at least two different types of chain ends each localised in a well-defined area of the macromolecule.

A method for accurate control over the number and placement of functional groups in the dendrimer is especially important for the synthesis of block copolymers. The convergent-growth approach is particularly suitable since there are a limited number of reactions required for generation growth.

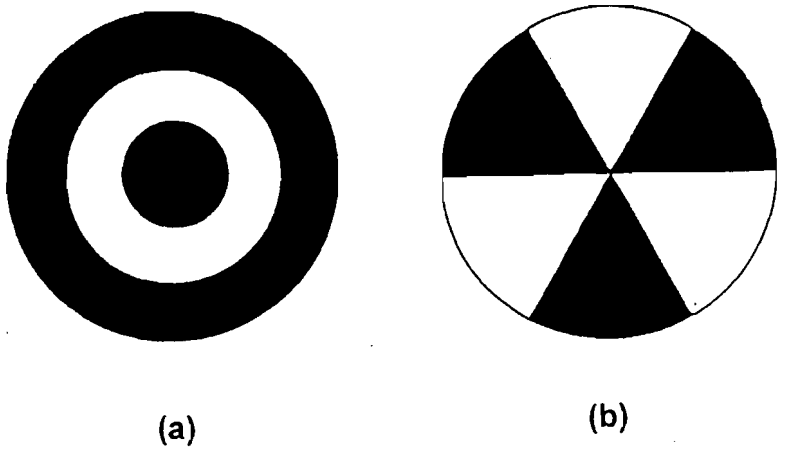


**Figure 5.1** Graphical representation of (a) dendritic segment-block and (b) dendritic layer-block copolymers.[1]

The preparation of dendritic segment-block and layer-block copolymers relies on the use of different building blocks and so the chemistries used in the attachment of these blocks to each other, and to a polyfunctional core, must be compatible. An example of a layer block copolymer is shown in Figure 5.2. The chiral layer-block dendrimer consists of an outer chiral layer having six (L)-tartrate units and an inner chiral layer having three antipodal (D)-chiral elements.[38] The dendrimers were synthesised using an iterative, convergent synthetic strategy starting from a $C_2$-symmetric phenol.

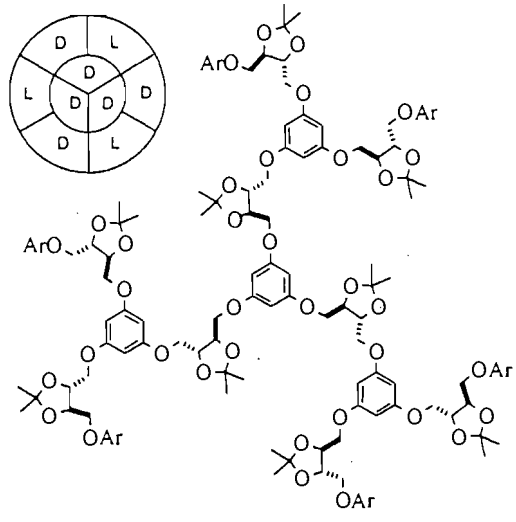


**Figure 5.2** A layer-block chiral dendrimer containing two different chiral elements which are derivatives of (D)- and (L)-tartaric acid.[3]

Hawker and Fréchet have reported the synthesis of several block copolymers.[156,162] A similar strategy is employed for the synthesis of dendritic segment block copolymers (schematic shown in Scheme 5.1).[162a] The starting material (a) contains what will eventually constitute the surface functional group "X" of one block, as well as a reactive functional group "$f_r$". Substrate (a) is then coupled with the monomer (b). Activation of "$f_p$" to "$f_r$" gives intermediate (c), which is again coupled to (b); this gives the second generation dendritic wedge (d). Repetition of this two-step procedure leads to (e). The corresponding unsubstituted dendritic wedge (f) is partially coupled to a polyfunctional core to give the tri-coupled core (g), which has a free coupling site. Coupling of the core with the substituted wedge (e) yields the final dendrimer (h), which consists of two different blocks.

**Hybrid linear-dendritic block copolymers**

A large number of possible bonding arrangements between the two polymeric blocks can be considered when hybrid linear-dendritic blocks are taken into account. The linear polymer can be attached to the chain ends or terminal groups of the dendrimer to give a multiarm star structure with a globular core. The dendrimer can also be attached through the focal-point group to either the chain ends or the backbone of a linear polymer. Poly(ethylene glycol) and pol(ethylene oxide) have been used in the preparation of such dendrimers (Figure 5.3).[4,156a]

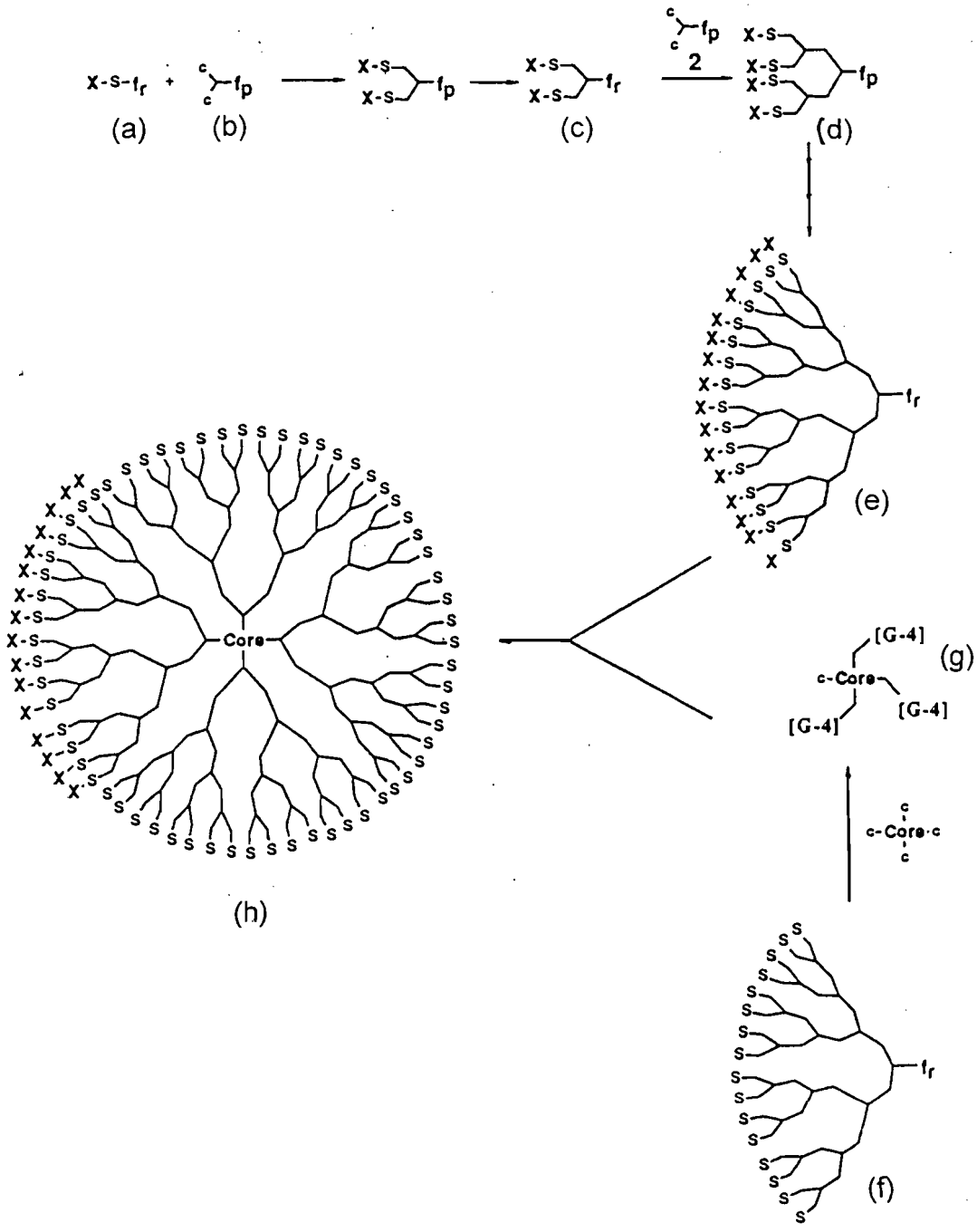


**Scheme 5.1**

Investigations of the physical properties of some novel hybrid block copolymers containing poly(ethylene)glycol showed their ability to form micelles in selected solvents. Phase separation leading to separate glass transition temperatures and crystallisation in the solid state has also been shown to occur after the linear polyethylene chains reached a threshold molecular weight.[156b]

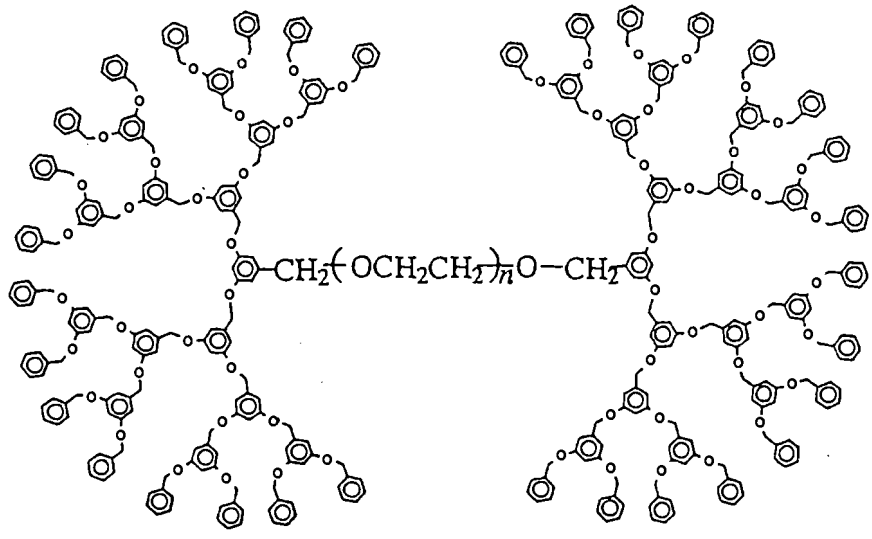


**Figure 5.3** A hybrid linear-dendritic block copolymer.[4]

In recent years, the scope of dendritic materials that have been prepared has increased dramatically from purely organic dendrimers to those including a variety of metals and non-metals such as iron, ruthenium, platinum, gold and silicon (see Chapters 2, 3 and 4). Until recently, there were no examples of organometallic dendritic molecules containing different transition metal in different layers. Perhaps, a reason for this is that the characterisation of inorganic and organometallic dendritic compounds can be exceedingly difficult. Standard methods of analysis are not always viable because of the dendrimers' large size, limited mobility and poor solubility. For example, Fréchet[156c] was able to characterise the purely organic benzyloxy benzyl dendrimer, $C_{5585}H_{4860}O_{765}$ using standard techniques, yet the smaller 1090 polypyridine-based cationic ruthenium dendrimer could not be characterised by simple methods due to its high charge ($44^+$) and low solubility.[123]

Dinuclear transition-metal complexes can be considered to represent the simplest model of metal surfaces and have the potential, through cooperativity of the metal centres, to effect unique transformations of simple organic substrates not possible with single metal centres.[157] Heterodinuclear complexes are especially interesting in this regard since each metal may be able to effect a reaction that is not possible for the other, or both metals together could orchestrate a conversion not possible to either metal alone. There would be a number of advantages to having more than one different metal in a dendrimer, one being in the area of catalysis. Several metals including iron, ruthenium

and nickel are known to catalyse the Fischer-Tropsch process.[78] For this reason, heterobimetallic complexes are expected to be good models for catalytic intermediates on the Fischer-Tropsch surface as the metals would be in close proximity.

Achar *et al.*[52b] reported the convergent synthesis of the first examples of heterometallic dendritic molecules. These compounds feature platinum(IV) units arranged in a concentric fashion around a central organic moiety, with ferrocenyl groups directed towards the periphery of the molecule (Figure 5.4).

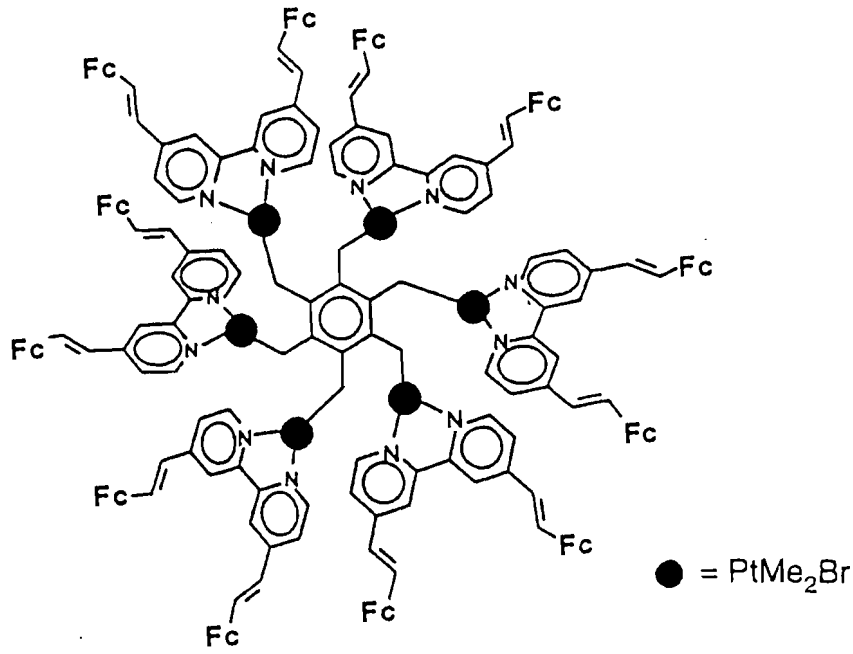


**Figure 5.4** A heterometallic dendrimer containing six platinum and twelve ferrocenyl units.[52b]

The above reactions occured under mild conditions (room temperature, atmospheric pressure) and in high yield (80-95%). The $^1$H NMR spectra of these complexes generally showed broad, poorly resolved peaks. Electrochemical studies on these ferrocene-containing dendritic molecules showed reversible multielectron oxidations corresponding to the Fe(III)/Fe(II) couple of the ferrocenyl units.[52b]

### Synthetic Approach

In this chapter, the synthesis and characterisation of several heterobimetallic dendrimer precursors and a first generation heterobimetaliic dendrimer are discussed. Two approaches have been used. In the first approach, both the metals were included in the dendritic wedge to form a heterobimetallic wedge. In the second approach, two different

wedges were attached to a core molecule to form a heterobimetallic dendrimer or block copolymer.

The synthesis of dendritic segment-block copolymers requires the preparation of dendritic fragments composed of different building blocks followed by coupling of these fragments to the same polyfunctional core. The convergent approach developed by Hawker and Fréchet is ideal for this type of synthesis because of its high degree of control over the number and placement of of functional groups at the periphery.

## 5.2 Synthesis and characterisation of heterobimetallic dendrimers and dendritic block copolymers

Haloalkyl metal complexes of the type $[Fp^*(CO)_2(CH_2)_3Br]$, $[Rp(CO)_2(CH_2)_3Br]$ and $[Wp(CO)_3(CH_2)_3I]$ were used as the starting materials for the preparation of the heterobimetallic dendrimers and dendritic block copolymers. The haloalkyl complexes were prepared as described in Chapters 2 - 4. The choice of solvent, base and reaction conditions were discussed in Chapter 2 and are retained in this chapter unless otherwise stated. We have again used convergent methodology of Hawker and Fréchet[28] for the reasons discussed above.

### 5.2.1 Iron-ruthenium systems

Two approaches were employed to prepare heterobimetallic dendrimers. The first involved preparation of a heterobimetallic dendritic wedge. In the preparation of the iron benzyl alcohol, a "mono-substituted" benzyl alcohol was isolated as a by-product (see Scheme 2.3, Chapter 2). This "mono-substituted" intermediate product was subsequently synthesised by adjusting the molar ratio of the haloalkyl complex to 3,5-dihydroxybenzyl alcohol (Scheme 5.2).

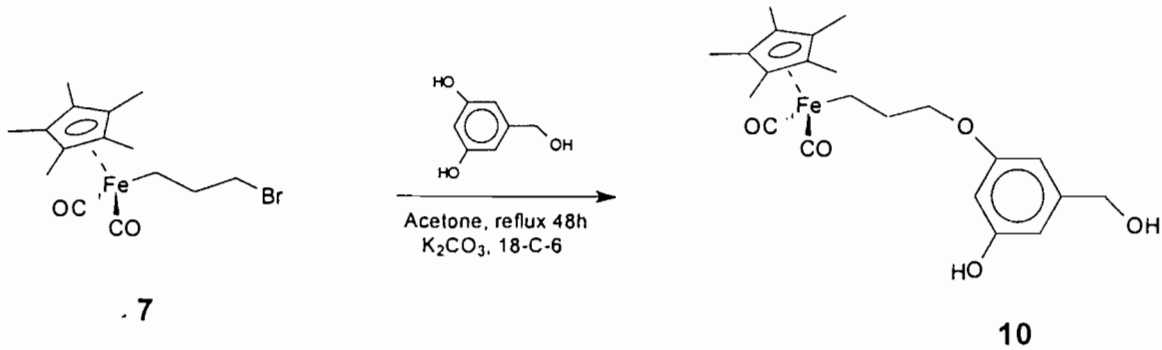


**7** **10**

+

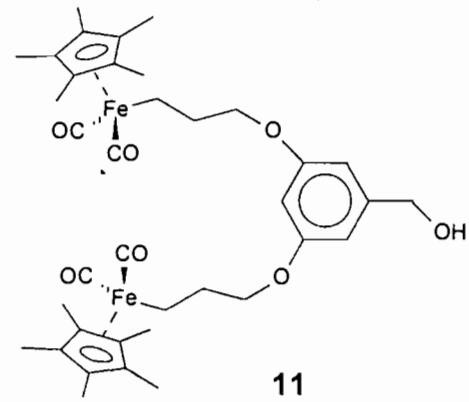


**11**

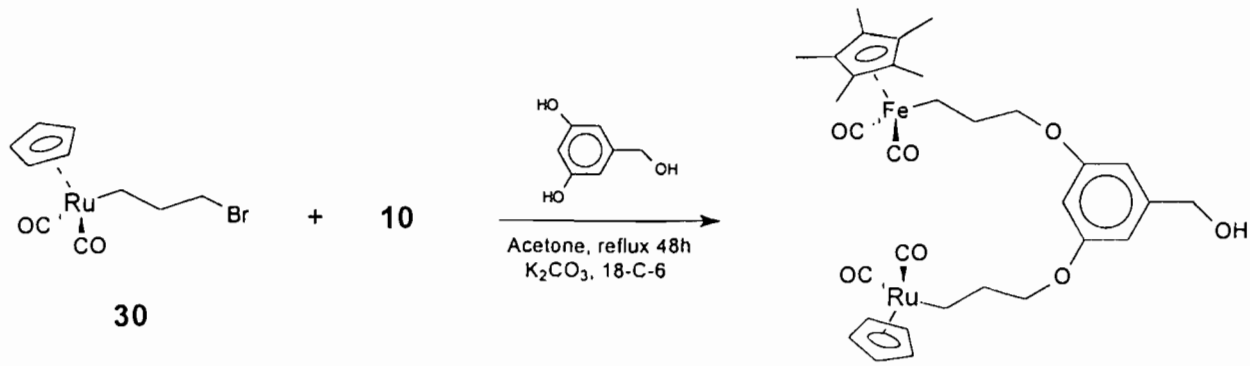


**30** **Fp*/Rp3G1OH (47)**

**Scheme 5.2**

The heterobimetallic dendritic wedges were synthesised as follows: For example, 1.3 molar equivalent of the bromopropyl iron complex, $Cp^*Fe(CO)_2(CH_2)_3Br$ **7** was reacted with 1 molar equivalent of 3,5-dihydroxybenzyl alcohol in the presence of potassium carbonate and 18-crown-6 in refluxing acetone for two days (Scheme 5.2). The reaction was followed by TLC on alumina plates eluting with a 70% $CH_2Cl_2$/hexane solution. The resulting "mono-substituted" complex **10** was purified by column chromatography and recrystallised from $CH_2Cl_2$/hexane to give a yellow solid in 37% yield. A small amount of the "di-substituted" benzyl alcohol **11** was also isolated. $^1H$ NMR spectroscopy (particularly the aromatic region) confirmed the formation of the "mono-substituted" product. The aromatic region of the $^1H$ NMR spectrum of **3** is shown in Figure 5. 5.

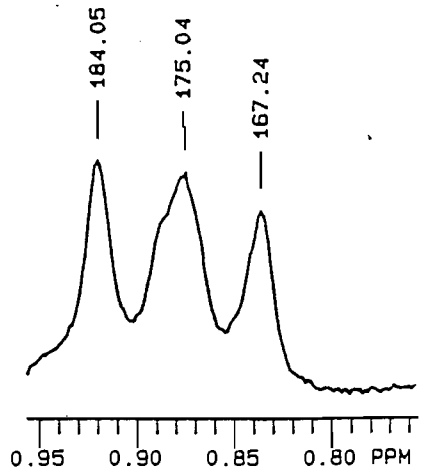


**Figure 5.3** The aromatic region of the $^1H$ NMR spectrum of **10**.

The analogous "mono-substituted" benzyl alcohol was not observed in the preparation of the ruthenium benzyl alcohols. This suggests that the bulkier $Cp^*Fe(CO)_2$- ligand (as opposed to $CpRu(CO)_2$-) causes steric congestion around the 3,5-dihydroxybenzyl alcohol unit and prevents the second $Cp^*Fe(CO)_2$- ligand from entering, thus causing the "mono-substituted" product to be formed predominantly.

This "mono-substituted" iron complex **10** was reacted with a second and different haloalkyl complex, $CpRu(CO)_2(CH_2)_3Br$ **30**. The complexes were refluxed in acetone in the presence of potassium carbonate and 18-crown-6 for a further two days (Scheme 5.2). Again the reactions were followed by TLC. The resulting heterobimetallic wedge **47** was purified on an alumina column and isolated as a yellow oil in 57% yield. In this way,

some iron/ruthenium and iron/tungsten heterobimetallic dendritic wedges have been synthesised and characterised.

In an attempt to prepare complex **47** in one step, the haloalkyl complexes **7** and **30** were refluxed together with the monomer unit in acetone for two days (Scheme 5.3). The heterobimetallic wedge, **47** was obtained as before together with some unreacted starting material.

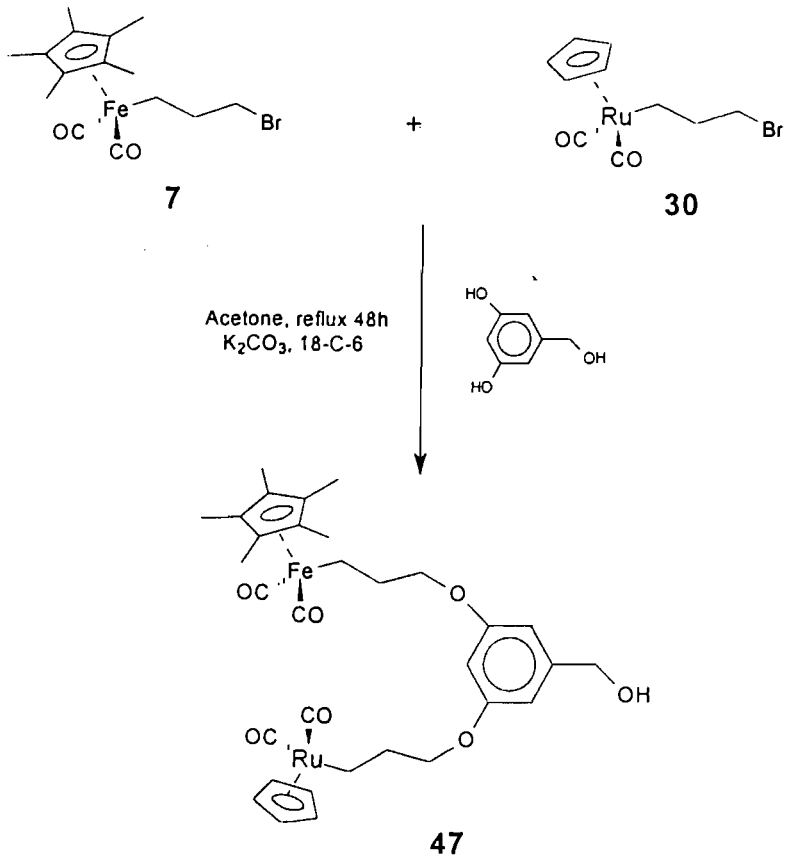


**Scheme 5.3**

Activation of the heterobimetallic benzyl alcohol **47** was carried out as before with a mixture of carbon tetrabromide and triphenylphosphine in THF (Scheme 5.4). The reaction was generally complete within 30 minutes and the resulting residue was then chromatographed on alumina using a $CH_2Cl_2$/hexane eluent system. Partial decomposition of the product occured while drying the sample under vacuum. Further

decomposition occurred upon running the $^{13}C$ NMR spectra so that broad unresolved resonances were obtained. This approach was therefore less successful.

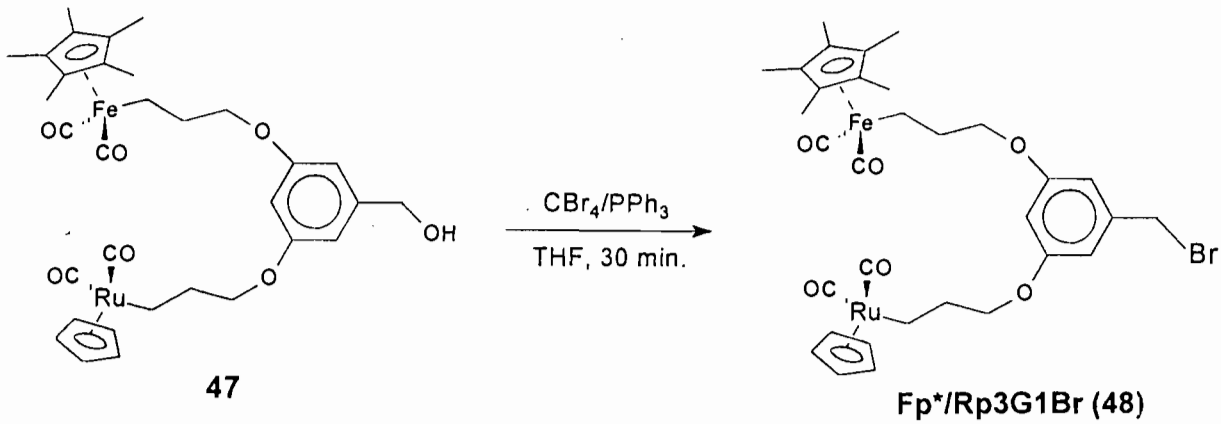


**Scheme 5.4**

The next approach was to prepare a heterobimetallic dendritic block copolymer. In the initial step, one equivalent of the iron dendritic wedge **7** was attached to the CORE molecule, 1,1,1-tris(4'-hydroxyphenyl) ethane (Scheme 5.5). The reaction mixture was refluxed in acetone for 44 hours and TLC was used to monitor the reaction. The resulting complex, **49** was reacted immediately with ruthenium benzyl bromide **32** to form the heterobimetallic block copolymer **50**. The reaction mixture was chromatographed on alumina and compound **50** was obtained as a pale yellow oily solid in 37% yield. The new complex was characterised by $^{1}H$ and $^{13}C$ NMR spectroscopy, IR and FAB mass spectrometry.

All the complexes were purified by column chromatography and recrystallisation where possible. The compounds were characterised by IR spectroscopy, $^{1}H$ and $^{13}C$ NMR spectroscopy and in some instances, mass spectrometry .

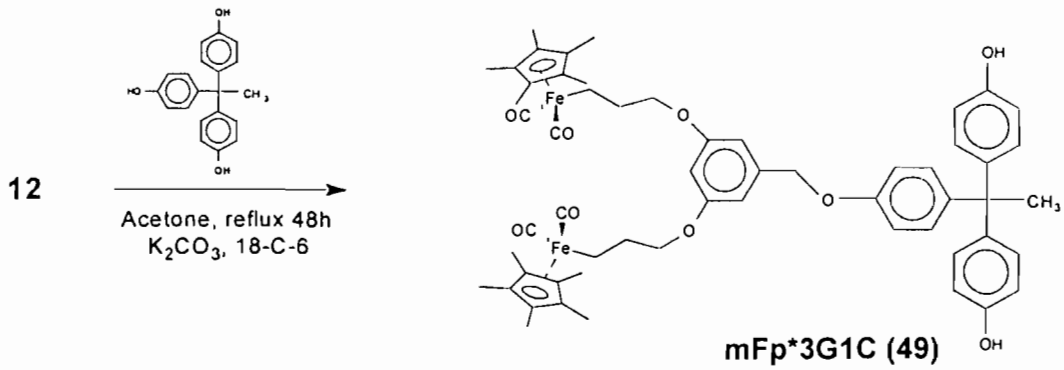
12
Acetone, reflux 48h
$K_2CO_3$, 18-C-6
mFp*3G1C (49)

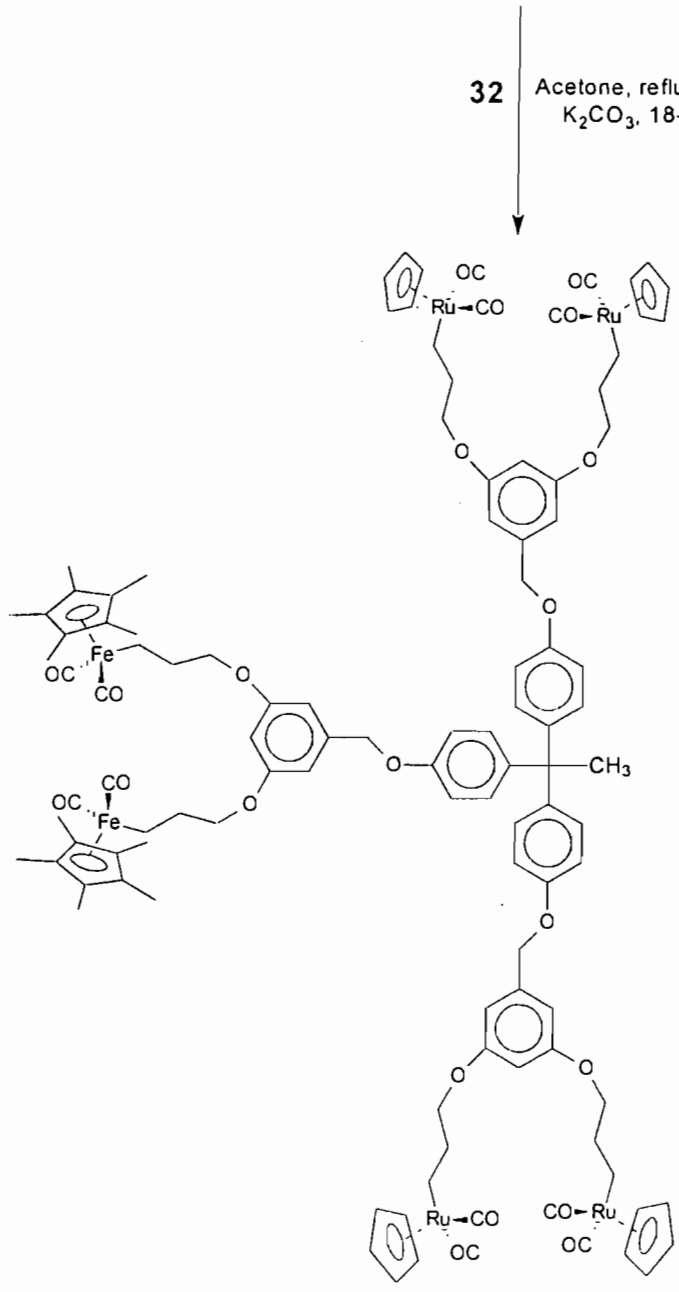
32
Acetone, reflux 48h
$K_2CO_3$, 18-C-6
Fp*/Rp3G1C (50)

Scheme 5.5

### 5.2.2 Iron-tungsten systems

Several tungsten dendritic wedges were also synthesised and characterised in order to compare their stability and reactivity with the iron and ruthenium dendrimers synthesised. The methodology used was as described in the previous chapters. In this case, the iodopropyltungsten complex **51** was used as the starting material. Again, a "mono-substituted" derivative **52** was formed during the reaction of the haloalkyl complex **51** with 3,5-dihydroxybenzyl alcohol in refluxing acetone (Scheme 5.6). The tungsten benzyl alcohol **53**[158] was isolated as a yellow oil while complex **52** was isolated as a yellow solid. Unreacted starting material **51** was observed from TLC and column chromatography. The complexes were characterised by IR, $^{1}H$ and $^{13}C$ NMR spectroscopy. Attempted activation of **53** with carbon tetrabromide and triphenylphosphine to form the expected benzyl bromide **54** was partly successful. The compound decomposed during NMR data collection.

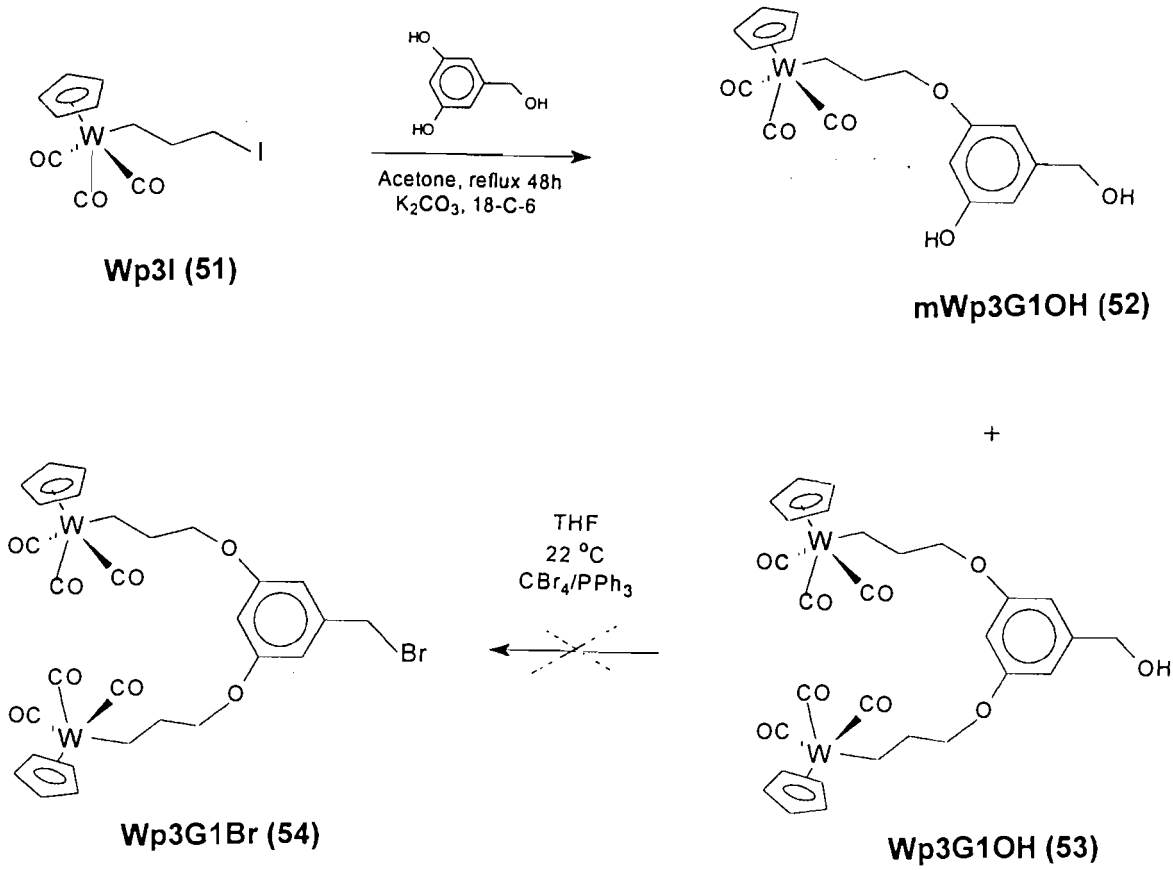


**Scheme 5.6**

A heterobimetallic iron-tungsten wedge was synthesised in the same manner as described in section 5.2.1. The "mono-substituted" iron benzyl alcohol **10** was reacted with the tungsten haloalkyl complex **51** in refluxing acetone to form the heterobimetallic benzyl alcohol **55** in low yield (21%).

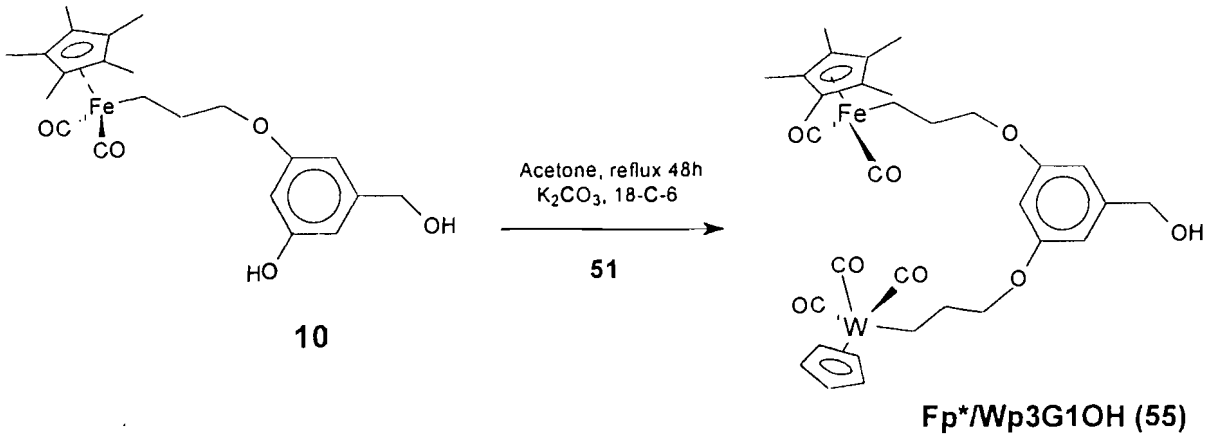


**10**

**Fp*/Wp3G1OH (55)**

**Scheme 5.7**

### 5.2.3 Dendritic phosphines and heterobimetallic dendrimers

Many homogeneous catalysts contain tertiary phosphine ligands. These ligands possess the correct steric and electronic properties that are necessary for catalytic reactivity and selectivity. One of the most important homogeneous catalysts known is Wilkinson's catalyst, $[RhCl(PPh_3)_3]$[78] which catalyses the hydrogenation of alkenes at 25 °C. As mentioned in Chapter 3, the idea of supporting a homogeneous catalyst on an inorganic support has both industrial and academic interest.

Dendrimers with surface phosphine groups have been shown to be useful for the complexation of other metals. For example, Reetz *et al.*[73] prepared dendritic phosphines up to the fifth generation and then complexed them with a variety of metal atoms including rhodium, platinum and nickel. In our case, we wished to prepare a dendritic phosphine wedge that could be reacted with a metal-containing core molecule to form a heterobimetallic dendrimer. Such dendrimer-supported metal complexes allow the possibility of combining the rich catalytic chemistry of transition metal phosphine complexes with highly structured dendrimer chemistry. In this section of the thesis, the

attempted synthesis of some novel iron- and ruthenium-containing dendritic phosphine metal complexes is discussed.

A preliminary reaction was carried out with a haloalkyl complex **7**. A solution of $LiPPh_2$ was prepared from lithium metal and triphenylphosphine and added to **7** at low temperature (-78 °C). The mixture was stirred at room temperature for 1.5 hours. Precipitation with hexane afforded the bright yellow solid **56**, along with a phosphine oxide decomposition product (Scheme 5.8).

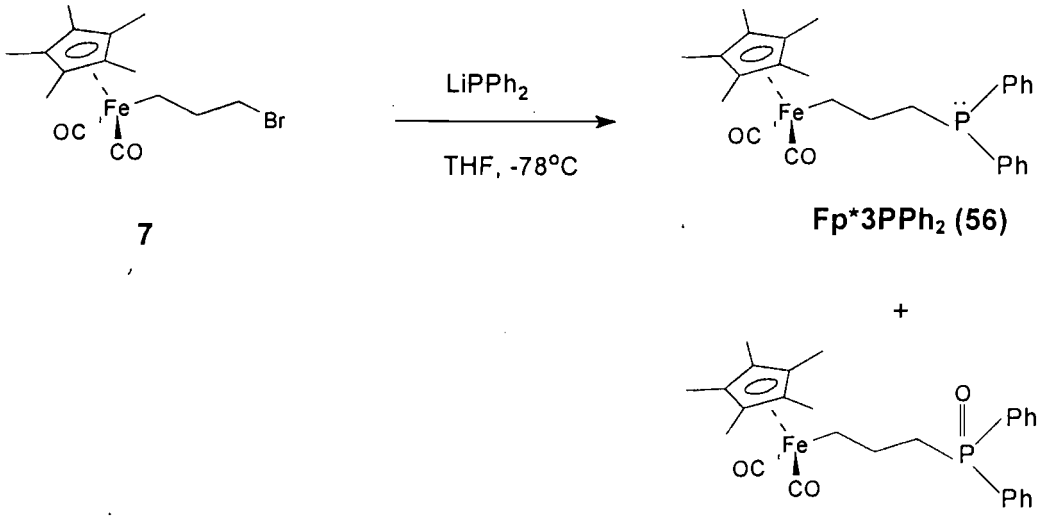


**7**

**Fp*3PPh$_2$ (56)**

**Scheme 5.8**

A model reaction with $LiPPh_2$ was then carried out on benzyl bromide. The reaction was carried out under the same conditions as described above. A white crystalline solid was obtained. The $^{31}P$ NMR spectrum again showed the presence of some oxidised product.

The dendritic iron and ruthenium benzyl bromides **14** and **32** were then reacted with $LiPPh_2$ at -78 °C (Scheme 5.9). A green oil was obtained for the iron compound and a yellow glassy solid **57** in the case of the ruthenium compound. Both compounds were extremely air sensitive and showed decomposition to the phosphine oxide product. This was clearly evident in the $^{31}P$ NMR spectrum (Figure 5.6).

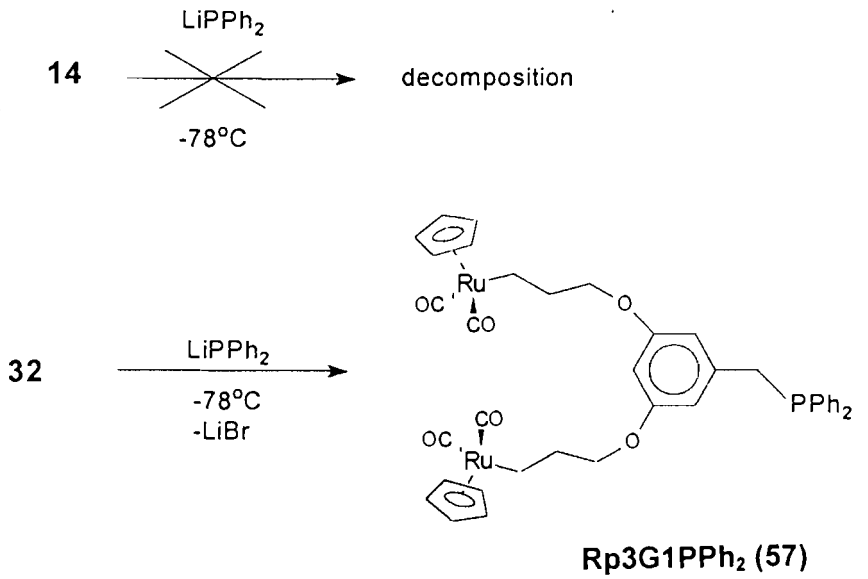


**Scheme 5.9**

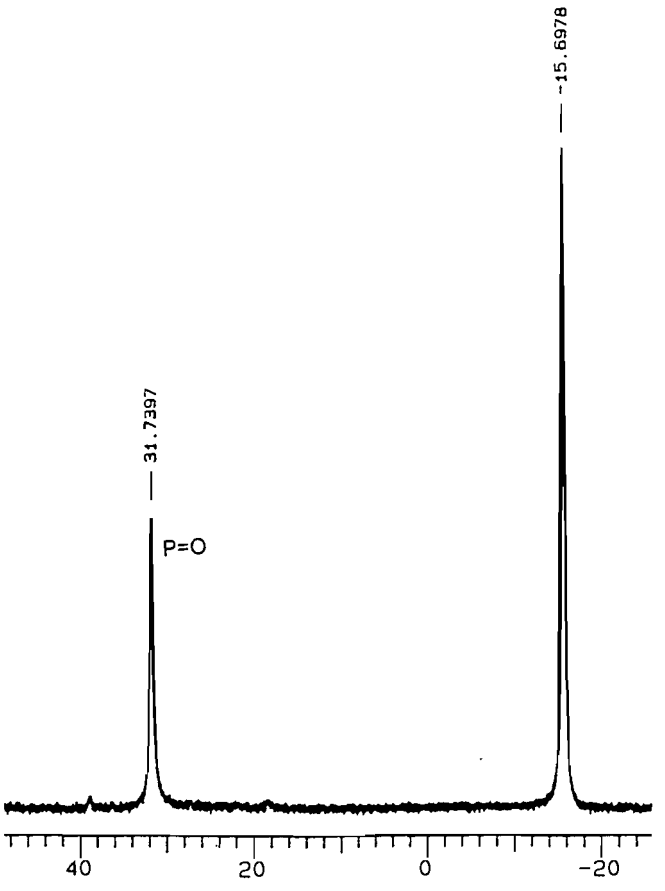


**Figure 5.6** $^{31}P$ NMR spectrum of **56** showing the formation of phosphine oxide.

**Complexation with metal cores**

The iron and ruthenium phosphine complexes were reacted with two different metal-containing cores; $Pt(COD)Cl_2$ and $Rh(III)Cl_3$. The COD ligand (1,5-cyclooctadiene) is labile due to the trans-influence of the Cl group and the high electronegativity of the Cl, which contracts the 5d orbitals of Pt and synergistically weakens the Pt-COD bond. As a model reaction, the iron phosphine complex **56** was reacted with the metal cores $Pt(COD)Cl_2$ and $Rh(III)Cl_3$. In both reactions, only decomposition products, and not the expected heterobimetallic complexes, were observed. $^{1}H$ and $^{31}P$ NMR spectroscopy confirmed this. In comparison, two molar equivalents of the ruthenium phosphine complex **57** were reacted with one molar equivalent of $Pt(COD)Cl_2$ at room temperature to produce complex **58** as a yellow glassy solid (Scheme 5.10).[159] Complex **58** is thermally unstable and decomposes at fairly low temperature (*ca.* 50 °C).

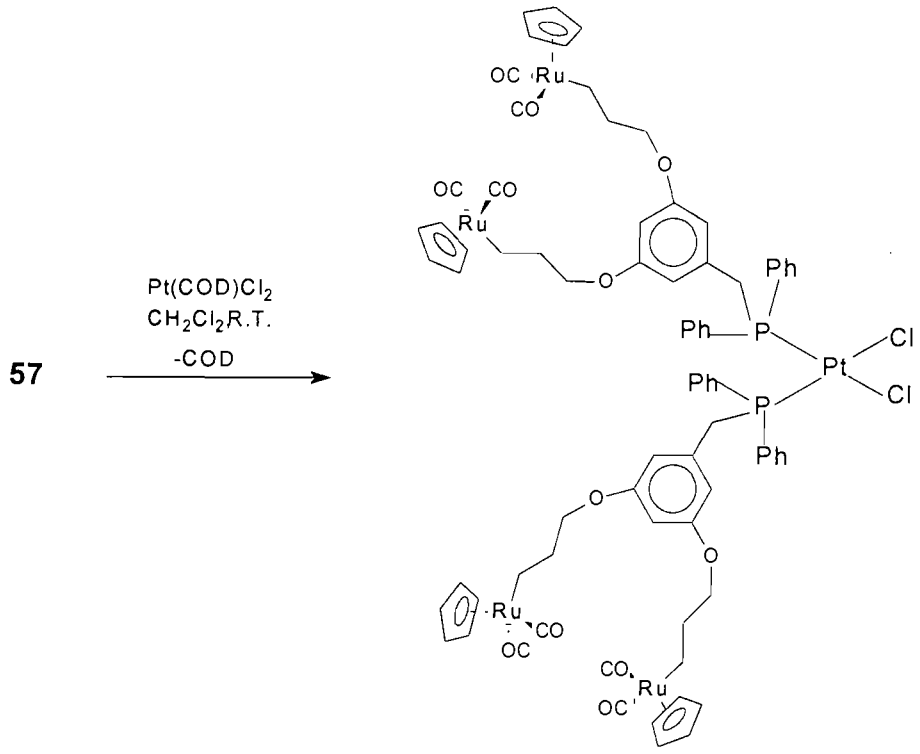


**58**

**Scheme 5.10**

### 5.2.4 Hybrid block copolymers

The first organic linear-dendritic block copolymers were reported by Fréchet and coworkers in 1991.[156] These block copolymers contained both flexible (linear polyethylene glycols) and more rigid (dendritic) blocks. Polyethylene glycols (PEG's) and their derivatives have applications as phase-transfer reagents and as materials that could potentially encapsulate other materials. This is due to the existence of both hydrophilic and hydrophobic parts of the molecule.

Polyethylene copolymers were prepared by attaching dendritic wedges with a reactive functional group at the core to the ends of bi-functional PEG's (Scheme 5.11). The reactions of the iron and ruthenium dendritic bromides with the PEG's were carried out in the presence of NaH. This was to avoid the association of acidic moieties with PEG[160a] and incomplete conversion of Williamson-type syntheses.[160b]

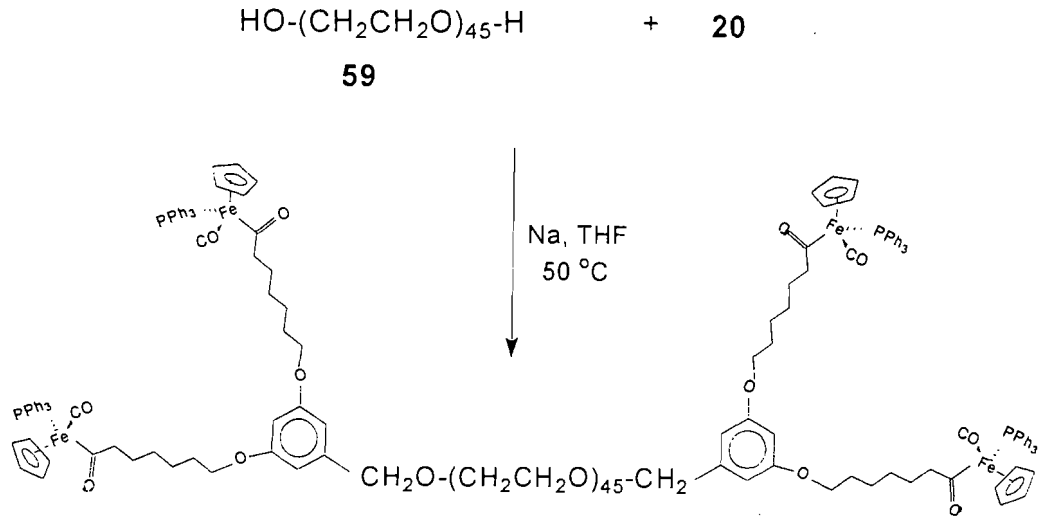


**Scheme 5.11**

For example, two molar equivalents of **20** were reacted with one molar equivalent of PEG 2000 **59** (average molecular weight of 2000 amu) in the presence of NaH at 50 °C (Scheme 5.11).[28c] The reaction was complete after 24 hours. The product was obtained

as a yellow oil **60**. The above reaction has also been performed on the ruthenium benzyl bromide **32** to produce compound **61** also a yellow oil. Full experimental details for sections 5.2.1 – 5.2.4 can be found in the experimental (section 7.5).

### 5.2.5 Characterisation of heterobimetallic dendrimers and dendritic block copolymers

The characterisation of all the dendrimers and dendritic fragments was carried out using a combination of $^{1}H$ and $^{13}C$ NMR spectroscopy (and $^{31}P$ NMR where appropriate) and mass spectrometry. Poor analytical data for these compounds was obtained as most of the complexes decomposed during the data collection. TLC was also extremely useful for confirming any unreacted starting material due to the large $R_f$ difference between the product and the starting material.

#### IR Spectroscopy

The reactions were monitored by IR spectroscopy since the carbonyl groups of the metal-ligand system remain on the surface of the dendrimer. For the heterobimetallic dendrimers such as **47**, four carbonyl bands were observed. The carbonyl region of the IR spectrum of the heterobimetallic complex **47** is shown in Figure 5.7.

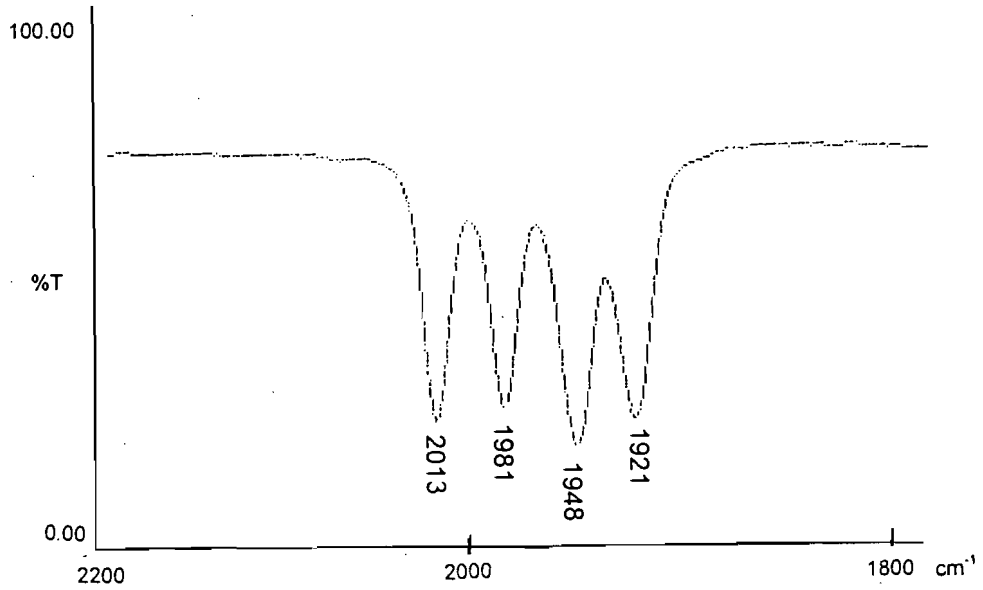


**Figure 5.7** The carbonyl region of the IR spectrum of **47**.

In the case of the heterobimetallic complexes such as **58**, two Pt-Cl stretching bands at 316 and 282 $cm^{-1}$, characteristic of the *cis*-complex were observed.

IR spectroscopy usually offers little information regarding the purity of the products. The functional groups within the molecule (aromatic and ether groups) make detection of the functional group at the focal point difficult.

**$^{1}$H, $^{13}$C and $^{31}$P NMR Spectroscopy**

As mentioned in the previous chapters, NMR spectroscopy proved to be the most useful method of characterisation for these types of complexes. In the $^{1}$H NMR, integration of the resonance due to the phenyl protons and comparison with other resonances in the spectrum allowed the generation number of the fragment to be confirmed and any unreacted starting material to be detected. Figure 5.8 shows the 100 MHz $^{13}$C NMR spectrum of **47**. Resonances for each metal environment can be seen. The functional groups on the periphery of the dendrimers give resonances at the following positions: δ88.5 ($C_5H_5$-Ru), 71.8, 71.0 ($CH_2O$), 38.5, 36.5 ($CH_2$), 9.3 ($C_5Me_5$-Fe), 7.1 ($FeCH_2$) and -9.3 ($RuCH_2$). The resonances of the aromatic protons occur in the region: δ160.8 – 95.0 ppm. Again activation of the dendritic wedges was confirmed by the shift of the benzyl protons from 4.60 ppm in the benzyl alcohol to 4.40 ppm in the dendritic benzyl bromide.

Coupling of the benzyl bromide to a polyfunctional core could readily be detected, since discrete resonances were observed in both the $^{1}$H and $^{13}$C NMR spectra for the core group. For copolymers such as **50**, unique resonances in the $^{1}$H and $^{13}$C NMR spectra are observed for each block. The aromatic region of the heterobimetallic dendrimer **50** is shown in Figure 5.9. The peaks for the two different environments of the aromatic protons are clearly seen.

The $^{1}$H NMR spectra of several of the complexes (particularly the benzyl bromides) showed broad, poorly resolved resonances, but integration of the spectra, together with analytical data (where possible) supports the proposed formulations.

$^{31}$P NMR spectroscopy was also very useful in the case of the phosphine complexes. The $^{1}J(^{195}Pt\text{-}^{31}P)$ coupling constant in complexes of the type $Pt(PPh_{3-n}R_n)_2Cl_2$ (R = alkyl; n = 1,2,3) has been shown to be larger for the *cis*-isomer than the *trans*-isomer.[161] This trend can be used to characterise the isomer formed. A $^{1}J(^{195}Pt\text{-}^{31}P)$ coupling constant of 3632 Hz was observed for complex **58** suggesting that the *cis*-isomer had been formed.[159]

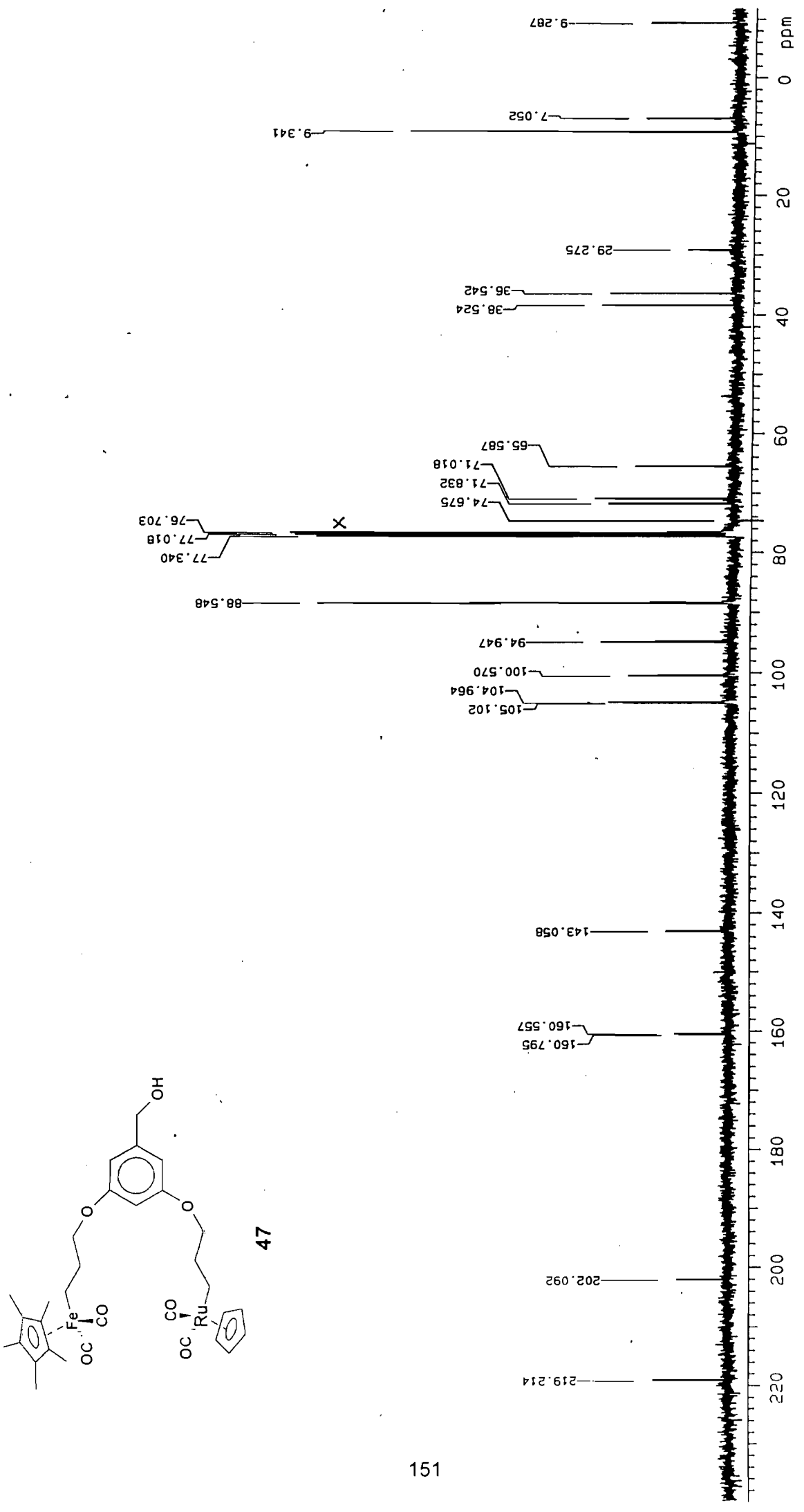


**Figure 5.8** A 100 MHz $^{13}C$ NMR spectrum of **47**. X = solvent

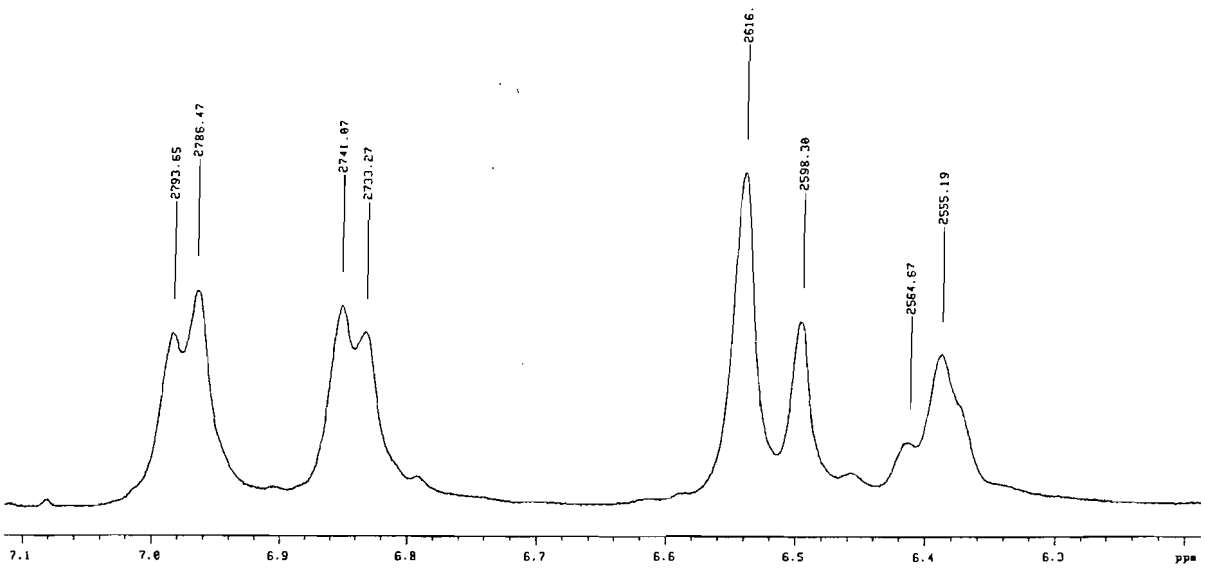


**Figure 5.9** The aromatic region of the $^{1}H$ NMR spectrum of **50**.

### Microanalysis

Many of the complexes described in this chapter were air sensitive and unstable in solution at room temperature. Difficulties in characterisation of organometallic dendrimers has been observed elsewhere.[11] For this reason, good microanalysis data was difficult to obtain for these complexes. The complexes are also obtained as oils in most cases and could not be purified by crystallisation. Microanalysis data was obtained where possible.

### Mass Spectrometry

Most of the spectra were recorded using fast atom bombardment (FAB) mass spectrometry. Mass spectrometry failed to yield parent ions: in most cases, loss of one or two carbonyl groups was observed. For example, the mass spectrum of the dendritic benzyl alcohol **47** showed peaks for (M + 1), (M – CO) and (M – 2CO). In the case of the phosphine complexes, decomposition occurred upon running the NMR spectra so that broad unresolved resonances were obtained.

## 5.3 Synthesis and attempted surface functionalisation of bromobenzyl-terminated dendrimers

The synthesis of many organic dendrimers have been reported in the literature over the past 10 years. Generally, organic dendrimers have the advantage of been synthesised in very high yields (often > 90%). High yields are one of the fundamental requirements of dendrimer synthesis. Organic dendrimers are usually more stable to moisture and heat than most organometallic dendrimers. For this reason, we have investigated the synthesis of bromobenzyl-terminated dendrimers. These dendrimers can be prepared in high yields and are air stable. We then attempted to functionalise the surface of the dendrimer with organometallic complexes.

The bromobenzyl dendrimers were synthesised according to literature procedure.[162] The bromobenzyl dendrimers and dendritic wedges were obtained as white solids or white crystals in good yields (60-80%). The complexes are also air stable. The products were purified by column chromatography on silica rather than by flash chromatography as mentioned in the literature procedure.

Schemes 5.12 and 5.13 show the reaction procedure that was followed. The dendritic benzyl alcohol **63** was synthesised by refluxing 4-bromobenzyl bromide **62** with 3,5-dihydroxybenzyl alcohol in acetone for 48 hours. The product was purified by column chromatography. An EtOAc/$CH_2Cl_2$ mixture was used to elute compound **63**. The activation procedure proceeded as before. The bromobenzyl alcohol **63** was stirred at room temperature together with a mixture of carbon tetrabromide and triphenyl phosphine to produce the bromobenzyl bromide **64**. The activation reactions are usually complete within 15 - 20 minutes. Column chromatography eluting with a $CH_2Cl_2$/hexane mixture gave product **64** as a white solid. The first generation dendrimer **65** was synthesised by reacting the benzyl bromide **64** with 1,1,1-tris(4'-hydroxyphenyl)methane in refluxing acetone. These two coupling and activation reactions were repeated to produce the second generation dendritic wedges, **66** (Scheme 5.13).

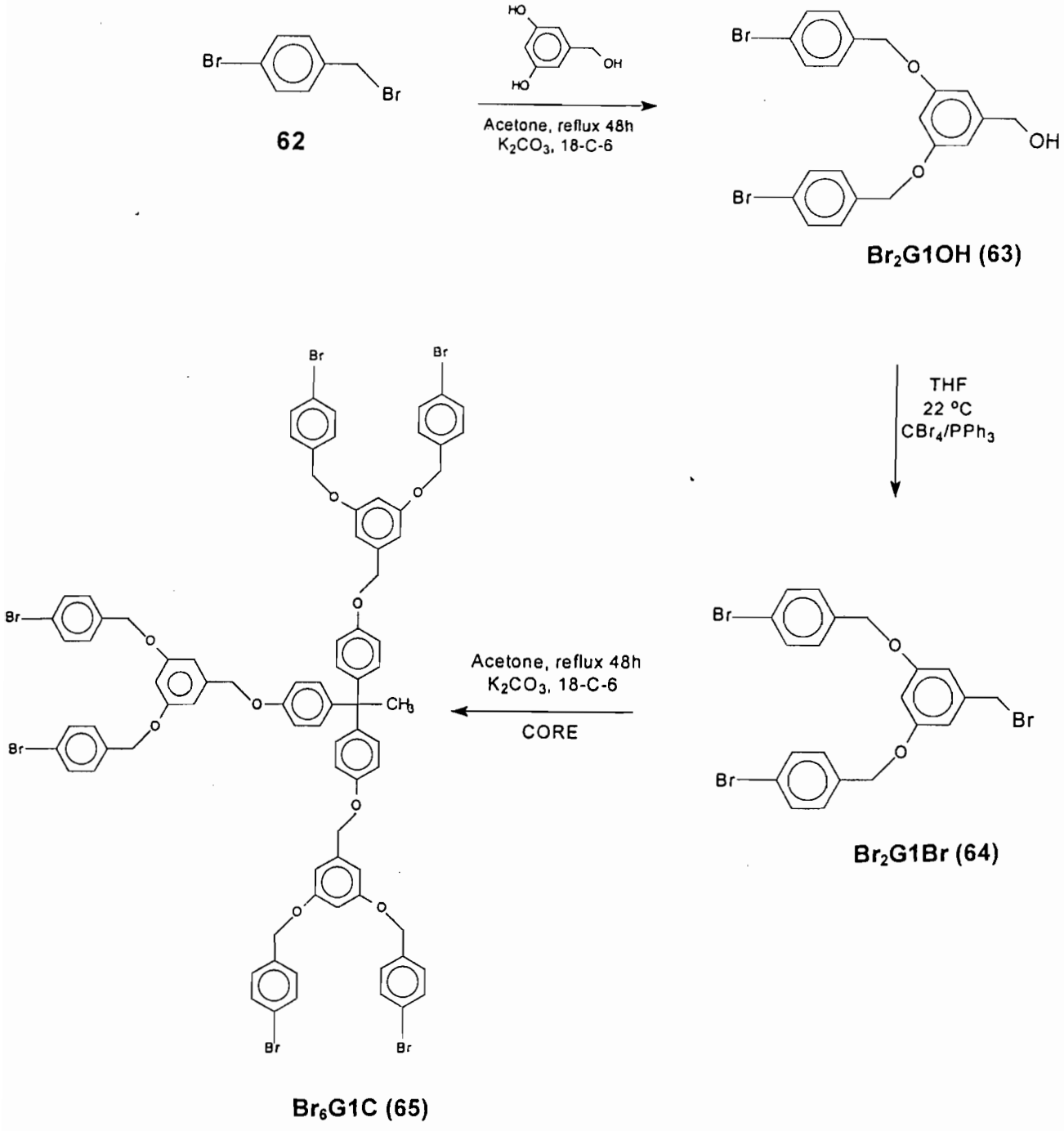
Br
Br
62
HO
OH
HO
Acetone, reflux 48h
$K_2CO_3$, 18-C-6
Br
O
OH
O
Br
$Br_2G1OH$ (63)
THF
22 °C
$CBr_4/PPh_3$
Br
O
Br
O
Br
$Br_2G1Br$ (64)
Acetone, reflux 48h
$K_2CO_3$, 18-C-6
CORE
Br
Br
Br
O
O
O
$CH_3$
Br
O
O
O
O
Br
Br
$Br_6G1C$ (65)

**Scheme 5.12**

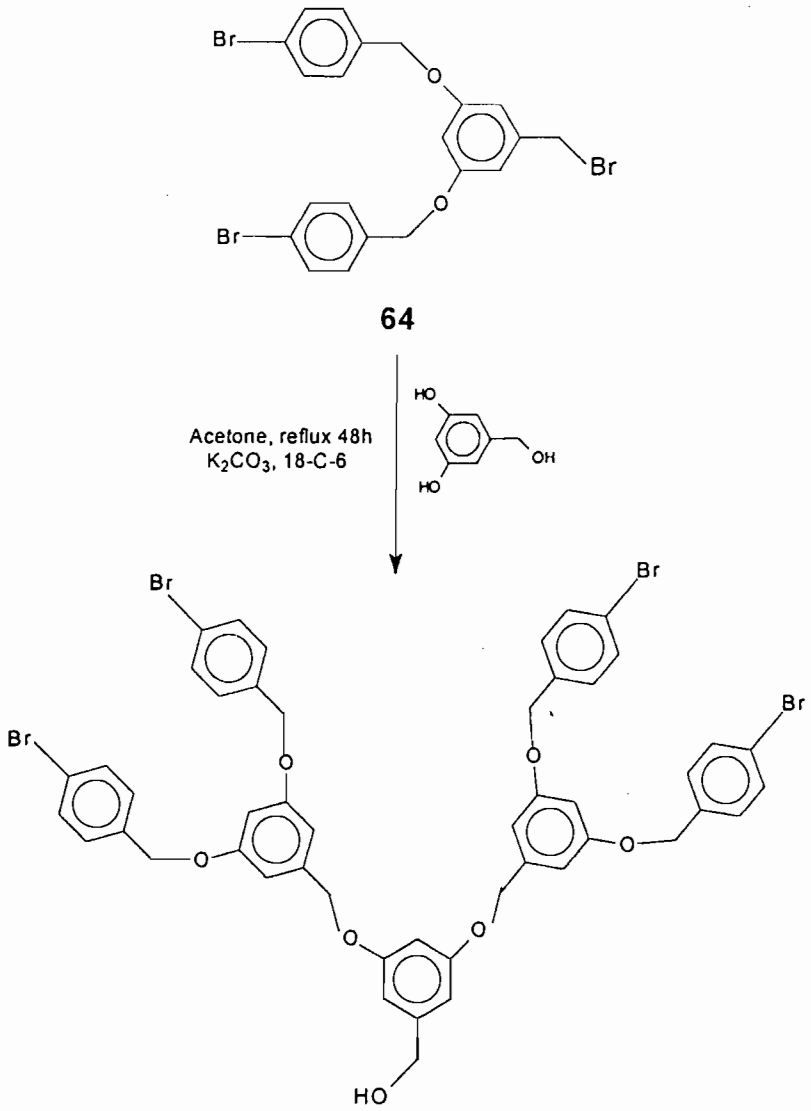
Br
Br
Br
O
O
64
Acetone, reflux 48h
$K_2CO_3$, 18-C-6
HO
OH
HO
Br
Br
Br
Br
O
O
O
O
O
O
HO
$Br_4G2OH$ (66)
higher generation
dendrimers

**Scheme 5.13**

The zero-generation dendrimer **67** was also synthesised by reacting bromobenzyl bromide **62** with 1,1,1-tris(4'-hydroxyphenyl)methane in refluxing acetone for 48 hours. The zero-generation dendrimer **67** was obtained as a white solid in good yield (Scheme 5.14).

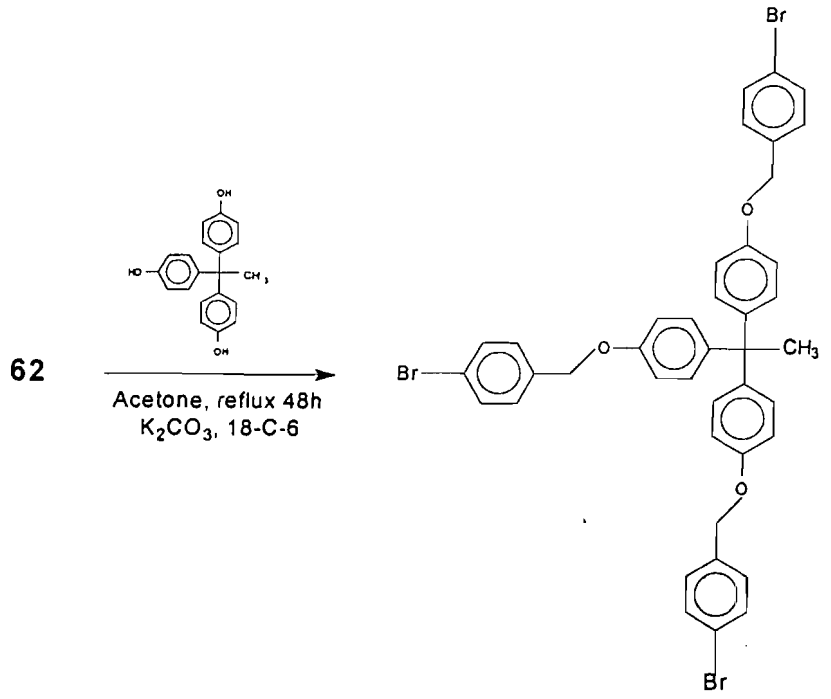


**$Br_3G0C$ (67)**

**Scheme 5.14**

The attempted activation reactions of the organic dendrimer with a metal complex were carried out on the zero-generation dendrimer **67**, a model compound. Several attempts were made to cleave the bromine atom from the bromobenzyl group. In the first attempt, $^n$butyl lithium was added to a cooled solution of the zero-generation dendrimer **67** (Scheme 5.15). The solution was stirred at low temperature (0 °C) for an hour, then cooled to -78 °C again to add $I(CH_2)_3I$. A creamy viscous oil was obtained after the work-up procedure. The $^1$H NMR product spectrum showed the presence of a new peak at *ca* 2.6 ppm (for the $CH_2$ group adjacent to the aromatic ring) but no peak at *ca.* 3.15 ppm (for the for the $CH_2$ group adjacent to iodine) suggesting that a dimer **68** had formed.

In a second attempt, the zero generation dendrimer was lithiated as before, and a solution of Fp3Br **1** added (Scheme 5.15). TLC showed that no reaction had taken place and the $^1$H NMR spectrum of the product mixture showed only unreacted starting material. Further attempts involved the reaction of **67** with $^t$butyl lithium at -78 °C. A two

molar excess of the lithium reagent was used to avoid possible coupling reactions. The solution was warmed to 60 °C after lithiation and the haloalkyl complex, **7** added. A creamy oil was obtained after the work-up procedure. The $^{1}H$ NMR spectrum of the reaction product showed an unresolved mixture of products. This suggested that the lithiation reaction produced an inseperable mixture of mono-, di- and tri-substituted lithiated products. Further complexation of the organic dendrimer with the metal-containing group was therefore not possible with this system. Full experimental details can be found in the experimental (section 7.5).

**Characterisation of the bromobenzyl-terminated dendrimers**

A combination of techniques were used to characterise the bromobenzyl-terminated dendrimers. These included IR spectroscopy, melting point, NMR spectroscopy and microanalysis. The data obtained in these syntheses agreed well with the literature data.[162]

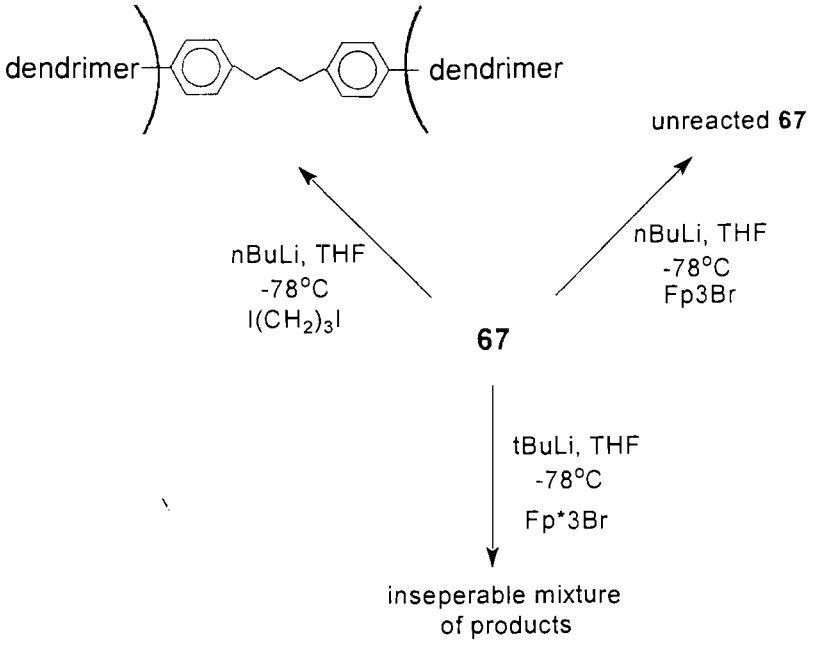


**Scheme 5.15**

## 5.4 Conclusions

The usefulness of the convergent growth approach for the synthesis of dendritic macromolecules with highly controlled architectures is demonstrated via the preparation of several dendritic block copolymers and heterobimetallic dendrimers. Such structures are not readily accessible through the procedures currently in use for divergent syntheses. The stepwise convergent growth approach allowed the preparation of block copolymers using monodispersed fragments containing a single reactive group at the focal point. Using this approach, a wide range of possible dendritic macromolecules can be synthesised where the structure, functional groups and three-dimensional architecture can be precisely controlled.

Several novel dendritic wedges containing iron-and-ruthenium and iron-and-tungsten were synthesised and characterised. The preparation of dendritic phosphines allowed complexation to metal-containing cores such as $Pt(COD)_2$ and $Rh(III)Cl_3$.

The complexes were characterised using conventional methods. In particular $^1H$ NMR spectroscopy allowed the different building blocks to be distinguished and subtle structural changes to be detected.

Finally, attempts were made to functionalise bromobenzyl-terminated dendrimers with metal-containing groups. The bromine atom appeared to be extremely stable to lithium reagents and a mixture of inseparable lithiated products was obtained.

Relatively few heterobimetallic dendrimers have appeared in the literature to date. Many new compounds containing a variety of metals and functional groups are expected to be prepared in the near future.

# Chapter 6

# Conclusions

The synthesis, structure and chemistry of several organometallic dendrimers and dendritic wedges have been investigated using a variety of techniques. Convergent methodology was used to build up the organometallic dendrimers. This methodology is particularly suitable for building organometallic dendrimers because of the high degree of control over the number and placement of ligands in the dendrimer associated with this method. Several new organometallic dendrimers and dendritic wedges have been synthesised and characterised by infrared spectroscopy, $^{1}H$ and $^{13}C$ NMR spectroscopy, mass spectrometry and microanalysis (where possible). The structures of selected dendrimers and dendrimer precursors were investigated using a combination of x-ray crystallography and molecular modelling. Finally, the chemistry of the first generation ruthenium dendrimer was investigated.

Fp, Fp* and Fp acyl dendrimers were synthesised using convergent methodology. A trend in the stability of the iron-containing dendrimers was observed. The Fp dendritic wedges were found to be very unstable, particularly the benzyl bromides, and decomposed rapidly in solution. The Fp* dendritic wedges were found to be more stable than the Fp analogues and it was possible to synthesise the first generation dendrimer and second generation dendritic wedges. The yields for the coupling reaction of the Fp* complexes were ,however, very low, which made preparation of higher generation dendrimers exceedingly difficult. In an attempt to improve the yields and stability of these iron-containing dendrimers, a series of iron acyl dendrimers were prepared. The iron acyl dendrimers proved to be more stable than the Fp and Fp* dendrimers.

Most of the iron-containing dendrimers were isolated as yellow oils after column chromatography. The compounds did not crystallise easily and tended to include solvent even after drying under vacuum for several hours. Consequently, microanalysis on these compound gave poor results. The iron benzyl bromides tended to be particularly sensitive under high vacuum and a trace amount of an impurity caused immediate decomposition. The X-ray crystal structures of $Cp^{*}Fe(CO)_{2}(CH_{2})_{3}Br$ and

$[CpFe(CO)(PPh_3)\{C(O)\}]_2(CH_2)_6$ showed the alkyl chain to lie in an extended conformation with the cyclopentadienyl and carbonyl ligands as far apart as possible. Cyclic voltammetry studies on some iron dendritic wedges and a first generation dendrimer all showed a single irreversible oxidation peak. These results suggest that the oxidation behaviour of one of the metals does not affect the oxidation of the remaining metals in the dendrimer. Thermogravimetric studies (DSC traces) of the dendritic wedges generally showed an endothermic peak which could be ascribed to melting.

Several attempts were made to link the metal centres of an iron dendritic wedge. Reactions with both nitrogen and phosphorus donor ligands resulted in coordination of the ligand to one metal centre only, rather than the expected bridged ligands. In addition, several novel iron dendrimers were synthesised by varying the core molecule.

A general trend in the stability and reactivity of the iron and ruthenium dendrimers was observed. The ruthenium-containing dendrimers are more stable at room temperature and in solution than the corresponding iron-containing dendrimers.

The structures of some organoruthenium dendrimers were investigated. The x-ray crystal structure of a first generation ruthenium dendritic wedge was obtained. The Cp groups in the dendritic wedge were found to be 'trans' to each other with respect to the plane of the benzyl ring. These crystal structure data can be useful for future molecular modelling studies on dendrimers.

As with the iron dendrimers, cyclic voltammetry studies on the first generation organoruthenium dendrimer and dendritic wedges showed single irreversible oxidation peaks. The metal sites in the dendrimer act independently of one another, suggesting that there is no communication or interaction between the metals. It was expected that the oxidation of one metal might influence the oxidation of the remaining metal sites, but this was not the case for either the iron or the ruthenium dendrimers.

The chemical reactivity of dendrimers has received little attention in the literature to date. In the present study, some chemical reactions of the first generation organoruthenium dendrimer have been investigated and compared with those of analogous mono-substituted compounds. The dendrimer was found to react differently from the mononuclear compounds. The reactions with the dendrimer were generally slower than

with the mononuclear compounds. In some of the reactions, only one of the six available metal sites on the dendrimer surface reacted.

Finally the first generation ruthenium dendrimer, Rp3G1C was tested as a supported heterogeneous catalyst in the Fischer-Tropsch synthesis. Although some $C_3$ and $C_4$ hydrocarbons were found in the product mixture, these were thought to result from decomposition of the dendrimer, rather than from the Fischer-Tropsch synthesis. The mono-atomic sites on the dendrimer were found to be insufficient for the catalysis of the synthesis of higher hydrocarbons.

Several cobaloxime dendritic wedges were synthesised and characterised. The alkyl chain length (in the haloalkyl starting complex) was found to influence the substitution of the 3,5-dihydroxybenzyl alcohol unit. The shorter chain compounds produced only the "mono-substituted" benzyl alcohol wedges whereas increasing the alkyl chain length produced a mixture of the "mono"-and "di"-substituted wedges. The bulkiness of the cobaloxime ligand made synthesis of even the first generation dendrimer difficult. The zero-generation cobaloxime dendrimer was however successfully prepared.

In the last section of work reported in this thesis, the synthesis of several heterobimetallic dendrimers and dendritic block copolymers was investigated. Convergent methodology has the advantage over a divergent synthetic approach for the synthesis of block copolymers. Two different approaches were used to synthesise the heterobimetallic complexes. Iron-ruthenium and iron-tungsten heterobimetallic dendritic wedges were successfully synthesised by isolating a "mono-substituted" intermediate, which was then reacted with a different haloalkyl complex. A heterobimetallic iron-ruthenium dendrimer was synthesised by complexation of two different wedges onto a single core molecule. An iron- and ruthenium dendritic phosphine was prepared and reacted with several different metal-containing cores. This represents yet another route to heterobimetallic dendrimers.

Finally a series of bromobenzyl-terminated dendrimers were synthesised. These organic dendrimers can be built up to the fifth generation in high yields. Several attempts were made to attach a metal-containing group to the surface of the dendrimer. Various lithium reagents were used to try to remove the bromo group. In all cases, a mixture of mono-, di- and tri-substituted lithiated products was obtained, which made purification and identification of the products very difficult. Grignard reagents are currently being

investigated as an alternative to the lithium reagents. Future work in this area will focus on building organic dendrimers with functional groups that are more easily cleaved.

Although large generation dendrimers were not synthesised in this work, many novel dendritic wedges and first generation dendrimers have been synthesised and characterised. Structural studies on the dendritic wedges have provided new information, as have the results obtained from the chemical reactivity studies. Future studies will be aimed at attaching metal groups to stable organic or inorganic cores. Finally, many interesting and useful applications for dendrimers are still waiting to be discovered, and so the focus of future dendrimer work is expected to be in this area of research.

# Chapter 7

# Experimental Details

## 7.1 General experimental details

### Chemicals

The starting materials $[CpFe(CO)_2]_2$, $[Cp^*Fe(CO)_2]_2$, $[CpW(CO)_3]_2$ and $[Ru_3(CO)_{12}]$ were obtained from Strem Chemicals. Bromobenzyl bromide was purchased from Sigma Aldrich. The haloalkyl metal complexes $[CpFe(CO)_2(CH_2)_nBr]$ (n = 3 or 6), $[Cp^*Fe(CO)_2(CH_2)_nBr]$ (n = 3 or 7 or 11), $[CpFe(CO)(PPh_3)\{C(O)\}(CH_2)_6Br]$, $[CpRu(CO)_2(CH_2)_3Br]$ and $[CpW(CO)_3(CH_2)_3I]$ were prepared by literature methods.[83,84,92] 3,5-dihydroxybenzyl alcohol was initially prepared by literature methods[163] and subsequently purchased from Sigma-Aldrich. Potassium carbonate was dried in the oven at 100°C. Alumina (Merck, 90, active, neutral) was deactivated before use and silica was used as is. All other reagents were obtained commercially, unless otherwise stated. Solvents were dried by standard methods, distilled, and stored under nitrogen over activated molecular sieves.

### Equipment

All reactions were carried out under nitrogen using standard Schlenk tube techniques. Melting points were recorded on a Kofler hotstage microscope (Reicher Thermovar). Microanalysis data were obtained from the University of Cape Town Microanalytical Laboratory. Infrared spectra were recorded on a Perkin-Elmer 983 spectrometer in solution cells with NaCl windows in hexane or $CH_2Cl_2$. In some cases, nujol mulls or KBr discs were also prepared. $^1H$ and $^{13}C$ NMR spectra were recorded on a Varian VXR 200 or a Varian Unity 400 spectrometer. The chemical shifts are reported according to the proton signal of deuterated solvent. Low resolution electron mass spectra were recorded on a Kratos MS 80 RFA spectrometer, operating at 70 eV ionizing voltage. Fast atom bombardment mass spectra were obtained from the University Chemical Laboratories, Cambridge, England, Sheffield University and Barcelona, Spain. Electrospray mass spectra were obtained from the University of Stellenbosch, Cape Town.

**Electrochemistry**

Cyclic voltammetry was performed on a BAS 100B Electrochemical Analyzer using a three-electrode system, comprising a platinum disk working electrode, a platinum wire auxiliary electrode and a $Ag/Ag^{+}$reference electrode (0.01M $AgNO_3$ and 0.1 M $[Bu_4N][ClO_4]$ in acetonitrile).Unless otherwise stated, all measurements were made on acetonitrile solutions which were 1-2 mM in sample and 0.1 M in $[Bu_4N][ClO_4]$. Under these conditions the ferrocene/ferrocenium couple, which was used a reference, had an $E_{1/2}$ value of 89 mV. All solutions were purged with argon and voltammograms were recorded under a blanket of argon.

**Thermal Analysis**

The differential scanning calorimetry (DSC) and thermogravimetric analysis (TGA) were carried out on the Perkin Elmer PC series DSC7 and TGA. Samples were heated under nitrogen from room temperature to 200 °C at a rate of either 10 or 20°/min in a hermetically sealed pan.

**Computer generated Structures**

Computer assisted molecular models for the dendrimers were generated using Hyperchem™.

**Crystal Structure Determination**

**Preliminary X-Ray photography**

Suitable single crystals were mounted and aligned on a Stoe optical goniometer. The space groups and preliminary cell parameters of all three structures were obtained photographically from oscillation, Weissenberg and precession photographs. The photographs were taken using various Weissenberg cameras and a Stoë Reciprocal Lattice Explorer for de Jong-Bouman, Buerger precession and cone-axis photographs. The crystals were irradiated with Ni-filtered CuKα radiation (λ = 1.5418Å) obtained from Philips PW1120 and PW1140 X-ray generators operating at 20 mA, 40 kV and 30 mA, 40 kV respectively.

**Intensity data-collection**

The data-collections were performed on an Enraf-Nonius CAD4 diffractometer with graphite-monochromated MoKα radiation (λ = 0.7107 Å ) obtained using a Philips PW 1730 model generator operating at 20 mA, 50 kV.

For data collections below ambient temperature, crystals were bathed in a constant stream of cold $N_2$ gas.

**Fp*3Br (7)**

X-ray intensity data collected at 21°C (294K) suffered from severe decay, allowing structure solution and refinement to a final R-factor of 0.173 only. The data were recollected at -25°C (248 K). Accurate cell parameters were obtained by least-squares analysis of the setting angles of 24 reflections in the θ range 16 -17°. Data were collected in the ω - 2θ scan mode with variable scan width ω = (0.85 + 0.35 tanθ)°, aperture width (1.12 + 1.05 tanθ) mm and speed, and a maximum recording time of 40s per reflection. Three reference reflections were periodically monitored for intensity and orientation control. Data were corrected for Lp-effects and for absorption.[164] The empirical absorption corrections were based on ψ-scans using several reflections with χ close to 90 °C. Table 2.5 shows details of the data collection.

**Fp dimer (23)**

X-ray intensity data were collected at -40°C (233K). The data were collected as described for Fp*3Br and details are shown in Table 2.6. Absorption corrections were applied.

**Rp3G1Br (32)**

X-ray intensity data were collected at -50 °C (223K). The data were collected as described for **7** and **23** and are shown in Table 3.1. Absorption corrections were also applied.

**Structure analysis and refinement**

In **7** and **23**, the heavy atoms, Fe and Br, were located by manual solution of a Patterson map and used as the initial phasing model. All of the remaining atoms, including hydrogen were located from difference Fourier maps. Full-matrix least-squares refinement was performed with SHELX-76 in which $\Sigma w||F_o| - |F_c||^2$ was minimised.[165] The weighting scheme was chosen to yield constant distributions of $\Sigma w(\Delta F)^2$ with $\sin\theta/\lambda$. In the final refinements, all non-H atoms were treated anisotropically in **7**, but only the Fe, P and carbonyl groups in **23** were. Hydrogen atoms were added from difference Fourier maps. The hydrogen atoms were then fixed in idealized positions with C-H = 1.00Å and were assigned common variable isotropic thermal parameters for chemically distinct groups. Complex neutral atomic scattering factors were taken from Cromer and Mann[166] for non-H atoms and from Stewart *et al.*[167] for H atoms, with dispersion corrections from Cromer and Liberman.[168] Molecular parameters were calculated with PARST[169] and molecular diagrams were plotted

using program PLUTO.[170] All computations were carried out on a VAX computer at the University of Cape Town.

An attempt was made to solve the structure of **32** using Patterson methods as well, but this attempt failed and so direct methods were used (SHELX-86) to find all non-hydrogen atoms.[171] The structure was refined using SHELX-76. Again, only the Ru, Br and O atoms were refined anisotropically as the other atoms gave abnormally high temperature factors when this was attempted. All details of structure refinement are listed in Tables 2.5, 2.6 and 3.1.

Several attempts were made to fully characterise all the compounds prepared in this study. Many of the compounds prepared were unstable and decomposed on the vacuum pump or during the analysis; for this reason they could not be fully characterised.

## 7.2 Experimental details pertaining to Chapter 2

**Synthesis of 3,5-dihydroxybenzyl alcohol (the monomer unit)**

Trimethylsilylchloride (400 μl, 2.95 mmol) was added to a stirred suspension of methyl-3,5-dihydroxy benzoate (5.00 g, 29.7 mmol) in hexamethyldisilazane (10 $cm^3$). The resulting mixture was refluxed for 5 h. The suspension changed to a solution which was stirred for a further 18 h at 25 °C, while a white deposit formed on the glass surface above the solution. Diethyl ether (20 $cm^3$) was added and the mixture was filtered. The solvent was removed under reduced pressure to give a pale yellow oil with low viscosity. The oil was dissolved in dry THF (2 $cm^3$) and slowly added over a 1.5 h to a heavily stirred suspension of lithium aluminium hydride (1.5 g, 39.5 mmol) in THF (100 $cm^3$). The mixture was refluxed for 4 h and left stirring at 25 °C for a further 17 h. Aqueous ammonium chloride (25 $cm^3$) was then added dropwise, followed by hydrochloric acid (*ca.* 6 $cm^3$) until the pH reached 3. The suspension was filtered and the solvent removed under reduced pressure to give a solid residue. The residue was washed with diethyl ether (3 x 50 $cm^3$) and then dried under reduced pressure to afford the product as a creamy white solid (3.40 g, 80%), m.p. 180–184 °C (lit.,[163] 181–184 °C); $\delta_H$(200 MHz; $d_6$-acetone) 6.35 (m, 2H, ArH), 6.24 (m, 2H, ArH), 4.46 (s, 2H, $CH_2OH$); $\delta_{C\{H\}}$(50 MHz; $d_6$-acetone) 158.4 (*m*-C), 144.7(*ipso*-C), 104.8 (*o*-C), 101.0 (*p*-C), 63.7 ($CH_2OH$).

The haloalkyl metal complexes listed below were prepared according to literature procedure[83,84,92] and purified by column chromatography and recrystallisation. Some characterisation data is listed in the table below.

| Complex | Yield (%) | m.p. /°C | ν(CO)[a] /cm$^{-1}$ |
|---|---|---|---|
| **Fp3Br (1)** | 70 | 22-25 | 2013, 1963 |
| **Fp6Br (2)** | 56 | 28-31 | 2009, 1956 |
| **Fp*3Br (7)** | 81 | 98-102 | 1991, 1938 |
| **Fp*7Br (8)** | 65 | oil | 1989, 1935 |
| **Fp*11Br (9)** | 64 | oil | 1988, 1934 |

[a] measured in hexane

**General procedure for the synthesis of benzyl alcohols, FpnG1OH (n = 3 or 6) and Fp*nG1OH (n = 3 or 7 or 11).**

A mixture of the appropriate metal-containing bromide, *e.g.* Fp3Br (2 equiv.), 3,5-dihydroxybenzyl alcohol (1 equiv.), potassium carbonate (3 equiv.) and 18-crown-6 (0.2 equiv.) in dry acetone was refluxed and stirred vigorously for 48 h (on average). The reaction was monitored by TLC eluting with a 70% $CH_2Cl_2$/hexane solution. The solution was allowed to cool and the solvent removed under reduced pressure to give a dark yellow or red/brown residue. The resulting residue was then extracted with 70% $CH_2Cl_2$/hexane and filtered. The filtrate was then concentrated and transferred to an alumina column. The polarity of the eluting solvent was gradually increased from 30% $CH_2Cl_2$/hexane to $CH_2Cl_2$. The purification procedure for each individual complex is outlined in the following text.

**Synthesis of Fp3G1OH (3)**

This was prepared from $[CpFe(CO)_2(CH_2)_3Br]$ **1** and purified by column chromatography eluting with a 70% $CH_2Cl_2$/hexane solution. The major yellow band was collected and the solvent removed to give a yellow oil **3** (40%), (Found: C, 56.6; H, 5.0%; $C_{27}H_{28}O7Fe_2$ requires C, 56.3; H, 4.9%) $\nu_{max}$/cm$^{-1}$ (CO) 1999, 1938 ($CH_2Cl_2$), $\delta_H$(200 MHz; $CDCl_3$) 6.42 (d, *J*(CH) 2 Hz, 2H, ArH), 6.31 (t, *J*(CH) 2 Hz, 1H, ArH), 4.69 (s, 10H, $C_5H_5$), 4.52 (br, 2H, $CH_2OH$), 3.80 (t, *J*(CH) 7 Hz, 4H, $CH_2O$), 1.82 (m, 4H, $CH_2$), 1.38 (m, 4H, $FeCH_2$); $\delta_{C\{H\}}$(50 MHz, $CDCl_3$) 217.3 (CO), 160.5, 143.2, 105.1, 100.5 (Ar), 85.4 ($C_5H_5$), 70.9 ($CH_2O$), 65.39 ($CH_2OH$), 37.13 ($CH_2$), -2.55 ($FeCH_2$); m/z (FAB) 548 (M - CO).

**Synthesis of Fp6G1OH (4)**

This was prepared from [$CpFe(CO)_2(CH_2)_6Br$] **2** and purified by column chromatography eluting with 70% $CH_2Cl_2$/hexane. The major yellow band was collected and the solvent removed to give a yellow oil **4** (32 %), $\nu_{max}/cm^{-1}$ (CO) 1999, 1938 ($CH_2Cl_2$), $\delta_H$(200 MHz; $CDCl_3$) 6.50 (br, 2H, ArH), 6.39 (t, *J*(CH) 3 Hz, 1H, ArH), 4.68 (s, 10H, $C_5H_5$), 4.59 (s, 2H, $CH_2OH$), 3.89 (t, *J*(CH) 7 Hz, $CH_2O$), 1.75, 1.42 (m, 16H, $CH_2$), 1.36 (m, 4H, $FeCH_2$), $\delta_{C\{H\}}$(50 MHz, $CDCl_3$) 217.7 (CO), 160.5, 143.1, 105.1, 100.6 (Ar), 85.3 ($C_5H_5$), 68.1 ($CH_2O$), 65.5 ($CH_2OH$), 38.1, 29.3, 25.7 ($CH_2$), 34.4($CH_2Br$), 3.4 ($FeCH_2$); m/z (FAB) 661 $(M + H)^+$.

**General procedure for the synthesis of benzyl bromides FpnG1Br (n = 3 or 6) and Fp*nG1Br ( n = 3 or 7 or 11).**

The appropriate benzyl alcohol *e.g.* Fp3G1OH (1 equiv.) with $CBr_4$ (1.25 equiv) was dissolved in the minimum volume of THF, followed by the addition of $PPh_3$ (1.25 equiv). The reaction mixture was stirred at R.T. and monitored by TLC (eluting with 30 % $CH_2Cl_2$/hexane). A large excess of $CBr_4$ and $PPh_3$ was often required to drive the reaction to completion. This was achieved by adding $PPh_3$ and $CBr_4$ at a rate of 1.25 equiv. every 10 min. until TLC showed no more starting material. The reaction was quenched with distilled water and the aqueous phase extracted with $CH_2Cl_2$ (3 x 20 $cm^3$). The combined organic phases were collected, dried over anhydrous $MgSO_4$ and filtered. The solvent was removed under reduced pressure to give a yellow oil. The crude product was purified by column chromatography, eluting with appropriate solvents.

**Synthesis of Fp3G1Br (5)**

This was prepared from Fp3G1OH **3** and purified by column chromatography, eluting with 30 % $CH_2Cl_2$/hexane. The major yellow band was collected and the solvent removed to give a dark yellow oil **5** (72%); $\nu_{max}/cm^{-1}$ (CO) 1999, 1938 ($CH_2Cl_2$); $\delta_H$(200 MHz, $CDCl_3$) 6.49 (br, 2H, ArH), 6.35 (br, 1H, ArH), 4.75 (s, 10H, $C_5H_5$), 4.39 (s, 2H, $CH_2Br$), 3.85 (br, 4H, $CH_2O$), 1.88 (br, 4H, $CH_2$), 1.43 (br, 4H, $FeCH_2$);$\delta_{C\{H\}}$(200 MHz, $CDCl_3$) 217.3 (CO), 160.5, 139.4, 107.4, 101.4 (Ar), 85.4 ($C_5H_5$), 71.0 ($CH_2O$), 37.1 ($CH_2$), 33.9 ($CH_2Br$), -2.6 ($FeCH_2$); m/z (FAB) 639 ($M^+$).

**Synthesis of Fp6G1Br (6)**

This was prepared from Fp6G1OH **4** and purified by column chromatography, eluting with 30 % $CH_2Cl_2$/hexane. The major yellow band was collected and the solvent removed to give a dark yellow oil **6** (70%); $\nu_{max}/cm^{-1}$ (CO) 1999, 1938 ($CH_2Cl_2$); $\delta_H$(200 MHz, $CDCl_3$) 6.49 (br, 2H, ArH), 6.41 (br, 1H, ArH), 4.75 (s, 10H, $C_5H_5$), 4.34 (s, 2H, $CH_2Br$), 3.88 (br, 4H, $CH_2O$),

1.88 (br, 8H, $CH_2$), 1.45 (br, 12H, $CH_2$ + $FeCH_2$); $\delta_{C\{H\}}$(200 MHz, $CDCl_3$) 217.3 (CO), 160.3, 139.6, 107.5, 101.5 (Ar), 85.3 ($C_5H_5$), 67.8 ($CH_2O$), 34.5, 32.7, 29.1, 27.9 ($CH_2$), 33.7 ($CH_2Br$), 1.1 ($FeCH_2$); m/z (FAB) 723 $(M+H)^+$.

**Synthesis of mFp*3G1OH (10)**

Fp*3Br **7** (0.613 g, 1.66 mmol) was added to a vigorously stirred mixture of 3,5-dihydroxybenzyl alcohol (0.211 g, 1.51 mmol), potassium carbonate (0.344 g, 2.49 mmol) and 18-crown-6 (0.044 g, 0.166 mmol) in acetone (20 $cm^3$). The mixture was refluxed for 48 h and monitored by TLC ($CH_2Cl_2$). The reaction mixture was cooled and the solvent removed under reduced pressure. The resulting dark yellow residue was extracted with $CH_2Cl_2$, concentrated and chromatographed on alumina. Elution with $CH_2Cl_2$ afforded some "di-substitued" product, Fp*3G1OH. The second yellow band eluted with acetone to yield the required "mono"-substituted product. The solvent was removed under reduced pressure to give a yellow residue. The product was recrystallised from $CH_2Cl_2$/hexane to give a yellow crystalline solid **10** (0.24 g, 37%), m.p. 124-129 °C (Found: C, 58.2; H, 6.4%; M-CO 400. $C_{22}H_{28}O_5Fe$ requires C, 61.7; H, 6.6%; M*428); $\nu_{max}/cm^{-1}$ (CO) 1981, 1921 ($CH_2Cl_2$); $\delta_H$(200 MHz, $CDCl_3$) 6.48 (s, 1H, ArH), 6.42 (s, 1H, ArH), 6.33 (s, 1H, ArH), 4.58 (s, 2H, $C\underline{H}_2OH$), 3.86 (t, *J*(CH) 7 Hz, 2H, $CH_2O$), 1.86 (m, 2H, $CH_2$), 1.73 (s, 15H, $C_5Me_5$), 0.82 (m, 2H, $FeCH_2$); $\delta_{C\{H\}}$(50 MHz, $CDCl_3$) 219.2 (CO), 161.0, 143.4, 105.7, 105.5, 101.25 (Ar), 94.96 ($\underline{C}_5Me_5$), 71.8 ($CH_2O$), 65.3 ($CH_2OH$), 36.5 ($CH_2$), 9.3 ($C_5\underline{Me}_5$), 7.0 ($FeCH_2$); m/z 400 (M - CO), 372 (M - 2CO).

**Fp*3G1OH (11)**

This was prepared from [$Cp^*Fe(CO)_2(CH_2)_3Br$] **7** and purified by column chromatography. A yellow band was collected and the solvent removed to give a yellow solid. A yellow solid **11** was obtained after recrystallisation from $CH_2Cl_2$/hexane at -15 °C (20%), m.p. 150-153 °C (Found: C, 62.0; H, 7.0%; $M^+$ 716. $C_{37}H_{48}O_7Fe_2$ requires C, 62.0; H 6.8 %; $M^+$ 716); $\nu_{max}/cm^{-1}$ (CO) 1980, 1919 ($CH_2Cl_2$); $\delta_H$(200 MHz, $CDCl_3$) 6.48 (s, 2H, ArH), 6.38 (s, 1H, ArH), 4.59 (s, 2H, $CH_2OH$), 3.85 (t, *J*(CH) 7 Hz, 4H, $CH_2O$), 1.82 (m, 4H, $CH_2$), 1.72 (s, 15H, $C_5Me_5$), 0.88 (m, 4H, $FeCH_2$); $\delta_{C\{H\}}$(50 MHz, $CDCl_3$) 219.2 (CO), 160.8, 142.9, 105.0, 100.7 (Ar), 94.9 ($C_5\underline{Me}_5$), 71.8 ($CH_2O$), 65.6 ($CH_2OH$), 36.5 ($CH_2$), 9.31 ($\underline{C}_5Me_5$), 7.1 ($FeCH_2$); m/z (FAB) 716 ($M^+$), 688 (M – CO), 660 (M – 2CO).

**Synthesis of Fp*7G1OH (12)**

This was prepared from [Cp*Fe(CO)$_2$(CH$_2$)$_7$Br] **8** and purified by column chromatography. A yellow band was collected with $CH_2Cl_2$ and the solvent removed to give **12** as a yellow oil (25%); (Found: C, 65.1; H, 7.7%; M$^+$ 829. $C_{45}H_{64}O_7Fe_2$ requires C, 65.2; H 7.8 %; M 716); $\nu_{max}$/cm$^{-1}$ (CO) 1980, 1919 ($CH_2Cl_2$); $\delta_H$(400 MHz, $CDCl_3$) 6.49 (br, 2H, ArH), 6.37 (br, 1H, ArH), 4.60 (s, 2H, $CH_2OH$), 3.93 (t, *J*(CH) 7 Hz, 4H, $CH_2O$), 1.87 (4 H, $CH_2$), 1.72 (m, 30 H, $C_5Me_5$), 1.45 (m, 16H, $CH_2$), 0.85 (m, 4H, $FeCH_2$); $\delta_{C\{H\}}$(100 MHz, $CDCl_3$) 219.6 (CO), 160.5, 160.5, 143.1, 105.1, 100.5 (Ar), 94.8 ($C_5\underline{Me}_5$), 68.0 ($CH_2O$), 65.4 ($CH_2OH$), 37.7, 33.9, 32.7, 28.3, 25.9 ($CH_2$), 14.0 3 ($FeCH_2$), 9.3 ($\underline{C}_5Me_5$); m/z (FAB) 913 (M + Rb)$^+$.

**Synthesis of Fp*11G1OH (13)**

This was prepared from [Cp*Fe(CO)$_2$(CH$_2$)$_{11}$Br] **9** and purified by column chromatography. The major yellow band was collected with $CH_2Cl_2$ and the solvent removed to give **13** as a yellow oil (30%); $\nu_{max}$/cm$^{-1}$ (CO) 1980, 1919 ($CH_2Cl_2$); $\delta_H$(400 MHz, $CDCl_3$) 6.49 (d, *J*(CH) 2 Hz, 2H, ArH), 6.36 (t, *J*(CH) 2 Hz, 1H, ArH), 4.60 (s, 2H, $C\underline{H}_2OH$), 3.92 (t, *J*(CH) 6 Hz, 4H, $CH_2O$), **1.76-1.27** (m, 36H, $CH_2$), 1.72 (m, 30H, $C_5Me_5$), 0.95 (m, 4H, $FeCH_2$); $\delta_{C\{H\}}$(100 MHz, $CDCl_3$) 219.61 (CO), 160.6, 143.2, 105.1, 100.5 (Ar), 94.7 ($\underline{C}_5Me_5$), 68.1 ($CH_2O$), 65.5 ($ArCH_2$), 37.8, 35.9, 29.8, 29.7, 29.6, 29.5, 29.4, 29.3, 26.1 ($CH_2$), 14.1 ($FeCH_2$), 9.3 ($C_5\underline{Me}_5$), m/z (FAB) 942 (M + 1)$^+$, 870 (M -2CO - $CH_3$)$^+$.

**Synthesis of Fp*3G1Br (14)**

This was prepared from Fp*3G1OH **11** and purified by column chromatography. The major yellow band was collected with 30%$CH_2Cl_2$/hexane and the solvent removed to give the product as a yellow oily solid. Recrystallisation with $CH_2Cl_2$/hexane gave **14** as yellow crystals (71%), m.p. 125 °C (dec.), (Found: C, 57.0; H, 6.5%; M$^+$ 778. $C_{37}H_{42}O_6Fe_2Br$ requires C, 57.0; H, 6.1%; M 779); $\nu_{max}$/cm$^{-1}$ (CO) 1980, 1920 ($CH_2Cl_2$); $\delta_H$(200 MHz, $CDCl_3$) 6.52 (br, 2H, ArH), 6.38 (br, 1H, ArH), 4.4 (s, 2H, $CH_2Br$), 3.85 (br, 4H, $CH_2O$), 1.95 (b, 4H, $CH_2$), 1.73 (s, 15H, $C_5Me_5$), 1.52 (b, 4H, $FeCH_2$); $\delta_{C\{H\}}$($CDCl_3$) 219.2 (CO), 160.6, 139.3, 107.3, 101.6 (Ar), 95.0 ($C_5\underline{Me}_5$), 71.9 ($CH_2O$), 36.5 ($CH_2$), 34.1 ($CH_2Br$), 9.4 ($\underline{C}_5Me_5$), 7.1 ($FeCH_2$); m/z 778 (M$^+$).

**Attempted synthesis of Fp*7G1Br and Fp*11G1Br**

The benzyl bromides were prepared from Fp*7G1OH **11** and Fp*11G1OH **13** respectively and purified by column chromatography. The major yellow bands were collected with

30%$CH_2Cl_2$/hexane and the solvent removed to give the products as yellow/green oils. The oils decomposed while drying on the vacuum pump.

**Synthesis of Fp*3G1C (15)**

A mixture of Fp*3G1Br **14** (0.06 g, 0.077 mmol), 1,1,1-tris(4-hydroxyphenyl)ethane (0.008 g, 0.026 mmol), potassium carbonate (0.09 g, 0.231 mmol) and 18-crown-6 (0.004 g, 0.007 mmol) in acetone (15 $cm^3$) was heated at reflux and stirred vigorously for 48 hours. The reaction was monitored by TLC, eluting with 50% $CH_2Cl_2$/hexane. The solvent was removed to give a dark yellow residue. The residue was then extracted with a 70%$CH_2Cl_2$/hexane and filtered. The filtrate was concentrated and transferred to an alumina column. The polarity of the eluting solvent was increased from 50% $CH_2Cl_2$/hexane to $CH_2Cl_2$. The major yellow band was collected and the solvent removed to give a yellow oil. A glassy solid **15** was obtained after drying the oil under high vacuum (30%), m.p. 48-52 °C, $\nu_{max}/cm^{-1}$ (CO) 1980, 1919 ($CH_2Cl_2$); $\delta_H$(200 MHz, $CDCl_3$) 6.99 (d, *J*(CH) 8 Hz, 6H, $Ar^{CORE}$), 6.86 (d, *J*(CH) 9 Hz, 6H, $Ar^{CORE}$), 6.55 (d, *J*(CH) 2 Hz, 6H, ArH), 6.42 (t, *J*(CH) 2 Hz, 3H, ArH), 4.93 (s, 6H, $ArCH_2O$), 3.86 (t, *J*(CH) 7 Hz, 12H, $CH_2O$), 2.10 (s, 3H, $CH_3$), 1.94 (m, 12H, $CH_2$), 1.72 (m, 90H, $C_5Me_5$), 0.9 (m, 12H, $FeCH_2$); $\delta_{C\{H\}}$(50 MHz, $CDCl_3$) 219.2 (CO), 160.7, 139.1, 105.7, 100.9 (Ar), 157.0, 142.0, 129.6, 114.0 ($Ar^{CORE}$), 94.94 ($C_5\underline{Me}_5$), 71.8 ($CH_2O$), 70.2 ($ArCH_2O$), 36.60 ($CH_2$), 29.71 ($CH_3$), 9.35 ($\underline{C}_5Me_5$), 7.12 ($FeCH_2$); (FAB) m/z 1187 $((M\text{-}CO)/2)^+$.

**Synthesis of Fp*3G2OH (16)**

Fp*3G1Br (0.023 g, 0.026 mmol) was added to a vigorously stirred mixture of 3,5-dihydroxybenzyl alcohol (0.002 g, 0.013 mmol), potassium carbonate (0.01 g, 0.039 mmol) and 18-crown-6 ( 0.069 g, 0.003 mmol) in dry acetone (15 $cm^3$) and the resulting mixture was refluxed for 72 h. The reaction was monitored by TLC eluting with a 70% $CH_2Cl_2$/hexane mixture. The solution was cooled and the solvent removed under reduced pressure to give an orange residue. The resulting residue was extracted with 50% $CH_2Cl_2$/hexane, filtered, concentrated and transferred to an alumina column. The polarity of the eluting solvent was increased from 70% $CH_2Cl_2$/hexane to $CH_2Cl_2$. A pale yellow fraction was eluted with 70% $CH_2Cl_2$/hexane and identified as unreacted starting material. Further elution with $CH_2Cl_2$ increasing to acetone afforded the product as a yellow oil (30%), $\nu_{max}/cm^{-1}$ (CO) 1982, 1922 ($CH_2Cl_2$); $\delta_H$(400 MHz, $CDCl_3$) 6.60 (d, *J*(CH) 2 Hz, 2H, ArH), 6.55 (d, *J*(CH) 2 Hz, 5H, ArH), 6.42 (t, *J*(CH) 2 Hz, 2H, ArH), 4.62 (d, *J*(CH) 6 Hz, 2H, $C\underline{H}_2OH$), 3.87 (t, *J*(CH) 7 Hz, 8H, $CH_2O$), 1.93 (m, 8H, $CH_2$), 1.72 (m, 60H, $C_5\underline{Me}_5$), 0.95 (m, 8H, $FeCH_2$); $\delta_{C\{H\}}$(100 MHz, $CDCl_3$) 219.2 (CO), 160.7, 160.3, 143.3, 138.7, 105.7, 101.3, 100.9 (Ar), 94.7

($\underline{C}_5Me_5$), 71.8 ($CH_2O$), 70.3 ($ArCH_2O$), 65.5 ($CH_2OH$), 36.6 ($CH_2$), 9.4 ($C_5\underline{Me}_5$), 7.1 ($FeCH_2$); m/z 1467 (M – 2CO – $CH_3$).

**Synthesis of Fp6ABr (18)**

This was synthesised according to literature procedure[84]. The compound was obtained as an orange solid after recrystallisation (80%) $\nu_{max}/cm^{-1}$ (CO) 1913, 1603 ($CH_2Cl_2$).

**Synthesis of Fp6AG1OH (19)**

CpFe(CO)(PPh3){C(O)}$(CH_2)_6$Br **18** (0.505 g, 0.84 mmol) was added to a vigorously stirred mixture of 3,5-dihydroxybenzyl alcohol (0.06 g, 0.42 mmol), potassium carbonate (0.18 g, 1.3 mmol) and 18-crown-6 ( 0.022 g, 0.084 mmol) in dry acetone (25 $cm^3$) and the resulting mixture was refluxed for 72 h. The reaction was monitored by TLC eluting with a 70% $CH_2Cl_2$/hexane mixture. The solution was cooled and the solvent removed under reduced pressure to give an orange residue. The resulting residue was extracted with 50% $CH_2Cl_2$/hexane, filtered, concentrated and transferred to an alumina column. The polarity of the eluting solvent was increased from 50% $CH_2Cl_2$/hexane to $CH_2Cl_2$ to yield a yellow fraction. Futher elution with 50% diethyl ether/$CH_2Cl_2$ increasing to $CHCl_3$ afforded the product as a yellow/orange solid. An orange foam **19** was obtained after the solvent was removed under reduced pressure (0.214 g, 43 %), m.p. 73-79°C (Found: C, 69.3; H, 6.1%; $M^+$ 1185. $C_{69}H_{70}O_7P_2Fe_2$•0.25 $CH_2Cl_2$ requires C, 69.0; H, 5.9%; M 1185); $\nu_{max}/cm^{-1}$ (CO) 1912, 1603 ($CH_2Cl_2$); $\delta_H$(200 MHz, $CDCl_3$) 7.37 (m, 30H, $P(C_6\underline{H}_5)_3$), 6.49 (br, 2H, ArH), 6.35 (br, 1H, ArH), 4.60 (br, 2H, $CH_2OH$), 4.41 (s, 10H, $C_5H_5$), 3.88 (t, *J*(CH) 6 Hz, 4H, $CH_2O$), 2.82, (m, 2H, C{O}$CH_2$), 2.59 (m, 2H, C{O}$CH_2$), 1.68 (m, 8H, $CH_2$), 1.27 (m, 4H, $CH_2$), 1.01 (m, 4H, $CH_2$); $\delta_{C\{H\}}$(50 MHz, $CDCl_3$) 221.0, 220.4 (CO), 160.5, 143.2, 105.0, 100.5 (Ar), 136.9 - 127.9 ($P(C_6\underline{H}_5)_3$), 85.2 ($C_5H_5$), 68.0 ($CH_2O$), 66.2, 66.1 ($CO\underline{C}H_2$), 65.4 ($CH_2OH$), 29.0, 28.8, 25.8, 25.0 ($CH_2$), $\delta_P$(80 MHz, $CDCl_3$) 75.9 ($P(C_6H_5)_3$); m/z (FAB) 1185 ($M^+$), 1157 (M - CO).

**Reaction of Fp6G1OH (4) with $PPh_3$**

$PPh_3$ (0.11 g, 0.43 mmol) was added to a solution of Fp6G1OH **4** (0.142 g, 0.22 mmol) in benzene (5 $cm^3$) and the resulting mixture refluxed for 27 h. IR spectroscopy confirmed the formation of the acyl product. The reaction mixture was allowed to cool and then filtered. The solution was concentrated and transferred to an alumina column. Elution with $CH_2Cl_2$ afforded some unreacted Fp6G1OH. Further elution with $CHCl_3$ and then acetone afforded the product as a yellow foam after drying under vacuum (0.14 g, 54%). IR spectroscopy and

$^1$H NMR spectroscopy confirmed the product as identical to that prepared in the previous experiment.

**Synthesis of Fp6AG1Br (20)**

Fp6AG1OH **19** (0.11 g, 0.093 mmol) and $CBr_4$ (0.38 g, 0.116 mmol) was dissolved in a minimum volume of THF (*ca.* 2 $cm^3$), and then $PPh_3$ (0.30 g, 0.116 mmol) added. The reaction mixture was stirred at R.T. and monitored by TLC (eluting with 30% $CH_2Cl_2$/hexane). A second batch of $CBr_4/PPh_3$ (1.29 mmol) was added. The formation of a precipitate was observed. The reaction mixture was quenched with distilled water, and the aqueous phase extracted with $CH_2Cl_2$ (3 x 20 $cm^3$). The solution was concentrated, and the residue columed on alumina with 50% $CH_2Cl_2$/hexane. A pale yellow fraction (identified as starting material) was obtained. Further elution with $CH_2Cl_2$ increasing to acetone afforded the product as a yellow/orange solid after the solvent was removed (0.081 g, 70%); m.p. 68-74 °C (Found: C, 65.0; H, 6.0%. $C_{69}H_{69}O_6P_2Fe_2Br \bullet 0.5\ CH_2Cl_2$ requires C, 64.7; H, 5.9%; M 1248); $\nu_{max}/cm^{-1}$ (CO) 1913, 1603 ($CH_2Cl_2$); $\delta_H$(200 MHz, $CDCl_3$) 7.37 (m, 30H, $P(C_6\underline{H}_5)_3$), 6.49 (br, 2H, ArH), 6.35 (br, 1H, ArH), 4.41 (br, 12H, $CH_2OH + C_5H_5$), 3.84 (t, *J*(CH) 6 Hz, 4H, $CH_2O$), 2.82, (m, 1H, C{O}$CH_2$), 2.59 (m, 1H, C{O}$CH_2$), 1.67 (m, 8H, $CH_2$), 1.27 (m, 4H, $CH_2$), 1.01 (m, 4H, $CH_2$); $\delta_{C\{H\}}$(50 MHz, $CDCl_3$) 221.0, 220.4 (CO), 160.4, 140.0, 107.3, 101.4 (Ar), 136.9 - 127.9 ($P(C_6\underline{H}_5)_3$), 85.2 ($C_5H_5$), 68.1 ($CH_2O$), 66.2, 66.1 ($CO\underline{C}H_2$), 33.8 ($CH_2Br$), 29.1, 28.8, 25.9, 25.0 ($CH_2$), $\delta_P$(80 MHz, $CDCl_3$) 75.9 ($P(C_6H_5)_3$); m/z (FAB) 1247 $(M - H)^+$.

**Synthesis of Fp6AG1C (21)**

Fp6AG1Br (0.165 g, 0.132 mmol) was added to a vigorously stirred mixture of 1,1,1tris-(4'hydroxyphenyl) ethane (0.013 g, 0.044 mmol), potassium carbonate (0.14 g, 1.04 mmol) and 18-crown-6 ( 0.008 g, 0.03 mmol) in dry acetone (15 $cm^3$) and the resulting mixture was refluxed for 48 h. The reaction was monitored by TLC eluting with a 50% $CH_2Cl_2$/hexane mixture. The solution was cooled and the solvent removed under reduced pressure to give a yellow/orange residue. The resulting residue was extracted with 50% $CH_2Cl_2$/hexane, filtered, concentrated and transferred to an alumina column. The polarity of the eluting solvent was increased from 50% $CH_2Cl_2$/diethyl ether to $CH_2Cl_2$ to yield the first yellow fraction (identified as unreacted starting material). Futher elution with $CHCl_3$ afforded the second yellow band. The product was obtained as a yellow/orange solid after the solvent was removed under reduced pressure (0.065 g, 39 %), m.p. 73-79 °C; $\nu_{max}/cm^{-1}$ (CO) 1913, 1605 ($CH_2Cl_2$); $\delta_H$(400 MHz, $CDCl_3$) 7.34 (m, 90H, $P(C_6\underline{H}_5)_3$), 6.98 (d, *J*(CH) 9 Hz, 6H, $Ar^{CORE}$), 6.84 (d, *J*(CH) 9 Hz, 6H, $Ar^{CORE}$), 6.56 (d, *J*(CH) 2 Hz, 6H, ArH), 6.39 (t, *J*(CH) 2 Hz, 3H, ArH), 4.93 (s, 6H, $ArCH_2O$), 4.39 (s, 30H, $C_5H_5$), 3.88 (t, *J*(CH) 6 Hz, 12H, $CH_2O$), 2.86

(m, 6H, C{O}$CH_2$), 2.57 (m, 6H, C{O}$CH_2$), 1.66 (m, 12H, $CH_2$), 1.35 (m, 12H, $CH_2$), 1.03 (m, 12H, $CH_2$); $\delta_{C\{H\}}$(100 MHz, $CDCl_3$) 220.1, 220.1 (CO), 160.5, 142.1, 105.7, 103.6 (Ar), 156.5, 139.9, 129.6, 113.9 ($Ar^{CORE}$),136.7 - 128.0 ($P(C_6\underline{H}_5)_3$), 85.2 ($C_5H_5$), 69.5 ($ArCH_2O$), 68.0 ($CH_2O$), 66.2 ($ArCH_2$), 53.8 ($CO\underline{C}H_2$), 31.7 ($CH_2$), 29.2, 28.9 25.9, 25.0 ($CH_2$); m/z (FAB) 3803 $(M - 4H)^+$.

**Synthesis of Fp6AG2OH (22)**

Fp6AG1Br (0.064 g, 0.05 mmol) was added to a vigorously stirred mixture of 3,5-dihydroxybenzyl alcohol (0.004 g, 0.026 mmol), potassium carbonate (0.01 g, 0.075 mmol) and 18-crown-6 (0.002 g, 0.005 mmol) in dry acetone (25 $cm^3$) and the resulting mixture was refluxed for 72 h. The reaction was monitored by TLC eluting with a 70% $CH_2Cl_2$/hexane mixture. The solution was cooled and the solvent removed under reduced pressure to give an orange residue. The resulting residue was extracted with 50% $CH_2Cl_2$/hexane, filtered, concentrated and transferred to an alumina column. The polarity of the eluting solvent was increased from 70% $CH_2Cl_2$/hexane to $CH_2Cl_2$ to yield a yellow fraction. Futher elution with $CH_2Cl_2$ increasing to $CHCl_3$ afforded the product as an orange solid. An orange foam was obtained after the solvent was removed under reduced pressure (56 %) $\nu_{max}/cm^{-1}$ (CO) 1912, 1603 ($CH_2Cl_2$); $\delta_H$(200 MHz, $CDCl_3$) 7.35 (m, 60H, $P(C_6\underline{H}_5)_3$), 6.59 (br, 2H, ArH), 6.53 (br, 5H, ArH + Ar'H), 6.38 (br, 2H, Ar), 4.93 (s, 4H, $ArCH_2O$), 4.60 (br, 2H, $CH_2OH$), 4.40 (s, 20H, $C_5H_5$), 3.87 (t, *J*(CH) 6 Hz, 8H, $CH_2O$), 2.81, (m, 8H, C{O}$CH_2$), 2.63 (m, 4H, C{O}$CH_2$), 1.65 (m, 12H, $CH_2$), 1.25 (m, 10H, $CH_2$), 1.01 (m, 10H, $CH_2$); $\delta_{C\{H\}}$(50 MHz, $CDCl_3$) 221.0, 220.2 (CO), 160.5, 160.2, 143.5, 105.7, 101.2, 100.8 (Ar), 139.0 (Ar'), 137.0 - 127.9 ($P(C_6\underline{H}_5)_3$), 85.2 ($C_5H_5$), 70.6 ($ArCH_2O$), 68.0 ($CH_2O$), 66.3, 66.2 ($CO\underline{C}H_2$), 65.2 ($CH_2OH$), 29.1, 28.8, 25.9, 25.0 ($CH_2$); m/z (FAB) fragments only

**Attempted synthesis of Fp6AG2Br**

Fp6AG2OH (0.141 g, 0.06 mmol) and $CBr_4$ (0.02 g, 0.07 mmol) was dissolved in a minimum volume of THF (*ca.* 2 $cm^3$), and then $PPh_3$ (0.019 g, 0.07 mmol) added. The reaction mixture was stirred at R.T. and monitored by TLC ( eluting with 30% $CH_2Cl_2$/hexane). A second batch of $CBr_4/PPh_3$ (1.29 mmol) was added. The formation of a precipitate was observed. The reaction mixture was quenched with distilled water, and the aqueous phase extracted with $CH_2Cl_2$ (3 x 20 $cm^3$). The solution was concentrated, and the residue columed on alumina with 30% $CH_2Cl_2$/hexane increasing to $CH_2Cl_2$. An orange oil was obtained after the solvent was removed. The resulting product decomposed on the vacuum pump.

**Fp dimer (23)**

This compound was isolated as a side product during the crystallisation of Fp6AG1OH. $\delta_H$(200 MHz, $CDCl_3$), 7.48 (m, 30H, $P(C_6H_5)_3$), 4.38 (s, 10H, $C_5H_5$), 2.78 (m, 1H, C{O}$CH_2$), 2.47 (m, 1H, C{O}$CH_2$), 1.70 (m, 4H, $CH_2$), 1.24 (m, 4H, $CH_2$).

**Reaction of Fp6G1OH with dppm, (1:1 mol ratio)**

Fp6G1OH (0.142 g, 0.22 mmol) was added to dppm (0.085 g, 0.22 mmol) in dry benzene (5 $cm^3$). The solution was refluxed for 22 h. IR showed two weak carbonyl bands for the expected product. The product was purified on a alumina column eluting with 70% $CH_2Cl_2$/hexane increasing to $CH_2Cl_2$ and finally acetone to elute the product as a yellow oil. After cooling and removal of the solvent under reduced pressure, the residue was chromatographed on alumina. Elution with 70% $CH_2Cl_2$/hexane gradually increasing to 100% $CH_2Cl_2$/hexane and then to $CHCl_3$ afforded two yellow bands. The solvent was removed under reduced pressure to yield the major fraction as a yellow oil (0.056 g, 24%) $\nu_{max}/cm^{-1}$ (CO) 2000, 1940, 1916, 1596 ($CH_2Cl_2$); $\delta_H$(200 MHz, $CDCl_3$), 7.46 (m, 10H, Ph), 7.21 (m, 10H, Ph), 6.50 (br, 2H, ArH), 6.37 (br, 1H, ArH), 4.70 (s, 5H, $C_5H_5$), 4.6 (br, 2H, $CH_2OH$), 4.52 (s, 5H, $C5H_5$), 3.92 (br, 4H, $CH_2O$), 2.81 (m, 1H, C{O}$CH_2$), 2.44 (m, 1H, C{O}$CH_2$), 2.1 (br, 2H, $PCH_2$), 1.71 (m, 8H, $CH_2$),1.43 (m, 2H, $FeCH_2$), 1.35 ( m, 8H, $CH_2$); $\delta_{C\{H\}}$(50 MHz, $CDCl_3$) 219.8, 219.2 (C{O}), 217.6 (CO), 160.42, 140.31, 133.1-127.5 (Ar + Ph), 105.0, 100.5 (Ar), 85.2, 84.8 ($C_5H_5$), 67.9 ($CH_2O$), 66.1, 66.0 (C{O}$CH_2$), 38.0, 34.4, 29.1, 25.8, 25.2 (CH2), 2.5 ($FeCH_2$); $\delta_P$(80 MHz, $CDCl_3$) 73.2 (d, *J*(PC) 16 Hz, 1P), 23.8 (d, *J*(CH) 17 MHz, 1P); the minor fraction: $\nu_{max}/cm^{-1}$ (CO) 2000, 1940, 1596 ($CH_2Cl_2$).

**Reaction of Fp6G1OH with dppm, (1:1.4 mol ratio)**

dppm (0.13 g, 0.34 mmol) Fp6G1OH (0.16 g, 0.2 mmol) benzene (5 $cm^3$). After cooling and removal of the solvent under reduced pressure, the residue was chromatographed on alumina. Elution with 70% $CH_2Cl_2$/hexane gradually increasing to 100% $CH_2Cl_2$/hexane and then to $CHCl_3$ afforded a yellow band. The solvent was removed under reduced pressure to yield a yellow oil (0.099 g, 28%) $\nu_{max}/cm^{-1}$ (CO) 2000, 1940, 1596 ($CH_2Cl_2$).

**Reaction of Fp6G1OH with 4,4'bipyridyl**

4,4'bipyridyl (0.053 g, 0.34 mmol) was added to a solution of Fp6G1OH (0.16 g, 0.2 mmol) in benzene (5 $cm^3$) and the solution refluxed for 23 h. After cooling and removal of the solvent under reduced pressure, the residue was chromatographed on alumina. Elution with 70% $CH_2Cl_2$/hexane gradually increasing to 100% $CH_2Cl_2$/hexane and then to $CHCl_3$

afforded the first yellow band. Further elution with ethyl acetate afforded second yellow band. The solvent was removed from both fractions under reduced pressure to yield the major fraction as a yellow oil (0.045 g, 23%) $\nu_{max}/cm^{-1}$ (CO) 1918, 1596 ($CH_2Cl_2$);$\delta_H$(200 MHz, $CDCl_3$), 7.21 (m, 16H, Ar'H), 6.48 (d, *J*(CH) 2 Hz, 2H, ArH), 6.35 (br, 1H, ArH), 4.55 (s, 10H, $C_5H_5$), 4.60 (br, 2H, $CH_2OH$), 3.87 (t *J*(CH) 7 Hz, 2H, $CH_2O$), 2.74 (m, 1H, C{O}$CH_2$), 2.32 (m, 1H, C{O}$CH_2$), 1.62 (m, 6H, $CH_2$), 1.23 (m, 8H, $CH_2$), 1.18 (m, 2H, $CH_2$).

**Reaction of Fp6G1OH (4) with 4,4'bipyridyl + oxidant**

4,4'bipyridyl (1.1 equiv.) was added to a solution of Fp6G1OH **4** (1 equiv.) in THF. The oxidant (ferricinium tetrafluoroborate) was generated by the addition of $AgBF_4$ to ferrocene in THF at R.T. and then added to the reaction mixture. The reaction was followed by IR spectroscopy. After several hours reaction at R.T., IR spectroscopy showed only unreacted starting material. A further portion of 4,4'bipyridyl (3 equiv.) was added and the solution refluxed overnight. The expected rapid conversion of **4** to the acyl product was not observed.

**Reaction Fp6G1OH (4) with phenylene diamine**

Phenylene diamine (1 equiv.) was added to a solution of Fp6G1OH **4** (1 equiv.) and 18-crown-6 (0.1equiv.) in diethyl ether and the solution refluxed for 48 h. The reaction was followed by IR spectroscopy. After cooling and removal of the solvent under reduced pressure, an IR spectum confirmed **28** as the product, $\nu_{max}/cm^{-1}$ (CO) 1992, 1947, 1597 ($CH_2Cl_2$).

**Reaction of Fp6AG1OH (4) with 1,3,5-tricarbonyl trichloride**

Triethylamine (0.004 g, 0.04 mmol) and benzene 1,3,5-tricarbonyl trichloride (0.03 g, 0.01 mmol) were added to Fp6G1OH **4** (0.049 g, 0.04 mmol) in dry THF (1 $cm^3$). The mixture was refluxed for 48 h. The product was isolated as a yellow oil after purification by column chromatography (0.014 g, 38%), $\nu_{max}/cm^{-1}$ (CO) 1912, 1601($CH_2Cl_2$); $\delta_H$(400 MHz, $CDCl_3$) 7.34 (m, 90H, $P(C_6\underline{H}_5)_3$), 7.22 (s, 1H, $Ar^{CORE}$), 7.18 (s, 1H, $Ar^{CORE}$), 7.16 (s, 1H, $Ar^{CORE}$), 6.38 (d, *J*(CH) 2 Hz, 6H, ArH), 6.36 (br, 3H, ArH), 4.39 (s, 30H, $C_5H_5$), 4.34 (br, 6H, $ArCH_2O$), 3.86 (t, *J*(CH) 7 Hz, 12H, $CH_2O$), 2.82 (m, 6H, C{O}$CH_2$), 2.56 (m, 6H, C{O}$CH_2$), 1.61 (m, 12H, $CH_2$), 1.28 (m, 12H, $CH_2$), 0.96 (m, 24H, $CH_2$). A large amount of unreacted starting material was evident in the $^1H$ NMR spectrum.

## 7.3 Experimental data for Chapter 3

Compounds **30** - **33** were synthesised according to literature procedures.[46] The characterisation data for these compounds is listed in Tables 3.1 and 3.2 in Chapter 3.

**Reaction Rp3G1OH (31) with $PPh_3$**

$PPh_3$ (0.08 g, 0.28 mmol) was added to Rp3G1OH **31** (0.095 g, 0.14 mmol) in benzene (5 $cm^3$) and the solution refluxed for 3 days. The reaction was monitored by IR spectroscopy (following the formation of a new acyl carbonyl band). After 3 days refluxing, the carbonyl region of the IR spectrum showed no evidence for an acyl product. The solution was cooled and the solvent removed under reduced pressure. Xylene was added and the solution refluxed for a further 25 h, after which a weak acyl peak appeared in the IR spectrum. After cooling the solution and removal of the solvent under reduced pressure, the residue was chromatographed on alumina. Elution with 50% $CH_2Cl_2$/hexane gradually increasing to $CH_2Cl_2$ afforded a pale yellow band (0.062 g, 37%), $\nu_{max}/cm^{-1}$ (CO) 1925, 1608 ($CH_2Cl_2$); $\delta_H$(400 MHz, $CDCl_3$) 7.46 (m, 30H, $P(C_6\underline{H}_5)_3$), 6.39 (d, *J*(CH) 2 Hz, 2H, ArH), 6.21 (t, *J*(CH) 2 Hz, 1H, ArH), 4.94 (s, 10H, $C_5H_5$), 4.60 (br, 2H, $CH_2OH$), 3.80 (br, 4H, $CH_2O$), 2.86, (m, 2H, C{O}$CH_2$), 2.38 (m, 2H, C{O}$CH_2$), 1.63 (m, 8H, $CH_2$), 2.0 (m, 4H, $CH_2$); $\delta_{C\{H\}}$(100 MHz, $CDCl_3$) 207.0, 205.1 (CO), 160.3, 143.1, 105.0, 100.6 (Ar), 136.4-127.9 (Ph), 88.7, 88.6 ($C_5H_5$), 67.5 ($CH_2O$), 61.4 ($CO\underline{C}H_2$), 65.3 ($CH_2OH$), 29.2 ($CH_2$); m/z (FAB) 1193 (M+2).

**Reaction of Rp3G1C (33) with $PPh_3$**

Rp3G1C **33** (1 equiv.) and $PPh_3$ (8 equiv.) were refluxed together in benzene. The reaction was followed by IR spectroscopy. After 3 days refluxing in benzene, the IR spectrum did not show the presence of an acyl peak. The solvent was replaced with xylene and the solution refluxed for a further 24 h, after which a weak acyl peak appeared. The product was purified and identified as **35**. A large amount of unreacted Rp3G1C was isolated as a side product. $\nu_{max}/cm^{-1}$ (CO) 1913, 1592 ($CH_2Cl_2$), $\delta_H$(400 MHz, $CDCl_3$) 7.33 (m, 90H, $P(C_6\underline{H}_5)_3$), 6.97 (d, *J*(CH) 8 Hz, 6H, $Ar^{CORE}$), 6.85 (d, *J*(CH) 9 Hz, 6H, $Ar^{CORE}$), 6.56 (d, *J*(CH) 2 Hz, 6H, ArH), 6.37 (t, *J*(CH) 2 Hz, 3H, ArH), 4.95 (s, 30H, $C_5H_5$), 4.92 (s, 6H, $ArCH_2O$), 3.86 (t, *J*(CH) 6 Hz, 12H, $CH_2O$), 2.85 (m, 6H, C{O}$CH_2$), 2.47 (m, 6H, C{O}$CH_2$), 2.10 (s, 3H, $CH_3$), 2.02 (m, 12H, $CH_2$).

**Reaction of Rp3G1C 33) with $I_2$**

Rp3G1C **33** (1 equiv.) was dissolved in $CH_2Cl_2$ and $I_2$ (6 equiv.) was added at R.T. The solution turned brown in colour. The reaction was monitored by IR spectroscopy. After about 5 min., IR showed that no starting material remained. The solvent was removed and the orange residue extracted with 30% $CH_2Cl_2$/hexane. The residue was chromatographed on alumina eluting with 30% $CH_2Cl_2$/hexane, the orange fraction collected and dried under vacuum. $^1H$ NMR spectroscopy showed the product to be a mixture of the new iodine terminated dendrimer **36** and $CpRu(CO)_2I$. $\delta_H$(400 MHz, $CDCl_3$) 6.97 (br, 6H, $Ar^{CORE}$), 6.82 (br, 6H, $Ar^{CORE}$), 6.58 (br, 6H, ArH), 6.40 (br, 3H, ArH), 4.92 (s, 6H, $ArCH_2O$), 3.96 (br, 12H, $CH_2O$), 3.34 (m, 12H, $CH_2I$), 2.10 (s, 3H, $CH_3$), 2.02 (m, 12H, $CH_2$).

**Reaction of Rp3G1C (33) with $Ph_3C^+PF_6^-$**

A solution of $Ph_3C^+PF_6^-$ (6 equiv.) in dry $CH_2Cl_2$ was added dropwise to a stirred solution of Rp3G1C **33** (1 equiv. ) in $CH_2Cl_2$ at R.T. The reaction was monitored by IR spectroscopy. After 24 h reaction at R.T., IR spectroscopy showed that most of the starting material has reacted. The solvent was removed under reduced pressure to yield a yellow/green oil. Acetone was added to precipitate product **37** as a grey/white solid (15%), $\nu_{max}/cm^{-1}$ (alkene) 2082, 2035 (CO) 2011, 1947(nujol).

**Experimental Procedure for the Catalysis experiments**

The Ru-dendrimer was synthesised according to literature procedure.[6] Silica gel (Davisil™, grade 646, $d_p$ = 200-250 μm, $d_{pore}$ = 150 A) was used as the support material. Rp3G1C (o.o55 g) was dissolved in *ca.* 1 $cm^3$ $CH_2Cl_2$ and loaded onto silica (0.445g ),resulting in a Ru loading of 3 wt%. The solvent was evaporated under a $N_2$ stream at room temperature. The known $Ru/SiO_2$ catalyst was prepared (for comparison) from an aqueous $RuCl_3$ solution, which was also loaded on silica. The incipient wetness method was used in both cases. In contrast to the dendrimer, the known catalyst (dried in air at 110 °C for 4 hours) was pretreated in the FT-synthesis reactor (see Figure 3.17) by a temperature programmed (4 °C/min, 300 °C, 4 hours) calcination in $N_2$, followed by reduction in $H_2$. The standard catalyst had a Ru content of 0.8 wt% assuming complete reduction of the ruthenium.

The stability of the Ru-dendrimer/$SiO_2$ in different environments was checked by TGA (Stanton Redcroft 780) in flow conditions under different environments. FT-synthesis was carried out on 0.4g of each catalyst in a U-tube plug flow reactor (0.25 inch, stainless steel, internal volume = 1.5 ml) at 170 °C, a total pressure of 2 bar, $v_{syngas}$ = 9 ml (NTP)/min and a

reaction pressure being maintained by addition of a pressure controlled argon stream before the pressure reducing valve. Samples of the product stream, to which a carefully measured reference gas stream (0.1 vol% cyclohexane in $N_2$) was added, were taken using the ampoule sampling technique. Gas chromatography (Varian 3400, flame ionisation detector, 50 m x 0.25 mm fused silica capillary column (Chrompack CP-Sil 5 CB), temperature program: -65 - 280 °C) was used to analyse the products. A rapid heat-up of the catalyst bed in the syngas (< 30s) was achieved by dipping the small reactor containing a small catalyst volume and a pre-heating zone for the syngas (0.5 ml) in a pre-heated silicon oil bath.

## 7.4 Experimental data for Chapter 4

Compounds [Co]3Br **38**, [Co]4Br **39** and [Co]6Br **40** were synthesised according to literature procedures[153] and characterised by m.p., IR and $^1$H NMR spectroscopy. Some characterisation data appears in Table 4.1. All these cobaloxime compounds are light sensitive and so aluminium foil was used to cover the Schlenk tube during the reactions and work-up procedures. The "mono"-substituted derivatives, [Co]6MG1OH and [Co]4MG1OH were isolated as side-products in the synthesis of the "di"-substituted benzyl alcohols, [Co]6G1OH and [Co]4G1OH respectively.

**General procedure for the synthesis of benzyl alcohols [Co]nG1OH (n = 4 or 6]**

A mixture of the appropriate metal-containing bromide *e.g.* [Co]6Br (2 equiv.), 3,5-dihydroxybenzylalcohol (1 equiv.), dried potassium carbonate (3 equiv.), 18-crown-6 (0.2 equiv.) in dry acetone (16 ml) was refluxed and stirred vigorously for 96 hours. The reaction was monitored by TLC eluting with ethyl acetate. Two new spots for the "di-substituted" and "mono-substituted" benzyl alcohols were observed. After the reaction was complete, the solvent was removed under reduced pressure to give a yellow residue. The residue was then extracted with ethyl acetate and filtered. The filtrate was concentrated and transferred to a silica column. The polarity of the eluting solvent was gradually increased from 30% ethyl acetate/hexane to ethyl acetate. The "di-substituted" benzyl alcohols were eluted with ethyl acetate and the "mono-substituted" products were eluted with acetone. The yellow/orange bands were collected and the solvent removed to give yellow/orange solids.

The purification procedure for each individual complex is outlined in the following text.

**Data for m[Co]4G1OH (41)**

A yellow/orange band was eluted with 10% acetone/ethyl acetate during the synthesis of **43**. The solvent was removed to yield a yellow oil **41** (39%). $\delta_H$(200 MHz, $CDCl_3$) 8.53 (d, *J*(CH)

2Hz, 2H, *o*H, py), 7.69 (t, *J*(CH) 8 Hz, 1H, *p*H, py), 7.26 (t, *J*(CH) 7 Hz, 2H, *m*H, py), 6.44, 6.34, 6.25 (s, 3H, ArH), 4.52 (s, 2H, $CH_2OH$), 3.77 (br, 2H, $CH_2O$), 2.10 (s, 12H, DMGO), 1.6 (m, $CH_2$).

**Data for m[Co]6G1OH (42)**

A yellow/orange band was eluted with acetone during the synthesis of **44**. The solvent was removed to yield a yellow oil **42** (36%). $\delta_H$(200 MHz, $CDCl_3$) 18.08 (br , 2H, OH...O, DMGO), 8.58 (d, *J*(CH) 5 Hz, 2H, *o*H, py), 7.66 (t, J(CH) 6 Hz, 1H, *p*H, py), 7.22 (t, J(CH) 4 Hz, 2H, *m*H, py), 6.46 (s, 1H, ArH), 6.37 (s, 1H, ArH), 6.31 (s, 1H, ArH), 4.58 (d, J = 12 Hz, 2H, $CH_2OH$), 3.83 (t, *J*(CH) 7 Hz, 2H, $CH_2O$), 2.10 (s, 12H, $CH_3$, DMGO), 1.52 (br, 2H, $CoCH_2$,) 1.21, (m, 8H, $CH_2$); $\delta_{C\{H\}}$(50 MHz, $CDCl_3$) 158.12, 151.06, 143.37, 106.35, 100.63 (Ar), 149.36 (C=N, DMGO), 149.96, 137.26, 125.10 (py), 68.08 ($CH_2OAr$), 65.32 ($ArCH_2$), 31.68, 30.13, 29.80, 29.26, 25.33 ($CH_2$), 12.53($CH_3$), m/z (FAB) $(M + 3H)^+$.

**Synthesis of [Co]4G1OH (43)**

This was prepared from [Co]4Br **39** and purified by column chromatography on silica eluting with acetone. The major yellow band was collected and the solvent removed to give a yellow/orange oily solid **43** (54%), m.p. 113-115 °C, $\delta_H$(400 MHz, $CDCl_3$) 8.54 (d, *J*(CH) 5Hz, 4H, *o*H, py), 7.67 (br, 2H, *p*H, py), 7.28 (t, *J*(CH) 6 Hz, 4H, *m*H, py), 6.41, (br, 2H, ArH), 6.24 (br, 1H, ArH), 4.56 (s, 2H, $CH_2OH$), 3.82 (t, *J*(CH) 6Hz, 4H, $CH_2O$), 2.08 (s, 24H, $CH_3$, DMGO), 1.60 (t, *J*(CH) 7Hz, 12H, $CoCH_2$ + $CH_2$), 1.01 (q, 4H, $CoCH_2C\underline{H}_2$) $\delta_{C\{H\}}$(100 MHz, $CDCl_3$) 160.41, 143.20, 105.13, 100.11 (Ar), 149.22 (C=N, DMGO),149.86, 137.37, 125.09 (py), 67.68 ($CH_2OAr$), 65.25 ($ArCH_2$), 30.76, 30.10, 26.67 ($CH_2$), 11.95 ($CH_3$,DMGO);

**Synthesis of [Co]6G1OH (44)**

This was prepared from [Co]6Br **40** and purified by column chromatography eluting with ethyl acetate. The major product, **44** was recrystallised from $CH_2Cl_2$/hexane to give a crystalline yellow/orange compound at -15 °C (0.066 g, 58 %). m.p. 180 °C(dec), (Found C, 50.9; H, 7.2%; $M^+$1043. $C_{45}H_{68}N_{10}O_{11}Co_2$ requires C, 51.8; H, 6.6%.; M 1043); $\nu_{max}/cm^{-1}$ (C=N, DMGO) 1556, (Co-N, DMGO) 515; δH(200 MHz, $CDCl_3$) 18.08 (br s, 4H, OH...O, DMGO), 8.58 (d, *J*(CH) 5 Hz, 4H, *o*H, py), 7.66 (t, *J*(CH) 6 Hz, 2H, *p*H, py), 7.22 (t, *J*(CH) 4 Hz, 4H, *m*H, py), 6.48 (br, 2H, ArH), 6.30 (d, *J*(CH) 2 Hz, 1H, ArH), 4.58 (d, *J*(CH) 12 Hz, 2H, $CH_2OH$), 3.83 (t, *J*(CH) 7 Hz, 4H, $CH_2O$), 2.10 (s, 24H, $CH_3$, DMGO) 1.61(q, *J*(CH) 8 Hz, 4H, $CH_2$), 1.52 (br, 4H, $CoCH_2$,) 1.24, (m, 8H, $CH_2$), 0.86 (m, 4H, $CoCH_2C\underline{H}_2$); $\delta_{C\{H\}}$(50 MHz, $CDCl_3$) 160.46, 143.37, 105.13, 101.11 (Ar), 149.13 (C=N, DMGO), 149.96, 137.34, 125.10

(py), 70.21 ($CH_2OAr$), 65.32 ($ArCH_2$), 31.88, 32.71, 30.44, 29.64, 28.60 ($CH_2$), 11.96 ($CH_3$,DMGO); mass spectrum (FAB) m/z 1042 $(M - H)^+$.

**General procedure for the synthesis of benzyl bromides [Co]nG1Br (n = 4 or 6)**

The appropriate benzyl alcohol *e.g.* [Co] 6G1Br (1 equiv.) with $CBr_4$ (1.25 equiv.) was dissolved in the minimum volume of THF, followed by the addition of $PPh_3$ (1.25 equiv). The mixture was maintained at 8 °C throughout the addition. The reaction mixture was stirred at R.T. After the addition was complete, the mixture was stirred for a further 15 minutes and then allowed to warm to R.T. The mixture was stirred for a further 1.5 hours and the reaction was monitored by TLC, eluting with a 50% ethyl acetate/acetone solution. The reaction was quenched with distilled water (10 $cm^3$) and the aqueous phase extracted with $CH_2Cl_2$ (2 x 15 $cm^3$). The organic layer was dried over $MgSO_4$, filtered and the solvent removed under vacuum to give an orange solid. The crude product was columned on alumina eluting with the appropriate solvents.

**Synthesis of [Co]6G1Br (45)**

This was prepared from [Co]6G1OH **44** and purified by column chromatography on alumina eluting with 30% ethyl acetate/hexane. A yellow/orange band was collected and the solvent removed to give a solid **45** (68%), δH(400 MHz, $CDCl_3$) 8.25 (d, 4H, *o*H, py), 7.69 (br, 2H, *p*H, py), 7.24 (m, 5H, *m*H, py + 3H, ArH), 4.34 (br, 2H, $CH_2OH$), 3.34 (t, 1H, $CH_2Br$), 2.21 (s, 24H, $CH_3$,DMGO), 1.72 (m, 8H, $CH_2$), 1.24 (m, 8H, $CH_2$)

**Attempted synthesis of [Co]6G1C**

A mixture of [Co]6G1Br **45** (1 equiv.), $K_2CO_3$ (3 equiv), 18-crown-6 (0.1 equiv.), CORE (0.3 equiv.) and dry acetone were refluxed under nitrogen for 40 hours. The reaction was monitored by TLC eluting with a 40% ethyl acetate/acetone mixture. The mixture was extracted with ethyl acetate, filtered and the solvent removed under high vacuum to yield an orange solid (13%). The solid was identified as unreacted starting material by $^1H$ NMR spectroscopy.

**Synthesis of [Co]4G0C (46)**

A mixture of [Co]6Br **39** (1 equiv.), $K_2CO_3$ (3 equiv), 18-crown-6 (0.1 equiv.), CORE (0.3 equiv.) and dry acetone were refluxed under nitrogen for 48 hours. The reaction was monitored by TLC eluting with a 40% ethyl acetate/acetone mixture. The compound was eluted with acetone/ethyl acetate and the solvent removed to give a yellow/orange oily solid **46** (20%); $\delta_H$(200 MHz, $CDCl_3$) 8.53 (d, *J*(CH) 2Hz, 6H, *o*H, py), 7.69 (t, *J*(CH) 8 Hz, 3H, *p*H,

eluted with acetone/ethyl acetate and the solvent removed to give a yellow/orange oily solid **46** (20%); $\delta_H$(200 MHz, $CDCl_3$) 8.53 (d, *J*(CH) 2Hz, 6H, *o*H, py), 7.69 (t, *J*(CH) 8 Hz, 3H, *p*H, py), 7.26 (t, *J*(CH) 7 Hz, 6H, *m*H, py), 6.94 (d, *J*(CH) 9Hz, 6H, Ar), 6.70 (d, *J*(CH) 9Hz, 6H, ArH), 3.84 (t, J(CH) 7Hz, 6H, $CH_2O$), 2.10 (s, 12H, $CH_3$, DMGO), 1.54 (m, 12H, $CoCH_2$ + $CH_2$), 1.05 (m, 6H, $CoCH_2C\underline{H}_2$).

## 7.5 Experimental data for Chapter 5

**Synthesis of Fp*/Rp3G1OH (47)**

Mono Fp*3G1OH **10** (0.129g, 0.3 mmol), Rp3Br (0.115g, 0.33 mmol), potassium carbonate (0.08g, 0.6 mmol) and 18-crown-6 (0.026g, 0.03 mmol) and acetone (15 $cm^3$) were refluxed together for 46 hours and the reaction was monitored by TLC ($CH_2Cl_2$). The yellow reaction mixture was cooled, concentrated and the resulting dark yellow residue was extracted with 70%$CH_2Cl_2$/hexane. The solvent was removed under reduced pressure and chromatographed on alumina. Elution with $CH_2Cl_2$ afforded a pale yellow fraction, some unreacted Rp3Br. The second dark yellow band eluted with acetone to yield the required heterobimetallic benzyl alcohol. The solvent was removed under reduced pressure to give a yellow oil (0.12g, 57%), (Found: C, 55.9; H, 6.2%; $M^+$ 692. $C_{32}H_{38}O_7FeRu$ requires C, 55.6; H, 5.5%; M 692); $\nu_{max}/cm^{-1}$ (CO) 2013, 1981, 1948,1921 ($CH_2Cl_2$); $\delta_H$(400 MHz, $CDCl_3$) 6.52 (d, *J*(CH) 8 Hz, 2H, ArH), 6.40 (m, 1H, ArH), 5.24 (s, 5H, $C_5H_5$), 4.60 (d, *J*(CH) 6 Hz, 2H, $C\underline{H}_2OH$), 3.86 ( t, *J*(CH) = 6.8 Hz, 2H, $CH_2O$), 2.01 (m, 2H, $CH_2$), 1.90 (m, 2H, $CH_2$), 1.72 (s, 15H, $C_5Me_5$), 1.62 (m, 2H, $RuCH_2$), 1.24(m, 2H, $FeCH_2$); $\delta_{C\{H\}}$(100 MHz, $CDCl_3$) 219.2 (FeCO), 202.1 (RuCO), 160.8, 160.6, 143.1, 105.1, 105.0, 100.6, 95.0 (Ar), 88.6 ($\underline{C}_5Me_5$), 71.8, 71.0 ($CH_2O$), 65.6 ($CH_2OH$), 38.5, 36.54 ($CH_2$), 9.3 ($C_5\underline{Me}_5$), 7.1 ($FeCH_2$), 9.3 ($RuCH_2$); m/z 693 $(M + H)^+$, 664 (M - CO), 636 (M - 2CO).

**One step synthesis of Fp*/Rp3G1OH (47)**

A mixture of Fp*3Br **7** (1.0g, 2.7 mmol), Rp3Br **30** (0.94g, 2.7 mmol), 3,5-dihydroxybenzyl alcohol (0.38g, 2.7 mmol), potassium carbonate (1.12g, 8.1 mmol ) and 18-crown-6 (0.07g, 0.27 mmol) was refluxed in dry acetone for two days. The solution changed from an initial yellow colour to a red colour after refluxing. The reaction mixture was concentrated and extracted with 70% $CH_2Cl_2$/hexane. The solvent was removed under reduced pressure and the residue chromatographed on alumina. A red fraction, Fp* dimer was eluted with 70% $CH_2Cl_2$/hexane. Further elution with $CH_2Cl_2$ yielded some unreacted Rp3Br and finally the heterobimetallic wedge, Fp*/Rp3G1OH, which was identical to that prepared in the previous experiment .

**Synthesis of Fp*/Rp3G1Br (48)**

$PPh_3$ (0.82g, 3.12 mmol) was added to a stirred solution of Fp*/Rp3G1OH **47** (0.710g, 1.03 mmol) and $CBr_4$ (0.97g, 2.91 mmol) in a minimum volume of THF (*ca* 2 $cm^3$). The reaction mixture was stirred for 10 min., followed by the addition of further portions of $PPh_3$ (0.39g, 1.5 mmol) and $CBr_4$ (0.46g, 1.4 mmol). The resulting mixture was stirred for a further 20 min, monitoring by TLC (70%$CH_2Cl_2$/hexane). The formation of a precipate indicated completion of the reaction. The reaction mixture was quenched with $H_2O$ (10 $cm^3$) and the residue partitioned between $H_2O$ and $CH_2Cl_2$ (15 $cm^3$). The aqueous phase was extracted with $CH_2Cl_2$ (3 x 20 $cm^3$), the combined organic phase was filtered, dried over $MgSO_4$ (anhydrous) and the solvent removed under reduced pressure. The resulting residue was chromatographed on alumina eluting with 70%$CH_2Cl_2$/hexane to give a bright yellow solution. Decomposition occured upon drying under vacuum. $\nu_{max}/cm^{-1}$ (CO) 2013, 1981, 1948,1921 ($CH_2Cl_2$); $\delta_H$(200 MHz, $CDCl_3$, 400 MHz) 6.51 (br, 2H, Ar), 6.36 (br, 1H, Ar), 5.25 (s, 5H, $C_5H_5$), 4.40 (s, 2H, $CH_2Br$), 3.84 (br t, 2H, $CH_2O$), 1.99 (m, 2H, $CH_2$), 1.82 (m, 2H, $CH_2$), 1.72 (s, 15H, $C_5Me_5$), 1.68 (m, 2H, $RuCH_2$)1.30 (m, 2H, $FeCH_2$).

**Reaction of one equivalent of Fp*3G1Br with the CORE (49)**

Fp*3G1Br **14** (0.17 g, 2.18 mmol), was added to a vigorously stirred mixture of 1,1,1-tris(4'-hydroxyphenyl)ethane (CORE) (0.803 g, 2.62 mmol), potassium carbonate (0.75 g, 5.45 mmol) and 18-crown-6 (0.17 g, 0.654 mmol) in acetone (30 $cm^3$) and the resulting mixture was refluxed for 48 hours. After cooling and removal of the solvent, the residue was extracted with $CH_2Cl_2$ to give a clear yellow solution. The solution was filtered and chromatographed on alumina. The first yellow band, unreacted Fp*3G1Br eluted with 50% $CH_2Cl_2$/hexane. A second pale yellow band was eluted with $CH_2Cl_2$ to give a yellow oil. This intermediate, "mono"Fp*3G1C was not fully characterised but reacted immediately with Rp3G1Br to form the heterobimetallic dendrimer, Rp2Fp*3G1C.

**Synthesis of Fp*/Rp3G1C (50)**

mFp*3G1C **49** (0.26 g, 0.026 mmol), Rp3G1Br **32** (0.041 g, 0.057 mmol), potassium carbonate (0.005 g, 0.039 mmol), 18-crown-6 (0.0007 g, 0.0026 mmol) were refluxed in acetone (15 $cm^3$) for 44 hours. TLC showed the presence of a new spot. After cooling of the reaction mixture and removal of the solvent, the residue was extracted with $CH_2Cl_2$ to give a yellow solution. The solution was filtered and chromatographed on alumina. A pale yellow oily solid was obtained by elution with 50% $CH_2Cl_2$/hexane. A "soft" oily solid remained upon drying under vacuum (0.032g, 37 %) m.p. 46 - 50 °C, $\nu_{max}/cm^{-1}$ (CO) $\delta_H$(400 MHz, $CDCl_3$, 400 MHz) 6.97 (d, *J*(CH) 9Hz, 6H, $Ar^{CORE}$), 6.86 (d, *J*(CH) 9 Hz, 6H, $Ar^{CORE}$), 6.54 (br, 6H,

ArH), 6.40 (br, 3H, ArH), 5.24 (s, 20H, $C_5H_5$), 4.95 (s, 6H, $CH_2OH$), 3.85 ( t, *J*(CH) 7 Hz, 12H, $CH_2O$), 2.11 (s, 3H, $CH_3$), 2.01 (m, 12H, $CH_2$ (Ru)), 1.85 (m, 4H, $CH_2$(Fe)), 1.72 (s, 30H, $C_5Me_5$), 1.67 (m, 8H, $RuCH_2$), 0.86 (m, 4H, $FeCH_2$); $^{13}C$ NMR $\delta(CDCl_3$, 100 MHz) 219.2 (FeCO), 202.1 (RuCO), 160.5, 156.9 ($Ar^{CORE}$), 142.0, 139.3, 129.5, 113.6 ($Ar^{CORE}$), 105.1, (Ar), 94.9 ($\underline{C}_5Me_5$), 88.9 ($C_5H_5$), 71.1, ($CH_2O$), 69.9 ($CH_2OH$), 50.7 ($\underline{C}CH_3$), 38.5 ($CH_2$), 33.9 ($C\underline{C}H_3$), 9.3 ($C_5\underline{Me}_5$), 7.1 ($FeCH_2$), -9.3 ($RuCH_2$); m/z 2274 (M - CO), 2247 ( M - 2CO).

**Synthesis of mWp3G1OH (52)**

This was isolated as a side product in the synthesis of **53**. The product was obtained as a yellow solid (18%), m.p. 45-50 °C, ν(CO) $cm^{-1}$ 1913, 2012 ($CH_2Cl_2$); Required for $C_{18}H_{18}O_6W$ m/z 486 (M - CO); $\delta_H(CDCl_3$, 200 MHz) 6.53 (s, 1H, Ar), 6.41(s, 1H, Ar), 6.34 (s, 1H, Ar), 5.40 (s, 5H, $C_5H_5$), 4.62 (s, 2H, $C\underline{H}_2OH$), 3.83 (t, *J*(CH) = 6.4 Hz, 4H, $CH_2O$), 2.02 (m, 2H, $CH_2$), 1.55 (m, 2H, $WCH_2$); $\delta_{C\{H\}}(CDCl_3$, 100 MHz) 218.8 (CO), 157.8, 143.5, 106.3, 104.9, 101.1 (Ar), 91.6 ($\underline{C}_5H_5$), 71.9 ($CH_2O$), 65.1 ($CH_2OH$), 36.2($CH_2$), -16.4 ($WCH_2$).

**Synthesis of Wp3G1OH (53)**

$Wp(CH_2)_3I$ **51** (0.0.79g, 1.57 mmol), potassium carbonate (0.33g, 2.34 mmol), 3,5-dihydroxybenzyl alcohol (0.11g, 0.79 mmol) and 18-crown-6 (0.041g, 0.157 mmol) and acetone (30 $cm^3$) were refluxed together for 46 hours, after which the reaction mixture had turned a yellow/brown colour. The reaction was monitored by TLC eluting with 70%$CH_2Cl_2$/hexane. The yellow reaction mixture was cooled, concentrated and the resulting dark yellow residue was extracted with $CH_2Cl_2$. The solvent was removed under reduced pressure and the residue chromatographed on alumina. Several fractions were collected. The first fraction eluted with 70% $CH_2Cl_2$/hexane yielded unreacted Wp3I. Elution with acetone afforded the product, Wp3G1OH. A third band was eluted with ETOH to give "mono"Wp3G1OH. The solvent was removed under reduced pressure to give yellow oils Wp3G1OH (20%); "mono"Wp3G1OH. Data for **53**: (Found: C, 40.35, H, 3.59%; $M^+$ . $C_{29}H_{28}O_9W_2$ requires C, 39.21; H, 3.18% M 888; $\nu_{max}/cm^{-1}$ (CO) 2011, 2004, 1912 ($CH_2Cl_2$); $\delta_H(CDCl_3$, 200 MHz) 6.49 (d, *J*(CH) 2 Hz, 2H, ArH), 6.36 (t, *J*(CH) 2 Hz, 1H, ArH), 5.40 (s, 5H, $C_5H_5$), 4.61 (s, 2H, $C\underline{H}_2OH$), 3.87 (t, *J*(CH) 6 Hz, 4H, $CH_2O$), 2.01 (m, 4H, $CH_2$), 1.57 (m, 4H, $WCH_2$); $\delta_{C\{H\}}(CDCl_3$, 100 MHz) 217.39 (CO), 160.52, 143.19, 105.13, 100.53 (Ar), 91.57 ($\underline{C}_5H_5$), 71.97 ($CH_2O$), 65.43 ($CH_2OH$), 36.21($CH_2$), -16.4 ($WCH_2$).

**Synthesis of Wp3G1Br (54)**

$PPh_3$ (0.11 g, 0.45 mmol) was added to a stirred solution of Wp3G1OH **53** (0.22 g, 0.25 mmol) and $CBr_4$ (0.14 g, 0.43 mmol) in a minimum volume of THF (*ca.* 2 $cm^3$). The reaction mixture was stirred for 10 min.after which the solution had turned green in colour. Further portions of $PPh_3$ (0.11g, 0.45 mmol) and $CBr_4$ (0.14g, 0.43 mmol) were added and the reaction mixture stirred for a further 10 min., monitoring by TLC (50 %$CH_2Cl_2$/hexane). The green reaction mixture was quenched with $H_2O$ (10 $cm^3$) and the residue partitioned between $H_2O$ and $CH_2Cl_2$ (*ca* 15 $cm^3$). The aqueous phase was extracted with $CH_2Cl_2$ (3 x 20 $cm^3$), the combined organic phase was filtered, dried over $MgSO_4$ (anhydrous) and the solvent removed under reduced pressure. The resulting brown residue was chromatographed on alumina eluting with 50%$CH_2Cl_2$/hexane to give a pale yellow solution. The solution was concentrated and crystallised at -15 °C. Decomposition occured upon recrystallisation of the yellow solid to give brownish coloured crystals (22%), m.p. 128 °C (dec); $\nu_{max}/cm^{-1}$ (CO) 2004, 1914 ($CH_2Cl_2$). The compound decomposed in solution before running the $^1H$ NMR spectrum.

**Synthesis of Fp*/ Wp3G1OH (55)**

A mixture of "mono"Fp*3G1OH (0.05 g, 0.117 mmol), Wp3I (0.04g, 0.129 mmol), potassium carbonate (0.024 g, 0.176 mmol ) and 18-crown-6 (0.003g, 0.012 mmol) was refluxed in dry acetone for 48 hours. The reaction was monitored by TLC ($CH_2Cl_2$). The solvent was removed and the reaction mixture extracted with 70% $CH_2Cl_2$/hexane. The solvent was removed under reduced pressure and the residue chromatographed on alumina. The first yellow band was eluted with 70% $CH_2Cl_2$/hexane and yielded some unreacted Wp3I. Further elution with $CH_2Cl_2$ yielded the benzyl alcohol complex, Wp3G1OH. (0.02 g, 21 %), $\nu_{max}/cm^{-1}$ (CO) 2012, 1982, 1920 ($CH_2Cl_2$); $\delta_H$($CDCl_3$, 200 MHz) 6.49 (br d, 2H, Ar), 6.38 (br t, 1H, Ar), 5.41 (s, 5H, $C_5H_5$), 4.58 (s, 2H, $C\underline{H}_2OH$), 3.87 (br t, 4H, $CH_2O$), 1.92 (m, 4H, $CH_2$), 1.73 (s, 15H, $C_5Me_5$), 1.61 (m, 2H, $WCH_2$)1.25 (m, 2H, $FeCH_2$); $\delta_{C\{H\}}$($CDCl_3$, 100 MHz) 219.2 (FeCO), 210 (WCO), 160.8, 143.1, 120.4, 105.2, 100.6, 94.9 (Ar), 91.6 ($\underline{C}_5Me_5$), 71.9 ($CH_2O$), 65.6 ($CH_2OH$), 36.5, 36.2 ($CH_2$), 9.3 ($C_5\underline{Me}_5$), 7.5 ($FeCH_2$), -16.4 ($WCH_2$); m/z 803 (M + H), 746 (M - 2CO).

**Synthesis of Fp*$(CH_2)_3PPh_2$ (56)**

Lithium metal (0.145 g, 20.8 mmol) was pressed into flat rods and added to a mixture of $PPh_3$ (0.513 g, 1.96 mmol) and dry THF (1.5 $cm^3$) under nitrogen. After stirring, the solution turned a dark red/ orange colour, indicating the formation of the diphenylphosphine ion. The solution was stirred at R. T. for 2 hours. 2-chloro-2-methyl propane (0.195 $cm^3$, 2.1 mmol)

was added by syringe. The dark red colour remained. The $LiPPh_2$ solution was then transferred to a clean dry Schlenk tube. A solution of Fp*3Br (0.555 g, 1,5 mmol) in dry THF (2 $cm^3$) was added dropwise to the $LiPPh_2$ solution at -78 °C. The reaction was stirred in a dry ice bath for 20 min, then warmed up to R.T. and stirred at R. T. for 1.5 hours. Degassed $H_20$ ( 10 $cm^3$) was added to quench the reaction. The product was extracted with degassed $CH_2Cl_2$ (3 x 20 $cm^3$), the organic phase collected, dried over MgSO4, filtered and concentrated. Degassed hexane (4 $cm^3$) was added to precipitate the product as a bright yellow solid (0.443 g, 45%), m.p. 155-160 °C (Found: C, 67.6; H, 6.60%, $M^+$ 474). $C_{27}H_{31}O_2PFe$ requires C, 68.4; H, 6.6%; M 474); ν(CO) 1982, 1922, 1187(P=O) ($CH_2Cl_2$); $\delta_H$ ($CDCl_3$) 7.41 (m, 10H, $P(C_6H_5)_2$); 2.15 (m, 2H, $CH_2P$), 1.67 (s, 15H, $C5Me_5$), 0.99 (m, 2H, $FeCH_2$); $\delta_{C\{H\}}$(50 MHz, $CDCl_3$)219.2 (CO), 132.9-128.1 ($P(C_6H_5)2$), 94.8 ($\underline{C}_5Me_5$), 34.0, 28.9 ($CH_2$), 15.4 ($FeCH_2$), 9.2 ($C_5\underline{Me}_5$); m/z 474 ($M^+$), 446 (M - CO), 418 (M - 2CO).

**Synthesis of $Rp3G1PPh_2$ (57)**

The phosphine complex was synthesised as decribed for **56**, starting from Rp3G1Br **32**. The complex was used *in situ*.

**Reaction of $Fp^*(CH_2)_3PPh_2$ with $Pt(COD)Cl_2$**

A $LiPPh_2$ solution was prepared as described previously. A solution of Fp*3Br (0.141 g, 0.37 mmol) in THF (1 $cm^3$) was added dropwise to a stirred $LiPPh_2$ solution (0.48 mmol) at -78 °C. The reaction was stirred at -78 °C for 20 min, then allowed to warm up to R.T. (1.5 hours). In a separate Schlenk tube, $Pt(COD)Cl_2$ (.069 g, 0.185 mmol) was dissolved in dry $CH_2Cl_2$ (2 $cm^3$) and the $Fp^*(CH_2)_3PPh_2$ solution (prepared above) was added dropwise. The mixture was stirred at R. T. for 2 hours. The solvent was removed under reduced pressure to yield a yellow solid. The solid was recrystallised from $CH_2Cl_2$/hexane (0.07g). The $^1H$ NMR spectrum showed only decomposed products. IR spectroscopy later showed a peak for P=O.

**Reaction of $Fp^*(CH_2)_3PPh_2$ with $Rh(III)Cl_3$**

An excess of $Fp^*(CH_2)_3PPh_2$ was added to a solution of $Rh(III)Cl_3$ in ethanol (7 $cm^3$). The yellow solution was refluxed for 2 hours, after which the solution went an opaque colour. The solution was cooled to R.T. and a fine yellow precipitate formed. Ethanol was added to the solution, the volume was concentrated and the flask transferred to the freezer at -15 °C. Orange crystals formed (0.04 g, 32%). $^{31}P$ NMR confirms the formation of the oxidised product by the presence of a strong P=O peak. The $^1H$ NMR spectrum showed only decomposed products.

**Reaction of Fp6AG1Br (20) with PEG 2000**

PEG 2000 **59** (0.03 g, 0.0148 mmol) was added to Fp6AG1Br **20** (0.03 g, 0.0148 mmol) in dry THF (1.5 $cm^3$). NaH (0.001 g, 0.04 mmol) was added slowly. The resulting mixture was refluxed for 24 h. TLC, eluting with 30% $CH_2Cl_2$/hexane. The solution was allowed to cool to R.T., then filtered, concentrated and extracted with acetone. Methanol was added to precipitate the product as an orange oily solid. The solid was recrystallised from a THF/hexane mixture (0.055 g, 44%), $\delta_H$(400 MHz, $CDCl_3$) 7.13 (m, 60H, Ph), 6.2 (br, 6H, ArH), 4.51 (br, 4H, $ArCH_2$), 3.83 (br, 8H, $CH_2O$), 3.43 (br, 180H, $OCH_2CH_2O$), 2.60 - 1.68 (m, 40H, $CH_2$).

**Reaction of Rp3G1Br (32) with PEG 2000**

PEG 2000 **59** (0.085 g, 0.042 mmol) was added to Rp3G1Br **32** (0.064 g, 0.087 mmol) in dry THF (2 $cm^3$). NaH (0.003 g, 0.12 mmol) was added slowly. The resulting mixture was stirred at 50 °C for 6 h. TLC, eluting with 30% $CH_2Cl_2$/hexane. The solution was allowed to cool to R.T., then filtered, concentrated and extracted with acetone. Methanol was added to precipitate the product as a white solid. The solid **61** was recrystallised from a THF/hexane mixture (0.086 g, 61%), m.p. 48-49 °C, $\delta_H$(200 MHz, $CDCl_3$) 6.44 (d, *J*(CH) 2 Hz, 4H, ArH), 6.33 (t, *J*(CH) 2 Hz, 2H, ArH), 4.45 (br, 4H, $ArCH_2$), 3.83 (t, *J*(CH) 7 Hz, 8H, $CH_2O$), 3.63 (br, 180H, $OCH_2CH_2O$), 2.01(m, 8H, $CH_2$), 1.67 (m, 8H, $RuCH_2$); $\delta_{C\{H\}}$(50 MHz, $CDCl_3$) 201.9 (CO), 160.3, 140.4, 105.8, 100.4 (Ar), 88.6 ($C_5H_5$), 70.9 ($CH_2OAr$), 70.5 ($OCH_2CH_2O$), 61.6 ($ArCH_2$), 38.4 ($CH_2$), -9.4 ($RuCH_2$).

**Synthesis of $Br_2$G1OH (63)**

Bromobenzyl bromide **62** (0.555 g, 2.20 mmol), potassium carbonate (0.45 g, 3.3 mmol), 3,5-dihydroxybenzyl alcohol (0.16 g, 1.1 mmol) and 18-crown-6 (0.058 g, 0.22 mmol) and acetone (20 $cm^3$) were refluxed together for 24h. TLC (acetone on silica) showed the presence of some starting material and so the reaction mixture was refluxed for a further 24h. The creamy/beige reaction mixture was cooled, concentrated and the resulting residue was extracted with $CH_2Cl_2$ (3 x 20 $cm^3$). The solvent was removed under reduced pressure to give the crude product as a white solid. The crude product was chromatographed on silica eluting with a $CH_2Cl_2$/EtOAc mixture (19:1 increased to 18:2). Compound **63** was obtained as a white solid (0.388 g, 74%), m.p. 96-99 °C (lit.,[162] 98-100 °C), (Found: C, 52.6; H, 3.8%. Calc. For $C_{21}H_{18}O_3Br_2$: C, 52.7; H, 3.8%; M 478); $\delta_H$($CDCl_3$, 400 MHz) 7.50 (Abq, *J*(CH) 10Hz, 8H, Ar'H), 7.29 (Abq, *J*(CH) 10Hz, 8H, Ar'H), 6.60 (d, *J*(CH) 2 Hz, 2H, ArH), 6.48 (t, *J*(CH) 2 Hz, 1H, ArH), 4.98 (s, 4H, $Ar'CH_2O$), 4.62 (s, 2H, $C\underline{H}_2OH$), 1.62 (br, 1H, $CH_2O\underline{H}$);

$\delta_{C\{H\}}$($CDCl_3$, 100 MHz) 159.8, 143.5, 135.8, 131.7, 129.0, 121.9, 105.8, 101.3 (ArC), 69.3 ($CH_2O$), 65.1 ($CH_2OH$).

**Synthesis of $Br_2G1Br$ (64)**

$PPh_3$ (0.25g, 0.96 mmol) was added to a stirred solution of $Br_2G1OH$ **28** (0.341g, 0.76 mmol) and $CBr_4$ (0.32g, 0.96 mmol) in a minimum volume of THF (*ca.* 2 $cm^3$). The reaction mixture was stirred for 15 min.,TLC still showed the presence of some starting material and so the reaction was stirred for a further 10 min. A white precipitate indicated completion of the reaction. The reaction mixture was quenched with $H_2O$ (10 $cm^3$) and the residue partitioned between $H_2O$ and $CH_2Cl_2$. The aqueous phase was extracted with $CH_2Cl_2$ (3 x 20 $cm^3$), the combined organic phase was filtered, dried over $MgSO_4$ (anhydrous) and the solvent removed under reduced pressure. The resulting residue was chromatographed on silica eluting with 70%$CH_2Cl_2$/hexane. Recrystallisation from acetone/water gave compound **29** as a white solid (0.252 g, 59%), m.p. 105-107 °C (lit.,[162] 106-107 °C), (Found: C, 46.6; H, 3.1%; Calc. for $C_{21}H_{17}O_2Br_3$: C, 46.6; H, 3.1%; M 478); $\delta_H$(400 MHz, $CDCl_3$) 7.51 (Abq, *J*(CH) 8Hz, 8H, Ar'H), 7.28 (Abq, *J*(CH) 8Hz, 8H, Ar'H), 6.62 (d, *J*(CH) 2 Hz, 2H, ArH), 6.48 (t, *J*(CH) 2 Hz, 1H, ArH), 4.98 (s, 4H, Ar'$CH_2O$), 4.40 (s, 2H, $CH_2Br$); $\delta_{C\{H\}}$($CDCl_3$, 100 MHz) 159.7, 139.9, 135.5, 131.7, 129.0, 121.9, 108.2, 101.2 (ArC), 69.3 ($CH_2O$), 33.3 ($CH_2Br$).

**Synthesis of Br6G1C (65)**

$Br_2G1Br$ **64** (0.223 g, 0.412 mmol), potassium carbonate (0.26 g, 0.618 mmol), 18-crown-6 (0.048 g, 0.062 mmol) and CORE (0.042 g, 0.137 mmol) were refluxed in acetone (10 $cm^3$) for 24 hours. TLC showed the presence of a new spot. After cooling of the reaction mixture and removal of the solvent, the residue was partitioned between $CH_2Cl_2$ and $H_2O$, and the aqueous layer extracted with $CH_2Cl_2$ (3 x 20 ml). The combined organic layers were dried over $MgSO_4$ and evaporated to dryness to give a creamy oil. The oil was chromatographed on alumina. A white solid **65** was obtained by elution with 50% $CH_2Cl_2$/hexane increasing $CH_2Cl_2$ to on silica (0.187 g, 81%), m.p. 60-65 °C (Found: C, 59.1; H, 4.0%; Calc. for $C_{83}H_{66}O_9Br_6$: C, 59.1; H, 4.0%; M 1687); $\delta_H$(400 MHz, $CDCl_3$) 7.49 (Abq, *J*(CH) 8Hz, 12H, Ar'H), 7.23 (Abq, *J*(CH) 8Hz, 12H, Ar'H), 7.02 (Abq, *J*(CH) 9Hz, 6H, $Ar^{CORE}$), 6.83 (Abq, *J*(CH) 9Hz, 6H, $Ar^{CORE}$), 6.64 (br, 2H, ArH), 6.52 (br, 1H, ArH), 4.98 (s, 18H, $ArCH_2O$), 2.12 (s, 3H, $CH_3$); $\delta_{C\{H\}}$($CDCl_3$, 100 MHz) 159.8, 139.8, 106.5, 101.5 (Ar), 156.7, 142.1, 129.6, 114.0 ($Ar^{CORE}$), 135.7, 131.7, 129.0, 121.9 (Ar'), 69.8 ($CH_2O$), 69.3 ($ArCH_2O$), 50.6 ($\underline{C}CH_3$), 30.1 ($C\underline{C}H_3$); m/z(FAB) 1672 (M – $CH_3$).

**Synthesis of $Br_4G1OH$ (66)**

$Br_2G1Br$ **64** (1.327 g, 2.45 mmol), potassium carbonate (0.312 g, 2.26 mmol), 3,5-dihydroxybenzyl alcohol (0.17 g, 1.21 mmol) and 18-crown-6 (0.059 g, 0.226 mmol) and acetone (30 $cm^3$) were refluxed together for 24h. TLC (acetone on silica) showed the presence of some starting material and so the reaction mixture was refluxed for a further 24h. The creamy/beige reaction mixture was cooled, concentrated and the resulting residue was extracted with $CH_2Cl_2$ (3 x 20 $cm^3$). The solvent was removed under reduced pressure to give the crude product as a white solid. The crude product was chromatographed on silica eluting with a $CH_2Cl_2$/EtOAc mixture (19:1 increased to 18:2). Compound **63** was obtained as a white solid (1.06 g, 83%), m.p. 154-157 °C (lit.,[162] 156-1158 °C), (Found: C, 55.9; H, 3.9%. Calc. For $C_{49}H_{40}O_7Br_4$: C, 55.5; H, 3.8%; M 1060); $\delta_H$($CDCl_3$, 400 MHz) 7.50 (Abq, *J*(CH) 10Hz, 16H, Ar'H), 7.25 (Abq, *J*(CH) 10Hz, 16H, Ar'H), 6.63 (d, *J*(CH) 2 Hz, 4H, ArH), 6.59 (d, *J*(CH) 2 Hz, 2H, ArH), 6.50 (m, 3H, ArH), 4.97 (s, 8H, Ar'$CH_2O$), 4.96 (s, 4H, $C\underline{H}_2OH$), 1.65 (br, 1H, $CH_2O\underline{H}$), $\delta_{C\{H\}}$($CDCl_3$, 100 MHz) 159.8, 159.7, 143.5, 139.2, 135.8, 131.7, 129.0, 121.9, 106.3, 105.8, 101.3, 101.1 (Ar), 69.7, 69.2 ($ArCH_2O$ + Ar'), 65.1 ($CH_2OH$).

**Synthesis of Br3G0C (67)**

Bromobenzyl bromide **64** (5.0 g, 20 mmol), potassium carbonate (4.1 g, 30 mmol), 18-crown-6 (0.79 g, 3 mmol) and CORE (2.048 g, 6.7 mmol) were refluxed in acetone (10 $cm^3$) for 24 hours. TLC showed the presence of a new spot. After cooling of the reaction mixture and removal of the solvent, the residue was partitioned between $CH_2Cl_2$ and $H_2O$, and the aqueous layer extracted with $CH_2Cl_2$ (3 x 20 ml). The combined organic layers were dried over $MgSO_4$ and evaporated to dryness to give a creamy coloured oil. The oil was chromatographed on alumina. A creamy white solid **67** was obtained by elution with 50% $CH_2Cl_2$/hexane increasing $CH_2Cl_2$ to on silica (0.187 g, 81%), m.p. 158-159 °C (Found: C, 60.1; H, 4.1%; Calc. for $C_{41}H_{33}O_3Br_3$: C, 60.5; H, 4.1%; M 813); $\delta_H$(400 MHz, $CDCl_3$) 7.50 (Abq, *J*(CH) 8Hz, 6H, Ar'H), 7.31 (Abq, *J*(CH) 8Hz, 6H, Ar'H), 7.00 (Abq, *J*(CH) 9Hz, 6H, $Ar^{CORE}$), 6.85 (Abq, *J*(CH) 9Hz, 6H, $Ar^{CORE}$), 4.98 (s, 6H, $ArCH_2O$), 2.10 (s, 3H, $CH_3$); $\delta_{C\{H\}}$($CDCl_3$, 100 MHz) 156.5, 142.1, 129.0, 113.9 ($Ar^{CORE}$), 136.1, 131.6, 129.6, 121.8 (Ar'), 69.2 ($ArCH_2O$), 50.6 ($\underline{C}CH_3$), 30.7 ($C\underline{C}H_3$); m/z(FAB) 813 $(M)^+$.

**Reaction of $Br_3G0C$ 67 with $^nBuLi/I(CH_2)_3I$**

$^nBuLi$ (1 $cm^3$, 1.5 mmol) was added to a solution of Br3G0C **67** (0.344 g, 0.42 mmol) in dry THF at -78 °C. The solution was allowed to warm up to R.T. and then kept at R.T. for 1 h. $I(CH_2)_3I$ (0.45 $cm^3$, 2.52 mmol) was added at -78 °C and the solution again warmed to R.T. The solution changed colour from yellow to almost colourless. TLC showed the presence of a new spot. The solution was cooled, filtered and the solvent removed. The crude product was purified by column chromatography on silica eluting with 30% $CH_2Cl_2$/hexane. The $^1H$ HNMR spectrum of the product showed that a dimer **68** had formed.

**Reaction of $Br_3G0C$ 67 with $^nBuLi/Fp3Br$**

$^nBuLi$ (1 $cm^3$, 1.5 mmol) was added to a solution of Br3G0C **67** (0.33 g, 0.41 mmol) in dry THF at -72 °C. The solution was allowed to warm up to R.T. and then kept at R.T. for 1 h. Fp3Br (0.33 g, 2.46 mmol) was added at -72 °C and the solution again warmed to R.T. The solution changed colour from yellow to almost colourless. TLC showed the presence of a new spot. The solution was cooled, filtered and the solvent removed. The crude product was purified by column chromatography on silica eluting with 30% $CH_2Cl_2$/hexane. The $^1H$ NMR spectrum of the product showed only unreacted starting material.

**Reaction of $Br_3G0C$ 67 with $^tBuLi/Fp3Br$**

$^nBuLi$ (1 $cm^3$, 1.64 mmol) was added to a solution of Br3G0C **67** (0.215 g, 0.26 mmol) in dry THF at -78 °C. The solution was warmed to 60 °C over 1 h and changed colour from red to almost colourless. Fp*3Br (0.30 g, 1.56 mmol) was added at -78 °C and the solution again warmed to R.T. The solution was stirred at R.T. overnight. TLC showed the presence of several new spots. The solution was cooled, filtered, dried over $MgSO_4$ and the solvent removed. A $^1H$ NMR spectrum of the product showed a mixture of products. Attempts to separate the product mixture failed.

# Chapter 8

# References


1 (a) D. A. Tomalia, H. M. Brothers II, L. T. Piehler and Y. Hsu, *Polym. Mater. Sci. Eng.*, 1995, **73**, 75 and references therein; (b) D. A. Tomalia, A. N. Naylor and W. A. Goddard III, *Angew. Chem., Int. Ed. Engl.*, 1990, **29**, 138.

2 C. J. Hawker and J. M. J. Fréchet, *New Methods Polym. Synth.*, 1995, 290 and references therein.

3 (a) S. C. Stinson, *Chem. Eng. News*, 1997, September 22, 28; (b) R. Dagani, *Chem. Eng. News*, 1993, February 1, 28; (c) R. F. Service, *Science*, 1995, **267**, 459; (d) M. Freemantle, *Chem. Eng. News*, 1999, November 1.

4 V. V. Narayanan and G. R. Newkome, in *Topics in Current Chemistry,* ed. E. Weber, Springer-Verlag, Berlin, Heidelberg, 1998, vol.197, pp. 20-77.

5 A. Archut and F. Vögtle, *Chem. Soc. Rev.*, 1998, **27**, 233.

6 H. Frey, C. Lach and K. Lorenz, *Adv. Mater.*, 1998, **10**, 279.

7 C. Gorman, *Adv. Mater.*, 1998, **10**, 295.

8 (a) C. N. Moorefield and G. R. Newkome, in *Advances in Dendritic Macromolecules,* ed. G. R. Newkome, JAI Press, Greenwich, CT, 1994, vol. 1, pp. 1-67; (b) G. R. Newkome, E. He and C. N. Moorefield, *Chem. Rev.*, 1999, **99**, 1689.

9 N. Ardoin and D. Astruc, *Bull. Soc. Chim. Fr.*, 1995, **132**, 875 and references therein.

10 F. Zeng and S. Zimmerman, *Chem. Rev.*, 1997, **97**, 1681 and references therein.

11 A. W. Bosman, H. M. Janssen and E. W. Meijer, *Chem. Rev.*, 1999, **99**, 1665.

12 (a) M. A. Hearshaw and J. R. Moss, *Chem. Commun.*, 1999, 1; (b) M. A. Hearshaw, A. T. Hutton, J. R. Moss and K. J. Naidoo in, *Advances in Dendritic Macromolecules,* ed. G. R. Newkome, JAI Press, Greenwich, CT, 1999, vol. 4, pp. 1-60.

13 Y. H. Kim, *J. Polym. Sci., Polym. Chem. Ed.*, 1998, **36**, 1685.

14 P. J. Flory, *J. Am. Chem. Soc.*, 1941, **63**, 3083; 3091; 3096.

15 E. Buhleier, W. Wehner, and F. Vögtle, *Synthesis*, 1978, 155.

16 R. G. Denkelwalter, J. F. Kolc and W. J. Lukasavage, *US Pat.*, 4 410 688, 1983.

17 (a) D. A. Tomalia, H. Baker, J. Dewald, M. Hall, G. Kallos, S. Martin, J. Roeck, J. Ryder and P. Smith, *Polymer*, 1985, **17**, 177; (b) D. A. Tomalia, R. J. Dewald, *US Pat.*, 4 507 466, 1985.

18 G. R. Newkome, C. N. Moorefield and G. R. Baker, *Aldrichim. Acta*, 1992, **25**, 31.

19 H.-F. Chow, I. Y.-K. Chan, C. C. Mak and M.-K. Ng, *Tetrahedron*, 1996, **52**, 4277.

20 G. R. Newkome and X. Lin, *Macromolecules*, 1991, **24**, 1443.

21 K. Lorenz, R. Mülhaupt and H. Frey, *Macromolecules*, 1995, **28**, 6657.

22 T. M. Miller, T. X. Neenan, R. Zayas and H. E. Bair, *J. Am. Chem. Soc.*, 1992, **114**, 1018.

23 T. Nagasaki, M. Ukon, S. Arimori and S. Shinkai, *J. Chem. Soc., Chem. Commun.*, 1992, 608.

24 D. O'Sullivan, *Chem. Eng. News*, 1993, August 16, 20.

25 (a) L.-L. Zhou and J. Roovers, *Macromolecules*, 1992, **26**, 963; (b) J. Roovers, P. M. Toporowski, L.-L. Zhou, *Polym. Preprints*, 1992, **33**, 182.

26 (a) A. W. van der Made, P. W. N. M. van Leeuven, J. C. de Wilde, R. A. C. Brandes, *Adv. Mater.*, 1993, **5**, 466; (b) A. W. van der Made and P. W. N. M. van Leeuven, *J. Chem. Soc., Chem. Commun.*, 1992, 1400.

27 (a) D. Seyferth and D. Y. Son, *Organometallics*, 1994, **13**, 2682; (b) S. W. Krska and D. Seyferth, *J. Am. Chem. Soc.*, 1998, **120**, 3604.

28 (a) C. Hawker and J. M. J. Fréchet, *J. Chem. Soc., Chem. Commun.*, 1990, 1010; (b) C. J. Hawker and J. M. J. Fréchet, *J. Am. Chem. Soc.*, 1990, **112**, 7638; (c) K. L. Wooley, C. J. Hawker and J. M. J. Fréchet, *Angew. Chem., Int. Ed. Engl.*, 1994, **33**, 82.

29 T. M. Miller and T. X. Neenan, *Chem. Mat.*, 1990, **2**, 346.

30 Z. Xu and J. S. Moore, *Acta Polym.*, 1994, **45**, 83.

31 (a) C. J. Hawker and J. M. J. Fréchet, *J. Am. Chem. Soc.*, 1992, **114**, 8405; (b) I. Gitsov, K. L. Wooley and J. M. J. Fréchet, *Angew. Chem., Int. Ed. Engl.*, 1992, **31**, 1200.

32 (a) K. Rengan and R. Engel, *J. Chem. Soc., Chem. Commun.*, 1992, 757; (b) K. Rengan and R. Engel, *J. Chem. Soc., Perkin Trans. 1*, 1991, 987.

33 G. R. Newkome, C. N. Moorefield, J. M. Keith, G. R. Baker and G. H. Escamilla, *Angew. Chem., Int. Ed. Engl.*, 1994, **33**, 666.

34 G. R. Newkome, V. K. Gupta, G. R. Baker and Z.-Q. Yao, *J. Org. Chem.*, 1985, **50**, 2003.

35 (a) R. Dagani, *Chem. Eng. News*, 1996, June 3, 30; (b) E. M. M de Brabander-van den Berg and E. W. Meijer, *Angew. Chem., Int. Ed. Engl.*, 1993, **32**, 1308; (c)

G. R. Newkome, C. N. Moorefield, G. R. Baker, M. J. Saunders and S. H. Grossman, *Angew. Chem., Int. Ed. Engl.*, 1991, **30**, 1178.

36 E. S. Friberg, M. Podzimek and D. A. Tomalia, *Mol. Cryst. Liq. Cryst.*, 1988, **164**, 157.

37 (a) V. Percec, P. Chu and M. Kawasumi, *Macromolecules*, 1994, **27**, 4441; (b) V. Percec and M. Kawasumi, *Macromolecules*, 1992, **25**, 3843.

38 H.-F. Chow and C. C. Mak, *J. Chem. Soc., Perkin Trans. 1*, 1997, 91.

39 C. Köllner, B. Pugin and A. Togni, *J. Am. Chem. Soc.*, 1998, **120**, 10274.

40 (a) S. C. Zimmerman, F. Zeng, D. E. C. Reichert and S. V. Kolotuchin, *Science*, 1996, **271**, 1095; (b) P. Thiyagarajan, F. Zeng, C. Y. Ku and S. C. Zimmerman, *J. Mater. Chem.*, 1997, **7**, 1221.

41 W. T. S. Huck, F. C. J. M. van Veggel and D. Reinhoudt, *J. Mater. Chem.*, 1997, **7**, 1213.

42 (a) N. Launay, A.-M. Caminade, R. Lahana and J.-P. Majoral, *Angew. Chem., Int. Ed. Engl.*, 1994, **33**, 1589; (b) J.-P. Majoral and A.-M. Caminade in, *Topics in Current Chemisty,* ed. E. Weber, Springer-Verlag, Berlin, Heidelberg, 1998, vol. 197, pp. 80-124; (c) C. Larré, D. Bressolles, C. Turrin, B. Donnadieu, A.-M. Caminade and J.-P. Majoral, *J. Am. Chem. Soc.*, 1998, **120**, 13070; (d) M. Slany, M. Bardaji, A.-M. Caminade, B. Chaudret and J.-P. Majoral, *Inorg. Chem.*, 1997, **36**, 1939; (e) M. Bardaji, A.-M. Caminade, J.-P. Majoral and B. Chaudret, *Organometallics,* 1997, **16**, 3489; (f) M. Bardaji, M. Kustos, A.-M. Caminade, J.-P. Majoral and B. Chaudret, *Organometallics*, 1997, **16**, 403.

43 (a) S. Serroni, G. Denti, S. Campagna, A. Juris, M. Ciano and V. Balzani, *Angew. Chem., Int. Ed. Engl*, 1992, **31**, 1493; (b) G. Denti, S. Campagna, S. Serroni, M. Ciano and V. Balzani, *J. Am. Chem. Soc.*, 1992, **114**, 2944; (c) S. Serroni, A. Juris, M. Venturi, S. Campagna, I. R. Resino, G. Denti, A. Credi and V. Balzani, *J. Mater. Chem.*, 1997, **7**, 1227. (d) M. Venturi, S. Serroni, A. Juris, S. Campagna and V. Balzani, in *Topics in Current Chemisty,* ed. E. Weber, Springer-Verlag: Berlin, Heidelberg, 1998, vol. 197, pp.194-228.

44 (a) G. R. Newkome, F. Cardullo, E. C. Constable, C. N. Moorefield and A. M. W. Cargill Thompson, *J. Chem. Soc., Chem. Commun.*, 1993, 925; (b) G. Newkome and E. He, *J. Mater. Chem*, 1997, **7,** 1237.

45 (a) E. Constable and P. Harverson, *Inorg. Chim. Acta*, 1996, **252**, 9; (b) E. Constable, *Chem. Commun.*,1997, 1073.

46 (a) Y.-H. Liao and J. R. Moss, *Organometallics*, 1996, **15**, 4307; (b) Y.-H. Liao and J. R. Moss, *Organometallics*, 1995, **14**, 2130; (c) Y.-H. Liao and J. R. Moss, *J. Chem. Soc., Chem. Commun.*, 1993, 1774.

47 (a) I. Cuadrado, C. Casado, B. Alonso, M. Morán, J. Losada and V. Belsky, *J. Am. Chem. Soc.,* 1997, **119**, 7613; (b) I. Cuadrado, M. Morán, J. Losada, C. M. Casado, C. Pascual, B. Alonso and F. Lobete, in *Advances in Dendritic Macromolecules*, ed. G. R. Newkome, JAI Press, Greenwich, CT, 1996, vol. 3, pp. 152-195; (c) I. Cuadrado, M. Morán, C. M. Casado, B. Alonso, F. Lobete, B. García, M. Ibisate and J. Losada, *Organometallics*, 1996, **15**, 5278; (d) R. Castro, I. Cuadrado, B. Alonso, C. M. Casado, M. Morán and A. E. Kaifer, *J. Am. Chem. Soc.*, 1997, **119**, 57; (e) F. Lobete, I. Cuadrado, C. M. Casado, B. Alonso, M. Morán and J. Losada, *J. Organomet. Chem.*, 1996, **509**, 109.

48 (a) J.-L. Fillaut, J. Linares and D. Astruc, *Angew. Chem., Int. Ed. Engl.,* 1994, **33**, 2460; (b) J.-L. Fillaut and D. Astruc, *J. Chem. Soc., Chem. Commun.*, 1993, 1320; (c) F. Moulines, L. Djakovitch, R. Boese, B. Gloaguen, W. Thiel, J.-L. Fillaut, M-H. Delville and D. Astruc, *Angew. Chem., Int. Ed. Engl.*, 1993, **32**, 1075; (d) C. Valério, J.-L. Fillaut, J. Ruiz, J. Guittard, J.-C. Blais and D. Astruc, *J. Am. Chem. Soc.*, 1997, **119**, 2588.

49 C. Gorman, *Adv. Mater.*, 1997, **9**, 1117.

50 (a) S. Achar and R. J. Puddephatt, *Angew. Chem., Int. Ed. Engl.,* 1994, **33**, 847; (b) S. Achar and R. J. Puddephatt, *Organometallics*, 1995, **14**, 1681; (c) S. Achar and R. J. Puddephatt, *J. Chem. Soc., Chem. Commun.*, 1994, 1895; (d) G.-X. Liu and R. J. Puddephatt, *Inorg. Chim. Acta*, 1996, **251**, 319; (e) S. Achar, J. J. Vittal and R. J. Puddephatt, *Organometallics*, 1996, **15**, 43.

51 (a) W. T. S. Huck, B. Snellink-Ruël, F. C. J. M. van Veggel and D. N. Reinhoudt, *Organometallics*, 1997, **16**, 4287; (b) W. T. S. Huck, L. J. Prins, R. H. Fokkens, N. M. Nibbering, F. C. J. M. van Veggel and D. N. Reinhoudt, *J. Am. Chem. Soc.*, 1998, **120**, 6240.

52 (a) N. Oshiro, F. Takei, K. Onitsuka and S. Takahashi, *Chemistry Letters*, 1996, 871; (b) S. Achar, C. E. Immoos, M. G. Hill and V. J. Catalano, *Inorg. Chem.*, 1997, **36**, 2314.

53 (a) P. Lange, A. Schier and H. Schmidbaur, *Inorg. Chem.*, 1996, **35**, 637; (b) P. Lange, A. Schier and H. Schmidbaur, *Inorg. Chim. Acta*, 1995, **235**, 263.

54 V. J. Catalano and N. Parodi, *Inorg. Chem.*, 1997, **36**, 537.

55 (a) E. C. Constable, O. Eich, C. E. Housecroft and L. A . Johnston, *Chem. Commun.*, 1998, 2661; (b) E. C. Constable, C. E. Housecroft and L. A. Johnston, *Inorg. Chem. Commun.*, 1998, **1**, 68.

56 (a) M. Zhao, L. Sun and R. M. Crooks, *J. Am. Chem. Soc.*, 1998, **120**, 4877; (b) L. Balogh and D. A. Tomalia, *J. Am. Chem. Soc.*, 1998, **120**, 7356.

57 (a) R. L. Lescanec and M. Muthukumar, *Macromolecules*, 1990, **23**, 2280; (b) M. L. Mansfield and L. I. Klushin, *Macromolecules*, 1993, **26**, 4262.

58 P. G. de Gennes and H. Hervet, *J. Phys. Lett.*, 1983, **44**, 351.

59 A. M. Naylor, W. A. I. Goddard, G. E. Keifer and D. A. Tomalia, *J. Am. Chem. Soc.*, 1989, **111**, 2339.

60 K. J. Naidoo, S. J. Hughes and J. R. Moss, *Macromolecules*, 1999, **32**, 331.

61 T. H. Mourey, S. R. Turner, M. Rubinstein, J. M. J. Fréchet, C. J. Hawker and K. L. Wooley, *Macromolecules*, 1992, **25**, 2402.

62 (a) K. L. Wooley, C. J. Hawker, J. M. Pochan and J. M. J. Fréchet, *Macromolecules*, 1993, **26**, 1514.

63 (a) B. L. Schwartz, A. L. Rockland, R. D. Smith, D. A. Tomalia and R. Splinder, *Rapid Commun. Mass Spec.*, 1995, **9**, 1552; (b) C. Moucheron and A. Kirsch-De Mesmaeker, *J. Am. Chem. Soc.*, 1996, **118**, 12834.

64 Z. Xu and J. S. Moore, *Angew. Chem., Int. Ed. Engl.*, 1993, **32**, 246.

65 P. L. Dubin, S. H. Edwards, J. I. Kaplan, M. S. Mehta and D. A. Tomalia, *Anal. Chem.*, 1992, **64**, 2344.

66 J. W. Kriesel, S. A. König, M. A. Freitas, A. G. Marshall, J. A. Leary and T. D. Tilley, *J. Am. Chem. Soc.*, 1998, **120**, 12207.

67 C. J. Hawker, K. L. Wooley and J. M. J. Fréchet, *J. Chem. Soc. Perkin Trans. 1*, 1993, 1287.

68 S. A. Evenson and J. P. S. Badyal, *Adv. Mater.*, 1997, **9**, 1097.

69 D. M. Junge, D. V. McGrath, *Chem. Commun.*, 1997, 857.

70 U. Kragl and C. Dreisbach, *Angew. Chem., Int. Ed. Engl.*, 1996, **35**, 642.

71 J. W. J. Knapen, A. W. van der Made, J. C. de Wilde, P. W. N. M. van Leeuwen, P. Wijkens, D. M. Grove and G. van Koten, *Nature*, 1994, **372**, 659.

72 A. Miedaner, C. J. Curtis, R. M. Barkley and D. L. DuBois, *Inorg. Chem.*, 1994, **33**, 5482 and references therein.

73 M. T. Reetz, G. Lohmer and R. Schwickardi, *Angew. Chem., Int. Ed. Engl*, 1997, **36**, 1526.

74 H. Brunner, *J. Organomet. Chem.*, 1995, **500**, 39.

75 H.-F. Chow and C. C. Mak, *J. Org. Chem*, 1997, **62**, 5116.

76 P. Bhyrappa, J. K. Young, J. S. Moore and K. Suslick, *J. Mol. Catal. A: Chem.*, 1996, 109.

77 L. L. Miller, R. G. Duan, D. C. Tully and D. A. Tomalia, *J. Am. Chem. Soc.*, 1997, **119**, 1005.

78 (a) F. A. Cotton and G. Wilkinson, in *Advanced Inorganic Chemistry*, Wiley-Interscience, New York, 5th edn., 1988, ch. 3, pp. 711; (b) A. J. Deeming, in

*Comprehensive Organometallic Chemistry*, ed. G. Wilkinson, F. Gordon, A. Stone and E. Abel, Pergamon Press, Oxford, England, 1982, vol. 4, pp. 377-512.

79 J. R. Green and W. A. Donaldson, in *Inorganic Synthesis,* Wiley, New York, pp. 1735-1784.

80 (a) T. J. Kealy and P. L. Paulson, *Nature (London)*, 1951, **168**, 1039; (b) S. A. Miller, J. A. Trebboth and J. F. Tremane, *J. Chem. Soc.*, 1952, 632.

81 R. B. King, *Coord. Chem. Rev.*, 1976, **20**, 155.

82 D. C. Calabro, J. L. Hubbard, C. H. Blevins, A. C. Campbell and D. L. Lichtenberger, *J. Am. Chem. Soc.*, 1981, **101**, 6839.

83 H. B. Fredrich, P. A. Makhesha, J. R. Moss and B. K. Williamson, *J. Organomet. Chem.*, 1990, **384**, 325.

84 J. R. Moss, *J. Organomet. Chem.*, 1982, **231**, 229.

85 (a) N. J. Coville, M. O. Albers, T. V. Ashworth and E. Singleton, *J. Chem. Soc., Chem. Commun.*, 1981, 408; (b) M. O. Albers, N. J. Coville and E. Singleton, *J. Organomet. Chem.*, 1982, **232**, 261.

86 G. R. Newkome, G. R. Baker, J. K. Young and J. G. Traynham, *J. Polym. Sci: A*:, 1993, **31**, 641.

87 C. K. Rofer-DePoorter, *Chem. Rev.*, 1981, 81, 447.

88 S. G. Davies, *Chem. Brit.*, 1989, 25, 268.

89 (a) S. G. Davies, I. M. Dordor-Hedgecock, K. H. Sutton and M. Whittaker, *J. Am. Chem. Soc.*, 1987, **109**, 5711; (b) J. R. Moss and L. Scott, *J. Organomet. Chem.*, 1989, **363**, 351.

90 J. Müller, *Angew. Chem., Int. Ed. Engl.*, 1972, **11**, 653.

91 S. Pignataro and F. P. Lossing, *J. Organomet. Chem.*, 1968, **11**, 571.

92 (a) R. B. King, *Inorg. Chem.*, 1966, **5**, 2227; (b) R. B. King, *J. Am. Chem., Soc.*, 1968, **90**, 1417.

93 R. K. Bohn and A. Haaland, *J. Organomet. Chem.*, 1966, **5**, 470.

94 R. O. Hill, C. F. Marais, J. R. Moss and K. J. Naidoo, *J. Organomet. Chem.*, 1999, **587**, 28.

95 M. Akita, A. Kondoh and Y. Moro-oka, *J. Chem. Soc., Dalton Trans.*, 1989, 1083.

96 B. K. Blackburn, S. G. Davies and M. Whittaker, in *Stereochemistry of Organometallic and Inorganic Compounds*, ed. I. Bernal, Elsevier, Amsterdam, 1989, vol. 3, pp. 141.

97 S. J. Archer, G. A. Harvey, J. R. Moss and A. M. Crouch, *Inorg. Chim. Acta*, 1992, **201**, 43.

98 L. Pope, P. Sommerville, M. Laing, K. J. Hindson and J. R. Moss, *J. Organomet. Chem.*, 1976, **112**, 309.

99 HYPERCHEM™-*Molecular Visualisation & Simulation*, Hypercube, Inc., 1994.

100 B.C. Gates, in *Catalytic Chemistry*, Wiley, New York, 1992.

101 A. J. Bard and L. R. Faulkner, in *Electrochemical Methods- Fundamentals and applications*, Wiley, New York, 1980.

102 Y.- H. Liao, Ph.D. Thesis, University of Cape Town, 1984.

103 (a) S. N. Anderson, C. W. Fong and M. D. Johnson, *J. Chem. Soc., Chem.* Commun., 1973, 163; (b) D. L. Reger, E. Mintz, L. Lebioda, *J. Am. Chem. Soc.*, 1986, **108**, 1940.

104 (a) D. C. Woska, J. Bartholomew, J. E. Greene, K. Eriks, A. Prock and W. P. Giering, *Organometallics*, 1993, **12**, 304; (b) A. A. Tracey, K. Eriks, A. Prock and W. P. Giering, *Organometallics*, 1990, 9, 1399.

105 M. J. Therien and W. C. Trogler, *J. Am. Chem. Soc.*, 1987, **109**, 5127.

106 (a) S. A. Evenson and J. P. S. Badyal, *Adv. Mater.*, 1997, **9**, 1097; (b) L. Zhang, Z. Bo, B. Zhao, Y. Wu, X. Zhang and J. Shen, in *Thin Solid Films*, 1998, 327-329, 221.

107 M. E. Brown, in *Introduction to Thermal Analysis - Techniques and Applications*, Chapman and Hall, London, 1988.

108 H. R. Alcock, F. W. Lampe, in *Contemporary Polymer Chemistry*, Prentice-Hall, U. S. A., 1981.

109 D. L. Reger and E. C. Culbertson, *J. Am. Chem. Soc.*, 1976, *98*, 2789.

110 S. J. Archer, K. P. Finch, H. B. Freidrich, J. R. Moss and A. M. Crouch, *Inorg. Chim. Acta*, 1991, **182**, 145.

111 J. D. Scott and R. J. Puddephatt, *Organometallics*, 1986, **5**, 1538.

112 R. H. Magnuson, R. Meirowitz, S. Zulu, and W. P. Giering, *Organometallics*, 1983, **2**, 460.

113 J. A. Howell and A. J. Rowan, *J. Chem. Soc., Dalton Trans.*, 1981, 297.

114 G. L'abbé, B. Haelterman and W. Dehaen, *J. Chem. Soc., Perkin Trans. 1*, 1994, 2203.

115 L. J. Twyman, A. E. Beezer and J. C. Mitchell, *J. Chem. Soc., Perkin Trans 1*, 1994, 407.

116 E. C. Constable, C. E. Housecroft, M. Cattalini and D. Phillips, *New J. Chem.*, 1998, 193.

117 X. Camps, H. Schönberger and A. Hirsch, *Chem. Eur. J.*, 1997, **3**, 561.

118 G. E. Oosterom, R. J. van Haaren, J. N. H. Reek, P. C. J. Kamer and P. W. N. M. van Leeuwen, *Chem. Commun.*, 1999, 1119.

119 (a) M. A. Bennet, M. I. Bruce and T. W. Matheson, in *Comprehensive*

*Organometallic Chemistry*, ed. G. Wilkinson, F. Gordon, A. Stone and E. Abel, Pergamon Press, Oxford, England, 1982, vol. 4, pp. 691-820; (b) F. M. Collins, M. O. Fildes, S. A. R. Knox and M. I. Yates, in *Organometallic Synthesis*, ed. R. B. King, Elsevier, Amsterdam, 1988, vol. 4, pp. 216.

120 (a) A. Yamamoto, *J. Organomet. Chem.*, 1986, **300**, 347; (b) W. J. Carter, J. W. Kellend, S. J. Okrasinski, K. E. Warner and J. R. Norton, *Inorg. Chem.*, 1982, **21**, 3955; (c) J. R. Moss and L. G. Scott, *Coord. Chem. Rev.*, 1984, **60**, 171; (d) W. Beck, N. Burkhard and M. Weiser, *Angew. Chem., Int. Ed. Engl.*, 1993, **32**, 923; (e) M. A. Gafoor, A. T. Hutton, J. R. Moss, *J. Organomet. Chem.*, 1996, **510**, 233.

121 M. O. Albers, D. J. Robinson, A. Shaver and E. Singleton, *Organometallics*, 1986, **5**, 2199.

122 P. D. Beer, O. Kocian, R. J. Mortimer and C. Ridgway, *J. Chem. Soc., Chem. Commun.*, 1991, 1460.

123 J. W. Kriesel, S. Konig, M. A. Freitas, A. G. Marshall, J. A. Leary and T. D. Tilley, *J. Am. Chem. Soc.*, 1998, **120**, 12207.

124 K. P. Finch, J. R. Moss and M. L. Niven, *Inorg. Chim. Acta*, 1989, **166**, 181.

125 R. George, J.-A. M. Andersen and J. R. Moss, *J. Organomet. Chem.*, 1995, **505**, 131.

126 J. P. Collman, L. S. Hegedus, J. R. Norton and R. G. Finke, in *Principles and Applications of Organotransition Metal Chemistry,* ed. J. P. Collman, L. S. Hegedus, J. R. Norton and R. G. Finke, University Science Books: Mill Valley, California, 2nd edn, 1987, pp. 433.

127 K. P. Finch, M. A. Gafoor, S. W. Mapolie and J. R. Moss, *Polyhedron*, 1991, **10**, 963.

128 (a) M. L. H. Green and P. L. I. Nagy, *J. Organomet. Chem.*, 1963, **1**, 58; (b) D. E. Laycock, J. Hartgerink and M. C. Baird, *J. Org. Chem.*, 1980, **45**, 291.

129 (a) J. W. Johnson and J. R. Moss, *Polyhedron*, 1985, **4**, 563; (b) R. B. King and M. B. Bisnette, *J. Organomet. Chem.*, 1967, **7**, 311; (c) M. Laing, J. R. Moss and J. Johnson, *J. Chem. Soc., Chem. Commun*, 1977, 656.

130 M. A. Gafoor, M.Sc. Thesis, University of Cape Town, 1991.

131 W. A. Hermann and B. Cornils, *Angew. Chem., Int. Ed. Engl.*, 1997, **36**, 1048.

132 G. W. Parshall and R. E. Putscher, *J. Chem. Educ.*, 1986, **63**, 189.

133 *Coordination Chemistry of Macrocyclic Compounds*, ed. G. A. Melson, Plenum, New York, 1979.

134 D. E. De Vos, F. Thibault-Starcyc, P. P. Knops-Gerrits, R. F. Parton and P. A. Jacobs, *Macromol. Symp.*, 1994, **80**, 157.

135 This work was done in collaboration with Dr M. Claeys and Dr. E. van Steen of the Catalysis Unit, Department of Chemical Engineering, U.C.T.

136 H. Schulz, *$C_1$Mol. Chem.*, 1985, **1**, 231.

137 M. A. Vannice, *J. Catal.*, 1977, **50**, 228.

138 H. Schulz, W. Böhringer, C.Kohl, N. Rahman, A. Will, *DGMK-Forschungsbericht*, DGMK, Hamburg, 1984, 320.

139 R. B. Anderson, *Catalysis*, ed. P. Emmett, Reinhold Publ., New York, 1956.

140 (a) H. Schulz, E. van Steen, and M. Claeys, Proc. DGMK Conference, Kassel, Germany, ed. M. Baerns, J. Weitkamp, DGMK-Tagungsbericht 9305, DGMK, Hamburg, 1993; (b) H. Schulz and M. Claeys, *Appl. Catal. A: General*, 1999, **186**, 71, 91.

141 V. A. Likholobov, B. L. Moroz, in *Handbook of Heterogeneous Catalysis*, ed. G. Ertl and H. Knözinger, Weinheim, VCH, 1997, vol. 5, pp. 2231.

142 R. D. W. Kemmitt and D. R. Russel, in *Comprehensive Organometallic Chemistry*, ed. G. Wilkinson, F. Gordon, A. Stone and E. Abel, Pergamon Press, Oxford, England, 1982, vol. 5, pp. 80-152.

143 (a) G. N. Schrauzer, *Angew. Chem. Int. Ed. Engl.*, 1976, **15**, 417; (b) G. N. Schrauzer and J. Kohnle, *Chem. Ber.*, 1964, **97**, 3056; (c) G. N. Schrauzer, *Acc. Chem. Res.*, **1**, 97; (d) G. N. Schrauzer, *Fortschr. Chem. Org. Naturst.*, 1974, **31**, 583; (e) D. G. Brown, *Progr. Inorg. Chem.*, 1973, **18**,177;

144 (a) G. Costa, G. Mestroni, G. Tauzher and L. Stefani, *J. Organomet. Chem.*, 1966, **6**, 181.; (b) G. Costa, G. Mestroni, and L. Stefani, *J. Organomet. Chem*, 1967, **7**, 49.

145 F. R. Jensen, V.Madan and D. H. Buchanan, *J. Am. Chem. Soc.*, 1970, **92**, 1414.

146 (a) G. N. Schrauzer and R. J. Windgassen, *J. Am. Chem. Soc.*, 1967, **89**, 1999; (b) E.A. Stadbauer, R. J. Holland, F. P. Lamn and G. N. Schrauzer, *Bioinorg, Chem.*, 1974, **4**, 67; (c) G. N. Schrauzer, *Inorganic Synthesis*, 1967, **11**, 937.

147 D. Dodd and M. D. Johnson, *Chem. Commun.*, 1971, 1371.

148 I. Das, S. Chowdhury, K. Ravikumar, S. Roy, B. D. Gupta; *J. Organomet. Chem.*, 1997, **532**, 101

149 R.Moors, F. Vögtle, *Chem. Ber.*, 1993, **126**, 2133.

150 D. Seyferth, T. Kugita, A. L. Rheingold, G. P. A. Yap, *Organometallics*, 1995, 14, 5362.

151 (a) B. González, C. M. Casado, B. Alonso, I. Cuadrado, M. Morán, Y. Wang and A. E. Kaifer, Chem. Commun., 1998, 2569; (b) I. Cuadrado, M. Morán, A. Moya, C. M. Casado, M. Barranco and B. Alonso, *Inorg. Chim. Acta*, 1996, **251**, 5.

152 E. C. Constable, C. E. Housecroft and L. A. Johnson, *Inorg. Chem. Commun.*, 1998, **1**, 68.

153 K. P. Finch and J. R. Moss, *J. Organomet. Chem.*, 1988, **346**, 253.

154 I. J. Mavunkal, unpublished work.

155 A. Adams, unpublished work.

156 (a) I. Gitsov, K. L. Wooley, C. J. Hawker, P. T. Ivanova and J. M. J. Fréchet, *Macromolecules*, 1992, **26**, 5621; (b) I. Gitsov and J. M. J. Fréchet, *Macromolecules*, 1993, **26**, 6536; (c) K. L. Wooley, C. J. Hawker and J. M.J. Fréchet, *J. Am. Chem.Soc.*, 1991, **113**, 4252.

157 D. A. Roberts and G. L. Geoffroy, in *Comprehensive Organometallic Chemistry*, ed. G. Wilkinson and E. Able, Pergamon Press, Oxford, England, 1982, vol. 6, chp. 40.

158 This complex had been prepared previously by X. Y. Yin; Ph.D. Thesis, University of Cape Town, 1996.

159 R. Zeng, unpublished work.

160 (a) J. M. Harris, *J. Macromolec. Sci., Rev. Macromolec. Chem. Phys. C*, 1985, **25**, 325; (b) J. M. Harris and M. G. Case, *J. Org. Chem.*, 1983, **48**, 5390 and references therein.

161 S. O. Grim, R. L. Keiter and W. McFarlane, *Inorg. Chem.*, 1967, **6**, 1133.

162 (a) K. L. Wooley, C. J. Hawker and J. M. J. Fréchet, *J. Chem. Soc., Perkin. Trans.1*, 1991, 1059; (b) C. J. Hawker and J. M. J. Fréchet, *Angew. Chem., Int. Ed. Engl.* 1992, **31**, 1200.

163 C. G. Pitt, H. H. Seltzman, Y. Sayed, C. E. Twine, Jr. and D. Williams, *J. Org. Chem.*, 1979, **44**, 677.

164 A. C. T. North, D. C. Phillips, F. S. Matthews, *Acta Crystallogr.*, 1968, **A24**, 351.

165 G. M. Sheldrick, SHELX-76, *Program for Crystal Structure Determination*; University of Cambridge, U. K. 1976.

166 D. T. Cromer and J. B. Mann, *Acta Crystallogr.*, 1986, **A24**, 321.

167 R. F. Stewart, E. R. Davidson and W. T. Simpson, *J. Chem. Phys.*, 1965, **42**, 3175.

168 D. T. Cromer and D. J. Liberman, *J. Chem. Phys.*, 1970, **53**, 1891.

169 M. Nardelli, *Comput. Chem.*, 1983, **7**, 95.

170 W. D. S. Motherwell, W. D. S., *PLUTO, a program for plotting molecular and crystal structures*, Cambridge University, U. K., 1976.

171 G. M. Sheldrick, SHELX-86, in *Crystallographic Computing 3*, ed. G. M. Sheldrick, C. Kruger and R. Goddard, Oxford University Press, 1985.

## ACKNOWLEDGEMENTS

I wish to express my sincere thanks and appreciation to the many people who have supported me throughout this thesis:

My supervisors, Professors John Moss and Mino Caira for their enthusiasm, encouragement and support in all areas of this thesis even when things were going badly!

To all the analytical staff for recording data, in particular:
Dr. Krassi Dimitrova, Ms. Margie Nair and Noel Hendricks for recording all the NMR spectra; Dr. Phillip Boshoff (Cape Technikon) and Sheffield University for recording FAB mass spectra and Mr Pierro Benincasa for the microanalysis.

Dr. Susan Bourne and Dr. Anita Coetzee for the data collections.

Dr. Alan Hutton for his help with the cyclic voltammetry experiments and proofreading parts of this thesis.

Dr. Shirley Churms for proofreading this thesis.

My colleagues and friends in the Chemistry Department, especially Dr. Ipe Mavunkal and Reinout Meijboom for many helpful discussions.

The Foundation for Research and Development and the University of Cape Town for financial assistance. The British Council is thanked for providing funding for an exchange visit to Sheffield University.

My parents and the rest of my family for all their encouragement and support over the course of this work.

My husband for his long suffering patience and support while I completed this thesis!

**Appendices 1, 2 and 3: Supplementary material**

Supplementary material for the three crystal structures solved in this study are on diskette in the following format:

**Appendix 1: Crystal structure data for Fp*3Br (7)**

"Appendix1a": Table A1: Fractional atomic co-ordinates
A2: Anisotropic displacement parameters
A3: Bond lengths
A4: Bond angles
A5: Torsion angles
A6: Hydrogen atomic co-ordinates

"Appendix1b": Observed and calculated structure factors

**Appendix 2: Crystal structure data for Fp dimer (23)**

"Appendix2a": Table A1: Fractional atomic co-ordinates
A2: Anisotropic displacement parameters
A3: Bond lengths
A4: Bond angles
A5: Torsion angles
A6: Hydrogen atomic co-ordinates

"Appendix2b": Observed and calculated structure factors

**Appendix 3: Crystal structure data for Rp3G1Br (32)**

"Appendix3a": Table A1: Fractional atomic co-ordinates
A2: Anisotropic displacement parameters
A3: Bond lengths
A4: Bond angles
A5: Torsion angles
A6: Hydrogen atomic co-ordinates

"Appendix3b": Observed and calculated structure factors

**Parts of this thesis have been presented at:**

1 "Investigation of the Polymorphism and Pseudopolymorphism of Tenoxicam." M. A. Timme, M. R. Caira and L. R. Nassimbeni, presented at the Academy of Pharmacetical Sciences, 15th Annual Congress, Grahamstown, June 1994.

2 "Synthesis, Structure and Chemistry of Novel Organometallic Dendrimers containing Iron." M. A. Timme, M. R. Caira and J. R. Moss, presented at Inorganic '95, University of Natal, January 1995.

3 "The Synthesis, Structure and Chemistry of Novel Organometallic Dendrimers." M. A. Timme, M. R. Caira and J. R. Moss, presented at the 33rd Convention of the South African Chemical Institute, University of Cape Town, January 1996.

4 "Organometallic Dendrimers of Iron and Ruthenium." Y-H. Liao, J. R. Moss, M. A Timme and R. Zeng, presented at the 17th International Conference on Organometallic Chemistry, Brisbane, Australia, July, 1996.

5 "The Synthesis, Structure and Chemistry of Novel Iron and Ruthenium Dendrimers." M. A. Timme, M. R. Caira and J. R. Moss, presented at the Anglo/German Inorganic Chemistry Meeting, Phillips-Universitat, Marburg, Germany, September 1997.

6 "The Synthesis and Structure of some Novel Organometallic Acyl Dendrimers." M. A. Timme, M. R. Caira and J. R. Moss, presented at Inorganic '97,University of Port Elizabeth, January 1997.

7 "Synthesis and Characterization of a Cobalt Dendrimer." M. A. Timme, A. Adams, I. Mavunkal, J. R. Moss, presented at the 34th South African Chemical Institute convention held together with the 7th International Conference on Chemistry in Africa, Durban, July 1998.

8 "Organometallic Dendrimers: Synthesis and Applications." J. R. Moss, M. Timme, S. J. Hughes and K. Naidoo, presented at the 33rd International Conference on Coordination Chemistry, August 1998.

(presented under maiden name: Timme)

COMPOUND REFERENCE GUIDE

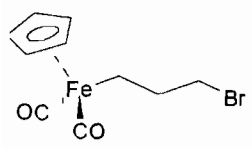

**Fp3Br (1)**

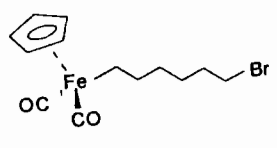

**Fp6Br (2)**

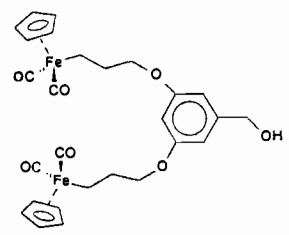

**Fp3G1OH (3)**

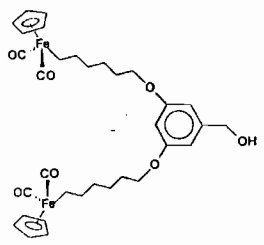

**Fp6G1OH (4)**

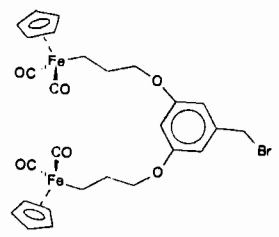

**Fp3G1Br (5)**

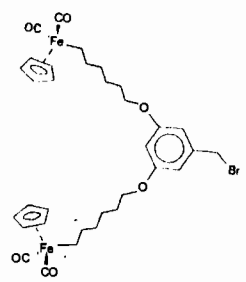

**Fp6G1Br (6)**

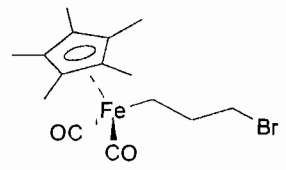

**Fp*3Br (7)**

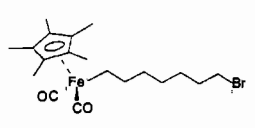

**Fp*7Br (8)**

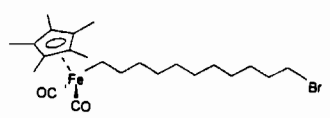

**Fp*11Br (9)**

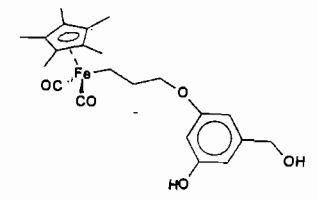

**mFp*3G1OH (10)**

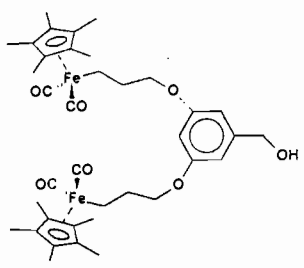

**Fp*3G1OH (11)**

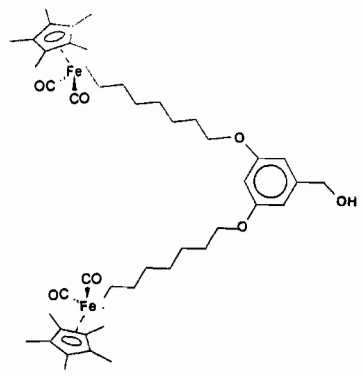

**Fp*7G1OH (12)**

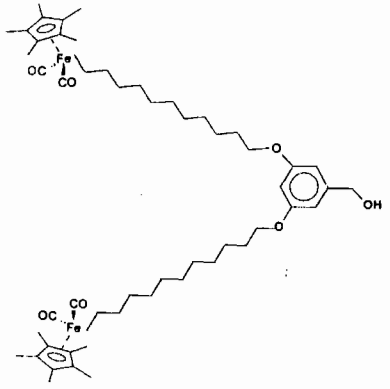

**Fp*11G1OH (13)**

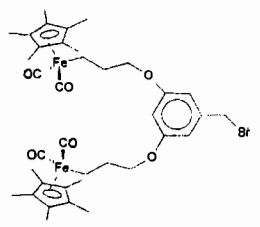

**Fp*3G1Br (14)**

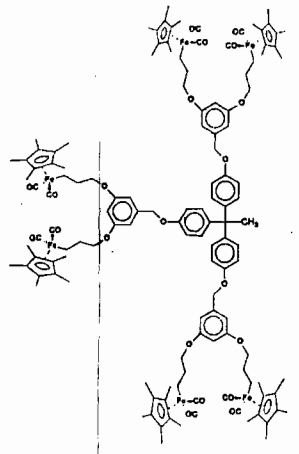

**Fp*3G1C(15)**

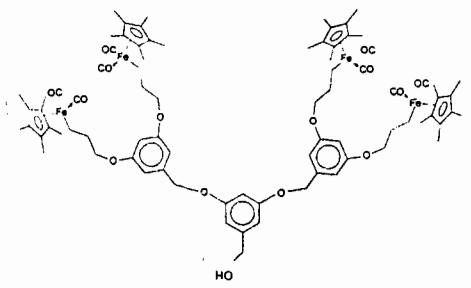

**Fp*3G2OH(16)**

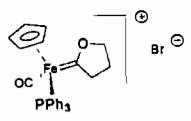

**Carbene(17)**

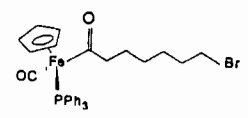

**Fp6ABr (18)**

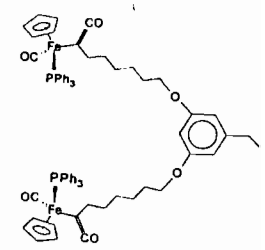

**Fp6AG1OH (19)**

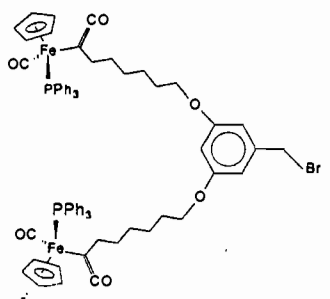

**Fp6AG1Br (20)**

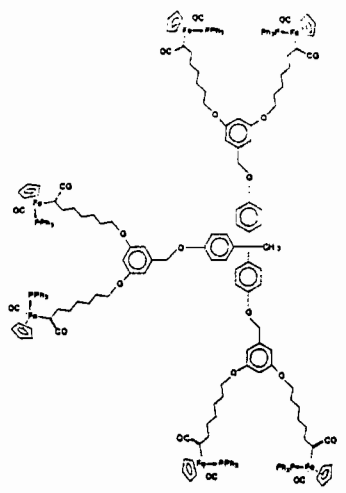

**Fp6AG1C (21)**

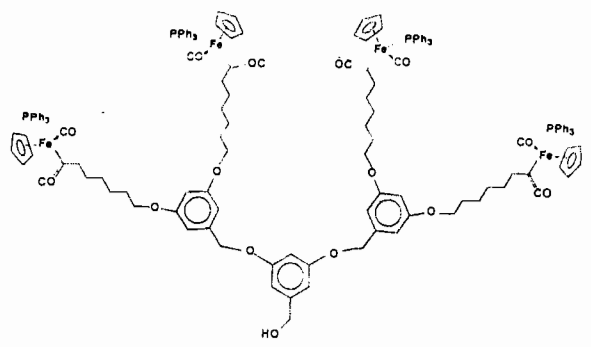

**Fp6AG2OH (22)**

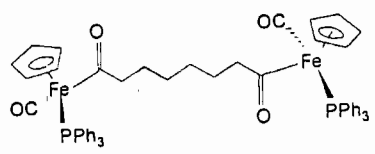

**Fp dimer (23)**

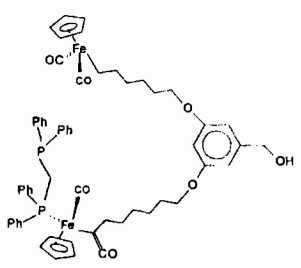

**(24)**

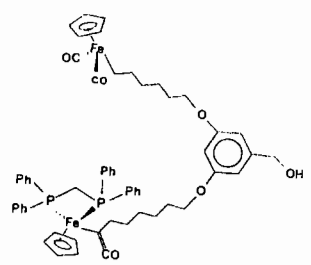

**(25)**

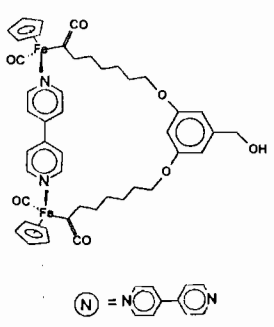

**(26b)**

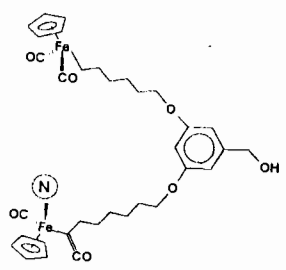

**(27)**

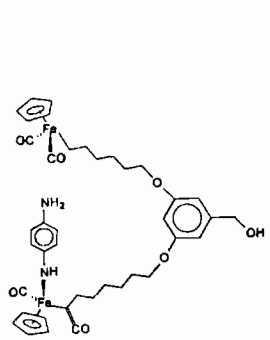

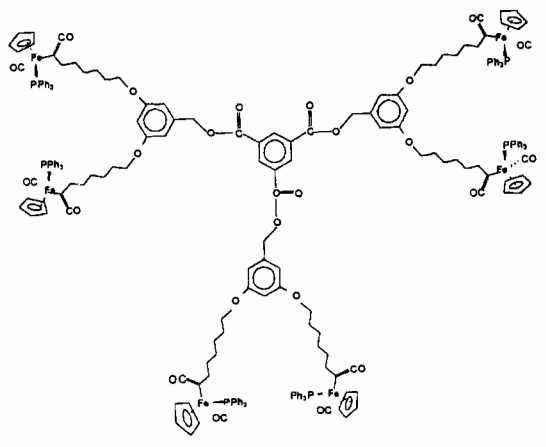

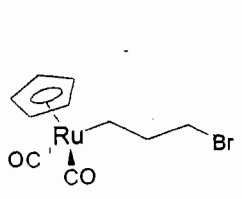

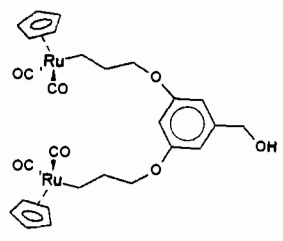

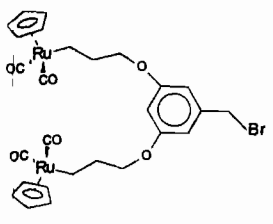

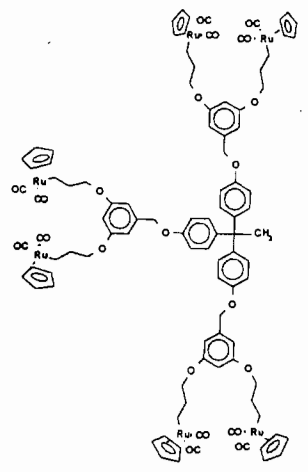

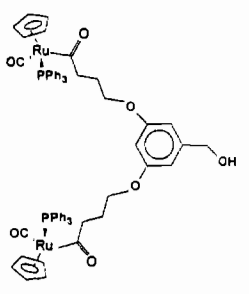

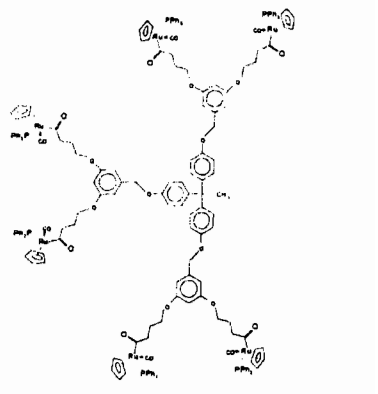

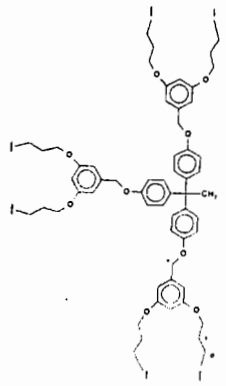

I3G1C (36)

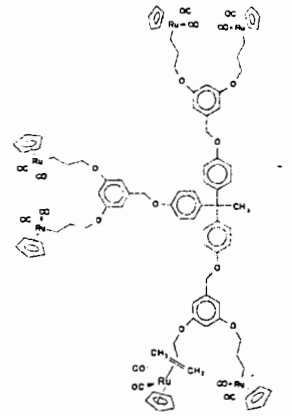

(37)

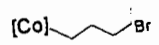


[Co]3Br (38)

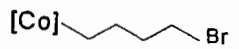


[Co]4Br (39)

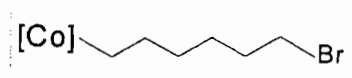


[Co]6Br (40)

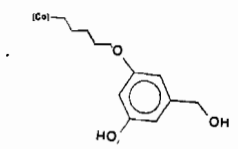


m[Co]4G1OH (41)

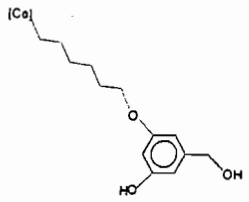


m[Co]6G1OH (42)

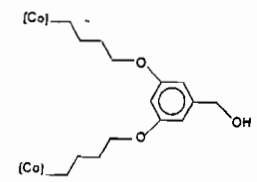


[Co]4G1OH (43)

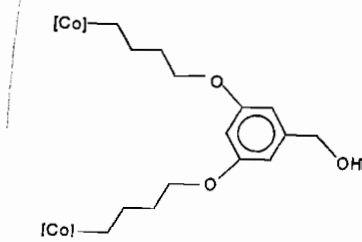


[Co]6G1OH (44)

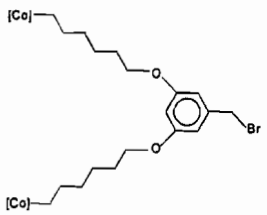


[Co]6G1Br (45)

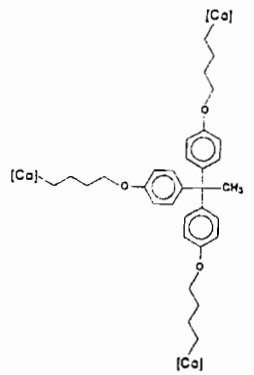


[Co]4G0C (46)

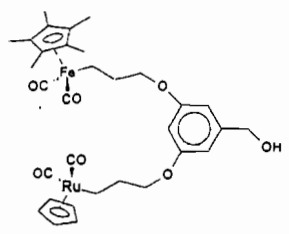


Fp*/Rp3G1OH (47)

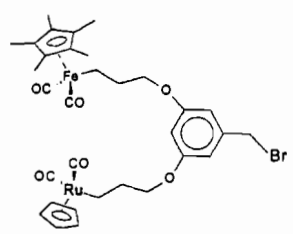


Fp*/Rp3G1Br (48)

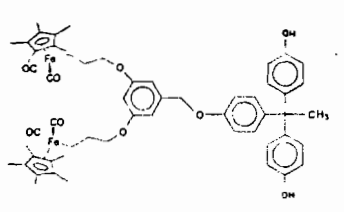


mFp*3G1C (49)

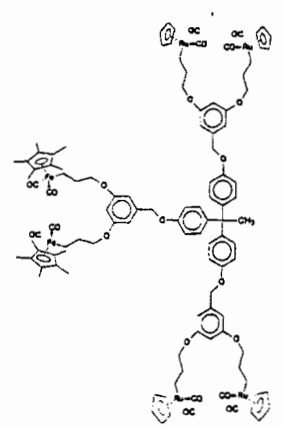

Fp*/Rp3G1C (50)

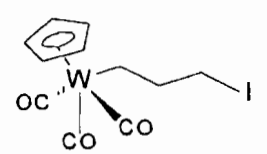


Wp3I (51)

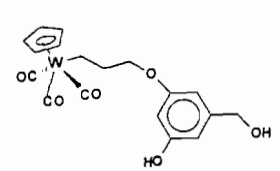


mWp3G1OH (52)

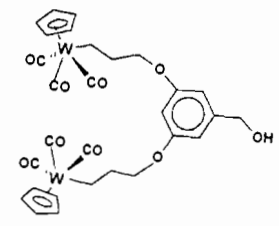


Wp3G1OH (53)

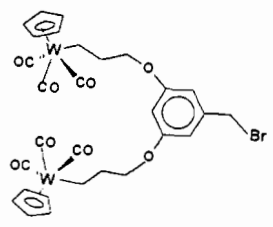


Wp3G1Br (54)

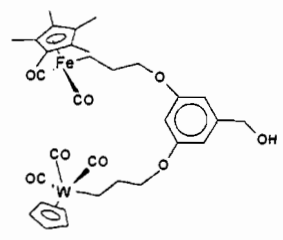


Fp*/Wp3G1OH (55)

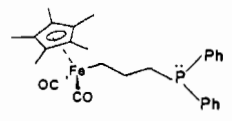


Fp*3PPh$_2$ (56)

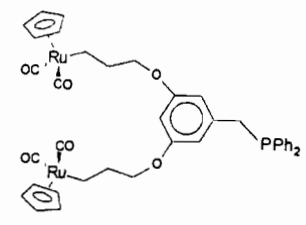


Rp3G1PPh$_2$ (57)

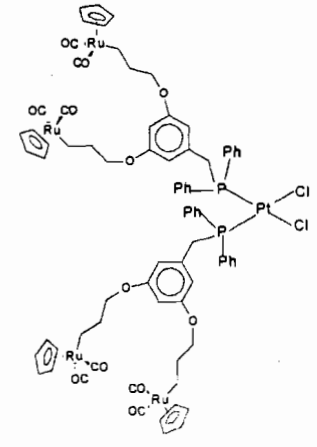


(58)

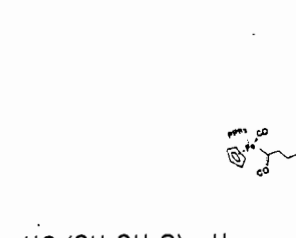


(59)

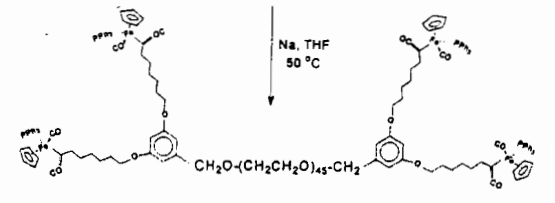


(60)

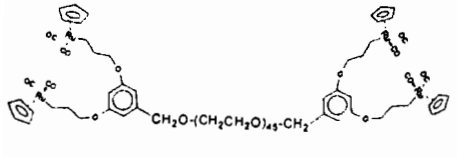


(61)

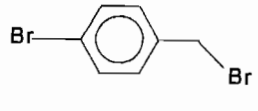


(62)

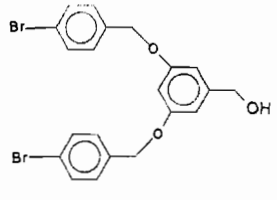


Br$_2$G1OH (63)

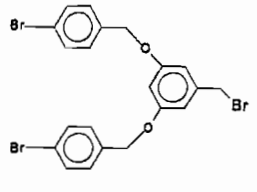


Br$_2$G1Br (64)

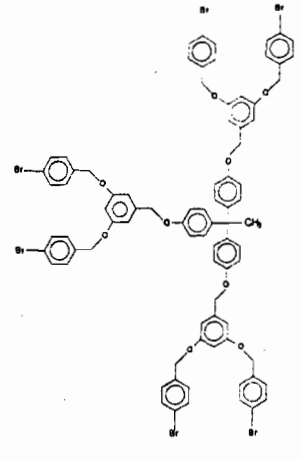

Br$_6$G1C (65)

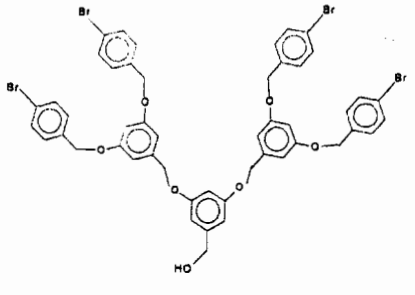


Br$_4$G2OH (66)

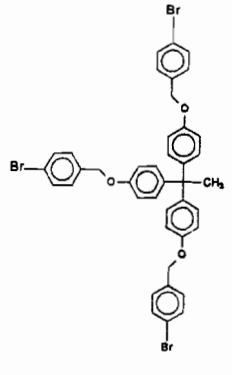


Br$_3$G0C (67)

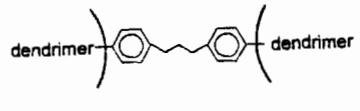


Br dimer (68)